

รายงานวิจัยฉบับสมบูรณ์

โครงการวิจัยเรื่อง: บริเวณรอยต่อเฟสของสารเฟร์โรอิเล็กทริกที่มี โครงสร้างแบบเพอรอฟสไกด์

โดย ผศ. ดร. นราชิป วิทยากร

สถาบันเทคโนโลยีพระจอมเกล้าเจ้าคุณทหารลาดกระบัง

สัญญาเลขที่ RSA5180002

รายงานวิจัยฉบับสมบูรณ์

โครงการ: บริเวณรอยต่อเฟสของสารเฟร์โรอิเล็กทริกที่มีโครงสร้างแบบ เพอรอฟสไกด์

ผศ. ดร. นราธิป วิทยากร

สถาบันเทคโนโลยีพระจอมเกล้าเจ้าคุณทหารลาดกระบัง

สนับสนุนโดยสำนักงานกองทุน สนับสนุนการวิจัย (ความเห็นในรายงานนี้เป็นของผู้วิจัย สกว.ไม่จำเป็นต้องเห็นด้วยเสมอไป)

กิตติกรรมประกาศ

งานวิจัยนี้สำเร็จได้ด้วยดีเนื่องจากการสนับสนุนจาก สำนักงานกองทุนสนับสนุนการวิจัย (สกว) ขอขอบคุณ คณะวิทยาศาสตร์ สถาบันเทค โนโลยีพระจอมเกล้าเจ้าคุณทหารลาดกระบังที่ อำนวยความสะดวกในการใช้เครื่องมือและสถานที่ ขอขอบคุณ วิทยาลัยนาโนเทคโนโลยีพระจอม เกล้าเจ้าคุณทหารลาดกระบัง ที่อำนวยความสะดวกในงานวิจัย ขอขอบคุณ รองศาสตราจารย์ ดร. จิติ หนูแก้ว และ ผู้ช่วยศาสตราจารย์ ดร. รัตติกร ยิ้มนิรัญ ที่คอยให้คำปรึกษา แนะนำ และ สนับสนุนในทุกๆ ด้านด้วยดีเสมอมา ขอบคุณผู้ร่วมวิจัย ดร. ธีรชัย บงการณ์ คุณรังสรรค์ เมืองเหลือ และนักศึกษาทุกคนที่ช่วยกันทำงานวิจัยอย่างเต็มที่จนสำเร็จลุล่วงไปด้วยดี สุดท้ายขอบคุณกำลังใจ และการสนับสนุนที่มีให้เสมอมาจากจาก พ่อ แม่ ภรรยา ลูก และน้องสาว

(ผู้ช่วยศาสตราจารย์ คร. นราธิป วิทยากร) หัวหน้าโครงการ

สารบัญ

	หน้า
กิตติกรรมประกาศ	1
บทคัดย่อภาษาไทย	3
บทคัดย่อภาษาอังกฤษ	4
Executive Summary	5
Output จากโครงการ	15
ภาคผนวก (reprint)	25

บทคัดย่อ

1. รหัสโรงการ: RSA5180002

2. ชื่อโครงการ บริเวณรอยต่อเฟสของสารเฟร์ โรอิเล็กทริกที่มี โครงสร้างแบบเพอรอฟไกด์

3. ชื่อหัวหน้าโครงการ

ผศ.คร. นราธิป วิทยากร ภาควิชา เคมี คณะวิทยาศาสตร์ สถาบันเทคโนโลยีพระจอมเกล้าเจ้าคุณ ทหารลาดกระบัง ถนนฉลองกรุง เขตลาดกระบัง กรุงเทพฯ 10520 E-mail Address: naratipcmu@yahoo.com, kvnarati@kmitl.ac.th

4. ระยะเวลาดำเนินงาน 3 ปี (1 พฤษภาคม 2551 ถึง 30 เมษายน 2554)

บทคัดย่อ

โครงการวิจัยนี้ได้ทำการศึกษาบริเวณรอยต่อเฟสของสารเฟร์โรอิเล็กทริกในกลุ่มดังต่อไปนี้ $PbZrO_{3}-Pb(Co_{1/3}Nb_{2/3})O_{3} - PbZrO_{3}-Pb(Ni_{1/3}Nb_{2/3})O_{3}, \ PbZrO_{3}-Pb(Zn_{1/3}Nb_{2/3})O_{3}, \ PbTiO_{3}-PbZrO_{3}-Pb(Zn_{1/3}Nb_{2/3})O_{3}, \ PbTiO_{3}-PbZrO_{3}-Pb(Zn_{1/3}Nb_{2/3})O_{3}, \ PbTiO_{3}-PbZrO_{3}-Pb(Zn_{1/3}Nb_{2/3})O_{3}, \ PbTiO_{3}-PbZrO_{3}-P$ $Pb(Zn_{1/3}Nb_{2/3})O_3$, $PbZrO_3$ -BiAlO₃, $PbZrO_3$ -Pb(Yb_{1/2}Nb_{1/2})O₃, $PbZrO_3$ -Pb(Y_{1/2}Nb_{1/2})O₃, $PbZrO_3$ -Pb(Y_{1/2}Nb_{1/2})O₃, $PbZrO_3$ -Pb(Yb_{1/2}Nb_{1/2})O₃, $PbZrO_3$ -Pb(Yb_{1/2}Nb_{1/2}Nb_{1/2})O₃, $PbZrO_3$ -Pb(Yb_{1/2}Nb_{1/2} $PbZrO_3$ - $Pb(Mg_{1/2}W_{1/2})O_3$ โดยสารละลายของแข็งที่ศึกษาเตรียมด้วย Pb(In_{1/2}Nb_{2/3})O₃ และ กระบวนการโคลัมใบต์ – (วุลแฟรไมต์) ซึ่งใช้เทคนิคการเลี้ยวเบนของรังสีเอกซ์ (X-ray diffraction หรือ XRD) และรามานสเปกโทรสโกปี (Raman spectroscopy) สำหรับการตรวจสอบโรงสร้างผลึก ของเซรามิกที่ผ่านการเผาซินเตอร์ (Sintering) แล้ว นอกจากนี้การตรวจสอบทางสัณฐานวิทยา (Morphology) สมบัติทางความร้อน (Thermal properties) การขยายตัวทางความร้อน (Thermal expansion) สมบัติใดอิเล็กทริก (Dielectric properties) และสมบัติเฟอร์ โรอิเล็กทริก (Ferroelectric properties) ของเซรามิกเทียบกับสัดส่วนองค์ประกอบนั้น ตรวจสอบโดยใช้กล้องจุลทรรศ์ อิเล็กตรอนแบบส่องกราด (Scanning Electron Microscopy หรือ SEM) เครื่องดิฟเฟอเรนเชียล สแกนนิ่งแคลอรีมิเตอร์ (Differential Scanning Calorimeter หรือ DSC) เครื่องใคลาโตมิเตอร์ (Dilatometer) ชุดวัด ใดอิเล็กทริก และชุดวัดวงวนฮิสเทอรีซิส P - E ตามลำดับ ความสัมพันธ์ ระหว่าง โครงสร้าง และ สมบัติ ถูกศึกษาและเชื่อมโยงให้เห็นในในกลุ่มสารละลายของแข็ง ผสม ระหว่าง เฟร์โรคิเล็กทริกแบบปกติ-รีแรกเซอร์-แอนติเฟร์โรคิเล็กทริก

Abstract

Project code: RSA5180002

Project Title: Morphotropic Phase Boundary in Ferroelectric Materials Based on

Perovskite Structure

Investigator: Asst. Prof. Dr. Naratip Vittayakorn

E-mail Address: naratipcmu@yahoo.com, kvnarati@kmitl.ac.th

Project Period: 3 years (1 May 2008 - 30 April 2011)

Abstract

The morphotropic phase boundary in many mixed ferroelectric system, such as PbZrO₃- $PbZrO_{3}-Pb(Ni_{1/3}Nb_{2/3})O_{3}$, $PbZrO_{3}-Pb(Zn_{1/3}Nb_{2/3})O_{3}$, $Pb(Co_{1/3}Nb_{2/3})O_3$ PbTiO,-PbZrO,- $Pb(Zn_{1/3}Nb_{2/3})O_{3},\ PbZrO_{3}-BiAlO_{3},\ PbZrO_{3}-Pb(Yb_{1/2}Nb_{1/2})O_{3},\ PbZrO_{3}-Pb(Y_{1/2}Nb_{1/2})O_{3},\ PbZrO_{3}-Pb(Y_{1/2}Nb_{1/2})O_{$ Pb(In_{1/2}Nb_{2/3})O₃ and PbZrO₃-Pb(Mg_{1/2}W_{1/2})O₃ system was investigated in this study. Ceramics were prepared by high temperature solid state reaction involving the use of high-purity starting oxides and columbite-(wolframite) precursor method. Compositions were selected across each solid solution so as to represent all of the phases that occur in the systems with special emphasis on compositions near MPBs and other regions of particular interest. Each composition was synthesized by ball-milling followed by calcining at temperatures ranging from 700-950 °C. Phase development of the calcined powders and the crystal structure of sintered ceramics were analyzed by X-ray diffraction. The properties of the ceramics were characterized by a combination of dielectric spectroscopy, polarization switching, and x-ray measurements. This project explores the structure-properties relationship of a number of normalrelaxor - antiferroelectric solid solution systems.

Executive Summary

โครงการวิจัยนี้ได้ทำการศึกษาบริเวณรอยต่อเฟสของสารเฟร์ โรอิเล็กทริกในกลุ่มดังต่อไปนี้ $PbZrO_3-Pb(Co_{1/3}Nb_{2/3})O_3$ $PbZrO_3-Pb(Ni_{1/3}Nb_{2/3})O_3$, $PbZrO_3-Pb(Zn_{1/3}Nb_{2/3})O_3$, $PbTiO_3-PbZrO_3-Pb(Zn_{1/3}Nb_{2/3})O_3$, $PbZrO_3-Pb(Yb_{1/2}Nb_{1/2})O_3$, $PbZrO_3-Pb(Y_{1/2}Nb_{1/2})O_3$, $PbZrO_3-Pb(Y_{1/2}Nb_{1/2})O_3$, $PbZrO_3-Pb(Ng_{1/2}Nb_{1/2})O_3$, $PbZrO_3-Pb(Ng_{1/2}Nb_{1/2})$

1. ผลการศึกษาในระบบ (1-x)PbZrO₃ - xPb(Co_{1/3}Nb_{2/3})O₃

เตรียมเซรามิกในระบบ (1-x)PbZrO₃-xPb(Co_{1/3}Nb_{2/3})O₃ เมื่อ $x = 0.00 \ 0.02 \ 0.04 \ 0.06 \ 0.08 \ 0.10$ 0.20 และ 0.30 ด้วยกระบวนการโคลัมไบต์ ทำการตรวจพิสูจน์เอกลักษณ์ด้วยเทคนิคการเลี้ยวเบน ของรังสีเอกซ์ (XRD) และรามานสเปกโทรสโกปี ตรวจสอบพฤติกรรมทางความร้อนด้วยเทคนิค DSC วัดค่าใดอิเล็กทริก ตรวจสอบสมบัติเฟอร์โรอิเล็กทริกโดยการวัดวงฮิสเทอรีซิส P-E และ ตรวจสอบสัณฐานวิทยาของเซรามิกด้วยกล้องจุลทรรศน์อิเล็กตรอนแบบส่องกราด (SEM) ผลการ ตรวจสอบโครงสร้างผลึกของเซรามิก PZ - PCoN ด้วยเทคนิค XRD พบว่ามีโครงสร้างเป็น เพอรอฟสไกต์ที่สัดส่วนองค์ประกอบ $0.00 \le x \le 0.30$ และไม่พบเฟสไพโรคลอร์ในทุกสัดส่วน องค์ประกอบ โดยพบว่าที่สัดส่วนองค์ประกอบ $0.00 \le x \le 0.10$ นั้นมีระบบผลึกเป็นแบบออร์ โทรอมบิก และจะเปลี่ยนไปเป็นรอมโบฮีครอลเมื่อปริมาณของ PCoN เพิ่มสูงขึ้น จากการผลของ DSC พบว่าเกิดการเปลี่ยนเฟสจาก AFE \rightarrow FE \rightarrow PE ที่สัดส่วนองค์ประกอบ $0.00 \le x \le 0.08$ โดย อุณหภูมิในการเปลี่ยนเฟสจากนั้นจะลดลงเมื่อสัดส่วนองค์ประกอบ x สูงขึ้น และช่วงกว้างของ อุณหภูมิของเฟส FE จะเพิ่มขึ้นเมื่อปริมาณของ PCoN เพิ่มขึ้น ส่วนที่ $x \ge 0.08$ พบการเปลี่ยนแปลง เพียงช่วงเคียวคือการเปลี่ยนเฟสจาก FE-PE ส่วนผลจากการวัดค่าคงที่ไดอิเล็กทริกนั้นพบว่าพีค ที่สัดส่วนองค์ประกอบ x=0.00 นั้นจะมีลักษณะเป็นพืกแหลม (Sharp peak) และที่อุณหภูมิ ประมาณ 237 °C มีการเปลี่ยนเฟสจาก AFE \rightarrow PE แต่ที่สัดส่วนองค์ประกอบ $0.02 \le x \le 0.06$ นั้น พบการเปลี่ยนแปลง 2 ช่วง โดยที่อุณหภูมิต่ำกว่าเป็นการเปลี่ยนเฟสจาก AFE-FE ส่วนช่วงที่ อุณหภูมิสูงกว่าเป็นพืกที่แสดงการเปลี่ยนเฟสจาก FE-PE โดยช่วงอุณหภูมิที่เป็น FE นั้นจะกว้าง ขึ้นเมื่อ x สูงขึ้น ส่วนที่ $x \geq 0.08$ พบการเปลี่ยนแปลงเพียงช่วงเดียวคือการเปลี่ยนเฟสจาก FE \longrightarrow PE ซึ่งอุณหภูมิในการเปลี่ยนเฟสจะมีแนวโน้มลดลงเมื่อปริมาณของ PCoN เพิ่มสูงขึ้น นอกจากนี้ ค่าคงที่ไดอิเล็กทริกสูงสุด ($\mathcal{E}_{\scriptscriptstyle
m r. \, max}$) มีแนวโน้มสูงขึ้นเมื่อปริมาณของ PCoN เพิ่มขึ้น โดยการเปลี่ยน เฟสที่พบจาก DSC และ ไดอเล็กทริกนั้นมีความสอดคล้องกัน จากการวัดวงวนฮิสเทอรีซิส P-E จะ พบลักษณะวงวนฮิสเทอรีซิสที่สมบูรณ์ที่สัคส่วนองค์ประกอบ $x \ge 0.08$ โดยค่าโพลาไรเซชันอิ่มตัว และโพลาไรเซชันคงเหลือนั้นมีค่าใกล้เคียงกัน และมีค่าเพิ่มขึ้นเมื่อ x เพิ่มขึ้น และจากการ

ตรวจสอบบริเวณรอยหักของเซรามิกในระบบ PZ-PCoN ด้วย SEM พบว่าการหักส่วนใหญ่เกิดขึ้น ที่บริเวณขอบเกรน และขนาดเกรนในช่วง $0.00 \le x \le 0.10$ มีแนวโน้มเพิ่มขึ้นเมื่อปริมาณ PCoN สูงขึ้น และมีขนาดเล็กลงเมื่อ x = 0.20 และ 0.30 ตามลำดับ โดยขนาดเกรนอยู่ในช่วง 0.57-0.59

2. ผลการศึกษาในระบบ (1-x)PbZrO $_3$ – xPb(Ni $_{1/3}$ Nb $_{2/3}$)O $_3$

เตรียมเซรามิกเพอรอฟสไกต์ในระบบ (1-x)PbZrO₃-xPb(Ni_{1/3}Nb_{2/3})O₃ (PZ-PNN) ที่ x เท่ากับ 0.00 0.02 0.04 0.06 0.08 0.10 0.20 0.30 0.40 และ 0.50 ด้วยเทคนิคกระบวนการรีแอกชั้น-ซิ นเทอริง และเทคนิคปฏิกิริยาสถานะของแข็ง ทำการตรวจสอบลักษณะเฟส และโครงสร้างผลึก ด้วยเทคนิคการเลี้ยวเบนของรังสีเอกซ์ พบว่าสามารถเตรียมเซรามิกเพอรอฟสไกต์ในระบบ PZ-PNN บริสุทธิ์ได้จากทั้งสองเทคนิค โดยที่สัดส่วน x เท่ากับ 0.00 ถึง 0.08 มีโครงสร้างผลึก เป็นแบบออร์โทรอมบิก เมื่อปริมาณของ x เพิ่มขึ้นเท่ากับ 0.10 ถึง 0.40 โครงสร้างผลึก เปลี่ยนไปเป็นแบบรอมโบฮีครอล และเปลี่ยนเป็นแบบคิวบิกเสมือนเมื่อ x เท่ากับ 0.50 ทำการ ตรวจสอบการเปลี่ยนเฟสด้วยเทคนิคดิฟเฟอเรนเชียลสแกนนิงแคลอริเมทรี เตรียมได้จากทั้งสองเทคนิคที่สัดส่วนของ x เท่ากับ 0.00 ถึง 0.08 มีการเปลี่ยนเฟสเกิดขึ้น 2 ครั้ง โดยที่อุณหภูมิต่ำจะเกิดการเปลี่ยนเฟสจากแอนติเฟอร์โรอิเล็กทริกเฟสไปเป็นเฟอร์โรอิเล็ก ทริกเฟส และจะเปลี่ยนจากเฟอร์โรอิเล็กทริกเฟสไปเป็นพาราอิเล็กทริกเฟสที่อุณหภูมิสูง ส่วน ที่สัดส่วน x เท่ากับ 0.10 ถึง 0.40 มีการเปลี่ยนเฟสเกิดขึ้นเพียงครั้งเดียว คือการเปลี่ยนเฟสจาก เฟอร์โรอิเล็กทริกเฟสไปเป็นพาราอิเล็กทริกเฟส และไม่พบการเปลี่ยนแปลงใด ๆ ที่ x เท่ากับ 0.50 นอกจากนี้ยังพบอีกว่าเมื่อปริมาณของ x เพิ่มสูงขึ้น อุณหภูมิการเปลี่ยนเฟสจะลดลง ตามลำดับ เมื่อทำการตรวจสอบสมบัติทางไดอิเล็กทริกเทียบกับอุณหภูมิที่ความถี่ต่าง ๆ พบว่า ที่ x เท่ากับ 0.00 เกิดพีคแหลมฐานแคบที่อุณหภูมิ 230 องศาเซลเซียส ค่าคงที่ใดอิเล็กทริกที่ใด้ ไม่ขึ้นกับความถี่ และเมื่อเพิ่มปริมาณของ x มากขึ้นพบว่าพืกที่ได้จะมีความแหลมลดลง ฐาน กว้างมากขึ้น ค่าคงที่ใดอิเล็กทริกที่ได้ก็ขึ้นกับความถี่มากขึ้นตามลำดับ ซึ่งเห็นได้ชัดเจนที่ สัดส่วน x เท่ากับ 0.50 และอุณหภูมิที่เกิดพีกก็ลดต่ำลงตามลำดับ จากนั้นตรวจสอบสมบัติทาง เฟอร์อิเล็กทริกพบว่าที่ x เท่ากับ 0.00 ถึง 0.06 มีสมบัติเป็นแอนติเฟอร์ โรอิเล็กทริก ที่ x เท่ากับ 0.08 เกิดวงวนเฟอร์โรฮีสเทอเรซิสที่กว้าง และจะแคบลงเมื่อปริมาณ x เพิ่มสูงขึ้น สุดท้ายทำ การตรวจสอบทางสัณฐานวิทยาพบว่าเซรามิกที่เตรียมได้มีความบริสุทธิ์ ไม่พบสิ่งแปลกปลอม ขอบเกรนติดชิดกันดี และมีขนาดเกรนเฉลี่ยอยู่ระหว่าง 0.91 ถึง 6.76 ใมโครเมตร

3. ผลการศึกษาในระบบ (1-x)PbZrO₃ - xPb(In_{1/2}Nb_{1/2})O₃

ทำการศึกษาสารละลายของแข็งของเซรามิกในระบบ เลคเซอร์โคเนต-เลคอินเคียมใน โอเบต ((1-x)PbZrO $_3$ - xPb(In $_{1/2}$ Nb $_{1/2}$)O $_3$; (1-x)PZ-xPIN) โดยทำการศึกษารูปแบบการเกิดเฟสเพ

อรอฟสไกต์ การเปลี่ยนเฟส สมบัติใดอิเล็กทริก และสมบัติเฟอร์โรอิเล็กทริกของเซรามิกที่เตรียม ได้ โดยทำการเตรียมผงผลึกของ (1-x)PZ-xPIN ที่สัดส่วน x เท่ากับ 0.00 0.02 0.04 0.06 0.08 0.10 0.20 0.30 0.40 และ 0.50 ด้วยวิธีการเตรียมสารตั้งต้นวูลแฟรไมต์ (Wolframite Precursor โดยใช้สารตั้งต้นเป็นโลหะออกไซด์ที่มีความบริสุทธิ์สูง (> 99.5%) เผาแคลไซน์ที่ อุณหภูมิ 850°C เป็นเวลา 2 ชั่วโมง อัตราการขึ้น/ลงอุณหภูมิ 10°C /นาที จากนั้นทำการอัดขึ้นรูป ์ ชิ้นงานเป็นรูปแผ่นกลม และเผาซินเตอร์ที่อุณหภูมิ 1200-1250°C เป็นเวลา 2 ชั่วโมง พบว่าเมื่อ ปริมาณ x เพิ่มสูงขึ้นอุณหภูมิซินเตอร์จะลดลง จากการตรวจสอบรูปแบบการเกิดเฟสเพอรอฟสไกต์ และ โครงสร้างผลึกของเซรามิก (1-x)PZ-xPIN ด้วยเทคนิคการเลี้ยวเบนของรังสีเอกซ์ (X-ray diffraction; XRD) พบว่าที่ x เท่ากับ 0.00 มีรูปแบบการเลี้ยวเบนของรังสีเอกซ์คล้ายคลึงกับรูปแบบ การ เลี้ยวเบนรังสีเอกซ์มาตรฐาน(ICDD File no. 75-1607) ของ PbZrO, ซึ่งมีโครงสร้างผลึกเป็น แบบออร์โทรอมบิก และที่ x เท่ากับ 0.02-0.10 ยังคงมีรูปแบบการเลี้ยวเบนของรังสีเอกซ์ใกล้เคียง กับรูปแบบการเลี้ยวเบนรังสีเอกซ์มาตรฐานของ $PbZrO_3$ เมื่อปริมาณ x เพิ่มขึ้นถึง 0.20 พบการ เปลี่ยนเฟสเกิดขึ้นจากออร์โทรอมบิก เป็นรอมโบฮีครอล เมื่อทำการตรวจสอบอุณหภูมิการเปลี่ยน เฟส ด้วยผลของค่าคงที่ใดอิเล็กทริก การวัดการขยายตัวทางความร้อน และดิฟเฟอเรนเชียลสแกน นิงแคลอริเมทรี (Differential scanning calorimetry; DSC) พบว่า ที่ x=0.02-0.4 เซรามิกส์เกิดการ เปลี่ยนเฟส 2 ครั้งจากแอนติเฟอร์โรอิเล็กทริกไปเป็นเฟอร์โรอิเล็กทริก และจากเฟอร์โรอิเล็กทริก ไปเป็นพาราอิเล็กทริกตามลำดับ ส่วนที่ x=0.5 เกิดการเปลี่ยนเฟสเพียงครั้งเดียวจากเฟอร์ โรอิเล็กท ริกไปเป็นพาราอิเล็กทริก และพบว่าอุณหภูมิการเปลี่ยนเฟสที่เกิดขึ้นทั้ง 2 ครั้ง จะลดลงเมื่อปริมาณ ของ x เพิ่มสูงขึ้น นอกจากนี้ที่อุณหภูมิห้องเซรามิกที่สัดส่วน $x=0.2\,$ สามารถวัดวงวนฮีสทีรีซิสได้ โดยมีลักษณะคล้ำยกับวงวนฮีสที่รีซิสของแอนติเฟอร์ โรอิเล็กทริก สัดส่วน x=0.3-0.5 แสดงสมบัติ เฟอร์โรอิเล็กทริก ผลการตรวจสอบโครงสร้างในระดับจุลภาคที่บริเวณรอยหักด้วยกล้องจุลทรรศ อิเล็กตรอนแบบส่องกราด (Scanning electron microscope) พบว่าที่บริเวณรอยหักของเม็ดเซรามิกส์ ส่วนใหญ่เกิดที่บริเวณขอบเกรน และมีขนาดเกรนในช่วง 2.26 - 3.16 µm

4. เซรามิกในระบบ (1-x) $PbZrO_3 - xPb(Yb_{1/2}Nb_{1/2})O_3$

ทำการศึกษาสารละลายของแข็งของเซรามิกในระบบ เลดเซอร์โคเนต-อิทเทอร์เบียมใน โอเบต ((1-x)PbZrO $_3$ - xPb(Yb $_{1/2}$ Nb $_{1/2}$)O $_3$; (1-x)PZ-xPYbN) โดยทำการศึกษารูปแบบการเกิดเฟสเพ อรอฟสไกต์ การเปลี่ยนเฟส สมบัติไดอิเล็กทริก และสมบัติเฟอร์โรอิเล็กทริกของเซรามิกที่เตรียม ได้ โดยทำการเตรียมผงผลึกของ (1-x)PZ-xPYbN ที่สัดส่วน x เท่ากับ 0.00 0.02 0.04 0.06 0.08 0.10 0.20 0.30 0.40 และ 0.50 ด้วยวิธีการเตรียมสารตั้งต้นวูลแฟรไมต์ (Wolframite Precursor Method) โดยใช้สารตั้งต้นเป็นโลหะออกไซด์ที่มีความบริสุทธิ์สูง (> 99.5%) เผาแคลไซน์ที่ อุณหภูมิ 900°C เป็นเวลา 2 ชั่วโมง อัตราการขึ้น/ลงอุณหภูมิ 20°C /นาที จากนั้นทำการอัดขึ้นรูป

ชิ้นงานเป็นรูปแผ่นกลม และเผาชินเตอร์ที่อุณหภูมิ 1200-1250°C เป็นเวลา 2 ชั่วโมง จากการ ตรวจสอบรูปแบบการเกิดเฟสเพอรอฟสไกต์ และโครงสร้างผลึกของเซรามิก (1-x)PZ-xPYbN ด้วย เทคนิกการเลี้ยวเบนของรังสีเอกซ์ (X-ray diffraction; XRD) พบว่าที่ x เท่ากับ 0.00 มีรูปแบบการ เลี้ยวเบนของรังสีเอกซ์กล้ายกลึงกับรูปแบบการ เลี้ยวเบนรังสีเอกซ์มาตรฐาน(ICDD File no. 75-1607) ของ ซึ่งมีโครงสร้างผลึกเป็นแบบออร์โทรอมบิก และที่ x เท่ากับ 0.02-0.20 ยังคงมีรูปแบบการเลี้ยวเบนรังสีเอกซ์มาตรฐานของ PbZrO₃ เมื่อ ปริมาณ x เพิ่มเป็น 0.30-0.50 พบเฟสแปลกปลอมเกิดขึ้น แสดงให้เห็นว่าเซรามิกส์ในระบบ (1-x)PZ-xPYbN ไม่สามารถเกิดเป็นสารละลายของแข็งที่มีโครงสร้างแบบเพอรอฟสไกต์ที่บริสุทธิ์ได้ เมื่อ x มากกว่า 0.2 จากนั้นทำการตรวจสอบอุณหภูมิการเปลี่ยนเฟส ด้วยผลของค่าคงที่ใดอิเล็กทริก และดิฟเฟอเรนเซียลสแกนนิงแคลอริเมทรี (Differential scanning calorimetry; DSC) พบว่า อุณหภูมิกูรีลดลง ลักษณะของพีกค่าคงที่ใดอิเล็กทริกจะมีฐานกว้างมากขึ้นเมื่อปริมาณของ x เพิ่ม สูงขึ้น และที่สัดส่วน x = 0.02-0.20 มีการเปลี่ยนเฟสในช่วงอุณหภูมิเคบๆ ก่อนถึงอุณหภูมิกูรี นอกจากนี้ยังพบว่าเซรามิกที่เตรียมได้ทุกสัดส่วน แสดงสมบัติแอนติเฟอร์โรอิเล็กทริกที่ อุณหภูมิห้อง

5. ผลการศึกษาเซรามิกในระบบ (1-x)PbZr O_3 – xPb($Y_{1/2}$ Nb $_{1/2}$) O_3

ทำการศึกษาสารละลายของแข็งของเซรามิกในระบบ เลคเซอร์โคเนต-อิทเทียมในโอเบต $((1-x)PbZrO_3 - xPb(Y_{1/2}Nb_{1/2})O_3; (1-x)PZ-xPYN)$ โดยทำการศึกษารูปแบบการเกิดเฟสเพอรอฟส ไกต์ การเปลี่ยนเฟส สมบัติใดอิเล็กทริก และสมบัติเฟอร์โรอิเล็กทริกของเซรามิกที่เตรียมได้ โดย ทำการเตรียมผงผลึกของ (1-x)PZ-xPYN ที่สัดส่วน x เท่ากับ 0.00 0.02 0.04 0.06 0.08 0.10 0.20 0.30 0.40 และ 0.50ด้วยวิธีการเตรียมสารตั้งต้นวูลแฟรไมต์ (Wolframite Precursor Method) โดยใช้สารตั้งต้นเป็นโลหะออกไซด์ที่มีความบริสุทธิ์สูง (> 99.5%) เผาแคลไซน์ที่อุณหภูมิ 900°C เป็นเวลา 2 ชั่วโมง จากนั้นทำการอัคขึ้นรูปชิ้นงานเป็นรูปแผ่นกลม และเผาซินเตอร์ที่อุณหภูมิ 1200-1300°C เป็นเวลา 2 ชั่วโมง พบว่าเมื่อปริมาณ x เพิ่มสูงขึ้นอุณหภูมิซินเตอร์จะลดลง จากการ ตรวจสอบรูปแบบการเกิดเฟสเพอรอฟสไกต์ และ โครงสร้างผลึกของเซรามิก (1-x)PZ-xPYN ด้วย เทคนิคการเลี้ยวเบนของรังสีเอกซ์ (X-ray diffraction; XRD) พบว่าที่ x เท่ากับ 0.00 มีรูปแบบการ เลี้ยวเบนของรังสีเอกซ์คล้ายคลึงกับรูปแบบการ เลี้ยวเบนรังสีเอกซ์มาตรฐาน(ICDD File no. 75-1607) ของ ซึ่งมีโครงสร้างผลึกเป็นแบบออร์โทรอมบิก และที่ x เท่ากับ 0.02-0.10 ยังคงมีรูปแบบ การเลี้ยวเบนของรังสีเอกซ์ใกล้เคียงกับรูปแบบการเลี้ยวเบนรังสีเอกซ์มาตรฐาน(1-x)PZ-xPYN ของ $PbZrO_3$ แต่เมื่อปริมาณ x เพิ่มขึ้นถึง 0.20 พบเฟสแปลกปลอมเกิดขึ้น แสดงว่าสารในระบบ (1x)PZ-xPYN สามารถเกิดเป็นสารละลายของแข็งที่มีโครงสร้างเป็นเพอรอฟสไกต์บริสุทธิ์ได้ที่ ปริมาณ $x \leq 0.1$ เมื่อทำการตรวจสอบอุณหภูมิการเปลี่ยนเฟสจากแอนติเฟอร์ โรอิเล็กทริกไปเป็น พาราอิเล็กทริก หรือที่เรียกว่า "อุณหภูมิคูรี (Curie temperature; T_c)" ด้วยผลของค่าคงที่ใดอิเล็กท ริก การวัดการขยายตัวทางความร้อน และดิฟเฟอเรนเชียลสแกนนิงแคลอริเมทรี (Differential scanning calorimetry; DSC) พบว่า ที่ x=0.02-0.20 พบว่าอุณหภูมิคูรีลดลงและลักษณะพีกที่เมื่อ ปริมาณของ x เพิ่มสูงขึ้น นอกจากนี้ยังพบอีกว่าที่อุณหภูมิห้องเซรามิกที่สัดส่วน x=0.02-0.10 แสดงสมบัติแอนติเฟอร์โรอิเล็กทริก และที่สัดส่วน x=0.20 แสดงสมบัติเฟอร์โรอิเล็กทริก

6. ผลการศึกษาเซรามิกในระบบ (1-x)PbZrO₃ - xPb(Zn_{1/3}Nb_{2/3})O₃

เตรียมเซรามิกส์ (1-x)PbZrO $_3 - x$ Pb $(Zn_{1/3}Nb_{2/3})O_3$ ที่ x = 0.0-0.5 ด้วยวิธี โคลัม ใบต์ ทำการตรวจ พิสูจน์เอกลักษณ์ด้วยเทคนิคการเลี้ยวเบนของรังสีเอ็กซ์ และรามานสเปกโทรสโกปี วัดการขยายตัว เชิงเส้น วัคค่าคงที่ ใคอิเล็กทริก วัควงวนฮิสเทอริซิส P-E และตรวจสอบ โครงสร้างในระดับจุลภาค ผลการตรวจสอบโครงสร้างผลึกพบว่า สามารถเตรียมเซรามิกส์ในระบบ PZ-PZN ที่มีโครงสร้าง แบบเพอรอฟสไกต์ ในสัคส่วน $0.00 \le x \le 0.50$ ได้โดยไม่พบเฟสแปลกปลอม จากผลที่ได้จาก XRD และรามานพบว่าที่สัดส่วน $0.00 \le x \le 0.10$ มีระบบผลึกเป็นแบบออร์โธรอมบิก และเกิด การเปลี่ยนเฟสจากออร์โธรอมบิกไปเป็นรอมโบฮีครอลที่ x=0.2 การตรวจสอบสมบัติไคอิเล็กทริก พบว่าที่ปริมาณ PZN เป็น 0.02-0.06 พบการเปลี่ยนเฟสเกิดขึ้น 2 ครั้ง จาก AFE→FE→PE โดย อุณหภูมิการเปลี่ยนเฟสจาก AFE→FE มีแนวโน้มลดลงเข้าใกล้อุณหภูมิห้องเมื่อปริมาณ PZN เพิ่มขึ้น และอุณหภูมิการเปลี่ยนเฟส FE→PE มีแนวโน้มลคลงเมื่อ PZN เพิ่มขึ้น และพบว่าช่วง อุณหภูมิของเฟสเฟอร์ โรอิเล็กทริกที่อยู่ระหว่างเฟสพาราอิเล็กทริกและแอนติเฟอร์ โรอิเล็กทริกของ PbZrO, จะเพิ่มขึ้นตามความเข้มข้นของ PZN ที่ $0.08 \le x$ พบการเปลี่ยนเฟสเกิดขึ้นเพียงครั้งเดียว จาก FE→PE โดยอุณภูมิการเปลี่ยนเฟสมีแนวโน้มลดลงเมื่อปริมาณ PZN เพิ่มขึ้น นอกจากนี้ ค่าคงที่ไดอิเล็กทริกสูงสุดจะค่อยๆ เพิ่มขึ้นเมื่อสัดส่วนองค์ประกอบเพิ่มสูงขึ้นถึง x=04 จากนั้นจะ กลับมามีค่าลดลงที่ x=0.5 ผลการวัดการขยายตัวเชิงเส้นที่ $0.02 \le x \le 0.06$ พบการเปลี่ยนเฟสและ แนวโน้มของอุณหภูมิการเปลี่ยนเฟสที่สอคคล้องกับผลการเปลี่ยนเฟสที่พบจากการวัดค่าไดอิเล็กท ริก ในการเปลี่ยนเฟสจาก AFE $\;
ightarrow\;$ FE จะเกิดการขยายตัวเชิงเส้น ส่วนการเปลี่ยนเฟสจาก FE \rightarrow PE จะเกิดการหดตัวของสาร แต่ที่ x=0.00 ผลที่ได้ขัดแย้งกับผลไดอิเล็กทริกคือพบการ เปลี่ยนเฟสเกิดขึ้น 2 ครั้ง ผลการวัควงวนฮิสเทอรีซิสพบวงวนฮิสเทอริซิสที่สมบรณ์ที่สัคส่วน 0.08 $\leq x \leq 0.50$ และพบลักษณะวงวนคล้ายกับวงวนของเฟอร์ โรอิเล็กทริกปกติ ผลการตรวจสอบ โครงสร้างในระดับจุลภาคที่บริเวณรอยหักของเม็ดเซรามิกส์พบว่าการหักส่วนใหญ่เกิดที่บริเวณ ขอบเกรน และขนาดเกรนในช่วง $0.02 \le x \le 0.06$ มีแนวโน้มเพิ่มขึ้นตามปริมาณ PZN จากนั้นจะมี ขนาดลดงเมื่อเพิ่มขึ้นที่ x=0.08 และ x=0.01 เมื่อปริมาณ PZN เพิ่มขึ้นถึง $0.20 \le x \le 0.50$ จะกลับ มีแนวโน้มเพิ่มขึ้นตามปริมาณ PZN อีกครั้ง

7. ผลการศึกษาเซรามิกในระบบ $(1-x)PbZrO_3 - xPb(Mg_{1/2}W_{1/2})O_3$

โครงสร้างผลึกและการเปลี่ยนเฟสของเซรามิกในระบบ เลดเซอร์โคเนต-เลดแมกนีเซียม ทั้งสเตต $((1-x)\text{PbZrO}_3-x\text{Pb}(\text{Mg}_{1/2})\text{O}_3; \text{PZ-PMW})$ ที่สัดส่วนขององค์ประกอบ (x) ตั้งแต่ 0.00-0.50 ด้วยเทคนิควุลแฟลมไมท์ (Wolframite precursor method) ทำการเตรียมผงผลึกโดยการเผา แคลไซน์ที่อุณหภูมิ 900°C เป็นเวลา 4 ชั่วโมงจากนั้นทำการตรวจสอบความบริสุทธิ์ด้วยเทคนิคการ ้เลี้ยวเบนของรังสีเอกซ์พบว่า ผงผลึกที่เตรียมได้มีความบริสุทธิ์ ซึ่งเมื่อสัดส่วนขององค์ประกอบอยู่ ที่ $0.00 \le x \le 0.10$ ผงผลึก PZ-PMW มีรูปแบบการเลี้ยวเบนรังสีเอกซ์สอคคล้องกับรูปแบบการ ้ เลี้ยวเบนรังสีเอกซ์ของ PbZrO, (PZ) จากฐานข้อมูลมาตรฐาน JCPDS เลขที่ 75-1607 แต่ที่สัดส่วน ขององค์ประกอบ $0.20 \le x \le 0.50$ พบพีกแปลกปลอมเกิดขึ้นซึ่งเมื่อทำการตรวจสอบแล้วพบว่า พีกที่ปรากฏนั้นสอดคล้องกับรูปแบบการเลี้ยวเบนรังสีเอกซ์ของ PMW จากฐานข้อมูลมาตรฐาน JCPDS เลขที่ 75-0004 โดยเมื่อทำการหาปริมาณของ PMW ที่เกิดขึ้นพบว่าปริมาณของ PMW จะ เพิ่มขึ้นตามสัดส่วนขององค์ประกอบที่เพิ่มขึ้น จากนั้นนำผงผลึกที่ได้มาทำการอัดขึ้นรูปแล้วนำไป เผาซินเตอร์ที่อุณหภูมิแตกต่างกันพบว่าเมื่อสัดส่วนขององค์ประกอบเพิ่มสูงขึ้น อุณหภูมิในการเผา ซินเตอร์จะเพิ่มสูงขึ้นด้วย จากนั้นนำเซรามิกที่เตรียมได้มาทำการตรวจสอบความบริสุทธิ์และ โครงสร้างผลึก (Crystal structure) ด้วยเทคนิคการเลี้ยวเบนของรังสีเอกซ์ (X-ray diffractometry; XRD) พบว่าเซรามิกที่เตรียมได้มีความบริสุทธิ์ โดยเมื่อสัดส่วนขององค์ประกอบอยู่ที่ $0.00 \le x \le$ 0.10 เซรามิก PZ-PMW มีรูปแบบการเลี้ยวเบนรังสีเอกซ์สอคคล้องกับรูปแบบการเลี้ยวเบนรังสี เอกซ์ของ $PbZrO_3$ (PZ) จากฐานข้อมูลมาตรฐาน JCPDS เลขที่ 75-1607 เมื่อเพิ่มสัดส่วนของ องค์ประกอบ (x) อยู่ที่ $0.20 \le x \le 0.50$ จะแบ่งการพิจารณาออกเป็นทีละสองสัดส่วนองค์ประกอบ ้ ดังนี้คือ ที่สัดส่วนขององค์ประกอบเท่ากับ 0.20 และ 0.30 พบว่าจากรูปแบบการเลี้ยวเบนของรังสี เอกซ์ที่ได้จากผงผลึกปรากฏพีกของ PMW แยกออกมาแต่เมื่อทำการเผาซินเตอร์แล้วไม่พบพีก ดังกล่าวแต่เมื่อสัดส่วนขององค์ประกอบเพิ่มขึ้นเป็น 0.40 และ 0.50 นั้นพบว่ายังคงปรากฏพีกของ PMW แยกออกมาอยู่เช่นเดิมแต่มีปริมาณของ PMW ลดลงและเมื่อทำการพิจารณาถึงโครงสร้าง แล้วพบว่ามีแนว โน้มในการเปลี่ยน โครงสร้างจากออ โทรอมบิกเป็นรอม โบฮีครอลเมื่อสัคส่วนของ องค์ประกอบ (x) สูงขึ้น จากนั้นทำการตรวจสอบสมบัติไดอิเล็กทริก (Dielectric properties) การ ขยายตัวทางความร้อน(Thermal expansion) สมบัติการเปลี่ยนแปลงทางความร้อนและยืนยันการ เปลี่ยนเฟสด้วยการตรวจสอบสมบัติเฟอร์โรอิเล็กทริก (Ferroelectric properties) พบว่าเซรามิก PZ-PMW ที่สัดส่วนขององค์ประกอบ $0.00 \le x \le 0.10$ มีการเปลี่ยนเฟสสองช่วงคือเปลี่ยนจากแอนติ เฟอร์โรอิเล็กทริกเป็นเฟอร์โรอิเล็กทริกและเปลี่ยนจากเฟอร์โรอิเล็กทริกเป็นพารา-อิเล็กทริกและ เมื่อสัดส่วนขององค์ประกอบ (x) สูงขึ้นพบว่าอุณหภูมิในการเปลี่ยนเฟสลดลง และที่สัดส่วนของ องค์ประกอบ $0.20 \le x \le 0.50$ มีการเปลี่ยนเฟสช่วงเดียวคือเปลี่ยนจากเฟอร์ โรอิเล็กทริกเป็นพาราอิ เล็กทริก

8. ผลการศึกษาในระบบ (1-x)PbZrTiO₃ - xPb(Zn_{1/3}Ta_{2/3})O₃

เซรามิกในระบบ PZT-PZnTa เตรียมสารละลายของแข็ง Pb[(1-x)(Zr_{1/2}Ti_{1/2})-x(Zn_{1/3}Ta_{2/3})]O₃ เมื่อ x=0.1-0.5 ด้วยกระบวนการ โคลัม ใบต์และวูลแฟร ใมต์ (columbite and wolframite methods) และ ใช้ เทคนิคการเลี้ยวเบนของรังสีเอกซ์ (XRD) กล้องจุลทรรศน์อิเล็กตรอนแบบส่องกราด (SEM) และ เครื่องวัด ใดอิเล็กทริก (dielectric spectroscopy) สำหรับตรวจสอบ โครงสร้างผลึก สัณฐานวิทยา และสมบัติ ใดอิเล็กทริกของเซรามิก ตามลำดับ จากผลที่ ได้พบว่า ปริมาณของเลดซิงค์แทนทาเลต [Pb(Zn_{1/3}Ta_{2/3})O₃; PZTa] ในสารละลายของแข็งนั้นส่งผลต่อเสถียรภาพของ โครงสร้างเพอรอฟส ใกต์ (perovskite) ของเลดเซอร์ โคเนต ใท [Pb(Zr_{1/2}Ti_{1/2})O₃; PZT] และเมื่อปริมาณ PZTa เพิ่มขึ้นจะ เกิดการเปลี่ยนเฟสจากเตตระ โกนอล (tetragonal) ไปเป็นซู โด-คิวบิก (pseudo-cubic) นอกจากนี้ยัง พบว่าที่สัดส่วนองค์ประกอบ x=0.1 นั้นมีทั้งสองเฟสของเตตระ โกนอลและซู โค-คิวบิก และจาก ค่าคงที่ ใดอิเล็กทริกที่ ได้พบว่ามีค่าคงที่ ใดอิเล็กทริกสูงสุดที่บริเวณรอยต่อเฟส (Morphotropic Phase Boundary; MPB) ซึ่งมีค่าเท่ากับ 19,600 ที่อุณหภูมิ 330 °C

9. <u>ผลการศึกษาเซรามิกในระบบ (1-x)Bi_{0.5}K_{0.5}O₃ - xBaTiO₃</u>

ทำการศึกษาสารละลายของแข็ง ของเซรามิกเพียโซอิเล็กทริกไร้สารตะกั่วในระบบ (1x)Bi_{0.5} $K_{0.5}$ O₃ - xBaTiO₃ (BKT - BT) ι $\mathring{\mathfrak{g}}$ 0 0 0.02 0.04 0.06 0.08 0.10 0.20 0.30 0.40 0.50 0.60 0.70 0.80 0.90 และ 1.00 โดยได้ทำการศึกษาโครงสร้างผลึก การเปลี่ยนเฟส และ สมบัติใดอิเล็กทริกของสารระบบนี้ โดยได้ทำการเตรียมผงผลึกที่มีความบริสุทธิ์สูงด้วยเทคนิค ปฏิกิริยาสถานะของแข็ง โดยใช้สารตั้งต้นเป็นสารประกอบประเภทออกไซด์หรือคาร์บอเนตที่มี ความบริสุทธิ์สูง และทำการเผาแคลไซน์ในช่วงอุณหภูมิ 850 – 1300 องศาเซลเซียส เป็นเวลา 2 ชั่วโมง นำผงผลึกที่ได้ทำการอัดขึ้นรูปชิ้นงานที่มีเส้นผ่านศูนย์กลาง 15 มิลลิเมตร หนา 5 มิลลิเมตร หลังจากนั้นนำไปทำการอัคขึ้นรูปแบบทุกทิศทุกทาง (Isostatic press) ด้วยความคัน 250 MPa ทำ การเผาซินเตอร์ในช่วงอุณหภูมิ 1040 – 1350 องศาเซลเซียส เป็นเลา 2 ชั่วโมง จากการศึกษาพบว่า เมื่อปริมาณของ BT เพิ่มขึ้น อุณหภูมิที่ใช้ในการเผาแคลไซน์และซินเตอร์เพิ่มสูงขึ้นตามลำดับ จาก การศึกษาความหนาแน่นของเซรามิกที่เตรียมได้ พบว่า ความหนาแน่นของเซรามิกเพิ่มสูงขึ้น ตาม ปริมาณสัคส่วนของ BT ที่เพิ่มขึ้น จากการตรวจสอบรูปแบบการเกิดเฟส เพอรอฟสไกต์ และ โครงสร้างผลึกของเซรามิก BKT – BT ด้วยเทคนิคการเลี้ยวเบนของรังสีเอกซ์ (X-ray diffraction; XRD) พบว่า สามารถเตรียมเซรามิกในระบบ BKT – BT ที่มีโครงสร้าง ความบริสุทธิ์สูงได้ทุกส่วนองค์ประกอบของสาร โดยที่ x เท่ากับ 0.00 มีรูปแบบการเลี้ยวเบนของ รังสีเอกซ์คล้ายคลึงกับรูปแบบการเลี้ยวเบนรังสีเอกซ์มาตรฐาน (ICDD File no. 36-0339) ของ $\operatorname{Bi}_{0.5} \mathrm{K}_{0.5} \mathrm{O}_3$ ซึ่งมีโครงสร้างผลึกเป็นแบบเททระโกนอล และเมื่อทำการเจือ BT เข้าไปในเซรามิก BKT พบว่า ยังคงมีโครงสร้างผลึกเป็นแบบเททระโกนอลทุกสัคส่วนองค์ประกอบของสาร อย่างไร

ก็ตาม เมื่อพิจารณาความเป็นเททระโกนอล (Tetragonality) ของเซรามิก พบว่า ความเป็นเททระโกนอลของเซรามิกมีค่าเพิ่มขึ้น ตามปริมาณสัดส่วนของ BT ที่เพิ่มขึ้น ยิ่งไปกว่านั้นยังพบว่า แลท ทิสพารามิเตอร์มีขนาดใหญ่ขึ้นตามปริมาณของ BT ที่เพิ่มขึ้นด้วย จากการตรวจสอบการเปลี่ยนเฟส และสมบัติทางไดอิเล็กทริก พบว่า ที่ x เท่ากับ 0.00 พบอุณหภูมิคูรีย์ที่ 400 องสาเซลเซียส ซึ่งเป็น อุณหภูมิการเปลี่ยนเฟสจากเฟสเฟอร์โรอิเล็กทริกแบบเททระโกนอลไปเป็นแฟสพาราอิเล็กทริกที่มี โครงสร้างเป็นแบบคิวบิก และเมื่อทำการเจือ BT มากขึ้น พบว่า อุณหภูมิคูรีย์จะลดลงตามลำดับ นอกจากนี้ยังพบว่า ที่ x เท่ากับ 0.00 กราฟไดอิเล็กตริกมีลักษณะเป็นพีคฐานกว้าง (Broad peak) ซึ่ง เป็นลักษณะของการเปลี่ยนเฟสแบบต่อเนื่อง (Diffuse phase transition) และเมื่อปริมาณของ BT เพิ่มขึ้นลักษณะของพิคเริ่มแหลมขึ้น (Shape peak) ซึ่งเป็นลักษณะของการเปลี่ยนเฟสแบบฉับพลัน (First order phase transition)

10. <u>ผลการศึกษาเซรามิกในระบบ (1-x)PbZrO, - xBiFeO</u>,

ทำการศึกษาสารละลายของแข็ง ของเซรามิกเพียโซอิเล็กทริกไร้สารตะกั่วในระบบ (1x)PbZrO $_3-x$ BiFeO $_3$ (PZ - BF) เมื่อ $x=0.00\,0.02\,0.04\,0.06\,0.08\,0.10$ และ $0.20\,$ โดยได้ ทำการศึกษาโครงสร้างผลึก การเปลี่ยนเฟส และสมบัติใดอิเล็กทริกของสารระบบนี้ โดยได้ทำการ เตรียมผงผลึกที่มีความบริสุทธิ์สูงด้วยเทคนิคปฏิกิริยาสถานะของแข็ง โดยใช้สารตั้งต้นเป็น สารประกอบประเภทออกไซด์ที่มีความบริสุทธิ์สูง และทำการเผาแคลไซน์ที่อุณหภูมิ 850องศา เซลเซียส เป็นเวลา 2 ชั่วโมง นำผงผลึกที่ได้ทำการอัดขึ้นรูปชิ้นงานที่มีเส้นผ่านศูนย์กลาง 15 มิลลิเมตร ทำการเผาซินเตอร์ในช่วงอุณหภูมิ 1050 – 1250 องศาเซลเซียส เป็นเวลา 2 ชั่วโมง จาก การศึกษาพบว่า เมื่อปริมาณของ BiFeO, เพิ่มขึ้น อุณหภูมิที่ใช้ในการเผาซินเตอร์ลดลงตามลำดับ จากการตรวจสอบรูปแบบการเกิดเฟสเพอรอฟสไกต์ และโครงสร้างผลึกของเซรามิก PZ – BF ด้วย เทคนิคการเลี้ยวเบนของรังสีเอกซ์ (X-ray diffraction; XRD) พบว่า สามารถเตรียมเซรามิกใน ระบบ PZ – BF ที่มีโครงสร้างเพอรอฟสไกต์บริสุทธิ์ได้สูงสุดที่ 20 %โมล ของ BiFeO, ที่เจือเข้าไป (รอยืนยันผล XRD $x=0.3\,\,0.4\,$ และเม็ด ได้ 20 เม.ย.) โดยที่ x เท่ากับ $0.00\,\,$ มีรูปแบบการเลี้ยวเบน ของรังสีเอกซ์คล้ายคลึงกับรูปแบบการเลี้ยวเบนรังสีเอกซ์มาตรฐาน (ICDD File no. 75-1607) ของ PbZrO, ซึ่งมีโครงสร้างผลึกเป็นแบบออร์โธรอมบิก และเมื่อทำการเจือ BiFeO, เข้าไปในเซรามิก $PbZrO_{3}$ ที่ x เท่ากับ 0.02 พบว่า ยังคงมีโครงสร้างผลึกเป็นแบบออร์โธรอมบิกอยู่ อย่างไรก็ตาม เมื่อ ปริมาณของ PbZrO, เพิ่มมากขึ้นเป็น x=0.10 กลับไม่พบโครงสร้างผลึกแบบออร์โธรอมบิก และ โครงสร้างน่าจะเปลี่ยนเป็นโครงสร้างแบบรอมโบฮีดรอล (รอผล XRD เม็ด) นอกจากนี้ยังพบว่า แลททิสพารามิเตอร์มีขนาดเล็กลงตามปริมาณของ BiFeO, ที่เพิ่มขึ้นด้วย จากการตรวจสอบการ เปลี่ยนเฟสและสมบัติทางไดอิเล็กทริก พบว่า ที่ x=0.00 พบอุณหภูมิคูรีย์ที่ 230 องศาเซลเซียส ซึ่ง เป็นอุณหภูมิการเปลี่ยนเฟสจากเฟสเฟอร์โรอิเล็กทริกแบบออร์โธรอมบิกไปเป็นเฟสพาราอิเล็กทริก

ที่มีโครงสร้างเป็นแบบคิวบิก และเมื่อทำการเจือ BiFeO_3 เพิ่มขึ้น พบว่า อุณหภูมิคูรีย์จะลดลง ตามลำดับ เมื่อพิจารณาค่าใดอิเล็กทริกสูงสุด ($\mathbf{\mathcal{E}}_{\max}$) พบว่า ในช่วงแรก เมื่อปริมาณของ BiFeO_3 เพิ่มขึ้น ค่า $\mathbf{\mathcal{E}}_{\max}$ มีค่าเพิ่มขึ้นตามลำดับ อย่างไรก็ตามเมื่อ x=0.08 กลับพบว่าค่า $\mathbf{\mathcal{E}}_{\max}$ มีค่าลดลงและ ลดลงอย่างต่อเนื่องเมื่อปริมาณของเพิ่มขึ้น นอกจากนี้ยังพบว่า ที่ x เท่ากับ 0.00 กราฟไดอิเล็กทริกมี ลักษณะเป็นพีคแหลม (Shape peak) ซึ่งเป็นลักษณะของการเปลี่ยนเฟสแบบฉับพลัน (First order phase transition) และเมื่อปริมาณของ BiFeO_3 เพิ่มขึ้น พีคเริ่มมีลักษณะฐานกว้าง (Broad peak) มาก ขึ้นตามลำดับ ซึ่งเป็นลักษณะของการเปลี่ยนเฟสแบบต่อเนื่อง ($\operatorname{Diffuse}$ phase transition)

11. <u>ผงผลึกในระบบ KNbO</u>,

ศึกษาการเตรียมผงผลึกไร้สารตะกั่วโพแทสเซียมในโอเบต (KNbO₃) โดยวิธีปฏิกิริยา โดยการใช้โพแทสเซียมออกซาเลตโมโนไฮเดรตเป็นสารตั้งต้น สถานะของแข็งแบบคัดแปลง (แทนโพแทสเซียมการ์บอเนตที่ใช้ในวิธีดั้งเดิม) โดยทำการศึกษาพฤติกรรมทางความร้อนของสาร ์ ตั้งต้น โดยเทคนิคเทอร์ โมกราวิเมตริกอนา ไลซิส (Thermo gravimetric analysis; TGA) และเทคนิค ดิฟเฟอร์เรนเชียลเทอร์มอลอนาใลซิส (Differential thermal analysis; DTA). เพื่อหาอุณหภูมิที่ ผงผลึกที่เตรียมได้ภายหลังจากการเผาแคลไซน์ถูกนำไปตรวจสอบ เหมาะสมในการเผาแคลไซน์ การเกิดเฟสเพอรอฟสไกต์และความบริสุทธิ์โดยเทคนิคการเลี้ยวเบนของรังสีเอกซ์ diffraction technique; XRD) และตรวจสอบสัณฐานวิทยาโดยกล้องจุลทรรศน์อิเล็กตรอนแบบส่อง กราด (Scanning electron microscope; SEM) พบว่าสามารถสังเคราะห์ผงผลึกไร้สารตะกั่ว โพแทสเซียมในโอเบต (KNbO₂) ได้ภายหลังจากการเผาแคลใชน์ที่อุณหภูมิ 550 องศาเซลเซียส เป็นเวลา 20 นาที (หรือมากกว่า) โดยใช้อัตราการขึ้นลงของอุณหภูมิเท่ากับ 20 องศาเซลเซียสต่อ นาที โดยผงผลึกที่เตรียมได้มีรูปแบบการเลี้ยวเบนของรังสีเอกซ์สอดคล้องกับรูปแบบการเลี้ยวเบน ของรังสีเอกซ์โพแทสเซียมในโอเบตมาตรฐาน JCPDS no.32-0822 ซึ่งมีโครงสร้างผลึกแบบออโธ รอมบิก (Orthorhombic) ผลึกมีรูปร่างคล้ายคลึงกัน ไม่สังเกตพบลักษณะผลึกที่แตกต่างซึ่งแสดงถึง เฟสไพโรคลอร์หรือเฟสแปลกปลอมอื่นใด โดยขนาดผลึกเฉลี่ย (Mean crystalline size; D) เมื่อ คำนวณจากรูปแบบการเลี้ยวเบนของรังสีเอกซ์ พบว่ามีค่าเท่า 33.15±9.22 นาโนเมตร ซึ่งเป็นค่า น้อยกว่าขนาดอนุภาคเฉลี่ยที่สังเกตได้จากรูปจากกล้องจุลทรรศน์อิเล็กตรอนแบบส่องกราคที่มีค่า เท่ากับ 222.14±81.51 นาโนเมตร ทั้งนี้อาจเป็นผลจากการเกาะกลุ่มหรือการจับตัวกันของผงผลึก นอกจากนั้นยังพบว่าอุณหภูมิและเวลาในการเผาแคลไซน์ มีผลต่อการเติบโตของผลึก สังเกตได้จาก รูปแบบการเลี้ยวเบนของรังสีเอกซ์เกิดพีกที่สูงขึ้น ค่าแลตทิชพารามิเตอร์และขนาดผลึกเฉลี่ย (D) ที่ คำนวณได้มีค่าเพิ่มขึ้นเมื่ออุณหภูมิและเวลาในการเผาแคลไซน์เพิ่มขึ้น

12. ผงผลึกในระบบ NaNbO,

ทำการศึกษาการเตรียมผงผลึกไร้สารตะกั่วโซเดียมในโอเบต (NaNbO.) โดยวิธีการสังเคราะห์ แบบเผาใหม้ (Combustion technique) โดยใช้โซเดียมในเตรท (NaNO,) และในโอเบียมเพนตะออก ใชด์ (Nb,O,) เป็นสารตั้งต้น โดยมีใกลซีน (NH,CH,COOH) เป็นสารเชื้อเพลิง โดยทำการศึกษา อิทธิพลของอัตราส่วนโคยโมลระหว่างสารตั้งต้นต่อสารเชื้อเพลิง (Φ) ที่มีผลต่อการเกิดเฟสเพ อรอฟสไกต์ของโซเดียมในโอเบต และศึกษาอิทธิพลของอณหภมิที่ใช้ในการเผาแคลไซน์เมื่อ อัตราส่วนระหว่างสารตั้งต้นต่อสารเชื้อเพลิง (Φ) คงที่ จากนั้นตรวจสอบเอกลักษณ์ของผงผลึกที่ เตรียมได้โดยเทคนิคการเลี้ยวเบนของรังสีเอกซ์ (X-ray diffraction technique; XRD) และเครื่องฟ เรียทรานสฟอร์มอินฟราเรคสเปกโตมิเตอร์ (Fourier transform infrared spectrometer; FTIR) จากนั้นตรวจสอบสัณฐานวิทยาโดยกล้องจุลทรรศน์อิเล็กตรอนแบบส่องกราด (Scanning electron microscope: SEM) จากผลการทดลองส่วนแรกพบว่าที่อัตราส่วน $\Phi < 0.7$ จะไม่เกิดปฏิกิริยาการ เผาใหม้ และไม่เกิดเฟสเพอรอฟสไกต์ในผงผลึก เมื่ออัตราส่วน $\phi \geq 0.7$ จึงเกิดปฏิกิริยาการเผา ใหม้และตรวจพบเฟสเพอรอฟสไกต์ของโซเคียมในโอเบต ที่มีรูปแบบการเลี้ยวเบนของรังสีเอกซ์ สอคคล้องกับรปแบบการเลี้ยวเบนของรังสีเอกซ์มาตรฐาน JCPDS ตรวจสอบสัญฐานวิทยาพบว่า อนุภาคที่เตรียมได้มีลักษณะเป็นทรงลูกบาศก์สี่เหลี่ยมมุมฉาก โดย ขนาดอนภาคเฉลี่ยของผงผลึกที่เตรียมได้มีค่าระหว่าง 55 ถึง 600 นาโนเมตร ทั้งนี้เมื่ออัตราส่วน **O** ≥ 1.0 พบว่านอกจากพบเฟสเพอร์รอฟสไกต์แล้ว ยังตรวจพบเฟสแปลกปลอมของในโอเบียมเพ นตะออกไซค์ซึ่งเป็นสารตั้งต้นหลงเหลืออย่ ซึ่งเฟสคังกล่าวจะมีปริมาณมากขึ้นเมื่ออัตราส่วน **O** เพิ่มมากขึ้น จากผลการทดลองส่วนที่สอง เมื่อนำผงผลึกที่เตรียมได้จากวิธีการสังเคราะห์แบบเผา ใหม้โดยใช้ $\mathbf{\phi}=1.0$ ไปผ่านกระบวนการเผาแคลไซน์ที่อุณหภูมิต่างๆ เป็นเวลา 4 ชั่วโมง พบว่า รูปแบบการเลี้ยวเบนของรังสีเอกซ์แสดงถึงการลดลงของปริมาณเฟส เมื่ออณหภมิเพิ่มสงขึ้น และแสดงเฟสเพอรอฟสไกต์ของโซเดียมในโอเบต แปลกปลอมของในโอเบียมเพนตะออกใชด์ บริสุทธิ์ เมื่อผงผลึกผ่านการเผาแคล ไซน์ที่อุณหภูมิอย่างน้อย 400 องศาเซลเซียส เป็นต้นไป อย่างไร ก็ตาม พบว่าอุณหภูมิที่สูงขึ้นจะส่งผลต่อการเพิ่มขึ้นของความเป็นผลึกของผงผลึกด้วย สังเกตจาก การสูงขึ้นและการแยกออกของพีกที่เกิดในรูปแบบการเลี้ยวเบนของรังสีเอกซ์

Output จากโครงการวิจัยที่ได้รับทุนวิจัย

1. ผลงานตีพิมพ์ในวารสารวิชาการระดับนานาชาติจำนวนทั้งสิ้น 46 เรื่อง

- Naratip Vittayakorn, Nopsiri Chaiyo, Rangson Muanghlua, Anuchar Ruangphanit and Wanwilai C. Vittayakorn "Effect of annealing on the structure and dielectric properties in PZT-PCoN ceramics" *Advance Materials Research*; Vol. 55-57(2008) pp 49-52
- Manun Sutapun, Rangson Muanghlua, Chian-Chih Huang, David P. Cann, Wanwilai C. Vittayakorn and Naratip Vittayakorn "Influence of Fabrication Processing on Perovskite Phase Formation of KNN-BZT" Advance Materials Research; Vol. 55-57(2008) pp 113-116
- Supamas Wirunchit, Pitak Laoratanakul and **Naratip Vittayakorn** "Effect of Lead Nickel Niobate Substitution on Phase Transitions of Lead Zirconate Ceramics Prepared by the Solid State Reaction Method" *Advance Materials Research*; Vol. 55-57(2008) pp 117-120
- Wanwimon Banlue, Rangson Muanfhlua, Wanwilai C. Vittayakorn and **Naratip Vittayakorn** "Synthesis, crystal structures, phase transition characterization and thermal properties of the (*1*–*x*)PbZrO₃-*x*Pb(Co_{1/3}Nb_{2/3})O₃ solid solution system" *Advance Materials Research*; Vol. 55-57(2008) pp 121-124
- Rangson Muanfhlua, Wanwilai C. Vittayakorn and **Naratip Vittayakorn** "Effects of Zr/Ti ratio on the structure and ferroelectric properties in PZT-PZN-PMN ceramics near the morphotropic phase boundary" *Advance Materials Research*; Vol. 55-57(2008) pp 125-128
- Nopsiri Chaiyo, Rangson Muanghlua, Anuchar Ruangphanit and Wanwilai C. Vittayakorn and **Naratip Vittayakorn** "Synthesis, phase formation and characterization of Co₄Nb₂O₉ powders synthesized by solid-state reaction" *Advance Materials Research*; Vol. 55-57(2008) pp 873-876
- S. Nabunmee, **N Vittayakorn**, D. P. Cann and G. Rujijanagul "Ferroelectric and Mechanical Properties of PZT-PZN-PNN ceramics" *Advance Materials Research*; Vol. 55-57(2008) pp 217-220

- T. Bongkarn, N Phungjitt and **N. Vittayakorn** "Effect of Calcination Temperatures on Microstructure and Phase Formation of Ba(Zr_{0.25}Ti_{0.75})O₃ Powders" *Advance Materials Research*; Vol. 55-57(2008) pp 205-208
- Wanwimon Banlue, **Naratip Vittayakorn**, Chien-Chih Huang and David P. Cann "Dielectric properties of $Pb[(1-x)(Zr_{1/2}Ti_{1/2})-x(Zn_{1/3}Ta_{2/3})]O_3$ ceramics prepared by columbite and wolframite methods" *Journal of Materials Science*, Volume 43, Number 12 / June, 2008, page 4220-4225 Impact factor = 0.99
- Supamas Wirunchit, Pitak Laoratanakul and **Naratip Vittayakorn** "Physical properties and phase transitions in perovskite $Pb[Zr_{I-x}(Ni_{1/3}Nb_{2/3})_x]O_3$ (0.0 $\leq x \leq$ 0.5) ceramics" *Journal of Physics D: Applied physics* Volume 41 Number 12, page 125406-125413; 21 Jane 2008: Impact Factor = 2.077
- Supamas Wirunchit and **Naratip Vittayakorn** "Structural transformation in antiferroelectric PbZrO₃-relaxor ferroelectric Pb(Ni_{1/3}Nb_{2/3})O₃ solid solution system" *Journal of Applied Physics* (2008)104 (2), p.p 024103 Impact factor = 2.2
- Nopsiri Chaiyo and **Naratip Vittayakorn** "Effect of calcinations conditions on phase formation of microwave dielectric cobalt niobate (CoNb₂O₆) powders via a mixed oxide synthesis route" *Journal of Ceramic Processing Research*, Vol. 9 No. 4, 2008 page 381-384, Impact factor = 0.534
- Wanwimon Banlue and **Naratip Vittayakorn** "Ferroelectric phase stabilization, phase transformations and thermal properties in (1-x)PbZrO₃-xPb(Co_{1/3}Nb_{2/3})O₃ solid solution" *Applied Physics A: Materials Science and Processing* (2008) 93 (2), pp. 565-569, Impact factor = 2.2
- Anurak Prasatkhetragarn, **Naratip Vittayakorn**, Supon Ananta, Rattikorn Yimnurun and David P. Cann "Synthesis and Dielectric and Ferroelectric Properties of Ceramics in (1-x)Pb(Zr_{1/2}Ti_{1/2})O₃–(x)Pb(Co_{1/3}Nb_{2/3})O₃ System" *Japanese Journal of Applied Physics* Vol. 47, No. 2, 2008, pp. 998–1002, Impact factor = 1.13
- Chien-Chih Huang, **Naratip Vittayakorn**, Anurak Prasatkhetragarn, Brady J. Gibbons, and David P. Cann "Phase Transitions and Dielectric Properties in Bi(Zn_{1/2}Ti_{1/2})O₃-(Na_{1-y}Li_y)NbO₃ Perovskite Solid Solutions" *Japanese Journal of Applied Physics* 48 (2009) 031401, Impact factor = 1.13

- W. Qu, X. Tan, **N. Vittayakorn**, S. Wirunchit, and M. F. Besser "High temperature phases in the $0.98 \text{PbZrO}_3 0.02 \text{Pb}(\text{Ni}_{1/3} \text{Nb}_{2/3}) \text{O}_3$ ceramic" *Journal of Applied Physics* (2009) 105, p.p 014106 Impact factor = 2.2
- Manoon Sutapun, Chien-Chih Huang David P. Cann and **Naratip Vittayakorn** "Phase transitional behavior and dielectric properties of lead free (K_{0.5}Na_{0.5})NbO₃-Bi(Zn_{0.5}Ti_{0.5})O₃ ceramics" *Journal of Alloy and Compound*.; Vol. 479 Page 462-466 (2009); Impact Factor 2007:1.455
- Nopsiri Chaiyo, Anucha Ruangphanit, Rangson Muanghlua, Surasak Niemcharoen, Atchara Sangseub, Saowanee Taopen, Sunanta Leelapattana, Wanwilai C. Vittayakorn, Naratip Vittayakorn "Synthesis and Morphology Evolution of Lead-Free Piezoelectric K_{1/2}Na_{1/2}NbO₃ Powder at Low Temperature" *Ferroelectrics*, Volume 383, Issue 1 2009, pages 8 14; Impact Factor: 0.427
- Rangson Muanghlua; Surasak Niemcharoen; Wanwilai C. Vittayakorn; Nattapong Tungsitvisetkul; Pimjan Chinwaro; Anucha Ruangphanit; Nopsiri Chaiyo; **Naratip Vittayakorn** "Preparation and Properties of Lead Free Bismuth Sodium Titanate-Bismuth Zinc Titanate Ceramics" *Ferroelectrics*, Volume 383, Issue 1 2009, pages 1 7; Impact Factor: 0.427
- Theerachai Bongkarn; Nalinee Phungjitt; **Naratip Vittayakorn** "Effect of Firing Temperatures on Phase Formation and Microstructure of Ba(Zr_{0.3}Ti_{0.7})O₃ Ceramics Prepared via Mixed Oxide Method" *Ferroelectrics*, Volume 383, Issue 1 2009, pages 65 72; Impact Factor: 0.427
- Wanwilai C. Vittayakorn and **Naratip Vittayakorn** "Hysteresis Response of Lead Zirconate —Lead Nickel Niobate Ferroelectric Ceramic Under Compressive Stress" *Ferroelectrics*, Volume 382, Issue 1 2009, pages 1–6; Impact Factor: 0.427
- Naratip Vittayakorn; Wanwimon Banlue "Synthesis, Ferroelectric Phase Stabilization, Phase Transition and Thermal Properties in (1-x)PbZrO₃-xPb(Zn_{1/3}Nb_{2/3})O₃ Solid Solution" *Ferroelectrics*, Volume 382, Issue 1 2009, pages 110–114; Impact Factor: 0.427
- Manoon Sutapun; **Naratip Vittayakorn** "Phase Transition and Dielectric Properties of Lead Free (K_{0.5}Na_{0.5})NbO₃- Bi(Zn_{0.5}Ti_{0.5})O₃ Piezoelectric Ceramics" *Ferroelectrics*, Volume 382, Issue 1 2009, pages 115–121; Impact Factor: 0.427

- Wanwimon Banlue; **Naratip Vittayakorn** "Effect of Pb(Zn_{1/3}Nb_{2/3})O₃ Additions on Phase Structure, Ferroelectric and Dielectric Properties of PbZrO₃ Ceramics" Ferroelectrics, Volume 382, Issue 1 2009, pages 122–126; Impact Factor: 0.427
- Supamas Wirunchit; **Naratip Vittayakorn** "Crossover from Antiferroelectric to Normal Ferroelectric Behavior in Lead Zirconate-Lead Nickel Niobate Ceramics Prepared by the Reaction Sintering Process" *Ferroelectrics*, Volume 382, Issue 1 2009, pages 135–140; Impact Factor: 0.427
- Supamas Wirunchit; Rangson Muanghlua; Surasak Niemcharoen; Wanwilai C. Vittayakorn; Pitak Laoratanakul; Naratip Vittayakorn "Preparation of Lead Zirconate-Lead Nickel Niobate Ceramics by the Reaction Sintering Process" Ferroelectrics, Volume 380, Issue 1 2009, pages 14–19; Impact Factor: 0.427
- G. Rujijanagul; **N. Vittayakorn**; S. Nabunmee "Effect of Annealing Time on Electrical and Mechanical Properties of 0.7(Pb(Zr_{1/2}Ti_{1/2})O₃)-0.3(Pb(Zn_{1/2}Nb_{2/3})O₃ Ceramics" Ferroelectrics, Volume 384, Issue 1 2009, pages 68 – 72; Impact Factor: 0.427
- B. Boonchom, M. Thongkam, S. Kongtaweelert and **N. Vittayakorn** "A simple route to synthesis new binary cobalt iron cyclotetraphosphate CoFeP₄O₁₂ using aqueous and acetone media" *Journal of Alloys and Compounds*, Volume 486, Issues 1-2, 3 November 2009, Pages 689-692 Impact Factor 2007:1.455
- Nalinee Phungjitt, perapong panya, Theerachai Bongkarn and **Naratip Vittayakorn** "The Structure phase and microstrucutres of perovskite Ba(Ti_{1-x}Zr_x)O₃ ceramics using the combustion routre" *Journal Functional Materials Letters*; Vol. 2 Page 169-174 (2009)
- Nopsiri Chaiyo, Banjong Boonchom and **Naratip Vittayakorn** "Solid State reaction of Sodium Niobate (NaNbO₃) powder at low temperature." *Journal of Materials Science*, Volume 45, 2010, pages 1443-1447; Impact Factor: 0.99
- Banjong Boonchom and **Naratip Vittayakorn** "One-step thermal synthesis of binary manganese iron cyclotetraphate MnFeP₄O₁₂" *Journal of Materials Science*, Volume 45, 2010, pages 1443-1447; Impact Factor: 1.4
- Banjong Boonchom, Montree Thongkam, Samart Kongtaweelert and **Naratip Vittayakorn** "Flower-like micro-particles and novel super paramagnetic properties of new binary Co_{1/2}Fe_{1/2}(H₂PO₄)₂.2H₂O obtained by a rapid solid state route at ambient temperature" *Materials Research Bulletin*, Volume 44, 2009, pages 2206-2210; Impact Factor: 1.7

- Banjong Boonchom and **Naratip Vittayakorn** "Synthesis and ferromagnetic property of new binary copper iron pyrophosphate CuFeP₂O₇" *Materials letters*, Volume 64, 2010, pages 275-277; Impact Factor: 1.7
- Banjong Boonchom and **Naratip Vittayakorn** "Floral-like microarchitectures of cobalt iron cyclotetraphosphate obtained by solid state synthesis" *Powder Technology* Volume 198, 2010, page 25-28; Impact Factor: 1.8
- Naratip Vittayakorn, Piyanut Charoonsuk, Panisara Kasiansin, Supamas Wirunchit, and Banjong Boonchom "Dielectric properties and phase transition behaviors in (1-x)PbZrO₃–xPb(Mg_{1/2}W_{1/2})O₃ ceramics" *Journal of Applied physics* Volume 106 page 064104, 2009; Impact factor: 2.4
- Usa Sukkha, Rangson Muanghlua, Surasak Niemcharoen, Banjong Boonchom and Naratip Vittayakorn "Antiferroelectric–ferroelectric phase transition in lead zinc niobate modified lead zirconate ceramics: crystal studies, microstructure, thermal and electrical properties" *Applied Physics A: Materials Science & Processing*, 2010, Volume 100, Number 2, Pages 551-559; Impact Factor = 1.595
- Banjong Boonchom, Rattanai Baitahe, Zongporn Joungmunkong, **Naratip Vittayakorn** "Grass blade-like microparticle $MnPO_4$ · H_2O prepared by a simple precipitation at room temperature" *Powder Technology*, Volume 203, Issue 2, 10 November 2010, Pages 310-314; Impact Factor = 1.745
- Banjong Boonchom, Rattanai Baitahe, Samart Kongtaweelert and **Naratip Vittayakorn** "Kinetics and Thermodynamics of Zinc Phosphate Hydrate Synthesized by a Simple Route in Aqueous and Acetone Media" *Industrial & Engineering Chemistry Research*, 2010, 49 (8), pp 3571–3576 ;Impact Factor =1.758
- Banjong Boonchom and **Naratip Vittayakorn** "Dehydration Behavior of Synthetic Al_{0.5}Fe_{0.5}PO₄·2.5H₂O" *Journal of Chemical & Engineering Data*, 2010, 55 (9), pp 3307–3311 Impact Factor =1.695
- Piyanut Charoonsuk, Supamas Wirunchit, Rangson Muanghlua, Surasak Niemcharoen, Banjong Boonchom, **Naratip Vittayakorn** "The phase evolution with temperature in 0.94PbZrO₃-0.06Pb(Mg_{1/2}W_{1/2})O₃ antiferroelectric ceramic" *Journal of Alloys and Compounds*, Volume 506, Issue 1, 10 September 2010, Pages 313-316; Impact Factor = 2.135

- Banjong Boonchom and **Naratip Vittayakorn** "Soft synthesis route and characterization of superparamagnetic Mn_{1/2}Fe_{1/2}(H₂PO₄)₂· 2H₂O and its decomposed product" *Industrial* & *Engineering Chemistry Research* Volume 50, 2011, pp 2021–2030 ;Impact Factor = 1.758
- Banjong Boonchom, Chanaiporn Danvirutai and **Naratip Vittayakorn** "A simple synthesis and characterization of binary Co_{0.5}Fe_{0.5}(H₂PO₄)₂·2H₂O and its final decomposition product CoFeP₄O₁₂" *Journal of Solid State Chemistry*, Volume 13 (2011) 77-81, Impact factor = 2.34
- Naratip Vittayakorn and Banjong Boonchom "Effect of BiAlO₃ modification on the stability of antiferroelectric phase in PbZrO₃ ceramics prepared by conventional solid state reaction" *Journal of Alloys and Compounds*, Volume 509, 2011, Pages 2304 2310; Impact Factor = 2.135
- Nopsiri Chaiyo, Rangson Muanghlua, Surasak Niemcharoen, Banjong Boonchom and Naratip Vittayakorn "Solution combustion synthesis and characterization of lead-free piezoelectric sodium niobate (NaNbO₃) powders" *Journal of Alloys and Compounds*, Volume 509, 2011, Pages 2445 2449; Impact Factor = 2.135
- Nopsiri Chaiyo, Anucha Ruangphanit, Rangson Muanghlua, Surasak Niemcharoen, Banjong Boonchom and **Naratip Vittayakorn** "Synthesis of potassium niobate (KNbO₃) nano-powder by a modified solid-state reaction" *Journal of Materials Science*, Volume 46 (2011) 1585–1590, Impact Factor = 1.4
- Rangson Muanghlua, Surasak Niemcharoen, Manoon Sutapun, Banjong Boonchom and Naratip Vittayakorn "Phase transition behaviour and electrical properties of lead-free (K_{0.5}Na_{0.5}) NbO₃-LiNbO₃-LiSbO₃ piezoelectric ceramics" *Current Applied Physics*, Volume 11 (2011) 434-437, Impact factor = 1.52

2. การนำเสนอผลงานวิจัยในที่ประชุมวิชาการทั้งสิ้น 30 เรื่อง

 Naratip Vittayakorn, Nopsiri Chaiyo, Rangson Muanghlua, Anuchar Ruangphanit and Wanwilai C. Vittayakorn "Effect of annealing on the structure and dielectric properties in PZT-PCoN ceramics" Smart/intelligent materials and nanotechnology & 2nd International workshop on functional materials and nanomaterials 22-25 April 2008 Chiang Mai ,Thailand

- 2. Wanwimon Banlue and Naratip Vittayakorn "Characterization of the (1-x)PbZrO₃-xPb(Co_{1/3}Nb_{2/3})O₃ ceramics by XRD, SEM, thermal and dielectric properties tests" The Asian Meeting on Electroceramics 22-24 October 2008, Tsukuba, Japan
- 3. Nabunmee, S., **Vittayakorn, N.**, Cann, D.P., Rujijanagul, G. "Ferroelectric and mechanical properties of PZT-PZN-PNN ceramics" Smart/intelligent materials and nanotechnology & 2nd International workshop on functional materials and nanomaterials 22-25 April 2008 Chiang Mai ,Thailand
- 4. Sutapun, M., Muanghlua, R., Huang, C.-C., Cann, D.P., Vittayakorn, W.C., Vittayakorn, N. "Influence of fabrication processing on perovskite phase formation of KNN-BZT" Smart/intelligent materials and nanotechnology & 2nd International workshop on functional materials and nanomaterials 22-25 April 2008 Chiang Mai ,Thailand
- 5. Wirunchit, S., Laoratanakul, P., **Vittayakorn, N**. "Effect of lead nickel niobate substitution on phase transitions of lead zirconate ceramics prepared by the solid state reaction method" Smart/intelligent materials and nanotechnology & 2nd International workshop on functional materials and nanomaterials 22-25 April 2008 Chiang Mai ,Thailand
- 6. Chaiyo, N., Muanghlua, R., Ruangphanit, A., Vittayakorn, W.C., **Vittayakorn, N**. "Synthesis, phase formation and characterization of Co₄Nb₂O₉ powders synthesized by solid-state reaction" Smart/intelligent materials and nanotechnology & 2nd International workshop on functional materials and nanomaterials 22-25 April 2008 Chiang Mai ,Thailand
- 7. Muanghlua, R., Niemchareon, S., Vittayakorn, W.C., Vittayakorn, N. "Effects of Zr/Ti ratio on the structure and ferroelectric properties in PZT-PZN-PMN ceramics near the morphotropic phase boundary" Smart/intelligent materials and nanotechnology & 2nd International workshop on functional materials and nanomaterials 22-25 April 2008 Chiang Mai ,Thailand
- 8. Bongkarn, T., Phungjitt, N., **Vittayakorn, N.** "Effect of calcination temperatures on microstructure and phase formation of Ba(Zr_{0.25}Ti_{0.75})O₃ powders" Smart/intelligent materials and nanotechnology & 2nd International workshop on functional materials and nanomaterials 22-25 April 2008 Chiang Mai, Thailand

- 9. Banlue, W., Muanghlua, R., Vittayakorn, W.C., **Vittayakorn N.** "Synthesis, crystal structures, phase transition characterization and thermal properties of the (1-x)PbZrO₃-xPb(Co_{1/3}Nb_{2/3})O₃ solid solution system" Smart/intelligent materials and nanotechnology & 2nd International workshop on functional materials and nanomaterials 22-25 April 2008 Chiang Mai ,Thailand
- 10. Nopsiri Chaiyo Anuchar Ruangphanit and **Naratip Vittayakorn** "Synthesis and Morphology evolution of lead-free piezoelectric KNbO₃ powder using a modified solid state reaction" The Twenty-sixth annual conference of the microscopy society of Thailand 28th January 2009 30th January 2009
- 11. C. Chansi, N. Adam, S. Vuttivong N. Chaiyo and N. Vittayakorn "Hydrothermal synthesis and characterization of lead-free piezoelectric $KNbO_3$ powders" The Twenty-sixth annual conference of the microscopy society of Thailand 28^{th} January $2009 30^{th}$ January 2009
- N. Chaiyo, A. Ruangphanit and N. Vittayakorn "Effect of calcinations condition on lead-free piezoelectric NaNbO₃ powder through a modified solid state reaction synthesis" The Twenty-sixth annual conference of the microscopy society of Thailand 28th January 2009 30th January 2009
- Nopsiri Chaiyo, Anucha Ruangphanit, Rangson Muanghlua, Surasak Niemcharoen, Atchara Sangseub, Saowanee Taopen, Sunanta Leelapattana, Wanwilai C. Vittayakorn, Naratip Vittayakorn "Synthesis and Morphology Evolution of Lead-Free Piezoelectric K_{1/2}Na_{1/2}NbO₃ Powder at Low Temperature" The Sixth Asian Meeting on Ferroelectric (AMF-6), 2 7 Aug. 2008. National Taipei University of Technology, Taipei, Taiwan.
- Rangson Muanghlua; Surasak Niemcharoen; Wanwilai C. Vittayakorn; Nattapong Tungsitvisetkul; Pimjan Chinwaro; Anucha Ruangphanit; Nopsiri Chaiyo; Naratip Vittayakorn "Preparation and Properties of Lead Free Bismuth Sodium Titanate-Bismuth Zinc Titanate Ceramics" The Sixth Asian Meeting on Ferroelectric (AMF-6), 2

 7 Aug. 2008. National Taipei University of Technology, Taipei, Taiwan.
- 15. Theerachai Bongkarn; Nalinee Phungjitt; Naratip Vittayakorn "Effect of Firing Temperatures on Phase Formation and Microstructure of Ba(Zr_{0.3}Ti_{0.7})O₃ Ceramics Prepared via Mixed Oxide Method" The Sixth Asian Meeting on Ferroelectric (AMF-6), 2 7 Aug. 2008. National Taipei University of Technology, Taipei, Taiwan.

- 16. Wanwilai C. Vittayakorn and Naratip Vittayakorn "Hysteresis Response of Lead Zirconate —Lead Nickel Niobate Ferroelectric Ceramic Under Compressive Stress" The Sixth Asian Meeting on Ferroelectric (AMF-6), 2 7 Aug. 2008. National Taipei University of Technology, Taipei, Taiwan.
- 17. **Naratip Vittayakorn**; Wanwimon Banlue "Synthesis, Ferroelectric Phase Stabilization, Phase Transition and Thermal Properties in (1-x)PbZrO₃-xPb(Zn_{1/3}Nb_{2/3})O₃ Solid Solution" The Sixth Asian Meeting on Ferroelectric (AMF-6), 2 7 Aug. 2008. National Taipei University of Technology, Taipei, Taiwan.
- 18. Manoon Sutapun; Naratip Vittayakorn "Phase Transition and Dielectric Properties of Lead Free (K_{0.5}Na_{0.5})NbO₃- Bi(Zn_{0.5}Ti_{0.5})O₃ Piezoelectric Ceramics" The Sixth Asian Meeting on Ferroelectric (AMF-6), 2 – 7 Aug. 2008. National Taipei University of Technology, Taipei, Taiwan.
- 19. Wanwimon Banlue; Naratip Vittayakorn "Effect of Pb(Zn_{1/3}Nb_{2/3})O₃ Additions on Phase Structure, Ferroelectric and Dielectric Properties of PbZrO₃ Ceramics" The Sixth Asian Meeting on Ferroelectric (AMF-6), 2 7 Aug. 2008. National Taipei University of Technology, Taipei, Taiwan.
- 20. Supamas Wirunchit; Naratip Vittayakorn "Crossover from Antiferroelectric to Normal Ferroelectric Behavior in Lead Zirconate—Lead Nickel Niobate Ceramics Prepared by the Reaction Sintering Process" The Sixth Asian Meeting on Ferroelectric (AMF-6), 2 7 Aug. 2008. National Taipei University of Technology, Taipei, Taiwan.
- 21. Supamas Wirunchit; Rangson Muanghlua; Surasak Niemcharoen; Wanwilai C. Vittayakorn; Pitak Laoratanakul; Naratip Vittayakorn "Preparation of Lead Zirconate-Lead Nickel Niobate Ceramics by the Reaction Sintering Process" The Sixth Asian Meeting on Ferroelectric (AMF-6), 2 7 Aug. 2008. National Taipei University of Technology, Taipei, Taiwan.
- 22. G. Rujijanagul; N. Vittayakorn; S. Nabunmee "Effect of Annealing Time on Electrical and Mechanical Properties of 0.7(Pb(Zr_{1/2}Ti_{1/2})O₃) 0.3(Pb(Zn_{1/2}Nb_{2/3})O₃ Ceramics" The Sixth Asian Meeting on Ferroelectric (AMF-6), 2 7 Aug. 2008. National Taipei University of Technology, Taipei, Taiwan.
- 23. Nopsiri Chaiyo, Banjong Boonchom and **Naratip Vittayakorn** "A modified solid-state reaction synthesis and characterization of sodium niobate (NaNbO₃) powders " The 3rd

- International Symposium on Functional Materials (ISFM2009) 15-18 June 2009, Jinju, KOREA
- 24. Usa Sukkha, Wanwimon Banlue, Banjong Boonchoma and Naratip Vittayakorn "Antiferroelectric-ferroelectric phase transition in lead zinc niobate modified lead zirconate ceramics: Crystal studies, Raman spectroscopy, Thermal expansion and electrical properties" The 3rd International Symposium on Functional Materials (ISFM2009) 15-18 June 2009, Jinju, KOREA
- 25. Manoon Sutapun, Rangson Muanghlua, Surasak Niemcharoen, Banjong Boonchom and Naratip Vittayakorn "Phase transition and dielectric properties of lead free $(K_{0.5}Na_{0.5})NbO_3$ LiNbO₃ LiSbO₃ piezoelectric ceramics" The 3rd International Symposium on Functional Materials (ISFM2009) 15-18 June 2009, Jinju, KOREA
- 26. Prapapim Phetnoi, Surasak Niemcharoen, Rangson Muanglua, Manoon Sutapun and Naratip Vittayakorn "Preparation of Bismuth Potassium Titanate Strontium Titanate Ceramics" The 27th Annual Conference of the Microscopy Society of Thailand, 20-22 Jan. 2010. Koh Samui, Surat Thani, Thailand.
- 27. Usa Sukkha and Naratip Vittayakorn "Influence of Pb(In_{1/2}Nb_{1/2})O₃ on the Phase transformations, Dielectric and Thermal properties of PbZrO₃ ceramic" The 27th Annual Conference of The Microscopy Society of Thailand (MST27), 20 22 Jan. 2010. The Fair House Beach Resort & Hotel, Surat Thani, Thailand.
- 28. Nopsiri Chaiyo, Anucha Ruangphanit, Naratip Vittaykorn "Solution Combustion Synthesis of Lead-free Piezoelectric Sodium Niobate (NaNbO3) Powders" The 27th Annual Conference of The Microscopy Society of Thailand (MST27), 20 22 Jan. 2010. The Fair House Beach Resort & Hotel, Surat Thani, Thailand.
- 29. Piyanut Charoonsuk, Panisara Kasiansin, Supamas Wirunchit, Banjong Boonchom and Naratip Vittayakorn "Ferroelectric phase transition and microstructure of the (1-x)PbZrO₃-xPb(Mg_{1/2}W_{1/2})O₃ system" The 27th Annual Conference of The Microscopy Society of Thailand, 20-22 Jan. 2010. Koh Samui, Surat Thani, Thailand.
- 30. C. Nawanil and **N. Vittayakorn**, "Synthesis of Blended Lead Zirconate (PbZrO₃) / Poly(Ethylene Oxide) Nanofibers via Electrospinning" The 27th Annual Conference of The Microscopy Society of Thailand, 20-22 Jan. 2010. Koh Samui, Surat Thani, Thailand.

Reprint

Effect of Annealing on the Structure and Dielectric Properties in PZT-PCoN Ceramics

N. Vittayakorn^{1,5,a}, N. Chaiyo¹, R. Muanghlua², A. Ruangphanit³ and W. C. Vittayakorn⁴

^a e-mail: naratipcmu@yahoo.com

Keyword: Ferroelectric Materials, Lead Zirconate Titanate, Lead Cobolt Niobate

Abstract The solid solution between the normal ferroelectric $Pb(Zr_{1/2}Ti_{1/2})O_3$ (PZT) and relaxor ferroelectric $Pb(Co_{1/3}Nb_{2/3})O_3$ (PCoN) was synthesized by the solid state reaction method. Sintered PZT-PCoN ceramics were annealed at temperatures ranging from 850 to 1,100°C for 4 h. X-ray diffraction patterns revealed changes of crystalline structure after annealing, which could be correlated to the accompanied changes in dielectric properties. Furthermore, significant improvements in the dielectric responses were observed in this system. After annealing, a huge increase of up to 200% occurred in the dielectric constants, especially near the temperature of maximum dielectric constant.

Introduction

Piezoelectric lead zirconate titanate (PZT) ceramic material has been widely used for transducer applications, due to its excellent piezoelectric properties, and was a candidate in a number of recent investigations [1, 2]. It is well known that PZT material is almost always used with a dopent, modifier or other chemical constituents to improve and optimize its basic properties for a particular application [1, 3]. Lead zirconate titanate ceramics and their solid solution, along with several complex perovskite oxides represented by Pb(B'B")O₃, have been investigated [4-6]. Among the various complex ferroelectric oxide materials, several niobates with transition temperatures below room temperature are $Pb(Mg_{1/3}Nb_{2/3})O_3$, $Pb(Ni_{1/3}Nb_{2/3})O_3$, and $Pb(Co_{1/3}Nb_{2/3})O_3$. Among them, lead cobalt niobate [Pb(Co_{1/3}Nb_{2/3})O₃ (PCoN)] is also a typical ferroelectric relaxor material with a transition temperature of -70°C, as reported by Smolenskii et al. [7] in 1958. In this compound, the octahedral sites of the crystal are occupied randomly by Co²⁺ and Nb⁵⁺ ions. Recently, our previous work has shown promise in producing phase pure perovskite PZT-PCoN ceramics with the solid state reaction method [5, 8]. A morphotropic phase boundary (MPB) between the PCoN-rich pseudo-cubic phase and the PZT-rich tetragonal phase reported $0.7Pb(Zr_{1/2}Ti_{1/2})O_3:0.3Pb(Co_{1/3}Nb_{2/3})O_3[5].$

In this study, we emphasized the effect of annealing on the crystal structure, and dielectric properties in PZT–PCoN ceramics. Based on our previous results for the PZT–PCoN system, PZT containing 30 mol% of PCoN was selected as the starting composition, which is close to the rhombohedral MPB in this system. For annealing, the samples were heat treated at 850-1,100°C for



¹ King Mongkut's Institute of Technology Ladkrabang Nanotechnology Research Center(NRC), King Mongkut's Institute of Technology Ladkrabang, Bangkok, Thailand 10520

²Electronics Research Center, Faculty of Engineering, King Mongkut's Institute of Technology Ladkrabang, Bangkok Thailand 10520

³ Department of Physics, Faculty of Science, Chiang Mai University, Chiang Mai, Thailand 50200

⁴ Thai Microelectronics Center (TMEC), National Electronics and Computer Technology Center, Nation Science and Technology Development Agency, Ministry of Science and Technology, Chachoengsao 24000, Thailand

Materials Science Research Unit, Department of Chemistry, Faculty of Science, King Mongkut's Institute of Technology Ladkrabang, Bangkok, Thailand 10520

4 hours in a sealed Al₂O₃ crucible, with PbO-rich atmosphere. This paper reports evolution of the perovskite phase, and crystal structure of the PZT–PCoN ceramics. Next, the temperature and frequency dependence of the dielectric constant are given for as-sintered and annealed samples. The results of influence on the post-sintering annealing of these properties are shown in brief.

Experiment

The 0.7Pb(Zr_{1/2}Ti_{1/2})O₃-0.3Pb(Co_{1/3}Nb_{2/3})O₃ ceramics were prepared by conventionally mixed-oxide processing, in which stoichiometric mixtures of reagent-grade metal oxide powders of 99% + purity (PbO, CoO, TiO₂, ZrO₂ and Nb₂O₅) were used as the starting raw materials. Thermal synthesis of blended and pressed mixture of the starting material was carried out at 900°C for a period of 4 h. Crumbled, milled and sieved material was pressed again in the form of cylinders and then sintered at 1,100°C for 4 h. The sintered pellets were then annealed at various temperatures from 850 to 1,100°C for 4 h. These annealing processes were performed in a double crucible, with interior PbO + ZrO₂ atmosphere, in order to maintain the established composition and, especially, avoid the loss of PbO caused by its sublimation. The Archimedes displacement method with distilled water was employed to evaluate sample density. The ceramic pellets were ground and polished to make parallel surfaces, and densities were determined geometrically. After gold sputtering onto the major faces of the pellets as electrodes, dielectric constants and losses at the frequency decades of 10 kHz were measured, using a computer-interfaced LCR meter.

Results and Discussions

The phase development in the annealed samples was analyzed by XRD and the results are presented in Figure 1. All samples show a single-phase powder diffraction pattern. No secondary reaction phases such as PbO, Pb-based compounds, unreacted oxide and so on, are observed in the pattern.

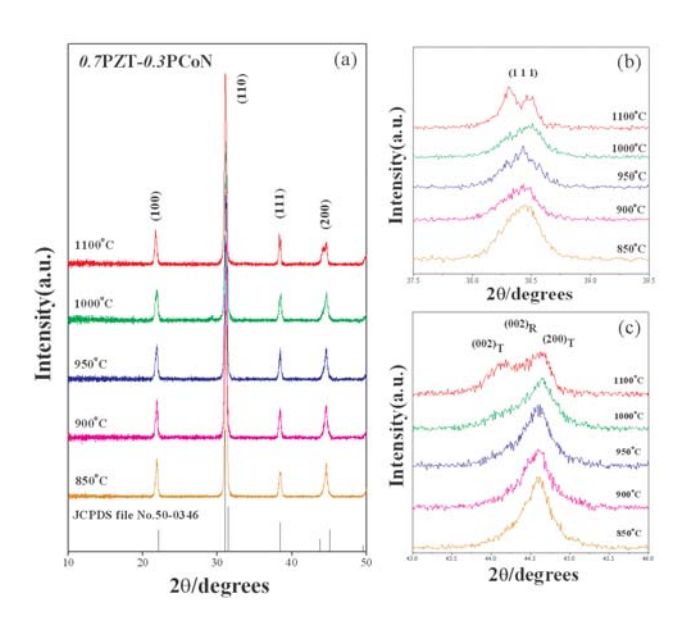


Figure 1 (a) XRD patterns of 0.7PZT-0.3PZN annealed samples at various temperatures for 4 h, (b) XRD pattern of the (1 1 1) peak, (c) XRD pattern of the (2 0 0) peak.

After annealing, a significant change in the crystal structure was observed, especially above an annealing temperature of $1,000^{\circ}$ C, where the crystal structure changes from pseudo-cubic to tetragonal and rhombohedral. On the basis of XRD and dielectric experiments, we have identified the MPB in the (1-x)PZT-xPCoN system from our previous work. The MPB resides at around $x \sim 0.2$, separating the tetragonal phase for $x \leq 0.2$ from the rhombohedral phase for $x \geq 0.3$. In this study, the XRD data show that splitting of the (200) and (111) peak is not observed in ceramic



samples annealed at temperatures below 1,000°C. These results indicated that the major phase in this ceramic sample had pseudo-cubic symmetry. Splitting of the (200) peak becomes more pronounced as the annealing temperature approaches 1,100°C, thus indicating stabilization of the tetragonal phase. Furthermore, the unambiguous splitting of the (111) peak indicated the coexistence of the rhombohedral and tetragonal phase. The co-existence of the tetragonal and rhombohedral phase is seen clearly when the XRD profile peak splits with increasing annealing temperature. From these results, it is clear that the composition of the annealed sample has shifted very closely to the MPB.

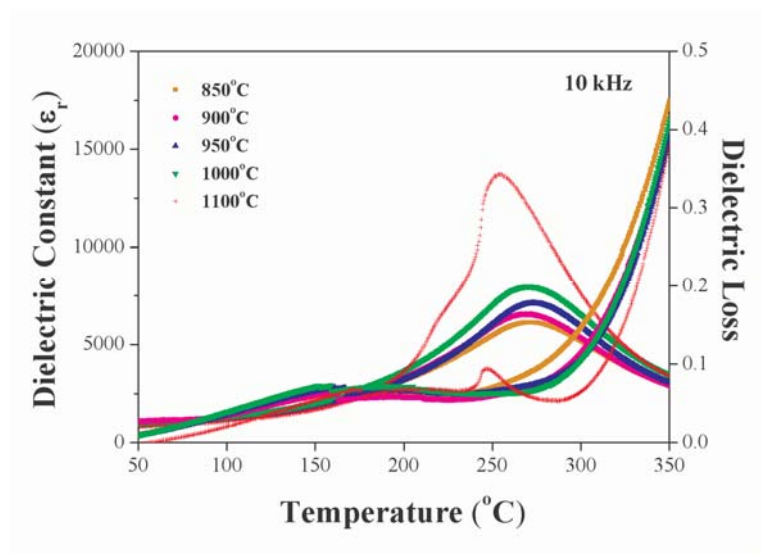
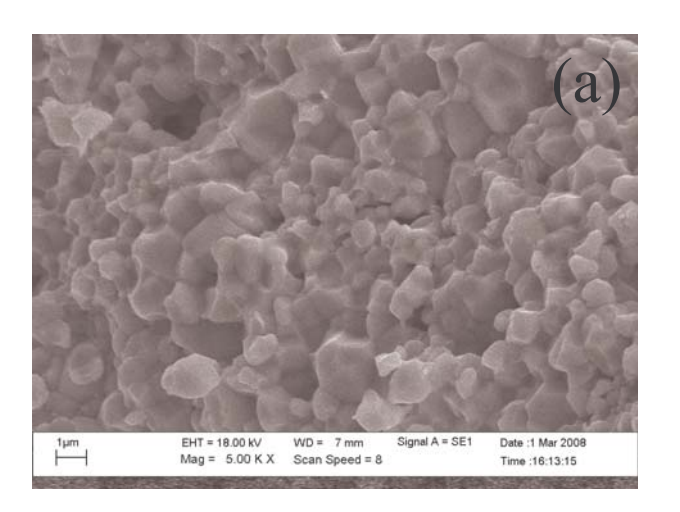


Figure 2 Variation of the dielectric constant (ε_r) and loss tangent $(\tan \delta)$ with different annealing temperatures at 10 kHz.



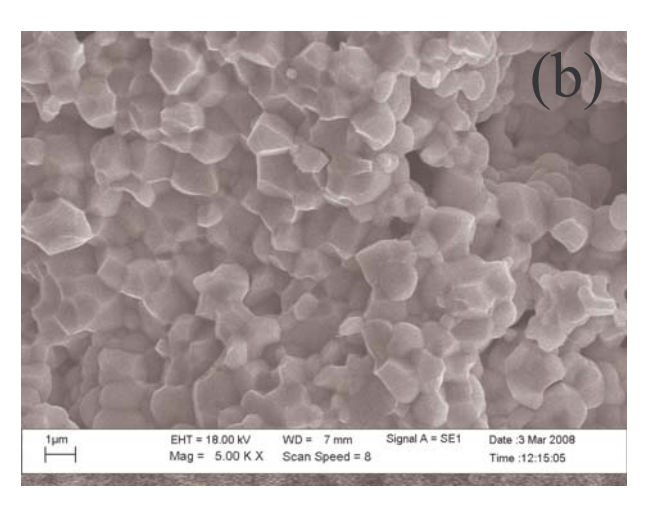


Figure 3 SEM photographs of 0.7PZT-0.3PCoN ceramics (a) as-sintered samples (b) annealing at 1,100°C.

Figure 2 shows the dielectric constant (ε_r) at 10 kHz versus the temperature for 0.7PZT-0.3PCoN ceramics annealed at different temperatures for 4 h. After annealing, a significant improvement in the dielectric constant was observed, especially near the temperature of the maximum dielectric constant (ε_m), where the improvement was up to 200%. This change in behavior might be due to a shift in a chemical composition close to the MPB, caused by thermal annealing. This behavior is consistent with the conclusions of Randall *et al.* [9]and Leite *et al.* [10] in the PMN–PT system. Figure 3 shows scanning electron microscopy (SEM) images of the fractured surfaces of 0.7PZT-



0.3PCoN ceramics before and after annealing at 1,100°C. There was no change in the grain size. The density of the samples decreased from 8.120 to 8.015 g/cm³ after annealing at 1,100°C for 4 h. Obviously, the decrease in density did not lead to an improvement of electrical responses.

Summary

The dielectric properties of 0.7PZT–0.3PCoN ceramics, formed via the solid state reaction, were investigated. Thermal annealing was seen to be effective at improving the dielectric and piezoelectric responses of PZT-based ferroelectric ceramics. The annealing time was found to have an effect on the electrical properties. After annealing at 1,100°C for 4h in a PbO-rich atmosphere, 0.7PZT-0.3PCoN ceramics with $\varepsilon_{\rm m}$ 14,400 were achieved in this study. The large improvements in dielectric properties after annealing were attributed to a shift in the phase composition to the MPB composition.

Acknowledgements

This work was supported by the Thailand Research Fund (TRF), the Commission on Higher Education (CHE), Thailand Graduate Institute of Science and Technology (TGIST), National Research Council of Thailand (NRCT) and King Mongkut's Institute of Technology Ladkrabang (KMITL).

References

- [1] G. H. Haertling: J. Am. Ceram. Soc. Vol. 82 (1999), p. 797.
- [2] K. Uchino: Ferroelectric Devices (Marcel Dekker, Inc., New York, 2000)
- [3] K. Uchino: Solid State Ionics Vol. 108 (1998), p. 43.
- [4] N. Vittayakorn, G. Rujijanagul, X. Tan, M. A. Marquardt and D. P. Cann: J. Appl. Phys. Vol. 96 (2004), p. 5103.
- [5] N. Vittayakorn and T. Tunkasiri: Phys. Scr. Vol. T129 (2007), p. 199.
- [6] N. Vittayakorn, G. Rujijanagul, X. Tan, H. He, M. A. Marquardt and D. P. Cann, J. Electroceramic Vol. 16 (2006), p. 141.
- [7] G. A. Smolenskii and A. L. Agranovskaya: Sov. Phys.-Tech. Phys. (1958), p. 1380.
- [8] N. Vittayakorn, S. Wirunchit, S. Traisak, R. Yimnirun and G. Rujijanagul: Curr. Appl Phys. Vol. 8 (2008), p. 128.
- [9] C. A. Randall, A. D. Hilton, D. J. Barber and T. R. Shrout: J. Mater. Res. Vol. 8 (1993), p. 880
- [10] E. R. Leite, A. M. Scotch, A. Khan, T. Li, H. M. Chan, M. P. Harmer, S.-F. Liu and S.-E. Park: J. Am. Ceram. Soc. Vol. 85 (2002), p. 3018.



Influence of Fabrication Processing on Perovskite Phase Formation of KNN-BZT

M. Sutapun¹, R. Muanghlua², C-C Huang³, D. P. Cann³, W. C. Vittayakorn⁴ and N. Vittayakorn^{1,a}

Keywords: Lead-free piezoelectric ceramics; Dielectric properties; perovskites; $(K_{0.5}Na_{0.5})NbO_3$; $Bi(Zn_{0.5}Ti_{0.5})O_3$

Abstract The binary system of $(1-x)(K_{1/2}Na_{1/2})NbO_3$ – $xBi(Zn_{1/2}Ti_{1/2})O_3$; x = 0.0-0.30 ceramics was fabricated by conventionally mixed oxide and two-stage mixed oxide methods. Phase development of calcined powders and the crystal structure of sintered ceramics were analyzed by X-ray diffraction (XRD). The microstructure analyses were undertaken by scanning electron microscopy (SEM). In the conventional method, the perovskite phases were obtained for compositions containing only 10 mol % KNN. For compositions above this amount, a complex mixture of phases was observed. However, the complete solid solution of perovskite phase, prepared by two–stage mixed oxide, was retained up to 20 mole % BZT content. The experiments in this study suggest that the two-stage mixed oxide method helps to stabilize the perovskite phase better, when compared with the conventional method.

Introduction

Piezoelectric materials based on Pb($Zr_{1-x}Ti_x$)O₃ (PZT) ceramics have been widely used, due to their excellent piezoelectric and dielectric properties at the morphotropic phase boundary(MPB) [1]. However, the use of lead-based ceramics has caused serious environmental problems because of the high toxicity of lead oxide [2]. Alkali niobate $K_{0.5}Na_{0.5}NbO_3$ (KNN), a solid solution of ferroelectric KNbO₃ and antiferroelectric NaNbO₃, is thought to be a promising candidate for lead-free piezoelectric ceramics because of its high Curie temperature (420 °C) and large electromechanical coupling factors [2]. Bi($Zn_{1/2}Ti_{1/2}$)O₃ (BZT) is a ferroelectric, which has a Zn^{2+} and Ti^{4+} complex on the B-site of ABO₃ perovskite structure, with a tetragonal symmetry [4, 5]. The BZT exhibits a high T_c and tetragonality enhanced through solid solution with PbTiO₃[4]. However, BZT is unstable in pure form and can only be stabilized under high pressures or in solid solutions with other perovskite end members [3, 4]. In order to develop lead-free piezoelectric materials, KNN was used for this research to stabilize the BZT perovskite phases in a solid solution. Both the conventionally mixed oxide and two-stage mixed oxide methods have been used in synthesizing the KNN-BZT ceramic. Finally, a comparison of the important dielectric properties was made to identify the optimum processing conditions.

Experimental

The $(1-x)(K_{1/2}Na_{1/2})NbO_3-xBi(Zn_{1/2}Ti_{1/2})O_3$; x = 0.0-0.30 lead-free ceramics were prepared by the conventionally mixed oxide and two-stage mixed oxide methods. Both methods used high purity



¹ Materials Science Research Unit, Department of Chemistry, Faculty of Science, King Mongkut's Institute of Technology Ladkrabang, Bangkok, Thailand 10520

²Electronics Research Center, Faculty of Engineering, King Mongkut's Institute of Technology Ladkrabang, Bangkok Thailand 10520

³Materials Science, School of Mechanical, Industrial, and Manufacturing Engineering, Oregon State University Corvallis, Oregon, 97331, USA

⁴ Department of Physics, Faculty of Science, Chiang Mai University, Chiang Mai, Thailand 50200 a e-mail: naratipcmu@yahoo.com

AR grade K₂CO₃ (99.0%), Na₂CO₃ (99.5%), Bi₂O₃ (99.5%), Nb₂O₅ (99.9%), ZnO (99.0%) and TiO₂ (99.0%). Alkali carbonates were used as a starting material, which had been treated carefully by a special drying process before use. These powders were placed in an oven at 230°C for 2 days and then stored in a moisture-free vessel. For the conventionally mixed oxide method, KNN-BZT ceramics were prepared by mixing starting reagent powders in the desieved stoichiometry and ball-milling in polyethylene, with ethanol and stabilized zirconia (YTZ) media, for 18 h After drying, the mixture was calcined at 850°C for 4 h. For the two-stage mixed oxide method, (K_{0.5}Na_{0.5})NbO₃ (KNN) powders were prepared first, followed by a reaction with Bi₂O₃, Nb₂O₅ and TiO₂ to form the KNN-BZT solid solution. Uncalcined powders were weighed according to the following chemical reaction equation and characterized by TG-DTA (Perkin Elmer). The microstructure analyses were undertaken by scanning electron microscopy (SEM, Leo 1455VP). The calcined powders, with polyvinyl alcohol (PVA) added as binder, were pressed into pellets of 15 mm diameter and ~ 2 mm thickness, and sintered at 1,000°C in KNN-atmosphere for 2 h in a closed alumina crucible. For dielectric measurement, sample surfaces were polished and painted with silver paste. Dielectric properties were measured using an LCR meter (HP-4284, Hewlett–Packard Inc.).

Results and Discussion

TG-DTA curves are given in Figure 1(a) and (b) for the conventional method (K₂CO₃, Na₂CO₃, Bi₂O₃, Nb₂O₅, ZnO and TiO₂) and two-stage method (KNN, Bi₂O₃, ZnO and TiO₂), respectively. The TGA curve, showing overall weight loss, was equal to 32.5% for the conventional method and ~24.5% for the two-stage method. The DTA curve showed an endothermic peak positioned at around 114-197°C and 115-179°C for the conventional method and two-stage method, respectively, which associated with the decomposition of water molecules. Furthermore, the TGA curve showed a 4.37 % and 3.51% weight loss at between 400°C and 600°C for the conventional method, which associated with the decarbonation of K₂CO₃ and Na₂CO₃, respectively. However weight loss was not observed at all in the same temperature for the two-stage method. The endothermic peaks, appearing at 850°C for both methods, should be correlated to the phase transition of perovskite structure because there was no weight loss on the TGA curves. These data were used to define the calcined temperature of the perovskite phase.

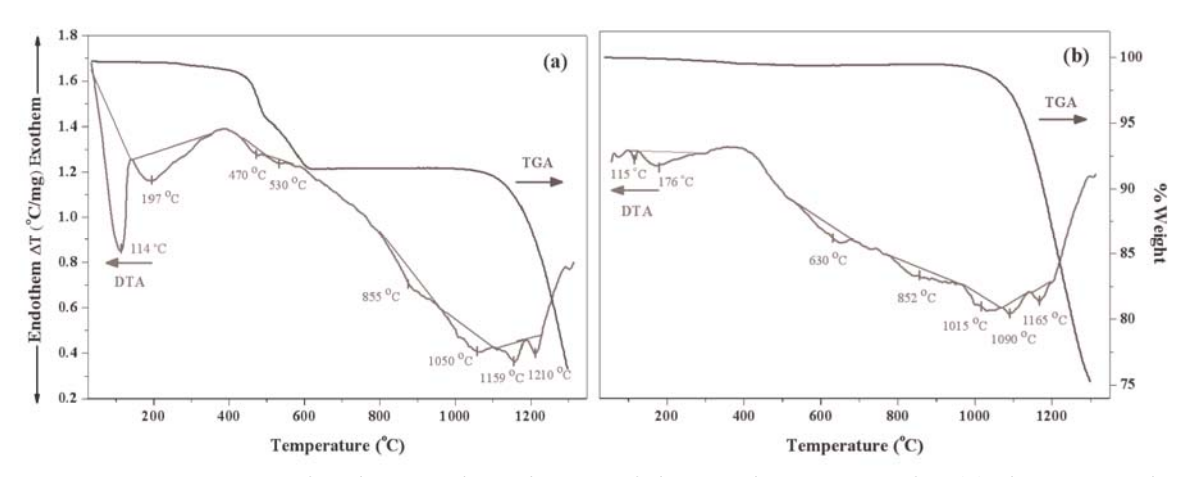


Figure 1 TG-DTA curves for the powder mixture of the starting reagent for (a) the conventionally mixed oxide method and (b) the two–stage mixed oxide method.

XRD patterns of the sintered (1-x) KNN – xBZT ceramics for both methods are shown in Figure 2(a) and (b). In the conventional method, the perovskite phases were obtained for compositions containing only 10 mol % KNN. For compositions above this amount, a complex mixture of phases was observed. However the complete solid solution of perovskite phase prepared by two stages was retained up to 20 mole% BZT content. The experiments in this study suggest that the two-stage method helps to stabilize the perovskite phase better, when compared to the conventional method.



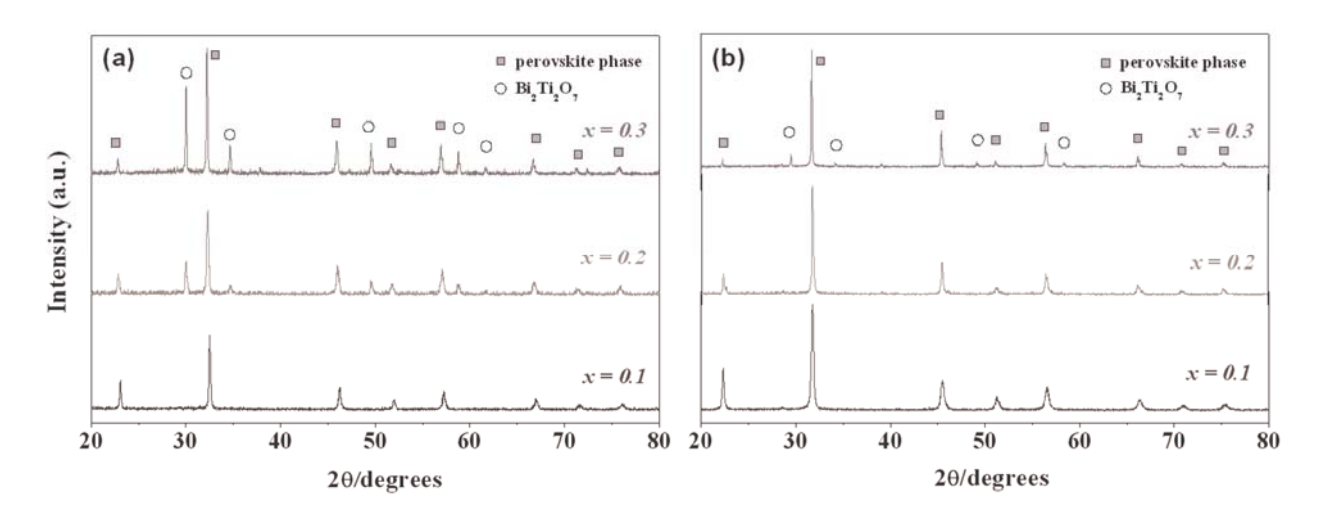


Figure 2 XRD patterns of the (1-x)KNN – xBZT powders calcined at 850 $^{\circ}$ C for 4 h, obtained by (a) the conventional mixed oxide method and (b) the two-stage mixed oxide method.

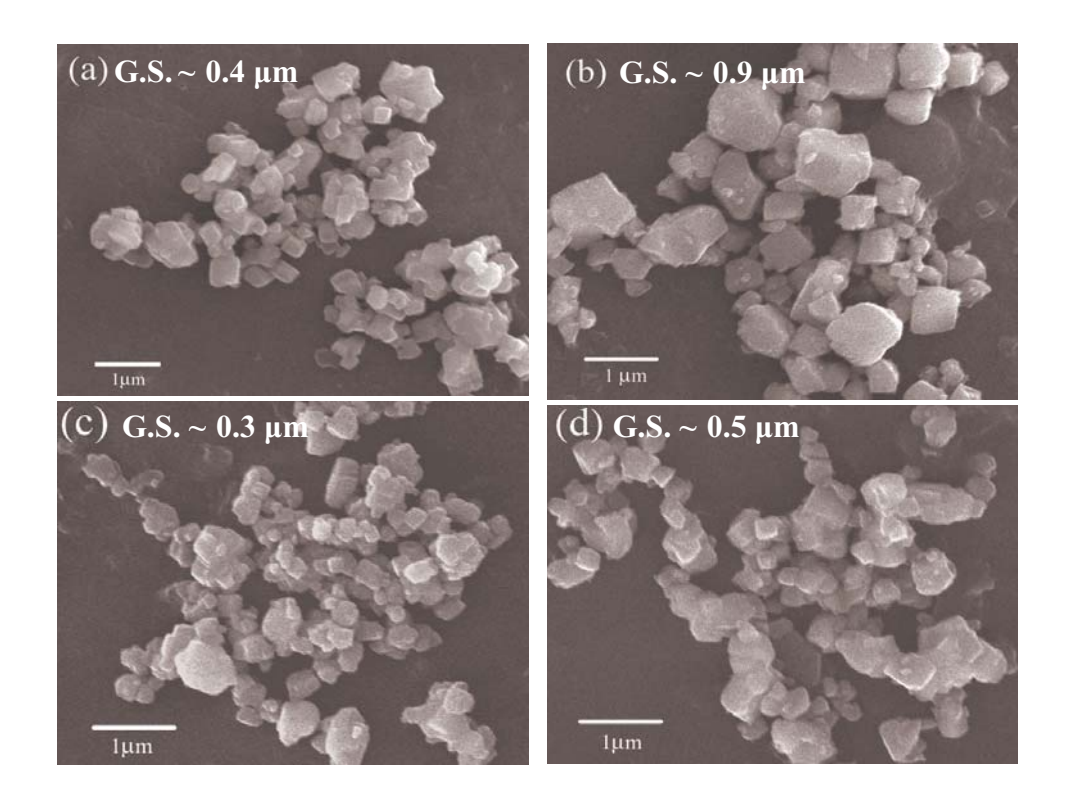


Figure 3 SEM micrographs of the (1-x)KNN – xBZT powders calcined at 850 $^{\circ}$ C for 4 h, obtained by the conventional mixed oxide method with (a) x = 0.1, (b) x = 0.2, and two-stage mixed oxide method with (c) x = 0.1 and (d) x = 0.2.

Figure 3 (a), (b), (c) and (d) show SEM micrographs of KNN-BZT powders for both methods, in which the average particle size was seen to increase with increasing BZT. However, there were no significant changes in grain size in the different preparation methods. Dielectric constant (ϵ_r) and loss tangent (tan (δ) at room temperature in both methods are shown in Figure 4. When compared to the conventional method, the two-stage method produces a slightly higher dielectric constant as well as a lower loss tangent. This may be attributed to the heterogeneous composition of ceramics synthesized by the conventional method. These results indicated that the two-stage method helps to



stabilize the perovskite phase and produces ceramics with better dielectric properties when compared to the conventional method.

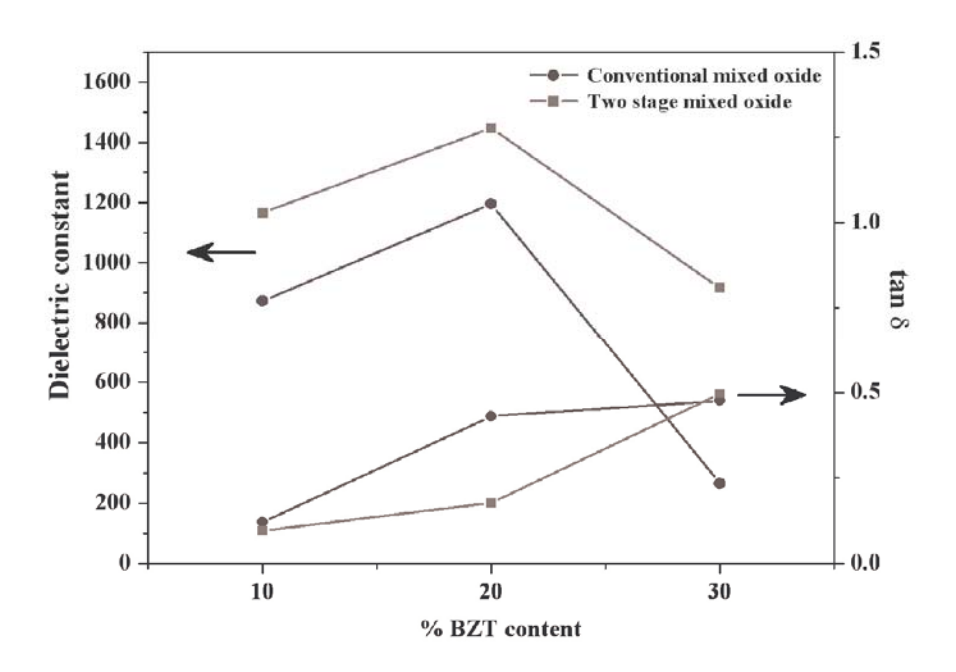


Figure 4 Dielectric constant (ε_r) and loss tangent $(\tan (\delta))$ of (1-x)KNN-xBZT ceramics at room temperature.

Summary

The properties of (1-x)KNN-xBZT; x = 0.0-0.3 ceramics prepared by conventional and two-stage methods were investigated. Perovskite phase formation behavior and dielectric properties were found to depend on the the methods of preparation. In the conventional method, the perovskite phases were obtained for compositions containing only 10 mol % KNN. For compositions above this amount, a complex mixture of phases was observed. However the complete solid solution of perovskite phase prepared by two-stage mixed oxide was retained up to 20 mole % BZT content. A better dielectric property was found for the ceramics synthesized by the two-stage method. The higher chemical homogeneity in ceramics synthesized by the two-stage method is the main reason for the higher dielectric constant.

Acknowledgements

This work was supported by the Thailand Research Fund (TRF), the Commission on Higher Education (CHE), National Research Council of Thailand (NRCT) and King Mongkut's Institute of Technology Ladkrabang (KMITL).

References

- [1] G. H. Haertling: J. Am. Ceram. Soc. Vol. 82 (1999), p. 797.
- [2] T. Takenaka and H. Nagata: J. Eur. Ceram. Soc. Vol. 25 (2005), p. 2693.
- [3] M. R. Suchomel and P. K. Davids: Appl. Phys. Lett. Vol. 86 (2005), p. 262905.
- [4] M. R. Suchomel, A. M. Fogg, M. Allix, H. Niu, J. B. Claridge and M. J. Rosseinsky: Chem. Mater. Vol.18 (2006), p. 4987.



Effect of Lead Nickel Niobate Substitution on Phase Transitions of Lead Zirconate Ceramics Prepared by the Solid State Reaction Method

S. Wirunchit¹, P. Laoratanakul² and N. Vittayakorn^{1,a}

¹Materials Science Research Unit, Department of Chemistry, Faculty of Science, King Mongkut's Institute of Technology Ladkrabang, Bangkok, Thailand 10520

²National Metal and Materials Technology Center (MTEC), Pathumthani 12120, Thailand ^anaratipcmu@yahoo.com

Keyword: Antiferroelectric Materials, Ferroelectric, Lead Zirconate

Abstract The solid solution between the antiferroelectric, PbZrO₃ (PZ), and relaxor ferroelectric, Pb(Ni_{1/3}Nb_{2/3})O₃ (PNN), was synthesized by the columbite method. The phase structure and phase transition of Pb(Zr_{1-x}(Ni_{1/3}Nb_{2/3})_xO₃ (PZNN), where $x = 0.0 \le x \le 0.50$, were investigated. The samples were kept at the calcination temperature of 900°C for 4 h and at the sintering temperature of 1,150°C for 2 h. Phase formation and phase transition of PZNN were investigated by x-ray diffraction (XRD) and thermal analysis, respectively. It was found that the structure of sintered pellets is orthorhombic for $0.0 \le x \le 0.10$, rhombohedral for $0.20 \le x \le 0.30$ and pseudo-cubic for x = 0.5. DSC measurement shows that in the antiferroelectric (AFE) phase – ferroelectric (FE) phase and FE to paraelectric (PE) phase; phase transformation temperatures decrease with increasing PNN concentration. The AFE–FE phase transformation was detected for compositions $0.00 \le x \le 0.08$.

Introduction

Lead zirconate, PbZrO₃ (PZ), is considered to be an excellent candidate as a key material of antiferroelectric ceramics [1-3]. At room temperature, PZ has an orthorhombic structure, with a = 5.87 Å, b = 11.74 Å and c = 8.20 Å [4], and an antiferroelectric (AFE) phase. It undergoes the AFE to a paraelectric (PE) phase and transforms from an orthorhombic structure to a cubic structure at 236°C [4]. It is reported that a ferroelectric (FE) phase exists over a very narrow temperature range (230-233°C) [5-8]. Lead nickel niobate (Pb(Ni_{1/3}Nb_{2/3})O₃;PNN) has a perovskite structure and typical relaxor ferroelectric properties. It exhibits a diffuse phase transition at around -120°C, with a much lower peak permittivity of about 4000 [9]. The crystal structure of PNN at room temperature is cubic (*Pm3m*), with a lattice parameter of 4.03 Å [9]. PNN based systems, such as Pb(Ni_{1/3}Nb_{2/3})O₃- Pb(Fe_{1/2}Nb_{1/2})O₃ [10] and Pb(Ni_{1/3}Nb_{2/3})O₃- Pb(Mg_{1/2}W_{1/2})O₃- PbTiO₃ [11], have been evaluated to possess low sintering temperatures and high dielectric constants. Thus, mixing PNN with PZ is expected to decrease the sintering temperature of PZ-based ceramics, a desirable move towards lower-cost electrodes [12].

In this work, the columbite precursor method was used to synthesize the $Pb(Zr_{I-x}(Ni_{1/3}Nb_{2/3})_xO_3$ (PZNN) with x = 0.0 - 0.5. The effect of PNN substitution on the phase transformation behavior of PZ was investigated. Phase structure, phase transitions and the related properties were studied by a differential scanning calorimeter.

Experimental

The perovskite structure of lead zirconate – lead nickel niobate ceramic, $Pb(Zr_{I-x}(Ni_{1/3}Nb_{2/3})_xO_3$ (PZNN), was prepared by the columbite precursor method via the ball-milling technique. The columbite structure (NiNb₂O₆) was synthesized first. Stoichiometric amounts of the precursor (NiO, Nb₂O₅) were mixed and milled in ethyl alcohol for 18 h. The mixture was dried and calcined at 1,100°C for 4 h. Then, NiNb₂O₆ and ZrO₂ were mixed with PbO, according to the composition of $Pb(Zr_{I-x}(Ni_{1/3}Nb_{2/3})_xO_3$ (PZNN), $0.0 \le x \le 0.5$, with an excessive content of 2 mol% PbO. After remilling and drying, the mixtures were calcined at 850°C for 4 h in a closed alumina crucible. Pellets



of 15 mm in diameter were pressed using 5% PVA. The binder was burnt out by slowly heating to 500°C over 2 h. The samples were sintered at temperatures ranging from 1,100°C to 1,150°C for 6 h. Phase formation and phase transition of PZ-PNN were investigated by x-ray diffraction (XRD) and a differential scanning calorimeter (DSC).

Results and Discussion

The XRD patterns of Pb($Zr_{I-x}(Ni_{1/3}Nb_{2/3})_xO_3$, $(0.0 \le x \le 0.5)$ ceramics, sintered at 1,150°C, are shown in Figure 1. From the patterns, PZ powder was identified as a single-phase material with a perovskite structure having orthorhombic symmetry, which could be matched with ICDD file no. 75-1607. The XRD patterns of the PZNN compositions showed a combination between PZ and PNN patterns, which indicated a perovskite structure having a symmetry that varied from orthorhombic to pseudo-cubic types. The ICDD file no. 34-0103 for PNN, with a cubic structural symmetry, showed a better comparison. The Pb($Zr_{I-x}(Ni_{1/3}Nb_{2/3})_xO_3$ was orthorhombic, rhombohedral and pseudo-cubic for compositions where $x = 0.00 \le x < 0.10$, $x = 0.10 \le x \le 0.40$ and x = 0.50, respectively.

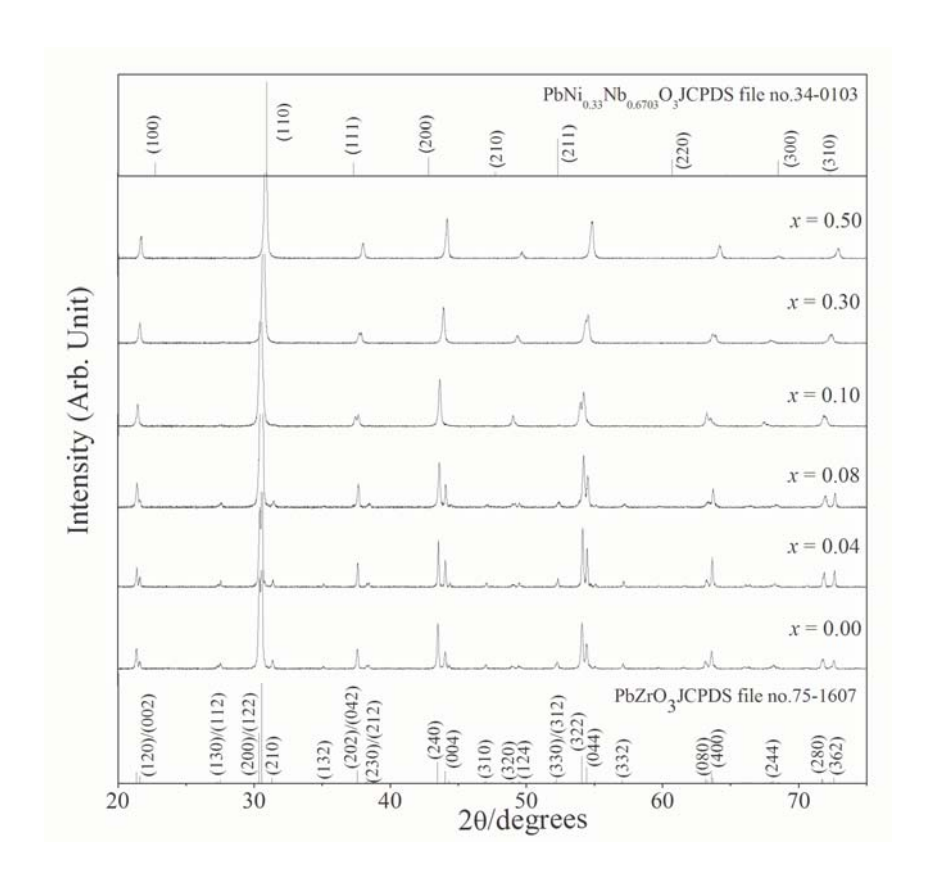


Figure 1 XRD patterns of Pb($Zr_{1-x}(Ni_{1/3}Nb_{2/3})_xO_3$ ceramics.

The DSC was used to investigate the phase transition in the Pb($Zr_{I-x}(Ni_{1/3}Nb_{2/3})_xO_3$ system. AFE-FE phase transition temperatures, enthalpy and paraelectric (PE) transitions are summarized in Table I. Figure 2 shows results of the DSC analysis of the PZNN ceramics. Two distinct endothermic peaks were observed for Pb($Zr_{I-x}(Ni_{1/3}Nb_{2/3})_xO_3$ samples with $0.0 \le x < 0.08$. The lower temperature corresponds to the transition temperature of the AFE \rightarrow FE phase transition, while the higher temperature corresponds to the FE \rightarrow PE phase transition.



Table 1 Phase transition temperatures of $Pb(Zr_{1-x}(Ni_{1/3}Nb_{2/3})_xO_3$ ceramics (R, Rhombohedral; O, Orthorhombic; C, pseudo-cubic)

Phase transition							
Composition	Crystal	Temperature (°C)		Enthalpy (J/g)			
(x)	Structure	AFE→FE	FE→PE	AFE→FE	FE→PE		
0.00	O	229.5	235.5	1.53	2.34		
0.04	O	150.1	220.8	1.33	2.89		
0.08	O	55	205.5	0.29	2.44		
0.10	R	-	200.2	-	1.88		
0.30	R	-	149.0	-	0.16		
0.50	C	-	-	-	-		

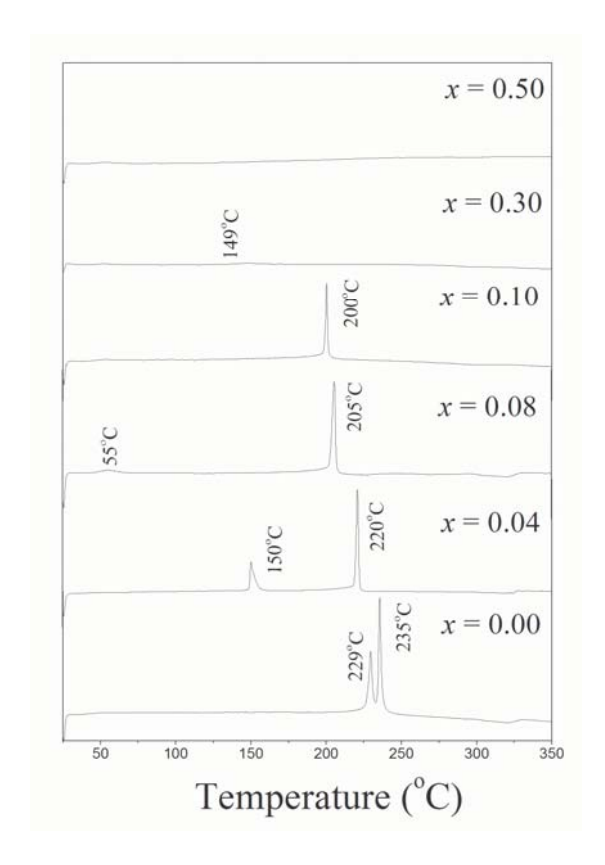


Figure 2 DSC thermographs of Pb($Zr_{1-x}(Ni_{1/3}Nb_{2/3})_xO_3$ ceramics.

Based on the results of XRD, and DSC data, the ferroelectric phase diagram for the $Pb(Zr_{1-x}(Ni_{1/3}Nb_{2/3})_xO_3)$ binary system has been established, as shown in Figure 3. The transition temperature decreases at approximate linearity with x. The phase diagram consists of three distinct crystallographic phases in this system; high temperature paraelectric cubic (Pm3m), rhombohedral (R3m), and ferroelectric orthorhombic [P2cb (no. 32)]. At low concentrations of PNN $x \le 0.08$, the symmetry can be defined as orthorhombic. The orthorhombic symmetry transforms into rhombohedral at a composition near x = 0.08.



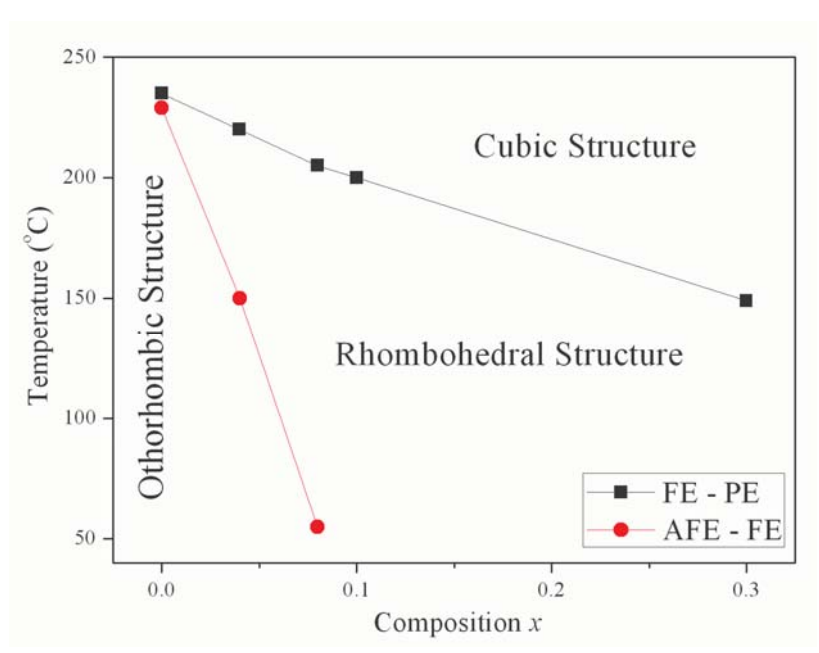


Figure 3 Phase diagram of the Pb($Zr_{1-x}(Ni_{1/3}Nb_{2/3})_xO_3$, x = 0.0-0.5 binary system.

Summary

The Structure of Pb($Zr_{I-x}(Ni_{1/3}Nb_{2/3})_xO_3$ (PZNN) is orthorhombic, rhombohedral and pseudo-cubic for compositions where $x = 0.00 \le x < 0.10$, $x = 0.10 \le x \le 0.40$ and x = 0.50, respectively. In the antiferroelectric (AFE) phase – ferroelectric (FE) phase and FE to paraelectric (PE) phase, phase transformation temperatures decrease with increasing PNN concentration. The AFE–FE phase transformation is detected for compositions $0.00 \le x \le 0.08$.

Acknowledgment

This work was supported by the Thailand Research Fund (TRF), the Commission on Higher Education (CHE), Thailand Graduate Institute of Science and Technology (TGIST) and King Mongkut's Institute of Technology Ladkrabang (KMITL).

- [1] E. Sawaguchi, G. shirane and S. Hosshino: Phys. Rev. Vol. 83 (1951), p. 1078.
- [2] E. Sawaguchi, G. shirane and Y. Takagi: J. Phys. Jpn. Soc. Vol. 6 (1951), p. 333.
- [3] N. Vittayakorn and S. Wirunchit, Smart Mater. Struct. Vol. 16 (2007), p. 851.
- [4] S. Roberts, J. Am. Ceram. Soc. Vol. 33 (1953), p. 63.
- [5] L. Goulpeau: Sov. Phys. Solid State. Vol. 8 (1967), p. 1970.
- [6] V. J. Tennery: J. Am. Ceram. Soc. Vol. 49 (1966), p. 483.
- [7] B. A. Scott and G. Burns: J. Am. Ceram. Soc. Vol. 55, (1972), p. 331.
- [8] R. W. Whatmore and A. M. Glazer: J.Phys. C: Solid state Physc. Vol. 12 (1979), p. 1505.
- [9] V. A. Bokov and I. E. Myl'nikova: Sov. Phys. Solid State. Vol. 3 (1961), p. 631.
- [10] T. R. Shrout, S. L. Swartz and J. M. Haun: Am. Ceram. Soc. Bull. Vol. 63 (1984), p. 808.
- [11] M. Yonezawa, Ferroelectrics. Vol. 68 (1986), p. 181.
- [12] Y. Xu, Ferroelectric Materials and Their Application (Elsevier Science Publishers B.V., 1991).



Synthesis, Crystal Structures, Phase Transition Characterization and Thermal Properties of the (1-x)PbZrO₃-xPb(Co_{1/3}Nb_{2/3})O₃ Solid Solution System

W. Banlue¹, R. Muanghlua², W. C. Vittayakorn³ and N. Vittayakorn^{1,a}

¹Materials Science Research Unit, Faculty of Science, King Mongkut's Institute of Technology Ladkrabang, Bangkok, Thailand 10520

²Electronics Research Center, Faculty of Engineering, King Mongkut's Institute of Technology Ladkrabang, Bangkok Thailand 10520

Keyword: Antiferroelectric Materials, Ferroelectric, Lead Zirconate

Abstract The phase transition behavior of the (1-x) PbZrO₃-xPb(Co_{1/3}Nb_{2/3})O₃ (PZCN) solid solution system ($0 \le x \le 0.30$) has been investigated by X-ray diffraction and DSC. In the solid solution, for $x \le 0.20$, the transition shows a first-order phase transition behavior and its antiferroelectric (AFE) crystal structure is orthorhombic. The transition temperature gradually decreases with increased Co²⁺/Nb⁵⁺ concentration. On the composition range $0.20 \le x \le 0.30$, a typical relaxor-like behavior is displayed. The low temperature crystal structure is pseudo-cubic in this composition range. With these data, the ferroelectric phase diagram between PZ and PCoN has been established.

Introduction

Lead zirconate [PbZrO₃, abbreviated as PZ] is an antiferroelectric ceramic with a Curie temperature of 230°C [1, 2]. PZ is a parent compound of PbZr_{1-x}Ti_xO₃ (PZT) solid solutions, which are of high scientific and technological interest for their ferroelectricity and piezoelectricity observed over a wide range of compositions [3]. It is reported that the antiferroelectric (AFE) to ferroelectric transition (under the application of a strong electric field to the ceramic in the antiferroelectric state) leads to significant energy storage for the DC field [4]. This feature of PbZrO₃ makes it a candidate material for energy storage applications [3]. Lead cobolt niobate [Pb(Co_{1/3}Nb_{2/3})O₃, abbreviated as PCoN] is a relaxor ferroelectric, characterized by frequency-dependent dielectric maxima and a diffuse phase transition [5, 6]. The diffuse phase transition characteristic of the PCoN was first explained by Smolenskii and Agranovskaya on the basis of local compositional fluctuations on a microscopic scale [6, 7]. PCoN-based ceramics are considered to possess low sintering temperatures. Therefore, these materials can be applied for fabricating multilayer capacitors with low-temperature melting inner electrodes [8]. There have been many studies concerning the solid solution of PZ and other perovskite materials such as PbTiO₃ [9], BaZrO₃, [4, 10] PbSnO₃ [11] and SrZrO₃ [9]. However, to the best of the authors' knowledge, no work has been done on the solid solution between PZ and PCoN. Therefore, the objective of our present study is to investigate phase transition of (1-x)PbZrO₃ – xPb(Co_{1/3}Nb_{2/3})O₃ (PZ – PCoN) with x = 0.00 - 0.30 as a function of composition and temperature.

Experimental

The (1-x)PbZrO₃ – xPb(Co_{1/3}Nb_{2/3})O₃ ceramics, where x = 0.00, 0.02, 0.04, 0.06, 0.08, 0.10, 0.20 and 0.30, were prepared by a columbite precursor. First, a columbite (CoNb₂O₆) precursor was prepared using reagent-grade CoO and Nb₂O₅ in stoichiometric proportions. The powders were thoroughly mixed in a ball mill for 18 h, using ethanol as a grinding medium, and the mixed powder was calcined at 1,100°C for 4 h to obtain the columbite precursor. Single-phase formation of the



³ Department of Physics, Faculty of Science, Chiang Mai University, Chiang Mai, Thailand 50200 a naratipcmu@yahoo.com

precursor was confirmed by X-ray diffraction. The columbite precursor was mixed with PbO (99% purity), and ZrO₂ (99% purity) in different proportions for making different compositions, and each mix was calcined at 900°C for 4 h to acquire the desired composition of (1-x)PZ-xPCoN. Two mol percent of excess PbO was added to all the compositions to compensate for the lead loss during sintering. Single-phase formation was verified by powder XRD. Powders were compacted in disk form with a diameter of 15 mm and thickness of 2–3 mm. These disks were sintered in PbO-rich atmosphere at 1,150°C for 2 h. The densities of the sintered samples were measured to ~95% of the theoretical values. The crystal structure of the sintered pellets was determined by X-ray diffraction (XRD). The phase transition temperatures and enthalpy (Δ H) of the phase transitions were determined by DSC. This was operated from room temperature to 250°C with a heating rate of 10°C/min.

Results and Discussion

Figure 1 illustrates the XRD patterns of (1-x)PZ-xPCoN sintered pellets for $0.00 \le x \le 0.30$. It can be seen that the sintered pellets are single-phase: all the lines in each XRD pattern could be indexed with a perovskite cell. The diffraction peaks move gradually towards higher angles with increasing PCoN contents, indicating smaller cell parameters.

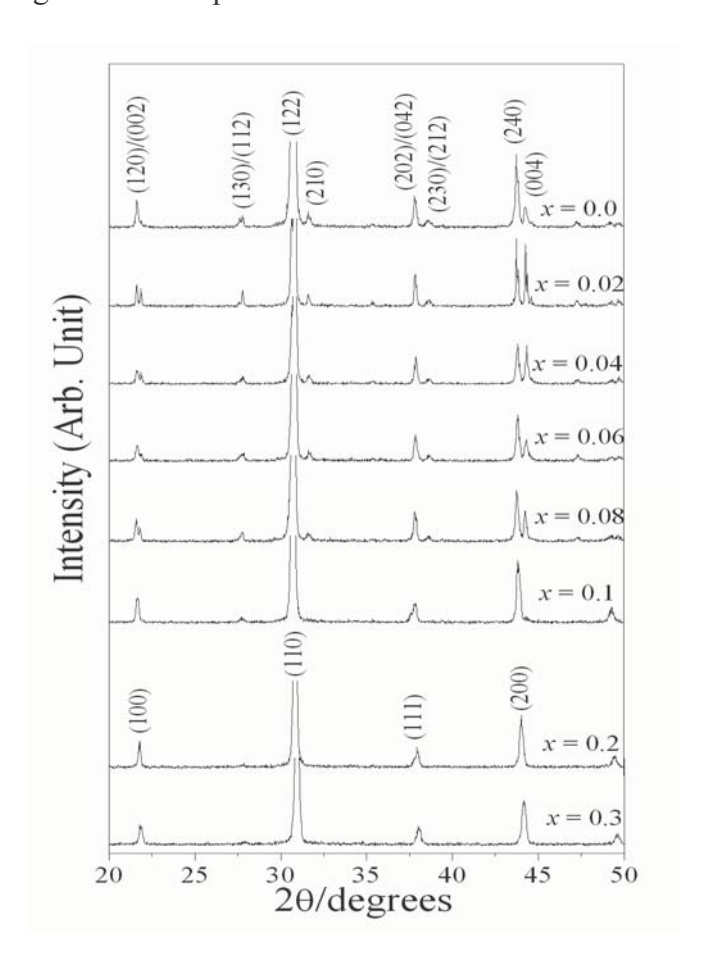


Figure 1 XRD patterns of (1-x)PbZrO₃ – xPb $(Co_{1/3}Nb_{2/3})O_3$ sintered pellets.



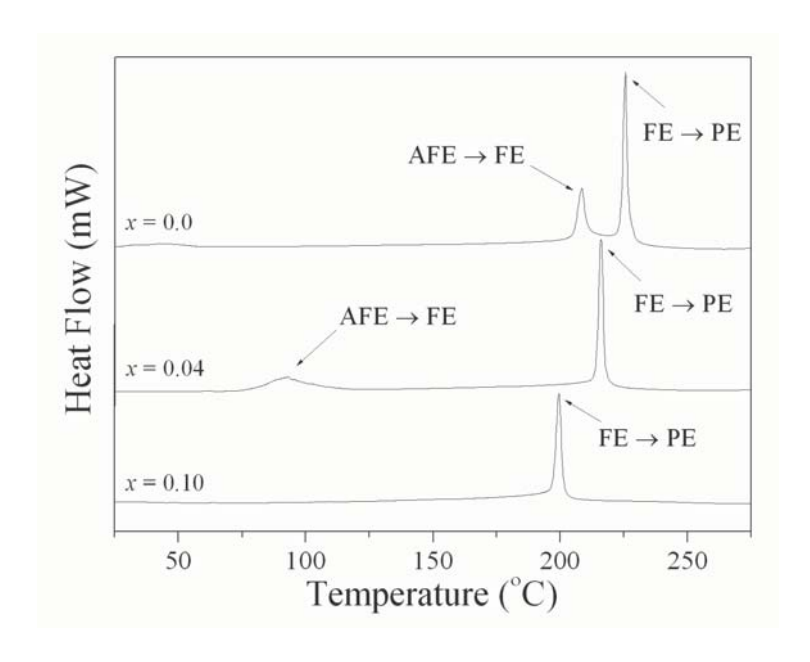


Figure 2 DSC thermographs of PZ-PCoN samples for: (a) x = 0, (b) x = 0.04 and (c) x = 0.10.

For the composition $0.00 \le x \le 0.10$, superstructure lines along with strong peaks are clearly observed, indicating that this composition belongs to the AFE orthorhombic phase. Furthermore, the samples with x = 0.1, 0.2 and 0.3 had a split (1 1 1) and (2 2 0) reflection and single (2 0 0) reflection, confirming that the crystal structure of the samples with x = 0.1, 0.2 and 0.3 is a rhombohedral perovskite. The DSC technique was used to investigate the phase transition of PZ-PCoN ceramics, with increasing PCoN concentration. A typical result of the DSC of PZ-PCoN for the composition x = 0, 0.04 and 0.10 is presented in Figure 2(a)-(c). Two distinct endothermic peaks observed for PZ at about 208.4 and 225.6°C are shown in Figure 2(a). The lower temperature corresponds to the transition temperature of the AFE phase transition, while the higher temperature corresponds to the FE

PE phase transition. In Figure 2(b), two endothermic peaks are shown at 92.8 and 216.1°C for the composition, x = 0.04. The AFE \rightarrow FE phase transition was found in the compositions of $0.00 \le x \le 0.10$. The peaks shift to lower temperatures, with a higher composition of x. This result corresponds to a decreasing AFE phase, with increasing amounts of PCoN content. Table 1 gives the transition temperature, including AFE→FE and FE→PE transitions of different PZ-PCoN compositions observed from DSC. The temperature range width of the FE phase increases progressively with PCoN content. After accumulating all these data, the ferroelectric phase diagram of (1-x)PZ-xPCoN has been finally established as a function of temperature and composition, as shown in Figure 3.

Table 1 Phase transitions temperature of (1-x)PZ-xPCoN ceramics

Composition	Phase transition temperature (°C)		
X	AFE→FE	FE→PE	
0.00	208.4	225.6	
0.02	145.2	220.9	
0.04	92.8	216.1	
0.06	33.3	209.9	
0.08	-	204.6	
0.10	-	199.4	
0.20	-	182.0	
0.30	-	158.2	



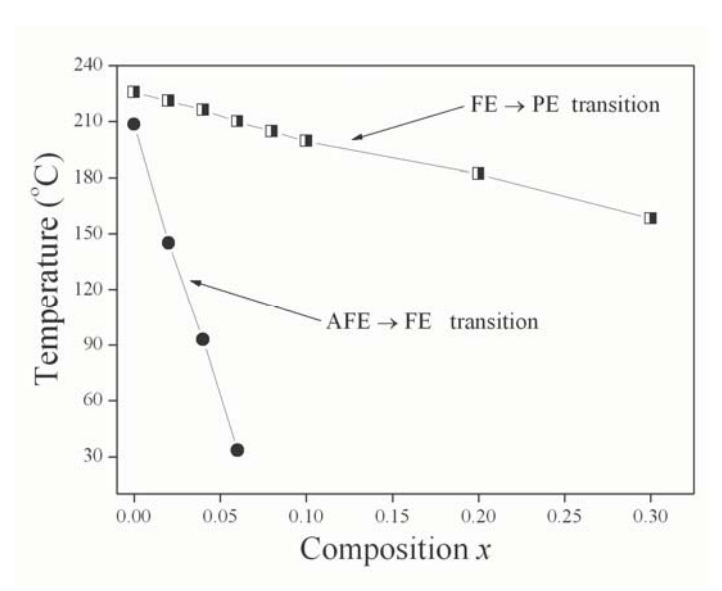


Figure 3 Ferroelectric phase diagram of the (1-x)PZ - xPCoN, x = 0.0-0.30 binary system.

The transition temperature decreases linearly with x, from approximately $T_c = 235^{\circ}C$ for x = 0.0 to $158.2^{\circ}C$ for x = 0.3. At room temperature, the phase boundary between the orthorhombic, antiferroelectric and rhombohedral ferroelectric phases was observed near x = 0.08. The phase diagram consists of three distinct crystallographic phases in this system; high temperature paraelectric cubic, rhombohedral, and ferroelectric orthorhombic.

Summary

Relaxor ferroelectric PCoN has been found to strongly influence crystal structure and thermal properties of PZ ceramics. The crystal structure data obtained from XRD indicate that the solid solution (I-x)PZ - xPCoN, where x = 0.0-0.3, successively transforms from orthorhombic to rhombohedral symmetry with increased PCoN concentration. The AFE \rightarrow FE phase transition is found in compositions of $0.0 \le x \le 0.08$. The AFE \rightarrow FE phase transition shifts to lower temperatures with higher compositions of x. The temperature range width of the FE phase increases with increased PCoN.

Acknowledgment

This work was supported by the Thailand Research Fund (TRF), the Commission on Higher Education (CHE), and King Mongkut's Institute of Technology Ladkrabang (KMITL).

- [1] E. Sawaguchi, G. Shirane and S. Hoshino: Phys. Rev. Vol. 83 (1951), p. 1078.
- [2] F. Jona, G. Shirane, F. Mazzi and R. Pepinsky: Phys. Rev. Vol. 105 (1957), p. 849.
- [3] G. H. Haertling: J. Am. Ceram. Soc. Vol. 82 (1999), p. 797.
- [4] B. P. Pokharel and D. Pandey: J. Appl. Phys. Vol. 86 (1999), p. 3327.
- [5] K. Uchino: Ferroelectrics Vol. 151 (1994), p. 321.
- [6] G. A. Smolenskii and Isupov: Sov. Phys. doklady. Vol. 9 (1954), p. 653.
- [7] N. Setter and L. E. Cross: J. Appl. Phys. Vol. 51 (1980), p. 4356.
- [8] A. Halliyal, U. Kumar, R. E. Newham and L. E. Cross: Am. Ceram. Soc. Bull. Vol. 66 (1987), p. 671.
- [9] B. Jaffe and W. R. Cook: *Piezoelectric ceramic* (R.A.N. Publishers, 1971).
- [10] B. P. Pokharel and D. Pandey, Phys. Rev. B. Vol. 65 (2002), p. 214108.
- [11] Y. Xu, Ferroelectric Materials and Their Application (Elsevier Science Publishers B.V., 1991).



Effects of Zr/Ti Ratio on the Structure and Ferroelectric Properties in PZT-PZN-PMN Ceramics Near the Morphotropic Phase Boundary

R. Muanghlua¹, S. Niemchareon ¹, W. C. Vittayakorn² and N. Vittayakorn^{3,a}

¹Electronics Research Center, Faculty of Engineering, King Mongkut's Institute of Technology Ladkrabang, Bangkok Thailand 10520

^a e-mail: naratipcmu@yahoo.com

Keyword: Ferroelectric Materials, Lead Zirconate titanate, Morphotropic phase boundary

Abstract The piezoelectric ceramics of $Pb(Zr_xTi_{1-x})O_3 - Pb(Zn_{1/3}Nb_{2/3})O_3 - Pb(Mn_{1/3}Nb_{2/3})O_3$; PZT-PZN-PMN with Zr/Ti ratios of 48/52, 50/50 and 52/48 were fabricated in order to investigate the effect of compositional modifications on the ferroelectric properties of PZT-PZN-PMN ceramics. The phase structure of ceramics sintered at 1,150°C was analyzed. Results show that the pure perovskite phase was in all ceramic specimens, and the phase structure of PZT-PZN-PMN piezoelectric ceramics transformed from tetragonal to rhombohedral, with the Zr/Ti ratios increased in the system. The PZT-PZN-PMN ceramics with a Zr/Ti ratio of 50/50 exhibited the most promising properties including high remanent polarization and low coercive field of 25.95 μ C cm⁻² and 12.5 kV cm⁻¹, respectively. Furthermore, the transition temperature decreased when the Zr/Ti ratio increased in the system.

Introduction

Lead zirconate titanate (PZT) is one of the most commonly used ferroelectric ceramic materials. The material has been studied intensively since discovery of the miscibility of lead titanate and lead zirconate in the 1950s. Due to their excellent dielectric, pyroelectric, piezoelectric and electro optic properties, they have a variety of applications in high energy capacitors, non-volatile memories (FRAM), ultrasonic sensors, infra red detectors, electro optic devices, and step-down multilayer piezoelectric transformers for AC–DC converter applications. Until now, many ternary and quaternary systems, such as PNW–PMN–PZT [1], PMN–PZN–PZT [2], PZT–PNN–PZN [3], and PZT–PFW–PMN [4] have been synthesized by modifications or substitutions to satisfy the requirements of the multilayered piezoelectric transformers. In this work, we studied influences of the Zr/Ti ratio on the crystal structure, and piezoelectric and dielectric properties of Pb(Zr_xTi_{1-x})O₃ – Pb(Zn_{1/3}Nb_{2/3})O₃ – Pb(Mn_{1/3}Nb_{2/3})O₃; PZT-PZN-PMN ceramics for multilayered piezoelectric transformer applications.

Experimental

The powders and ceramics with compositions of $Pb_{0.97}Sr_{0.03}[(Mn_{1/3}Nb_{2/3})_{0.07}(Zn_{1/3}Nb_{2/3})_{0.06}(Zr_{(1-x)}Ti_x)_{0.87}]O_3$ were prepared via a conventional mixed-oxide process, where x=0.48, 0.50 and 0.52. Reagent-grade oxide powders PbO (99.0%), ZrO_2 (99.0%), TiO_2 (99.5%), Nb_2O_5 (99.5%), ZnO(99.9%) and MnO_2 (99.0%) were mixed, consecutively. The mixtures were milled in ethanol using zirconium ball as media in a polyethylene jar for 18 h. The mixed slurry was dried at 80°C and calcined at 850°C for 4 h. Then, the calcined powders were ground again under the same condition in order to obtain fine uniform powders. After drying, the powders were added to 5 wt.% polyvinyl alcohol (PVA) solution, and then pressed into 15 mm diameter plates under a pressure of 100 MPa. The pressed plates were sintered at 950–1,100°C for 6 h in a sealed alumina crucible with lead atmosphere. The sintered ceramics were examined by X-ray diffractometry (XRD, D8



Department of Physics, Faculty of Science, Chiang Mai University, Chiang Mai, Thailand 50200
 Materials Science Research Unit, Faculty of Science, King Mongkut's Institute of Technology Ladkrabang, Bangkok, Thailand 10520

Advance) to determine the phase structure. Subsequently, the sintered disks were polished, and silver-paste electrodes were fired at 850° C. In addition, the polarization (P) was measured as a function of electric field (E), using a ferroelectric tester system (Radiant Technologies, Inc., PT66A).

Results and Discussion

Figure 1 (a) and (b) show the XRD patterns of $Pb_{0.97}Sr_{0.03}[(Mn_{1/3}Nb_{2/3})_{0.07}(Zn_{1/3}Nb_{2/3})_{0.06}(Zr_{(1-x)}Ti_x)_{0.87}]O_3$ sintered pellets for x=0.48, 0.50 and 0.52. The sintered pellets can be seen as a single-phase: all the lines in each XRD pattern could be indexed with a perovskite cell. No secondary reaction phases, such as PbO, Pb-based compounds, unreacted oxide and so on, are observed in the pattern.

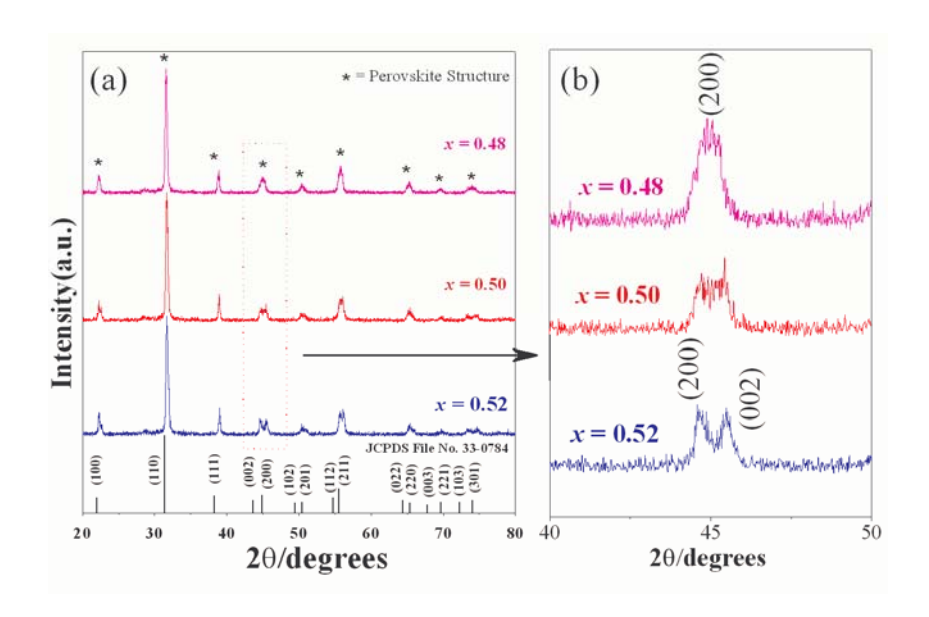


Figure 1 XRD patterns of $Pb_{0.97}Sr_{0.03}[(Mn_{1/3}Nb_{2/3})_{0.07}(Zn_{1/3}Nb_{2/3})_{0.06}(Zr_{(1-x)}Ti_x)_{0.87}]O_3$ sintered pellets.

Based on the careful XRD study of $(2\ 0\ 0)$ reflections in Figure 1(b), we found that a phase transformation from the pseudo-cubic structure to the tetragonal structure occurs with increasing x content. The ceramics with x=0.48 exist as a pseudo-cubic phase revealed by the single $(2\ 0\ 0)_R$ peak. At x=0.50, the ceramics coexist as a tetragonal and pseudo-cubic phase revealed by the coexistence of $(0\ 0\ 2)_T$ and $(2\ 0\ 0)_R$ peaks in the 2θ range of 43.5° to 45.5° . The ceramics exist as a tetragonal phase when indicated by the splitting of $(0\ 0\ 2)$ and $(2\ 0\ 0)$ peaks in the 2θ range of 43.5° to 46.5° at x=0.52.

Table 1 Characteristics of $Pb_{0.97}Sr_{0.03}[(Mn_{1/3}Nb_{2/3})_{0.07}(Zn_{1/3}Nb_{2/3})_{0.06}(Zr_{(1-x)}Ti_x)_{0.87}]O_3$ ceramics with optimized processing conditions

Composition <i>x</i>	Crystal structure	Theoretical Density (%)	Grain Size (µm)
0.48	PC	94.05	2.84
0.50	PC+T	94.03	2.72
0.52	PC	95.21	2.94



In the first approximation, it could be said that the composition between x=0.50 is close to the morphotropic phase boundary (MPB) of this system, where the structure of the $Pb_{0.97}Sr_{0.03}[(Mn_{1/3}Nb_{2/3})_{0.07}(Zn_{1/3}Nb_{2/3})_{0.06}(Zr_{(1-x)}Ti_x)_{0.87}]O_3$ compositions is gradually changing from pseudo-cubic to tetragonal. The physical properties do not vary significantly with the ceramic compositions, as listed in Table 1.

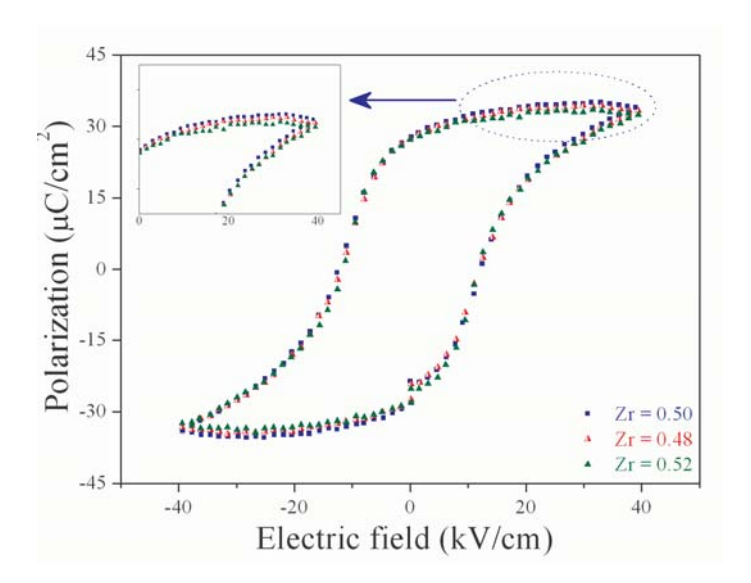


Figure 2 Hysteresis loops of the $Pb_{0.97}Sr_{0.03}[(Mn_{1/3}Nb_{2/3})_{0.07}(Zn_{1/3}Nb_{2/3})_{0.06}(Zr_{(1-x)}Ti_x)_{0.87}]O_3$ ceramics with x = 0.48, 0.50 and 0.52 measured at 40 kV/cm.

Figure 2 illustrates the P–E curves of the samples, with x = 0.48, 0.50 and 0.52 measured at 25 kV/cm. All compositions show symmetry in shape and reveal rectangular hysteresis loops, which is typical of a phase that contains long-range cooperation between dipoles. No evidence of pinning effect or asymmetric loop was detected in any electric field strengths. From the fully saturated loops, the remanent polarization P_r and coercive field E_c were determined. The values of P_r and E_c for composition x = 0.50 are 25.95 μ C/cm² and 12.5 kV/cm, respectively, whereas the remanent polarization P_r is 25.7 μ C/cm² for composition x = 0.48. Maximum remanent polarization was observed in the ceramic with composition x = 0.5. It has been seen that the samples with compositions x = 0.5 exhibit the highest saturation and remnant polarization among all the ceramics studied. As indicated by the above XRD, the composition with x = 0.5 contains both tetragonal and pseudo-cubic phases, so it should favor a strong ferroelectric effect. This is due to the increased ease of reorientation during poling by the transformation of a number of 180° domains into 90° ones. Also revealed from these results, the MPB coexisting in the tetragonal and pseudo-cubic phases in the present system is a broad composition region of x = 0.5, which exhibits high ferroelectric properties around the center of the MPB.

Summary

The Zr/Ti ratio has been found to influence crystal structure and ferroelectric properties of $Pb_{0.97}Sr_{0.03}[(Mn_{1/3}Nb_{2/3})_{0.07}(Zn_{1/3}Nb_{2/3})_{0.06}(Zr_{(1-x)}Ti_x)_{0.87}]O_3$ ceramics. The crystal structure data obtained from XRD indicate that the solid solution $Pb_{0.97}Sr_{0.03}[(Mn_{1/3}Nb_{2/3})_{0.07}(Zn_{1/3}Nb_{2/3})_{0.06}(Zr_{(1-x)}Ti_x)_{0.87}]$, where x=0.48, 0.50 and 0.52, successively transforms from pseudo-cubic to tetragonal symmetry with increased x concentration. More interestingly, XRD analysis and ferroelectric property measurements indicated the existence of the MPB composition at between x=0.50.



Acknowledgment

This work was supported by the Thailand Research Fund (TRF), the Commission on Higher Education (CHE), and Faculty of Engineering, King Mongkut's Institute of Technology Ladkrabang and King Mongkut's Institute of Technology Ladkrabang (KMITL).

- [1] Z. Yang, R. Zhang, L. Yang and Y. Chang: Materials Research Bulletin. Vol. 42 (2007), p. 2156.
- [2] J. Yoo, K. Kim, C. Lee, L. Hwang, D. Paik, H. Yoon and H. Choi: Sensors and Actuators A: Physical. Vol. 137 (2007), p. 81.
- [3] N. Vittayakorn and D. P. Cann; Appl. Phys. A. Vol. 86 (2007), p. 403.
- [4] Z. Yang, X. Chao, C. Kang and R. Zhang: Materials Research Bulletin. Vol. 43 (2008), p. 38.



Synthesis, Phase Formation and Characterization of Co₄Nb₂O₉ Powders Synthesized by Solid-State Reaction

N. Chaiyo¹, R. Muanghlua², A. Ruangphanit³, W. C. Vittayakorn⁴ and N. Vittayakorn^{1,5,a}

- ¹ King Mongkut's Institute of Technology Ladkrabang Nanotechnology Research Center (NRC), King Mongkut's Institute of Technology Ladkrabang, Bangkok, Thailand 10520
- ²Electronics Research Center, Faculty of Engineering, King Mongkut's Institute of Technology Ladkrabang, Bangkok Thailand 10520
- ³ Thai Microelectronics Center (TMEC), National Electronics and Computer Technology Center, Nation Science and Technology Development Agency, Ministry of Science and Technology, Chachoengsao 24000, Thailand
- ⁴ Department of Physics, Faculty of Science, Chiang Mai University, Chiang Mai, Thailand 50200
- Materials Science Research Unit, Department of Chemistry, Faculty of Science, King Mongkut's Institute of Technology Ladkrabang, Bangkok, Thailand 10520

^a e-mail: naratipcmu@yahoo.com

Keywords: Co₄Nb₂O₉; Calcinations; Powder synthesis; Microwave dielectric

Abstract. A corundum-type structure of cobalt niobate $(Co_4Nb_2O_9)$ has been synthesized by a solid-state reaction. The formation of the $Co_4Nb_2O_9$ phase in the calcined powders was investigated as a function of calcination conditions by differential thermal analysis (DTA) and X-ray diffraction (XRD) techniques. Morphology and particle size have been determined by scanning electron microscopy (SEM). It was found that the minor phases of unreacted Co_3O_4 tend to form together with the columbite $CoNb_2O_6$ phase at a low calcination temperature and short dwell time. It seems that the single-phase of $Co_4Nb_2O_9$ in a corundum phase can be obtained successfully at the calcination conditions of $900^{\circ}C$ for 60 min, with heating/cooling rates of $20^{\circ}C$ /min.

Introduction

A variety of microwave dielectric ceramics have been utilized for microwave dielectric applications including the filters and resonators in the wireless communication system [1]. There are three important properties required, i.e., a high dielectric constant ε_r , high quality factor $Q \times f$ and low temperature coefficient of resonant frequency τ_f , in order to miniaturize the size of the microwave dielectric resonator and reach suitability for application at high frequency, and the resonant frequency must be stable at various operating temperatures. A high $Q \times f$ value of more than 30,000 GHz is required to withstand high electric loads, especially for microwave dielectric ceramics used in the base stations of mobile phones. However, still higher $Q \times f$ – value materials are required for new digital systems [2]. Over the past few years, the demand for smaller, lighter and temperature stable devices has increased. Cobalt niobate CoNb₂O₆ is one of the best known microwave dielectric materials, which recently gained considerable attention. In general, production of single-phase CoNb₂O₆ is not straightforward, as a minor concentration of Co₄Nb₂O₉ sometimes forms alongside the major phase of CoNb₂O₆. The crystal structure of Co₄Nb₂O₉ ceramic is known to have a corundum-type structure. The oxygen ions are located at the lattice sites of a hexagonal closed-packed unit cell. In the HCP crystal structure, as in the FCC structure, there are as many octahedral interstitial sites as there are atoms in the unit cell. In recent study, the microwave dielectric properties of a corundum-type structure such as Mg₄Nb₂O₉ ceramic was reported to have a high $Q \times f$ value, which was comparable to that of Al₂O₃. Thus far, although Co₄Nb₂O₉ is identical



in stoichiometry to Mg₄Nb₂O₉, it has not been synthesized to the corundum-type structure. Interestingly, the mixed oxide route for the production of Co₄Nb₂O₉ powders has not received detailed attention, and the effects of calcination conditions have not yet been studied extensively. The objective of this work was to study the reaction between the starting cobalt oxide and niobium oxide precursors, phase formation and microstructure of corundum-type structure cobalt niobate powder.

Experimental

Reagent-grade oxides of Co_3O_4 (99.99 %, Aldrich, USA) and Nb_2O_5 (99.9%, Aldrich, USA) were used in this study. $Co_4Nb_2O_9$ powders were synthesized by the solid-state reaction of Co_3O_4 and Nb_2O_5 powders that were homogenized by ball milling with ethyl alcohol in the required stoichiometric ratio. The mixed slurry was dried at 80° C. The reactions of the uncalcined $Co_4Nb_2O_9$ powder, taking place during heat treatment, were investigated by differential thermal analysis (DTA; Perkin-Elmer 7 series) using a heating rate of 10° C /min in air from room temperature to 1,350 °C. According to the DTA results, various calcination conditions (i.e. temperatures ranging from 700 – 1,100 °C and dwell times from 15 to 240 min) were applied, with a heating/cooling rate of 20° C/min in order to investigate the formation of $Co_4Nb_2O_9$. Calcined powders were subsequently examined by room temperature X-ray diffraction (XRD; Bruker D8 Advance) using Ni-filtered CuK_{α} radiation to identify the phase formed and optimum calcination condition for the formation of $Co_4Nb_2O_9$ powders. Powder morphologies and grain size were directly imaged using scanning electron microscopy (LEO, LEO 1455VP, Cambridge, England).

Results and Discussion

The DTA curve for the powder mixed in the stoichiometric proportions of $Co_4Nb_2O_9$ is shown in Figure 1. Three endothermic peaks centered at $121^{\circ}C$, $294^{\circ}C$ and $837^{\circ}C$ were observed. The first and second endothermic peaks should correspond to the evaporation of water molecules and decomposition of the organic species from the milling process, respectively [3, 4]. The third endothermic peak, at $837^{\circ}C$, was assigned to the formation of $Co_4Nb_2O_9$ by combination reactions of Co_3O_4 and Nb_2O_5 . Based on the DTA measurements, these data were used to define the range of calcination temperature at between 700 to 1,100 $^{\circ}C$ for XRD investigation.

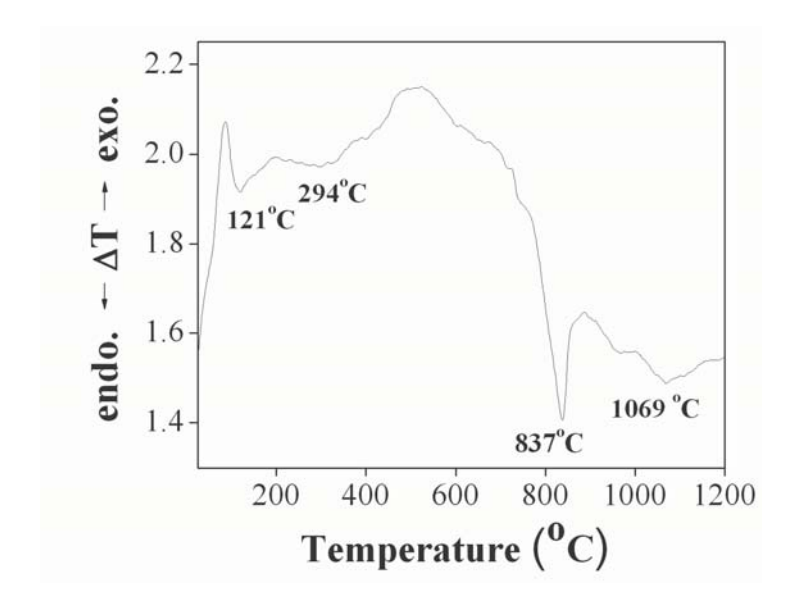


Figure 1. DTA curve for the mixture of Co₃O₄-Nb₂O₅ powder.



XRD patterns of all calcined powders are given in Figure 2. At a clacination temperature as low as 800°C, the strongest reflections were apparent in the majority of the XRD patterns, which indicated the formation of a columbite phase of $CoNb_2O_6$ (A) that could be matched with JCPDS file numbers 32-0304. The minor phase of unreacted cubic- Co_3O_4 (Y), which could be matched with JCPDS files No 78-1969, were found. As the calcination temperature increased to 900°C, intensity of the corundum $Co_4Nb_2O_9$ peaks was enhanced further and became the monophasic phase. This $Co_4Nb_2O_9$ phase was indexable according to a hexagonal corundum-type structure, with a lattice parameter of a = 517 pm and c = 1412 pm, and space group P3c1 (no. 165), consistent with JCPDS file numbers 38-1457. Upon calcinations at 1,000 and 1,100 °C, an essentially monophasic phase of $Co_4Nb_2O_9$ was obtained. However, in this work, there were no significant differences between the powders calcined at temperatures ranging from 900 to 1,100 °C.

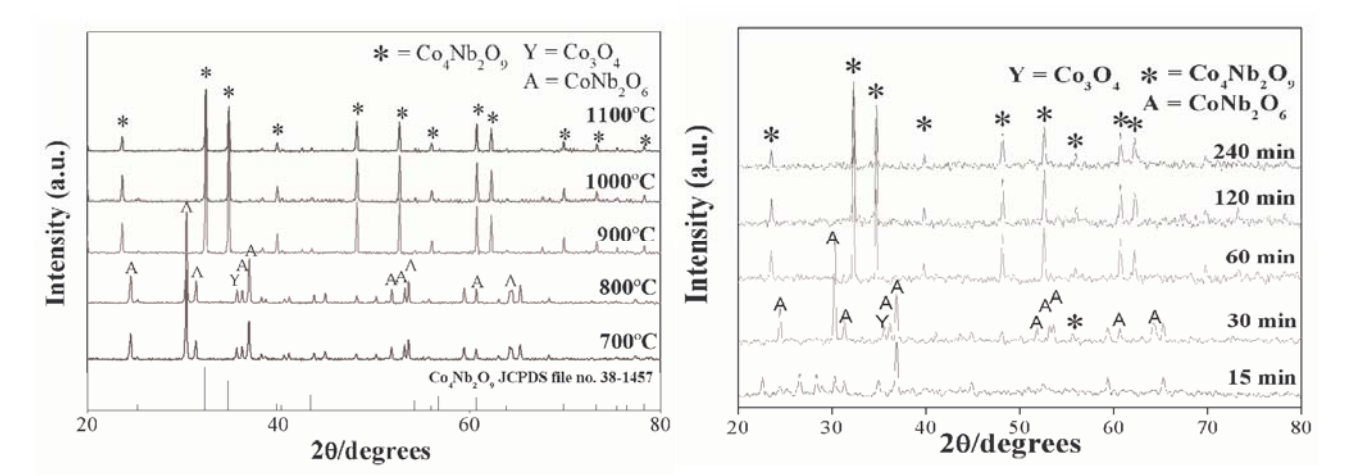


Figure 2. XRD patterns of Co₄Nb₂O₉ powder calcined at various temperatures for 4 h with heating/cooling rates of 20 °C /min.

Figure 3. XRD patterns of Co₄Nb₂O₉ powder calcined with heating/cooling rates of 20 °C /min at 900 °C for 15-240 min.

After obtaining the optimum calcination temperature, dwell times ranging from 15 min to 120 min, with a constant heating/cooling rate of 20°C/min were applied at 900 °C, as shown in Figure 3. It was observed that the single-phase of Co₄Nb₂O₉ (yield of 100% within the limitations of the XRD technique) powder was possible in powders calcined at 900°C, with a dwell time of 60 min or more applied. Observation that the dwell time effect may also play an important role in obtaining a single-phase product is also consistent with other systems [5, 6].

The average grain sizes were determined from the XRD pattern according to the Scherrer's equation

$$D = \frac{k\lambda}{\beta\cos\theta_B}$$

where D is the average grain size, k is a constant equal to 0.89, θ_B is the (3 1 1) peak angle, λ is the X-ray wavelength equal to 1.5406 Å and β is the half peak width. The average grain size of Co₄Nb₂O₉ powders was about 280 nm at 900 °C, with a dwell time of 60 min. The morphology of the calcined Co₄Nb₂O₉ powders was investigated by scanning electron microscopy (SEM), which is illustrated in Figure 4(a) and 4(b). In general, the particles are agglomerated and basically irregular in shape, with a substantial variation in particle size and morphology. The particle size can be estimated in the range of 300-400 nm from SEM micrographs. A detailed study at higher



magnification [Fig. 5(b)] shows that the particles had spherical secondary particles, composed of nano-sized primary particulates.

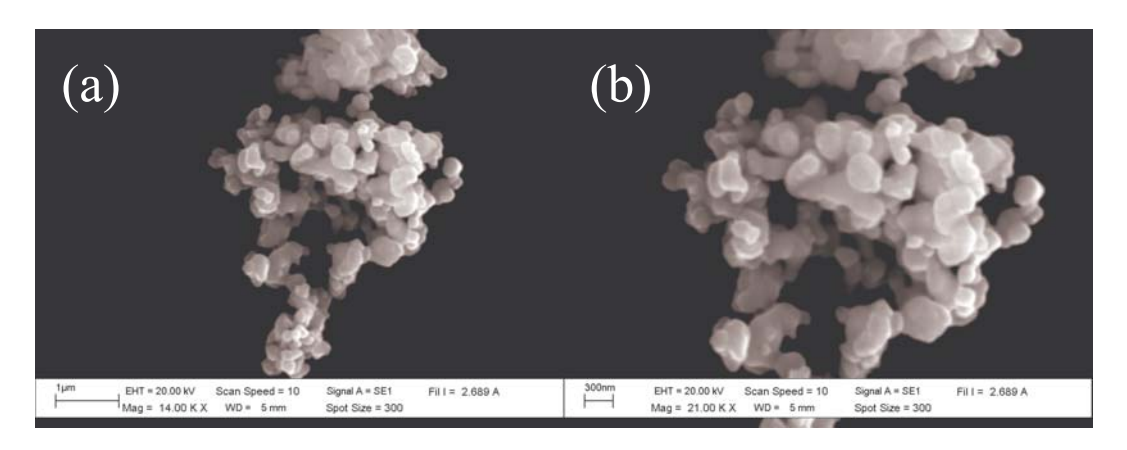


Figure 4. Scanning electron micrographs of the Co₄Nb₂O₉ powders calcined at 900 °C for 60 min, with a heating/cooling rate of 20 °C /min.

Summary

The corundum-structure, $Co_4Nb_2O_9$, was synthesized by solid state reaction using oxides as starting materials. The content of the impurity phases decreased with increasing calcination temperature and dwell time. Evidence has been obtained of a 100% yield of $Co_4Nb_2O_9$ at a calcination temperature of 900°C for 60 min, with heating/cooling rates of 20°C/minute. XRD showed the compound to have a corundum structure, with hexagonal lattice parameters of a = 5.1669(\pm 0.0014) and c = 14.1248 (\pm 0.0072). The particle size can be estimated in the range of 300-400 nm from SEM micrographs.

Acknowledgements

This work was supported by the Thailand Research Fund (TRF), the Commission on Higher Education (CHE), Thailand Graduate Institute of Science and Technology (TGIST), National Research Council of Thailand (NRCT) and King Mongkut's Institute of Technology Ladkrabang (KMITL).

- [1] A. Kan, H. Ogawa, A. Yokoi and Y. Nakamura: J. Euro. Ceram. Soc. Vol. 27 (2007), p. 2977.
- [2] A. J. Moulson and J. M. Herbert: *Electroceramics: Materials, Properties, Applications* (Chapman and Hall, New York, 1990)
- [3] S. Ananta, Mater. Lett. Vol. 58 (2004), p. 2530.
- [4] R. Wongmaneerung, T. Sarakonsri, R. Yimnirun and S. Ananta: Materials Science and Engineering: B. Vol. 130 (2006), p. 246.
- [5] R. Wongmaneerung, R. Yimnirun and S. Ananta: Mater. Lett. Vol. 60 (2006), p. 2666.
- [6] S. Wongsaenmai, R. Yimnirun and S. Ananta: Mater. Lett. Vol. 61 (2007), p. 2426.



Ferroelectric and Mechanical Properties of PZT-PZN-PNN Ceramics

S. Nabunmee, N. Vittayakorn, D. P. Cann and G. Rujijanagul*

Department of Physics, Faculty of Science, Chiang Mai University, Chiang Mai 50200, Thailand *rujijanagul@yahoo.com

Keywords: Dielectric permittivity, Phase transition, PZT-PZN-PNN ceramics

Abstract. Ceramics in the system $0.05(Pb(Zn_{1/3}Nb_{2/3})O_3-0.15Pb(Ni_{1/3}Nb_{2/3})O_3-0.8Pb(Zr_{1/2}Ti_{1/2})O_3$ (0.05PZN-0.15PNN-0.8PZT) were synthesized via the columbite method. Ferroelectric properties of the samples prepared by different sintering conditions were investigated. The mechanical property of the ceramics was also determined. The best ferroelectric properties were observed for the sample sintered at 1250°C.

Introduction

In the last decade, normal ferroelectric such as lead zirconate titanate [PbZ r_{1-x} Ti $_x$ O $_3$, PZT] has become an important commercially produced piezoelectric materials.[1-3] Excellent piezoelectric properties of PZT have been observed in compositions close to the morphotropic phase boundary(MPB Zr:Ti ,52:48). [1-3] Locating the MPB for the ferroelectric materials is very important for making the phase diagram and for obtaining excellent electrical properties. Therefore, most commercial PZT and other ferroelectric ceramics are thus designed in the vicinity of the MPB with various dopings in order to achieve high properties.

Lead-based relaxor perovskites, such as $Pb(Zn_{1/3}Nb_{2/3})O_3$ (PZN) and $Pb(Ni_{1/3}Nb_{2/3})O_3$ (PNN), having the general formula $Pb(B'B'')O_3$ have received significant attention since the 1970s because of their peculiar dielectric and piezoelectric behavior. These materials have been applied in many areas such as electrostrictive actuators, transducers, and multilayer ceramic capacitors. [4-9]

Recently, binary or ternary systems containing a combination of relaxor ferroelectrics with rhombohedral symmetry and normal ferroelectric tetragonal symmetry near the MPB have attracted particular attention owing to their high dielectric and piezoelectric properties. The excellent electrical properties can be applied to many areas such as multilayer ceramic capacitors, electrostrictive transducers, sensors, and actuators. [10-12] In the present work, solid solution of 0.05PZN-0.15PNN-0.8PZT ternary system was synthesized via a columbite method. Various sintering temperature were carried out, to find out the optimum processing condition.

Experimental

The ternary system of 0.05PZN-0.15PNN-0.8PZT was synthesized by a columbite method. The wolframite precursor ZrTiO₄ was formed by reaction between ZrO₂ with TiO₂ at 1400 °C for 4 h. The columbite precursor ZnNb₂O₆ was prepared from the reaction between ZnO and Nb₂O₅ at 975 °C for 4 h. The precursors ZrTiO₄, ZnNb₂O₆ were then mixed with PbO (99.9%) according to the stoichiometric ratio for the desired compositions with 2 mol% excess PbO added. The mixed powders were calcined at temperatures ranging, 900°C at a dwell time of 2 h in a double crucible configuration with a heating rate of 20 °C/min. The calcined powders were isostatically cold pressed into pellets at a pressure of 100 MPa. Sintering occurred between 1100 and 1350 °C with a dwell time of 2 h at 500°C with heating rate 1°C/min and 2 h at 1250°C with heating rate 5°C/min. The perovskite phase was examined by x-ray diffraction (XRD). The density of the sintered samples was measured by Archimedes' method with distilled water as the fluid medium. The polarization-Electric field (P-E) property and mechanical property of the sintered samples were measurement.



Results and Discussion

The perovskite and pyrochlore phase formation at different sintering temperatures in 0.05PZN-0.15PNN-0.8PZT ceramics were studied and analyzed by XRD.

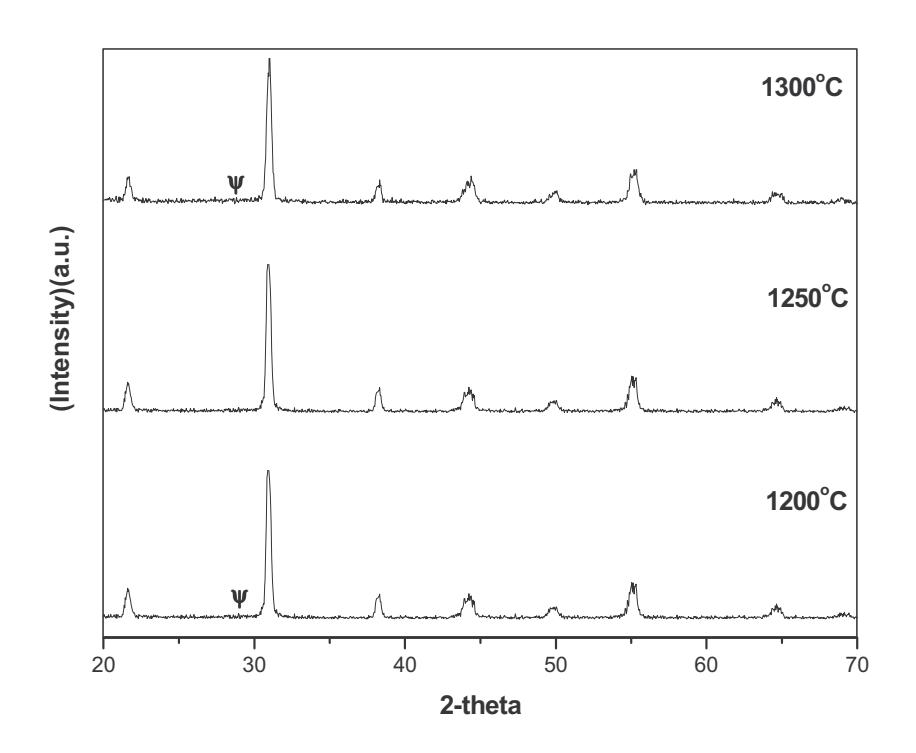


Figure 1. XRD patterns at room temperature of 0.05PZN-0.15PNN-0.8PZT ceramics.

Fig. 1 illustrates XRD patterns from this system. The pyrochlore-type structure was found in the sample sintered at 1200 and 1300°C, as indicated by ψ . In the other hand, pure peroskite was observed for the 1250 °C sintered sample. The formation of pyrochlore phase may be due to reaction between PbO and the columbite precursors or due to lead lose at high temperature.

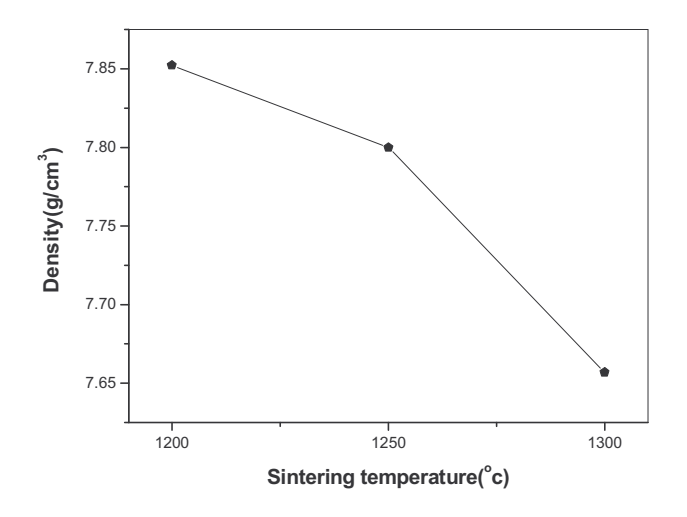


Figure 2. Density as a function of sintering temperature of 0.05PZN-0.15PNN-0.8PZT ceramics.

Fig. 2 shows the typical sintered densities of 0.05PZN-0.15PNN-0.8PZT ceramics for various sintering temperature. Although the pure perovskite phase was found at 1250°C, the density of the sample was observed to decrease with increasing sintering temperature. The decreasing in density may be due to the PbO evaporation at high temperature.



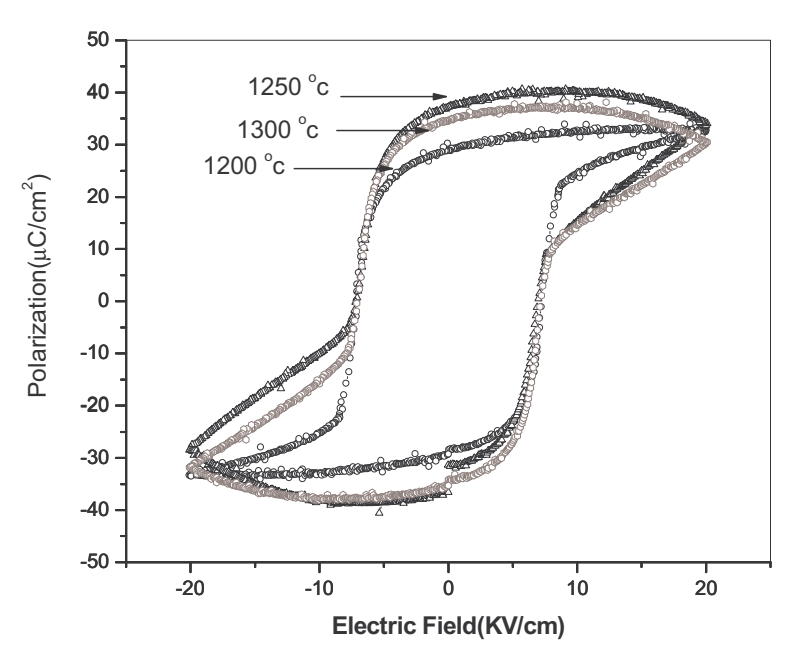


Figure 3. Polarization vs. electrical field for 0.05PZN-0.15PNN-0.8PZT ceramics.

The result of polarization-field (P-E) measurements for the ceramics sintered at various temperatures is shown in Fig. 3. All samples showed normal ferroelectric behavior with a rectangular loop. High polarization was observed for all samples. The optimum ferroelectric with higher remanent polarization (Pr) of 40 μ C/cm² was observed for the sample sintered at 1250°C, as expected. The lower remanent polarization in other sintering conditions may due to the formation of pyrochlore phase in the samples which made the ceramics have lower ferroelectric behavior. However, coercive field (E_c) was ~ 7.2 kV/cm for all sintering conditions.

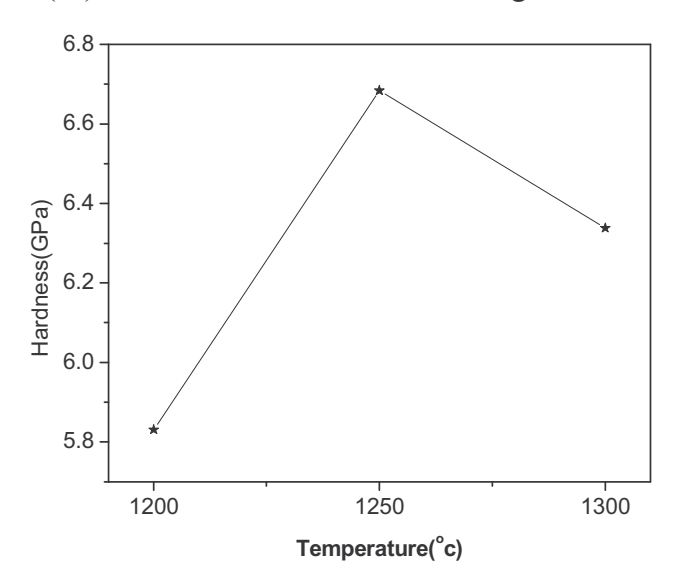


Figure 4. The 1250°C sintered sample displayed a higher hardness than the other samples.

The results of hardness measurements are shown in Fig. 4. The higher hardness value was 6.7 GPa. In the present work, the grain size of the system was found to increase with increasing the sintering temperature. Therefore, the existent of pyrochlore phase may result in the lower mechanical property of the samples.



Summary

In this work, 0.05PZN-0.15PNN-0.8PZT ceramics were synthesized via a columbite method. The sintering temperature of 1250°C was selected as the optimum sintering condition for preparation of the 0.05PZN-0.15PNN-0.8PZT ceramics. Pyrochlore phase was found to effect on the ferroelectric and mechanical properties of the ceramics.

Acknowledgements

This work was supported by The Thailand Research Fund (TRF), National Metal and Materials Technology Center (MTEC), Faculty of Science and Graduate School Chiang Mai University, and Commission on Higher Education (CHE) Thailand. The authors would like to thank Prof. Dr. Tawee Tunkasiri for his help in many facilities.

- [1] K. Uchino: Ferroelectric Devices (Marcel Dekker, New York, 2000).
- [2] A. J. Moulson and J. M. Herbert: *Electroceramics Materials Properties and Applications* (Chapman and Hall, New York, 1990).
- [3] K. Uchino: Solid State Ionics Vol. 108 (1998), p. 43.
- [4] L.E. Cross: Ferroelectrics Vol.76 (1987), p. 241.
- [5] T.R. Shrout and A. Halliyal: Journal of American Ceramics Society Bull. (1987).
- [7] K. Uchino: Ferroelectrics Vol.151 (1994), p. 321.
- [8] K. Uchino: Solid State Ionics Vol.108 (1998), p. 43.
- [9] K. Uchino: *Piezoelectric Actuators and Ultrasonic Motors* (Kluwer Academic Publishers, Boston, MA, 1996).
- [10] N. Vittayakorn, C. Puchmark, G. Rujijanagul, X. Tan, and D. P. Cann: J. Appl. Phys. Vol.6 (2006), p. 303.
- [11] N. Vittayakorn, G. Rujijanagul, X. Tan, M. A. Marquardt, and D. P. Cann: J. Appl. Phys. Vol. 96 (2004), p. 5103.
- [12] S. Nabunmee, G. Rujijanagul, N. Vittayakorn, D. P. Cann: J. Appl. Phys. Vol.102 (2007), p. 094108.



Effect of Calcination Temperatures on Microstructure and Phase Formation of Ba(Zr_{0.25}Ti_{0.75})O₃ Powders

T. Bongkarn^{1,a*}, N. Phungjitt^{2,b} and N. Vittayakorn^{3,c}

¹Department of Physics, Faculty of Science, Naresuan University, Phitsanulok, Thailand ²Department of Physics, Faculty of Science, Uttaradit Rajabhat University, Uttaradit, Thailand ³Department of Chemistry, Faculty of Science, King Mongkut's Institute of Technology Ladkrabang, Bangkok, Thailand

^areseachcmu@yahoo.com, ^bnalinee_amp@hotmail.com, ^cnaratipcmu@yahoo.com

Keywords: Barium zirconate titanate, Microstructure, Phase formation, Solid state reaction

Abstract. In this work, the effect of calcination temperatures on the microstructure and phase formation of Ba($Zr_{0.25}Ti_{0.75}$)O₃ (BZT) powders were investigated. The BZT powders were prepared via the solid state reaction method under various calcination temperatures. It was found that the second phases such as BaCO₃, ZrO_2 , Ba ZrO_3 and Ba $_2ZrO_4$ existed in samples with calcination temperature below 1200 °C. Homogeneity and a highly pure perovskite phase of the BZT powders were obtained with calcination condition at 1300 °C for 4 h. Lattice parameter *a* and the percentage of cubic perovskite phase tended to increase with increasing calcination temperatures. The TG-DTA results corresponded to the XRD investigation. The microstructures of calcined powders exhibited an almost-spherical morphology and had a porous agglomerated form in all samples. The average particle sizes were increased from 0.2 to 1.1 μm when calcination temperatures were increased from 800 to 1350 °C.

Introduction

Barium titanate (BaTiO₃; BT) is well known as a fundamental ferroelectric perovskite oxide and is often used in multilayer ceramic capacitors (MLCs) due to its high dielectric constant [1,2]. BaTiO₃ displays dielectric anomalies at 130, 0, and -90 °C with respective transformations in symmetry from cubic to tetragonal, from tetragonal to orthorhombic, and from orthorhombic to rhombohedral. Those anomalies are accompanied by a high dielectric constant near the phase transition [3]. Barium zirconate titanate Ba(Zr_xTi_{1-x})O₃ is obtained by substituting ions at the B site of BaTiO₃ with Zr ions. This substitution results were in a decrease of the temperature and a broadening of the permittivity maximum [4-6]. At a Zr/Ti ratio greater than 0.10, the three dielectric constant peaks coalesce into a single broad maximum [7]. Moreover, the transition temperature of BZT shifts to a lower temperature region with the increase of the Zr content. The dielectric study of the [Ba(Zr_xTi₁₋₁] _x)O₃] ceramics with x=0.20 and 0.25 showed a normal ferroelectric with weak diffuse phase transition behaviors [8]. The diffuse phase transition and a relaxor-like behavior were found at higher Zr contents (x=0.30 and 0.35). The high tunability and the value of figure of merit (FOM) of the $[Ba(Zr_xTi_{1-x})O_3]$ with x=0.25 ceramic measured at room temperature under the biasing field 20 kV/cm are 58% and 135, respectively [8,9]. This makes [Ba(Zr_xTi_{1-x})O₃] ceramic a promising material for tunable capacitor applications. Successfully, [Ba(Zr_xTi_{1-x})O₃] ceramics were prepared via sol-gel process and mixed oxide method [8,9]. However, the detail of calcined temperatures affected crystal structure and morphology evolution of [Ba(Zr_xTi_{1-x})O₃] powders, which synthesis by solid state reaction method have been reported yet. Therefore, in the present work, the effect of calcination temperatures on microstructure and the phase formation of [Ba(Ti_{0.75}Zr_{0.25})O₃; BZT] powders prepared via a solid state reaction method was studied.



Experimental

The starting materials were commercially available barium carbonate; BaCO₃ (99%), titanium (IV) oxide; TiO₂ (99%) and zirconium (IV) oxide; ZrO₂ (99%). Barium zirconate titanate [Ba(Zr_{0.25}Ti_{0.75})O₃, BZT] powder was synthesized by the solid state reaction of thoroughly ground mixtures of BaCO₃, TiO₂ and ZrO₂ powders that were by a ball milling procedure (zirconia milling media under ethanol for 24 h). Drying was carried out at 120 °C for 4 h. After sieving, various calcination temperatures, ranging from 800 to 1350 °C, with a dwell time of 4 h and a heating /cooling rate of 5 °C/min, were performed. The reaction of the uncalcined BZT powders taking place during heat treatment were investigated by thermogravimetric and differential thermal analysis (TG-DTA) using a heating rate of 10 °C/min from room temperature up to 1350 °C. Calcined powders were subsequently examined at room temperature by X-ray diffraction (XRD; Philip PW3040/60 X' Pert Pro) to identify the phase formed and the optimum calcination temperature of BZT powders. Powder morphologies and particle sizes were directly imaged, using scanning electron microscopy (SEM; LEO 1455 VP).

Results and discussion

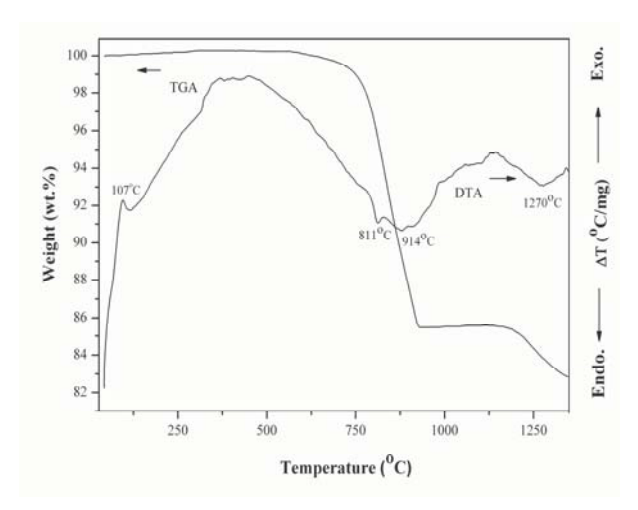


Figure 1. The DTA-TGA curve for the mixture of BZT powders.

The TG-DTA curves recorded at a heating rate of 10 °C/min in air for an equimolar mixture in the stoichiometric proportion of BZT is displayed in Fig. 1. The TG curve shows two distinct weight losses. The first weight loss occurs around 780 °C and the second one above 1190 °C. The sample shows a small exothermic peak in the DTA curve ~107 °C. This DTA peak can be attributed to the vaporization of water. No anomaly was observed from the TG pattern at this temperature. This may indicate that the small amount of vaporization of water could not be detected by the TG measurement. The first weight loss is attributed to the transition from witherite orthorhombic BaCO₃ to the rhombohedral phase [10]. In the second fall of specimen weight, a solid state reaction between BaCO₃, TiO₂ and ZrO₂ was observed. The broad endothermic characteristic of the DTA curve showed

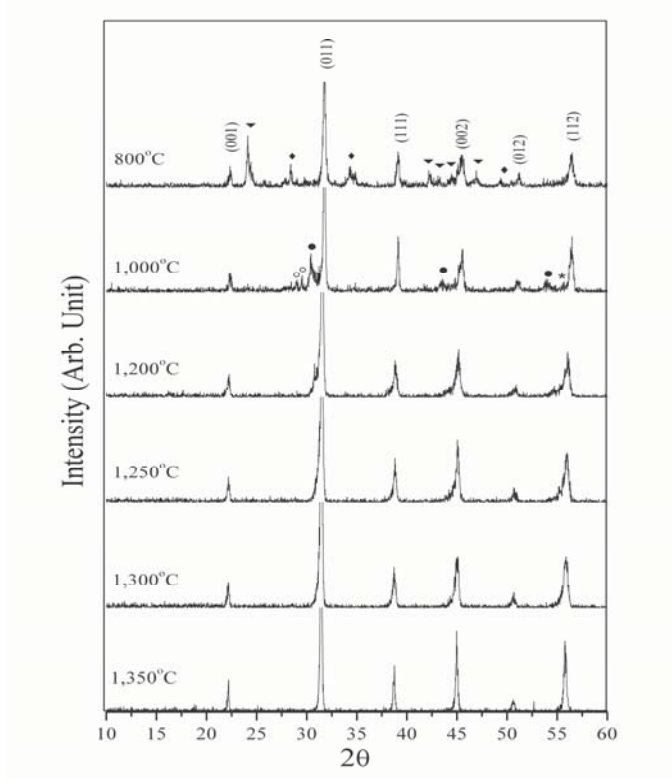
that these chemicals reacted most strongly at a minimum peak of 914 °C. Moreover, another endothermic peak with a minimum at 1270 °C was also observed in this profile. These data were used to define the range of optimum calcination temperatures from 800 to 1350 °C.

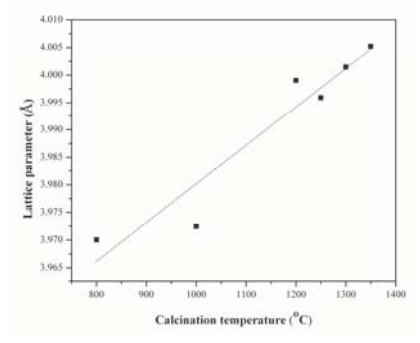
To further study the phase development with increased calcination temperatures in the powders, they were calcined for 4 h in normal air at various temperatures up to 1350 °C, followed by phase analysis using XRD. XRD patterns of the BZT powders formed with different calcinations temperatures are given in Fig. 2. After calcination at 800 °C, the crystalline phase of BZT was accompanied with BaCO₃ and ZrO₂ as separate phases, whose X-ray peak matched with the JCPDS file number 41-0373 and 24-1165. As the temperature increased to 1000 °C, the peaks corresponding to the raw materials disappeared, while the intensity of the BaZrO₃, BaTiO₃ and Ba₂ZrO₄ peaks become minor phases, which can correlate with JCPDS file number 41-0726 and 24-0130, respectively. After calcination at 1250 °C, the peaks corresponding to BaZrO₃ and Ba₂ZrO₄ were not detectable, whereas the BaTiO₃ phase remained. Evidently, a single phase of BZT is formed by calcination at 1300 °C. This observation agrees well with those derived from the TG-DTA results.

The strong reflections in the majority of the XRD patterns indicate the formation of the BZT perovskite phase, which can be matched with the JCPDS file number 36-0019. To a first approximation, this phase has a cubic perovskite type structure in the space group Pm-3m (no.221)



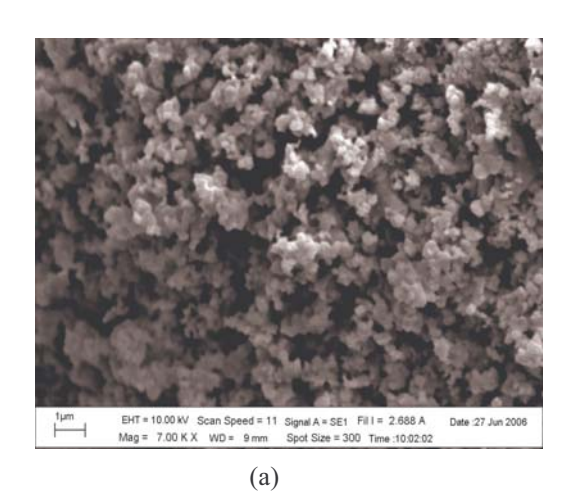
with a cell parameter a=4.0520 Å. The lattice parameter a as a function of calcination temperatures of this study is shown in Fig. 3. The lattice parameter was increased with the increasing of calcinations temperatures. This indicated that the calcination temperatures have a direct significance on lattice parameter and unit cell volume. The relative amount of perovskite and impurity phases were determined by measuring the major XRD peak intensities of the perovskite and impurity phases. Fig. 4 shows the percentage of the BZT perovskite phase as a function of calcination temperatures. The percentage of the BZT perovskite phase was increased with increasing calcination temperatures. The calcined powders, ranging from 800 to 1250 $^{\circ}$ C, were not achieved 100% of the time. The single phase of perovskite of the calcined samples at higher temperatures than 1300 $^{\circ}$ C is formed.





SEM photographs of BZT powders calcined at 1000 and 1300 $^{\circ}$ C are shown in Fig. 5. These powders exhibited an almost spherical morphology and have a porous agglomerated form. As the temperatures increased, more agglomerate particles could be observed. The average particle size tended to increase as calcination temperatures increased. The average particle size was 0.2, 0.3, 0.6, 0.8, 0.9 and 1.1 μ m for the powders calcined at 800, 1000, 1200, 1250, 1300 and 1350 $^{\circ}$ C, respectively.





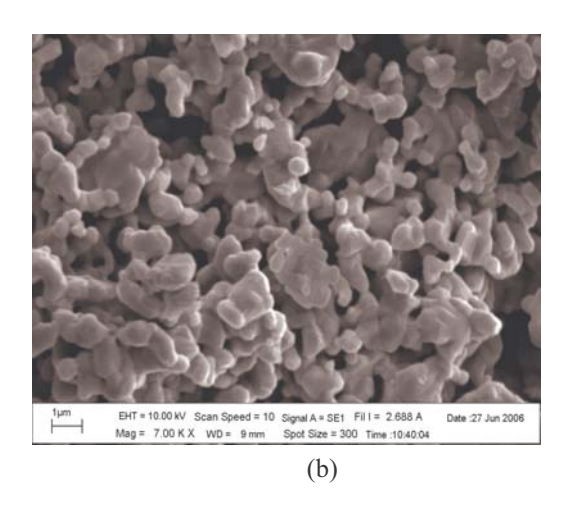


Figure 5. SEM photomicrographs of BZT powders calcined at (a) 1000 °C and (b) 1300 °C.

Summary

It has been shown that the pure perovskite phase of $Ba(Ti_{0.75}Zr_{0.25})O_3$ powders can be formed through the reaction of barium carbonate, titanium (IV) oxide and zirconium (IV) oxide with calcined temperatures at 1300 °C. Evidence of the formations of minor phases of $BaZrO_3$, $BaTiO_3$ and Ba_2ZrO_4 , which coexists with the perovskite phase, is found at calcinations temperatures ranging from 1000-1250 °C. The calcination temperatures have a strong influence on the crystal structure, homogeneity and the unit cell volume of the calcined powders. The resulting microstructure of the BZT powders were more agglomerated as the calcination temperatures increased.

Acknowledgments

This work was supported financially by the Thailand Research Fund (TRF), Commission on Higher Education (CHE), and Naresuan University. Thanks also to the Uttaradit Rajabphat University and King Mongkut's Institute of technology, Ladkrabang (KMITL) for supporting facilities. Acknowledgement is also given to Mr. Don Hindle, for his helpful comments and correction of the manuscript.

- [1] W.S. Clabaugh, R. Swiggard and R.Gilchrist: J. Res. Nat. Bur. Stds. Vol. 56 (1956), p. 289.
- [2] Y. Sakabe, K. Minai and K. Wakino: Jpn. J. Appl. Phys. Suppl. Vol. 20 (1981), p.147.
- [3] B. Jaffe, J. Cook and H. Jaffe: *Piezoelectric Ceramics* (Academic Press, London, U.K., 1997).
- [4] E. J. Brajer: U.S. Patent 2, 708, 243. (1955).
- [5] F. Kulscar: U.S. Patent 2, 735, 024. (1956).
- [6] W. Ulrich, G. Georg B. Ulrich, W. Sophie, H. Detlev and W. Rainer: J. Am. Ceram. Soc. Vol. 84 (2001), p. 759.
- [7] D. Hennings, A. Schnell and G. Simon: J. Am. Ceram. Soc. Vol. 65 (1982), p. 539.
- [8] X.G. Tang, K.H. Chew and H.L.W. Chan: Acta Mater. Vol. 52 (2004), p. 5177.
- [9] R. Liang, X. Dong, Y. Chen, F. Cao and Y. Wang: Ceram. Int. Vol. 33 (2007), p. 957.
- [10] A. S. Seveyrat, A. Hajjaji, Y. Emziane, B. Guiffard and D. Guyomar: Ceram. Int. Vol 35 (2007), p. 35.



Dielectric properties of Pb[$(1-x)(Zr_{1/2}Ti_{1/2})-x(Zn_{1/3}Ta_{2/3})]O_3$ ceramics prepared by columbite and wolframite methods

Wanwimon Banlue · Naratip Vittayakorn · Chien-Chih Huang · David P. Cann

Received: 15 January 2008/Accepted: 24 March 2008/Published online: 9 April 2008 © Springer Science+Business Media, LLC 2008

Abstract Polycrystalline samples of Pb[$(1 - x)(Zr_{1/2}Ti_{1/2})$] $-x(\text{Zn}_{1/3}\text{Ta}_{2/3})]O_3$, where x = 0.1-0.5 were prepared by the columbite and wolframite methods. The crystal structure, microstructure, and dielectric properties of the sintered ceramics were investigated as a function of composition via X-ray diffraction (XRD), scanning electron microscopy (SEM), and dielectric spectroscopy. The results indicated that the presence of Pb(Zn_{1/3}Ta_{2/3})O₃ (PZnTa) in the solid solution decreased the structural stability of overall perovskite phase. A transition from tetragonal to pseudo-cubic symmetry was observed as the PZnTa content increased and a co-existence of tetragonal and pseudo-cubic phases was observed at a composition close to x = 0.1. Examination of the dielectric spectra indicated that PZT-PZnTa exhibited an extremely high relative permittivity at the MPB composition. The permittivity showed a ferroelectric to paraelectric phase transition at 330 °C with a maximum value of 19,600 at 100 Hz at the MPB composition.

Introduction

Lead zirconate titanate $Pb(Zr_{1-x}Ti_x)O_3$ perovskite solid solutions (PZT) are normal ferroelectric ceramic materials

W. Banlue · N. Vittayakorn (⋈)
Materials Science Research Unit, Department of Chemistry,
Faculty of Science, King Mongkut's Institute of Technology
Ladkrabang, Bangkok 10520, Thailand
e-mail: naratipcmu@yahoo.com

C.-C. Huang · D. P. Cann Materials Science, School of Mechanical, Industrial, and Manufacturing Engineering, Oregon State University, Corvallis, OR 97331, USA

with many important practical applications including piezoelectric devices, ferroelectric memories, high ε capacitors, and infrared pyroelectric detectors, by utilizing their excellent piezoelectric, ferroelectric, and pyroelectric properties [1, 2]. The anomalous piezoelectric properties of PZT ceramics near the morphotropic phase boundary (MPB) separating two ferroelectric phases, namely, rhombohedral and tetragonal phases at low and high Ti contents, respectively [3]. Recently, the new free energy formulation automatically predicts equilibrium PZT phase diagram with two-phase region replacing the linear MPB and satisfying the Gibbs phase rule [4]. Identifying the MPB in the phase equilibria in ferroelectric systems is very important in order to obtain the optimum electrical properties. Therefore, most commercial ferroelectric ceramics are designed in the vicinity of the MPB with various doping schemes in order to take advantage of the superior dielectric and piezoelectric properties [5, 6].

Recently, many piezoelectric ceramic materials have been developed from binary systems containing a combination of normal ferroelectrics with tetragonal symmetry and relaxor ferroelectrics with rhombohedral symmetry near the MPB. These systems can yield high dielectric permittivities such as in PMN-PT [7] and PZN-PT [8], excellent piezoelectric coefficients such as in PZN-PZT [9] and PSN-PT [10], and high pyroeletric coefficients such as in PNN–PT–PZ [11]. The low phase-transition temperature of some members of the lead-based tantalate family $Pb(B_{1-x}Ta_x)O_3$, in which B is Zn^{2+} , Mg^{2+} and Ni^{2+} , make them important candidates for utilization in devices such as low-temperature capacitors and actuators for space applications [12]. Lead zinc tantalate Pb(Zn_{1/3}Ta_{2/3})O₃ solid solutions (PZnTa) possess the perovskite structure and exhibit relaxor ferroelectric behavior. Nevertheless, synthesis of perovskite lead zinc tantalate Pb(Zn_{1/3}Ta_{2/3})O₃

(PZnTa) has been unsuccessful until now [13]. It is well-known that during the phase-formation process of lead-based perovskite materials a pyrochlore-type phase $(A_2B_2O_{7-\delta})$ with low dielectric permittivity precedes the formation of the perovskite phase. The failure can be attributed to the higher covalency of Zn^{2+} and Ta^{5+} as well as to the somewhat larger ionic size of Zn^{2+} as compared to the sixfold lattice sites formed by the oxygen octrahedra. A columbite–wolframite process was then introduced to promote the development of the perovskite phase and to suppress the formation of the pyrochlore phase [13–15].

Since both PZT and PZnTa have the perovskite structure, it is suggested that PZnTa can be alloyed with PZT in order to stabilize and optimize the PZnTa ceramics. Recently our previous work [9, 16] has shown promise in producing phase-pure perovskite solid solutions based on $Pb(Zr_{1/2}Ti_{1/2})$ O_3 -Pb($Zn_{1/3}Nb_{2/3}$) O_3 (PZT-PZN) via the columbite method. The binary system of (1 - x)PZT - xPZN exhibited two MPBs at the compositions x = 0.5 and $x \sim 0.2-0.3$. The maximum value of d_{33} (>600 pC/N) and the highest k_n (~ 0.7) were recorded for the composition x = 0.3. In addition, Nb and Ta belong to the same group in the periodic table and the have the same ionic radii. It is expected that excellent properties can be obtained from ceramics in PZT-PZnTa system. So far, there have been no systematic studies on the structural and dielectric properties over the entire range of PZT-PZnTa solid solutions. In the present study, PZT and PZnTa were chosen as end components to prepare solid solutions via a columbite-wolframite precursor method. Crystal structure and microstructure were investigated by XRD and SEM analysis, respectively. Finally, the dielectric properties of PZT-PZnTa ceramics were determined as a function of temperature and frequency to establish structure-property relationships.

Experimental

The perovskite-phase powders were synthesized using a columbite–wolframite precursor method in order to avoid the formation of a pyrochlore phase. Powders of ZnO (99.9%), Ta_2O_5 (99.9%), PbO (Fluka, >99% purity), TiO_2 (99.8%), and ZrO_2 (99%) were used as the starting materials. The following reaction sequences are proposed for the formation of PZT–PZnTa:

$$ZnO_{(s)} + Ta_2O_{5(s)} \rightarrow ZnTa_2O_{6(s)}$$
 (1)

$$ZrO_{2(s)} + TiO_{2(s)} \rightarrow ZrTiO_{4(s)}$$
 (2)

$$\begin{array}{l} PbO_{(s)} \,+\, (1-x)/2 \; Zr TiO_{4(s)} \,+\, x/3 \; Zn Ta_2 O_{6(s)} \\ \to Pb \big[(1-x) \big(Zr_{1/2} Ti_{1/2} \big) - x \big(Zn_{1/3} Ta_{2/3} \big) \big] O_{3(s)} \end{array} \eqno(3)$$

The columbite precursor $ZnTa_2O_6$ was prepared from the reaction between ZnO and Ta_2O_5 at 1,100 °C for 4 h and

then ZrO₂ was reacted with TiO₂ at 1,400 °C for 4 h to form ZrTiO₄. The precursors ZnTa₂O₆, ZrTiO₄ and PbO (with 2 mol% excess PbO) were weighed according to the compositions of Pb[$(1 - x)(Zr_{1/2}Ti_{1/2}) - x(Zn_{1/3}Ta_{2/3})]O_3$ with x = 0.1-0.5. Each mixture of the starting powders was milled and mixed in a ball mill, as well as wet-homogenized with ethanol using nylon-coated YTZ zirconia milling as media for 18 h. After drying, the mixtures were calcined at 700-950 °C for 4 h in an alumina crucible and configured with a heating rate of 20 °C/min. The calcined powders were milled for 3 h in order to reduce the particle size. After grinding and sieving, the calcined powders were mixed with 5 wt% polyvinyl alcohol binder and uniaxially pressed into pellets. Binder burnout occurred by slowly heating to 500 °C and holding for 2 h. Sintering occurred between 1,100 and 1,250 °C with a dwell time of 4 h. To mitigate the effects of lead loss during sintering, the pellets were sintered in a closed alumina crucible containing PbZrO₃ powder. PZT-PZnTa ceramics were subsequently examined by room temperature X-ray diffraction (XRD; Philips PW 1729 diffractometer), using Ni-filtered CuK_{\alpha} radiation to identify the perovskite structure. The relative amounts of perovskite and pyrochlore phase were then determined by measuring the primary X-ray peak intensities of the perovskite and pyrochlore phase. The density of the sintered PZT-PZnTa pellets was measured by the water immersion method (Archimedes method). The relative density of all the sintered pellets in this study was approximately 94–96% of the theoretical density. To determine the dielectric properties, the maximum density sample for each composition samples was ground on both surfaces and silver electrodes were applied using a low-temperature silver paste by firing at 500 °C for 30 min. The capacitance was measured with a HP4284A LCR meter in connection with a sample holder (Norwegian Electroceramics) capable of high temperature measurement. The relative permittivity (ε_r) was calculated using the geometric area and thickness of the discs.

Result and discussion

The XRD patterns of (1 - x)PZT - xPZnTa ceramics with various x values are shown in Fig. 1. The patterns show a single-phase perovskite for the compositions x = 0.1 and 0.2. A cubic pyrochlore phase $Pb_{1.83}(Zn_{0.29}Ta_{1.71})O_{6.39}$ (Powder diffraction Files No. 34-395), identified with "*", began to develop at x = 0.3 and increased in intensity with increasing PZnTa concentration. No evidence of a cubic phase of $Pb_{1.49}Ta_2O_{6.28}$ (Powder diffraction Files No. 84-1732) was found. These results indicate that the presence of PZnTa in the solid solution decreased the structural stability of the PZT perovskite phase due to its tolerance factor and electronegativity [13]. It is interesting to note that the pure



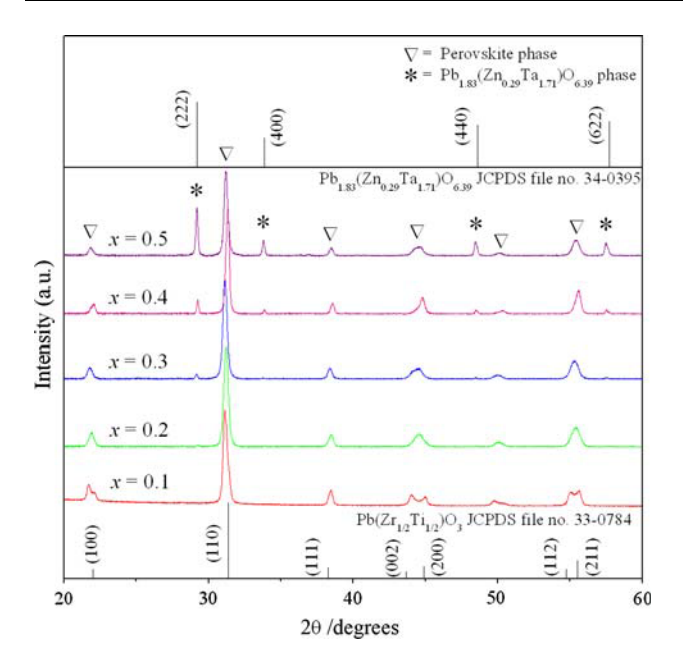


Fig. 1 XRD patterns of (1 - x)PZT - xPZnTa ceramics prepared by columbite-wolframite method as a function of composition

perovskite phase in (1 - x)PZT - xPZnTa can only be obtained for $x \le 0.2$. This is a significant contrast to the $(1 - x)PZT - xPb(Zn_{1/3}Nb_{2/3})O_3$ system in which the perovskite phase can be obtained up to $x \le 0.5$. The results indicate that it is more difficult to obtain a pure perovskite phase in tantalate systems than in niobates.

Although Nb and Ta belong to the same periodic group, Ta⁵⁺ has stronger covalent properties [17]. It is well known that an increase in covalent bond strength decreases the thermodynamic stability of the perovskite structure [13]. This is likely the main reason it is difficult to obtain the perovskite phase in the tantalate system. Studies on the stabilization of the perovskite phase in solid solutions of PZN and PZnTa with BT, PMN and PMT also showed an easier stabilization of the perovskite structure in PZN, due to the higher ionic strength of Nb–O bonds [18].

SEM micrographs of a fractured surface of PZT–PZnTa ceramics are shown in Fig. 2a and b, respectively. The micrograph of 0.9PZT–0.1PZnTa (Fig. 2a) shows a highly homogeneous microstructure. These micrographs indicate that average grain size was in the range of 1.27 μm , and the fracture occurred mostly by intergranular mechanisms. The 0.5PZT–0.5PZnTa ceramic showed a very heterogeneous microstructure (Fig. 2b) with a large amount of pyrochlore phase, as XRD patterns also indicated.

The $PbZrO_3-PbTiO_3$ phase diagram predicts that at room temperature $Pb(Zr_{1/2}Ti_{1/2})O_3$ falls within the tetragonal phase field near the MPB. The crystal symmetry for PZnTa-based perovskite is cubic at room temperature. Below the phase transition temperature the symmetry changes to rhombohedral. Since PZnTa has a low phase

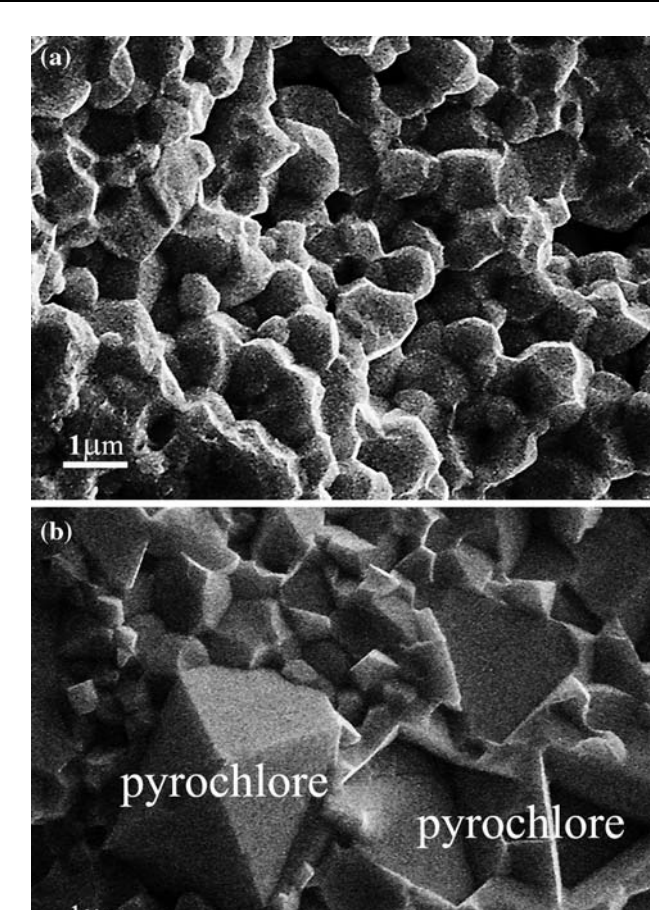


Fig. 2 SEM images of the grain morphology in (1 - x)PZT - xPZnTa ceramics for (**a**) x = 0.1 and (**b**) x = 0.5

transition temperature, with increasing x the crystal symmetry should change due to the decrease in phase transition temperature. It is well known that in the pseudo-cubic phase the $\{2\ 0\ 0\}$ profile will show a single narrow peak because all the planes of $\{2\ 0\ 0\}$ share the same lattice parameters, while in the tetragonal phase the $\{2\ 0\ 0\}$ profile should be split into two peaks with the intensity height of the former being half of the latter because the lattice parameters of $(2\ 0\ 0)$ and $(0\ 2\ 0)$ are the same but are slightly different from those of $(0\ 0\ 2)$.

Figure 3 shows the evolution of the $(2\ 0\ 0)$ peak as a function of composition. At low PZnTa concentrations, the XRD pattern shows strong (200) peak splitting which is indicative of tetragonal symmetry. As the PZnTa concentration increased, the $(2\ 0\ 0)$ reflection transformed to a single peak which suggests pseudo-cubic symmetry. To a first approximation, it could be said that the composition with x=0.1 is close to the MPB, where the structure of the PZT–PZnTa compositions gradually shifts from tetragonal to pseudo-cubic symmetry as the PZnTa content increased. Dielectric data described later further supports this



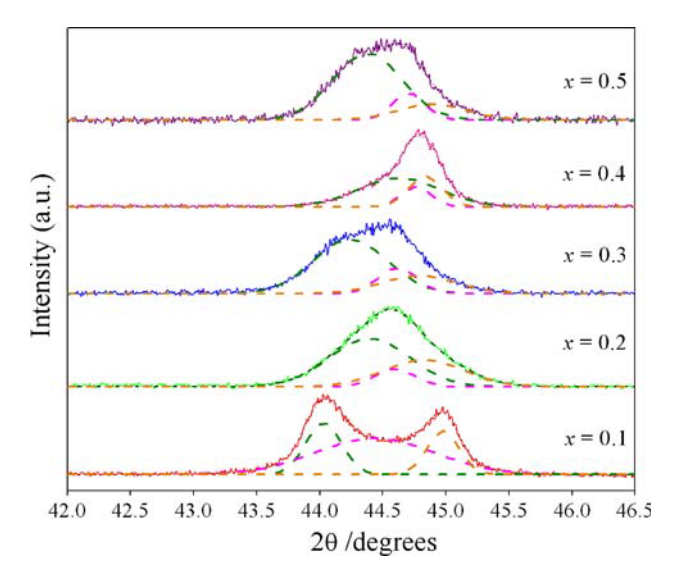


Fig. 3 XRD pattern of the (200) peak of (1 - x)PZT - xPZnTa ceramics, for x = 0.0–0.5

assumption. It is interesting to note that the influence of the addition of PZnTa on the phase transition of Pb(Zr $_{1/2}$ Ti $_{1/2}$)O $_3$ is similar to that of the Pb(Zr $_{1/2}$ Ti $_{1/2}$)O $_3$ -Pb(Ni $_{1/3}$ Nb $_{2/3}$)O $_3$, Pb(Zr $_{1/2}$ Ti $_{1/2}$)O $_3$ -Pb(Co $_{1/3}$ Nb $_{2/3}$)O $_3$, and Pb(Zr $_{1/2}$ Ti $_{1/2}$)O $_3$ -Pb(Zn $_{1/3}$ Nb $_{2/3}$)O $_3$ systems [9, 19–21].

The characteristic temperature dependence of the dielectric constant at 100 Hz for (1-x)PZT - xPZnTa, where x = 0.1–0.5, is shown in Fig. 4. The transition temperatures and maximum dielectric constants of the 0.9PZT–0.1PZnTa ceramics in this work were 330 °C and 19,600, respectively. The frequency dependence of dielectric properties for x = 0.1 and 0.5 ceramics are shown in Fig. 5a and b. For 0.9PZT–0.1PZnTa (Fig. 5a), the dielectric constants peak is sharp and approaches 19,600. The dielectric properties of 0.9PZT–0.1PZnTa ceramic change significantly with

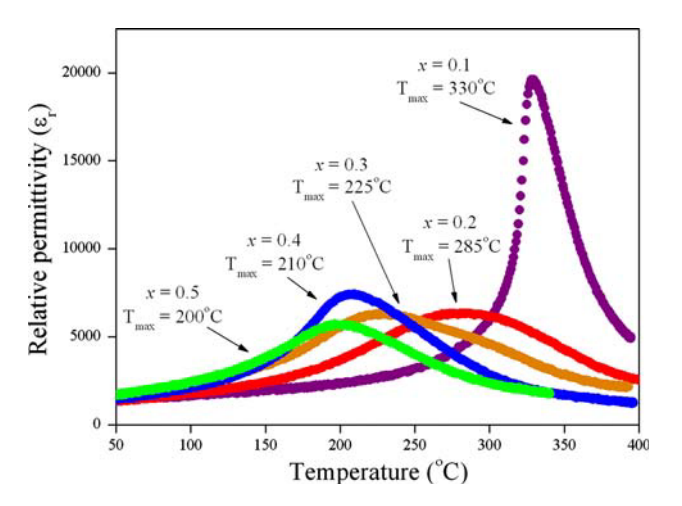
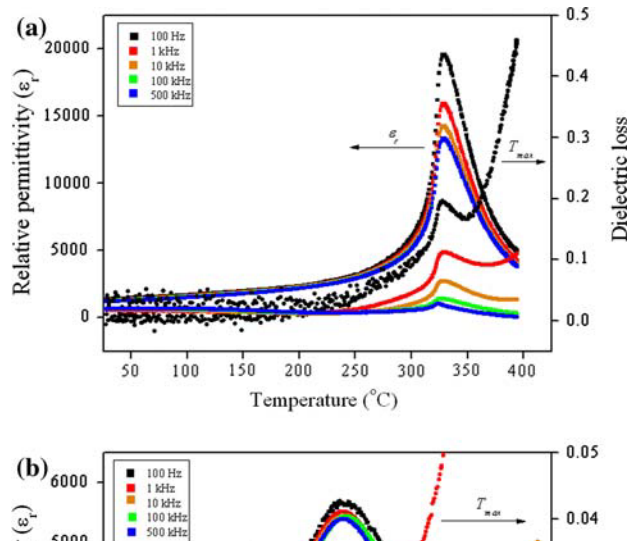


Fig. 4 Variation of the dielectric constant with temperature for (1 - x) PZT - xPZnTa ceramics at 100 Hz



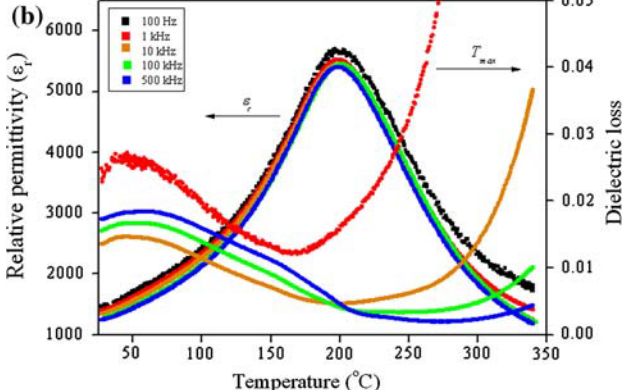


Fig. 5 Temperature and frequency dependence of the dielectric properties for: (a) x = 0.1 and (b) x = 0.5 ceramics

temperature, but are nearly independent of frequency, except in the vicinity of the phase transformation temperature [22, 23]. This is a typical characteristic of ferroelectric ceramics with a long-range ordered structure. It is well known that PZT exhibits normal ferroelectric behavior and PZnTa is a relaxor ferroelectric material as a result of a short-range ordered structure with a nanometer scale compositional heterogeneity [24]. The nature of the homogeneously polarized states is believed to be primarily controlled by the concentration of PZnTa. When PZnTa is added to form the binary system with PZT, a clear shift of the transition temperature to lower temperatures was observed. Furthermore, the dielectric peak broadened indicating an increase in the diffuseness of the phase transition. It should also be noted here that, in all compositions, the dielectric properties increased significantly at high temperatures as a result of thermally activated space charge conduction. The variation in the transition temperature with composition and other dielectric data is listed in Table 1. The Curie temperature significantly decreased with increasing PZnTa content up to 30 mol%. However, for the compositions 0.3 < x < 0.5, transition temperature remained at a nearly constant value between 200 and 225 °C. This is consistent with the X-ray



diffration findings that indicated the co-existence of a pyrochlore phase for these compositions.

A modified Curie–Weiss law can be used to model the dielectric behavior of a normal ferroelectric in solid solution with a relaxor ferroelectric with a diffuse phase transition. The formulation is as follows:

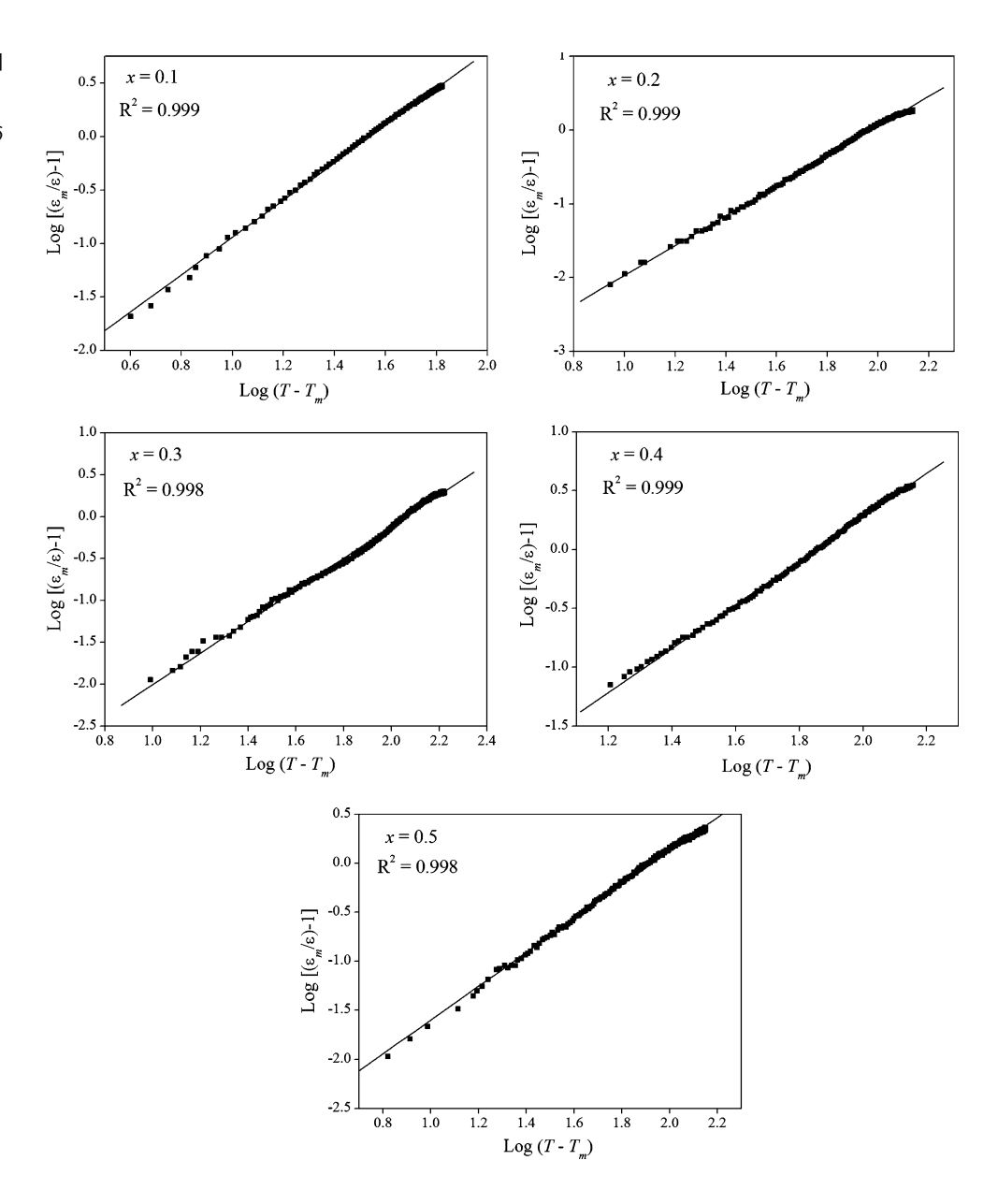
$$\frac{\varepsilon'_{\rm m}}{\varepsilon'(f, T)} = 1 + \frac{(T - T_{\rm m}(f))^{\gamma}}{2\delta_{\gamma}^2} \tag{4}$$

where $1 \le \gamma \le 2$. When $\gamma = 1$, Eq. 4 simplifies to the Curie–Weiss law; when $\gamma = 2$ this equation describes the ideal relaxor behavior with a quadratic dependence. The

Table 1 Dielectric properties of (1 - x)PZT - xPZnTa ceramics at 100 Hz

PZTa content (x)	ε_r at room temp.	tan δ at room temp.	T_{max} (°C)	ε_r at T_{\max}	tan δ at $T_{\rm max}$	δ_{γ} (°C)	γ
0.1	1,430	0.0102	330	19,600	0.193	13.51	1.74
0.2	1,280	0.0429	285	6,310	0.081	22.36	1.98
0.3	1,500	0.0282	225	6,290	0.066	21.11	1.89
0.4	1,340	0.0289	210	7,410	0.072	12.57	1.80
0.5	1,520	0.0163	200	5,690	0.039	11.87	1.72

Fig. 6 Plots of $\log[(\varepsilon_{\rm m}/\varepsilon)-1)]$ vs. $\log(T-T_{\rm m})$ for (1-x) PZT -xPZnTa ceramics. The solid lines are fits to Eq. 5. γ , δ and R^2 indicate fitting parameters (γ and δ) and correlation of the fit (R^2)





parameter $\varepsilon'_{\rm m}$ is the maximum value of the relative permittivity at $T=T_{\rm m}$ (f) and $\varepsilon'(f,T)$ is the relative permittivity of the sample. If $\log{[\varepsilon'_{\rm m}/\varepsilon'(f,T)-1]}$ is plotted versus $\log{[T-T_{\rm m}(f)]}$, the values of γ and δ_{γ} can be determined as seen in Fig. 6. The parameter γ was determined to be in the range of 1.72–1.98 and the diffuseness parameter δ_{γ} was measured to be 11.87–22.36, which confirms the diffuse phase transitions in PZT–PZnTa due to a high degree of disorder. The calculations suggest that the addition of PZnTa into PZT leads to lower degree of disorder but can be attributed to the pyrochlore phase present in high PZnTa-content compositions.

Conclusions

Ceramic solid solutions based on (1 - x) Pb $(Zr_{1/2}Ti_{1/2})$ $O_3 - (x)Pb(Zn_{1/3}Ta_{2/3})O_3$ (where x = 0.1, 0.2, 0.3, 0.4,and 0.5) were prepared via a columbite-wolframite method. The PZT-PZnTa solid solutions exhibit a singlephase perovskite structure for $x \le 0.2$. As the content of PZnTa increases (i.e., $x \ge 0.3$), a secondary pyrochlore phase Pb_{1.83}(Zn_{0.29}Ta_{1.71})O_{6.39} was formed. The results indicate that it is more difficult to obtain pure perovskite in tantalate solid solutions than it is in niobates solid solutions. The dielectric response of 0.9PZT-0.1PZnTa is closer to normal ferroelectric behavior, while the other compositions exhibit a diffuse phase transition. Investigations of the structure and properties of the PZT-PZnTa system over the range x = 0.1-0.5 have revealed an MPB at x = 0.1, separating a tetragonal phase from a pseudocubic phase. Examination of the dielectric spectra indicates that PZT-PZnTa exhibits a high relative permittivity at the MPB composition. The permittivity shows a ferroelectric to paraelectric phase transition at 330 °C with a maximum value of 19,600 at 100 Hz at the MPB composition.

Acknowledgements This work was supported by the Thailand Research Fund (TRF), the Commission on Higher Education (CHE),

the National Research Council of Thailand (NRCT), and the King Mongkut's Institute of Technology Ladkrabang (KMITL).

- Uchino K (2000) Ferroelectric devices. Marcel Dekker, Inc., New York
- Bhalla AS, Guo R, Roy R (2000) Mat Res Innovat 4:3. doi: 10.1007/s100190000062
- Jaffe B, Cook WR (1971) Piezoelectric ceramic. R.A.N. Publishers
- George A Rossetti J, Zhang W, Khachaturyan AG (2006) Appl Phys Lett 88:072912. doi:10.1063/1.2173721
- 5. Haertling GH (1999) J Am Ceram Soc 82:797
- Xu Y (1991) Ferroelectric materials and their application. Elsevier Science Publishers B.V
- Seung-Eek P, Shrout TR (1997) IEEE Trans Ultrason Ferroelectr Freq Control 44:1140
- Takenaka T, Muramata K, Fujii T (1992) Ferroelectrics 134:133. doi:10.1080/00150199208015577
- Vittayakorn N, Puchmark C, Rujijanagul G, Tan X, Cann DP (2006) Curr Appl Phys 6:303
- Bing Y-H, Ye Z-G (2006) J Cryst Growth 287:326. The 16th American Conference on Crystal Growth and Epitaxy – ACCGE 16
- Cornejo IA, Jadidian B, Akdogan EK, Safari A (1998) Dielectric and Electromechanical properties of PNN-PT-PZ system: a processing-property study. In: Proc IEEE ISAF'98
- 12. Kuwata J, Uchino K, Nomura S (1982) Jpn J Appl Phys 21:1298
- 13. Shrout TR, Halliyal A (1987) Am Ceram Soc Bull 66:704
- 14. Vittayakorn N, Wirunchit S (2007) Smart Mater Struct 16:851
- Vittayakorn N, Rujijanagul G, Tunkasiri T, Tan X, Cann DP (2003) J Mater Res 18:2882
- Vittayakorn N, Rujijanagul G, Tunkasiri T, Tan X, Cann DP (2004) Mater Sci Eng B 108:258
- 17. Ahn B-Y, Kim N-K (2002) J Mater Sci 37:4697
- 18. Kim J-S, Kim N-K (2003) J Am Ceram Soc 86:929
- Vittayakorn N, Rujijanagul G, Tan X, He H, Marquardt MA, Cann DP (2006) J Electroceram 16:141
- Vittayakorn N, Rujijanagul G, Tan X, Marquardt MA, Cann DP (2004) J Appl Phys 96:5103
- 21. Vittayakorn N, Tunkasiri T (2007) Phys Scr T129:199
- Koval V, Alemany C, Brianin J, Bruncková H (2004) J Electroceram 10:19
- Yimnirun R, Ananta S, Laoratanakul P (2005) J Eur Ceram Soc 25:3235
- Randall CA, Bhalla AS, Shrout TR, Cross LE (1990) Ferroelectrics 11:103



J. Phys. D: Appl. Phys. 41 (2008) 125406 (7pp)

Physical properties and phase transitions in perovskite $Pb[Zr_{1-x}(Ni_{1/3}Nb_{2/3})_x]O_3$ $(0.0 \leqslant x \leqslant 0.5)$ ceramics

1

Supamas Wirunchit¹, Pitak Laoratanakul² and Naratip Vittayakorn^{1,3}

- ¹ Material Science Research Unit, Department of Chemistry, Faculty of Science, King Mongkut's Institute of Technology Ladkrabang, Bangkok 10520, Thailand
- ² National Metal and Materials Technology Center (MTEC), Pathumthani 12120, Thailand

E-mail: naratipcmu@yahoo.com

Received 5 February 2008, in final form 30 March 2008 Published 23 May 2008 Online at stacks.iop.org/JPhysD/41/125406

A hetract

A solid solution of lead zirconate–lead nickel niobate ceramics, Pb[Zr_{1-x}(Ni_{1/3}Nb_{2/3})_x]O₃ (PZNN) with x=0.0–0.5, was synthesized via the columbite precursor method. The crystal structures as well as the thermal and dielectric properties were investigated in terms of the lead nickel niobate (PNN) concentration. X-ray diffraction indicated that all samples exhibited a single-phase perovskite structure. At room temperature, Pb[Zr_{1-x}(Ni_{1/3}Nb_{2/3})_x]O₃ is orthorhombic for a composition where x=0, rhombohedral for the compositions where x=0.1, 0.2 and 0.3 and pseudo-cubic for compositions where x=0.4 and 0.5. The results of the addition of lead nickel niobate to the lead zirconate ceramic showed enhancement of the room-temperature dielectric permittivity. Lead nickel niobate substitution also led to lower transition temperatures. Furthermore, this transition from normal to relaxor FE ceramics was typified by a quasi-linear relationship between the diffuseness parameter δ_{γ} and the PNN mole fraction x.

(Some figures in this article are in colour only in the electronic version)

1. Introduction

Since the discovery of antiferroelectricity in the perovskite structure in the 1950s, lead zirconate oxide (PbZrO₃ or PZ) has been the focus of extensive experimental and theoretical studies [1]. PbZrO₃ has a phase transition which occurs at ca $230\,^{\circ}$ C, but the transition from the orthorhombic antiferroelectric (AFE) structure to the rhombohedral ferroelectric (FE) structure a few degrees below the paraelectric (PE) transition temperature has been reported by several authors [2, 3]. Both AFE-to-FE and FE-to-PC phase transitions are first order and show a thermal hysteresis of around $10\,^{\circ}$ C [3, 4]. The structure of the PbZrO₃ is orthorhombic with $a = 5.87\,\text{Å}$, $b = 11.74\,\text{Å}$ and $c = 8.20\,\text{Å}$. Antiparallel shifts of Pb²⁺ ions in the PbZrO₃ are responsible for the quadrupling of the pseudo-cubic cell and the AFE behaviour [5, 6]. The characteristic double hysteresis loop

resulting from forward phase switching with zero remanent polarization makes AFE material compositions suitable for high charge storage applications [7, 8]. The most intensively studied AFE PbZrO₃ is chemically modified by adding Sn, Ti, Nb and Ba or La to adjust the critical field for the phase transition and to optimize properties for processing and applications [3,4]. PbZrO₃ was also studied for its microwave dielectric properties, but it shows a dielectric relaxation near microwave frequencies [9]. The FE relaxor PNN exhibits a broad maximum in the dielectric constant and a diffuse phase transition. Its Curie temperature is about -120 °C, and the maximum dielectric constant is about 3500 at 1 kHz [10].

Recently, many piezoelectric ceramic materials have been developed from binary systems containing combination types of piezoelectric materials which have high piezoelectric and dielectric properties [7, 8]. Much research has been done on solid solutions containing PZ, such as $Pb_{1-x}Ba_xZrO_3$ (PBZ) [4], $Pb(Zr_{1-x},Ti_x)O_3$

³ Author to whom any correspondence should be addressed.

PMN) [11, 12], $PbZrO_3-PbTiO_3-Pb(Zn_{1/3}Nb_{2/3})O_3$ (PZ-PT-PZN) [13–15] and $Pb(Zn_{1/3}Nb_{2/3})O_3-PbZrO_3$ (PZN–PZ) [16]. New piezoelectric ceramics for high-frequency ultrasonic transducer applications using modified PbZrO₃ ceramic compositions in a (1-x-y)PbZrO₃ + xPb $(Mn_{1/3}Nb_{2/3})$ O₃ + yPbTiO₃ system with an FE rhombohedral phase near the AFE orthorhombic phase $(0.0 < x \le 0.1 \text{ and } 0.0 < y \le 0.2)$ have been reported by Takeuchi et al [17]. Changes in the electromechanical properties of ceramics with compositions at the morphotropic phase boundary (MPB) in the rhombohedral phase (y = 0.05 and x = 0.05 and y = 0.025 and x = 0.1) were rather sharp, although no noticeable changes could be observed in the lattice parameters. The anisotropy of electromechanical coupling factors (k_t/k_p ratio) was 24 for x = 0.05 and y = 0.00, which is a boundary composition between the AFE orthorhombic phase and the FE rhombohedral phase. One of the most famous systems is the solid solution of the PbNi_{1/3}Nb_{2/3}O₃-PbTiO₃-PbZrO₃ (PNN-PT-PZ) system which has a MPB at a lead zirconate (PZ) concentration around 0.20-0.45 [18, 19]. At these PZ concentrations the longitudinal electromechanical coupling coefficient (k_{33}) in the compound reaches 0.8 [18]. As a part of a series of investigations on the solid solution with PbZrO₃, this study deals with the PZ-PNN binary compound because no detailed report on the structural and dielectric properties of this entire system exists.

In this work, the effect of PNN substitution on the phase transformation behaviour of PZ was investigated. The phase structure, phase transitions and related properties are studied by a differential scanning calorimeter and dielectric measurement. Furthermore, the influence of the PNN content in the system that was studied on the diffuseness of the dielectric peaks is discussed.

2. Experimental

Ceramic powders with a composition of Pb[Zr_{1-x} $(Ni_{1/3}Nb_{2/3})_x$]O₃ with x = 0.0-0.5 (hereinafter abbreviated as PZNN) were synthesized using the columbite precursor method in order to avoid the formation of a pyrochlore phase. Commercial oxide powders of PbO, NiO and Nb₂O₅ (99.9% purity, Aldrich Chemicals, USA) and ZrO₂ (99% purity, Aldrich Chemicals, USA) were used as the starting materials. The columbite precursor NiNb₂O₆ was prepared from the reaction between NiO and Nb₂O₅ at 1100 °C for 4 h and then the precursor was mixed with PbO and ZrO₂. Each mixture of the starting powders was milled and mixed in a ball mill as well as wet-homogenized with ethanol using nylon-coated YTZ zirconia milling as media for 18 h. The mixture was dried and reacted at 650-900 °C; dwell times of 4 h and heating/cooling rates of 20 °C min⁻¹ in a closed alumina crucible were utilized. Calcined powders were subsequently examined by room-temperature x-ray diffraction (XRD; Philips PW 1729 diffractometer) using Ni-filtered Cu K_{α} radiation to identify the phases formed and the optimum calcination conditions for the formation of PZNN powders. The calcined powders

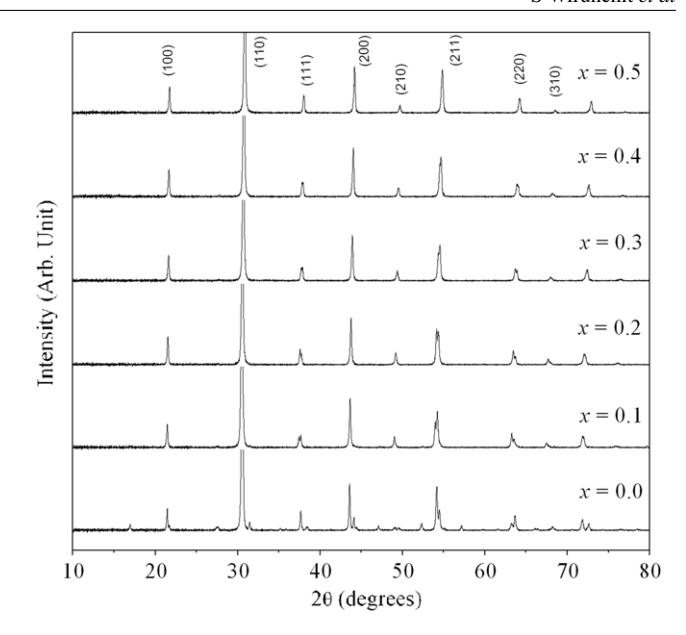


Figure 1. XRD profiles of Pb[Zr_{1-x}(Ni_{1/3}Nb_{2/3})_x]O₃; x = 0.0–0.5 ceramics at optimum sintering conditions.

were milled for 3 h to reduce the particle size. After grinding and sieving, the calcined powder was mixed with a 5 wt% polyvinyl alcohol binder and uniaxially pressed into a pellet. Binder burnout occurred by slowly heating the pellets to 500 °C and holding them at that temperature for 2 h. Sintering occurred between 1100 and 1250 °C with a dwell time of 4 h depending on the composition. To mitigate the effects of lead loss during sintering, the pellets were sintered in a closed alumina crucible containing PbZrO₃ powder. The density of the sintered PZNN pellets was measured by the Archimedes water immersion method. The relative density of all the sintered pellets was approximately 94-96% of the theoretical density. Lattice parameters of the perovskite phases were determined by Cohen's method in conjunction with the least squares method [20]. Ceramic morphologies were directly imaged using scanning electron microscopy ((SEM) JEOL JSM-840A). To determine the dielectric and FE properties, the maximum density of each composition sample was mapped on their major faces, and silver electrodes were made from a low-temperature silver paste by firing at 500 °C for 30 min to enable electrical measurements to be taken. The relative permittivity (ε_r) and dissipation factor $(\tan \delta)$ of stress-free samples were measured using an HP-4284A LCR meter. The capacitance and dissipation factors of the samples were measured at 100 Hz-1 MHz; the temperature varied between 25 and 300 °C, and a heating rate of 2 °C min⁻¹ was used during the measurements. The phase transitions were also measured by a differential scanning calorimeter (DSC 2920, TA Instrument) between ambient and 350 °C at a rate of 10 °C min⁻¹.

3. Results and discussion

3.1. Crystal structure

X-ray diffraction (XRD) was performed on the sintered samples with the composition in the range x = 0.0–0.5. As shown in figure 1, all samples exhibited the characteristics

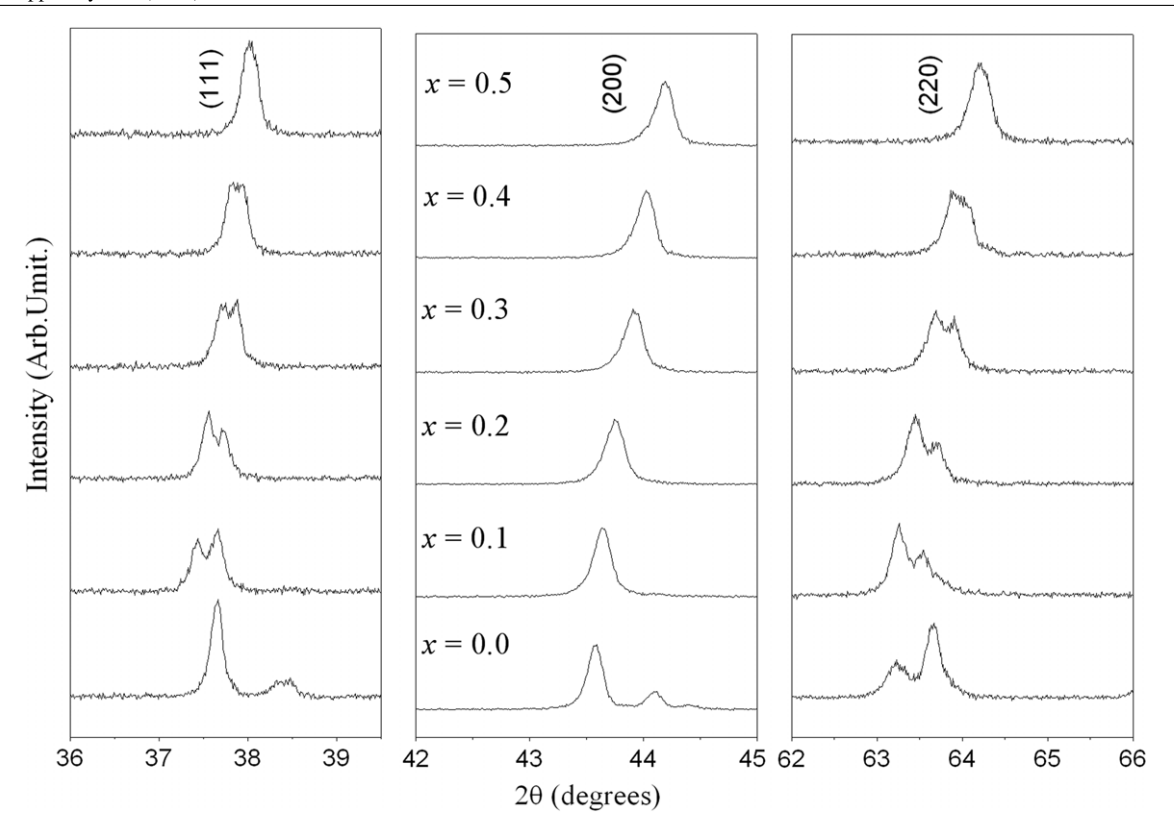


Figure 2. X-ray pattern of the (1 1 1), (2 0 0) and (2 2 0) peaks of $Pb[Zr_{1-x}(Ni_{1/3}Nb_{2/3})_x]O_3$; x = 0.1-0.5 ceramics.

of a single-phase perovskite structure. The XRD patterns of the PZNN compositions show a combination of PZ and PNN patterns with the symmetry varying between orthorhombic and pseudo-cubic types. The PNN composition at room temperature was determined to be cubic with the lattice parameter $a = 4.031 \,\text{Å}$, space group Pm3m. Superstructure lines along with strong peaks are clearly observed in the composition x = 0.0, indicating that this composition belongs to the AFE phase. At room temperature, pure PZ has an orthorhombic perovskite-type structure with lattice parameters a = 8.231 Å, b = 11.77 Å and c = 5.881 Å,space group P2cb (no. 32) [21, 22]. For the composition x = 0.0, the 004, 240, 130, 112 and 110 peaks are observed, indicating that the major phase in this composition had an orthorhombic symmetry which could be matched with ICDD file no. 75–1607 [23]. However, for x = 0.1, 0.2 and 0.3, the enlarged profiles of the diffraction lines 111, 200 and 220 are shown in figure 2. Although a single peak is indicated for 200, splitting was clearly observed for 1 1 1 and 2 2 0, and therefore the crystal structure is rhombohedral. These results indicate that the phase transition from the orthorhombic to the rhombohedral phase should be located between the composition x = 0.0-0.1. The substitution of larger $(Ni_{1/3}Nb_{2/3})^{4+}$ ions with Zr^{4+} sites, implying the transition of the Pb[$Zr_{1-x}(Ni_{1/3}Nb_{2/3})_x$]O₃ structure from orthorhombic to rhombohedral as shown in figure 2, may facilitate parallel displacement along the [1 1 1] direction and the associated displacements of three oxygen ions in the Pb[$Zr_{1-x}(Ni_{1/3}Nb_{2/3})_x$]O₃ structure, resulting in an improvement in the ferroelectricity. The presence of a polar axis in the [111] direction has been reported for the FE rhombohedral structure [24]. For the composition x = 0.4and 0.5, the XRD data show that splitting of the 200 and 111 peaks is not observed. Only a single 220 peak is visible, indicating that the major phase in these compositions has pseudo-cubic symmetry, reflecting the phenomenon that these compositions have a transition temperature higher than room temperature as shown in the dielectric section. With the peaks properly indexed, a lattice parameter was determined using UnitCell, a linear least squares refinement program. The calculated lattice parameters of the perovskite structures are presented in table 1. In the PZ-PNN system, the A site is occupied by Pb²⁺ (0.1630 nm) ions, and the Ni²⁺, Nb⁵⁺ and Zr⁴⁺ ions occupy the B site of the ABO₃ perovskite crystal structure. The average ionic radius of B site ions in the composition $Pb[Zr_{1-x}(Ni_{1/3}Nb_{2/3})_x]O_3$ can be calculated from the following equation:

$$r_{\text{B site}} = (1 - x)[r_{\text{Zr}^{4+}}] + x[\frac{1}{3}r_{\text{Ni}^{2+}} + \frac{2}{3}r_{\text{Nb}^{5+}}],$$
 (1)

where the ionic radii of Ni²⁺, Nb⁵⁺ and Zr⁴⁺ are 0.0830 nm, 0.0780 nm and 0.0860 nm, respectively [25]. In general, the lattice parameters of the perovskite structure also gradually decrease as x increases, undoubtedly because of the introduction of the smaller nickel/niobium ion ($r=0.79\,\text{Å}$) into the zirconium site ($r=0.86\,\text{Å}$), resulting in a decrease in the unit cell according to the Vegard rule [26]. The influence of the addition of Ni²⁺/Nb⁵⁺ ions on the lattice constant of the Pb[Zr_{1-x}(Ni_{1/3}Nb_{2/3}) $_x$]O₃ system is similar to that of the PbZrO₃–Pb(Cd_{1/2}W_{1/2})O₃ and the PbZrO₃–Pb(Mn_{1/2}W_{1/2})O₃ systems [27].

Table 1. Characteristics of Pb[$Zr_{1-x}(Ni_{1/3}Nb_{2/3})_x$]O₃ ceramics with optimized processing conditions (R, rhombohedral; PC, pseudo-cubic).

x	Crystal structure	Lattice parameter (Å)	$T_{\rm m}$ (°C) at 100 Hz	Relative permittivity at 25 °C	Relative permittivity at T_{max}	γ	δ_{γ}
x = 0.1	R	4.149 ± 0.0061	200	325	13 000	1.06	7.9
x = 0.2	R	4.134 ± 0.0032	175	580	19 400	1.20	14.1
x = 0.3	R	4.126 ± 0.0025	155	960	17 200	1.39	16.3
x = 0.4	PC	4.110 ± 0.0040	123	1415	16 500	1.57	22.0
x = 0.5	PC	4.099 ± 0.0027	80	2635	12 000	1.70	30.3

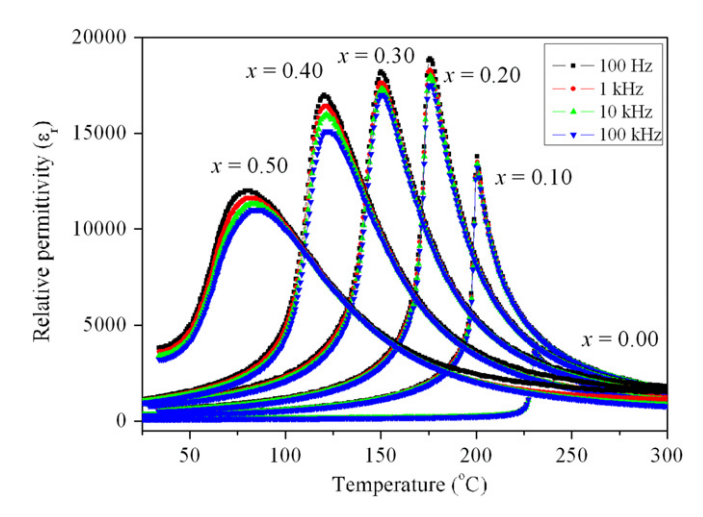
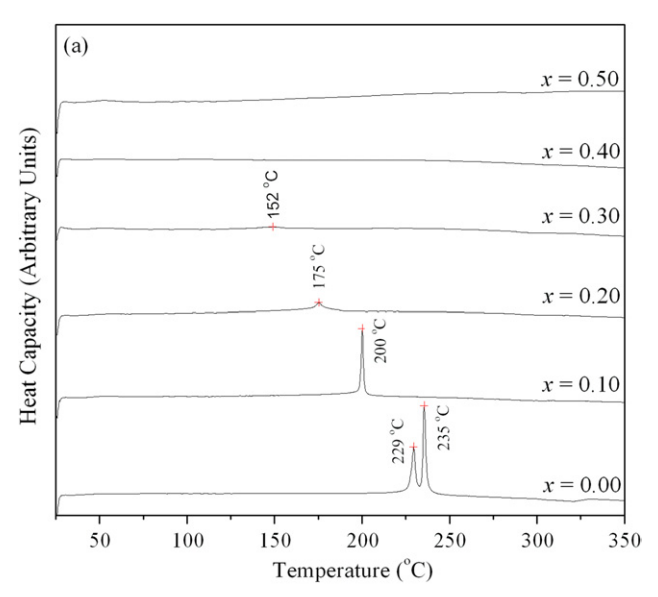


Figure 3. Temperature dependence of the relative permittivity ε_r for Pb[Zr_{1-x}(Ni_{1/3}Nb_{2/3})_x]O₃; x = 0.0–0.5 ceramics.

3.2. Dielectric and thermal properties

The compositional dependence of the dielectric response characteristics for PZNN ceramics where the normal and relaxor FE behaviour cross over is shown in figure 3 for the compositions x = 0.0-0.5 taken at measurement frequencies of 0.1, 1, 10 and 100 kHz. For composition = 0.0, the relative permittivity increased slowly until the temperature approached 230 °C. At 235 °C the relative permittivity increased considerably, passing through a maximum at about 236 °C. With further heating, the relative permittivity decreased in accordance with the Curie-Weiss law, $\varepsilon_{\rm r} = C/(T-T_{\rm o})$, where $\varepsilon_{\rm r}$ is the relative permittivity of a stress-free sample, T is the temperature and C and T_0 are constants which, in this study, were 1.04×10^5 and 460.7 K, respectively. With an increase in the PNN concentration to x = 0.3, the first-order dielectric features of the spontaneous transformation became increasingly less distinct, whereas the relaxor-like dielectric dispersion became increasingly more pronounced, existing over a broader temperature range near $T_{\rm max}$. These results clearly show that dielectric response crossovers between the relaxor and the normal states exist over a relatively wide PNN content range between x = 0.3and 0.4. Upon increasing the PNN concentration to x = 0.5, the ceramic exhibits a broad maximum of relative permittivity with a strong frequency dispersion which is reminiscent of the relaxor FE behaviour of a PNN crystal. The maximum value of the relative permittivity decreases with increased frequency. The dielectric dispersion below the transition



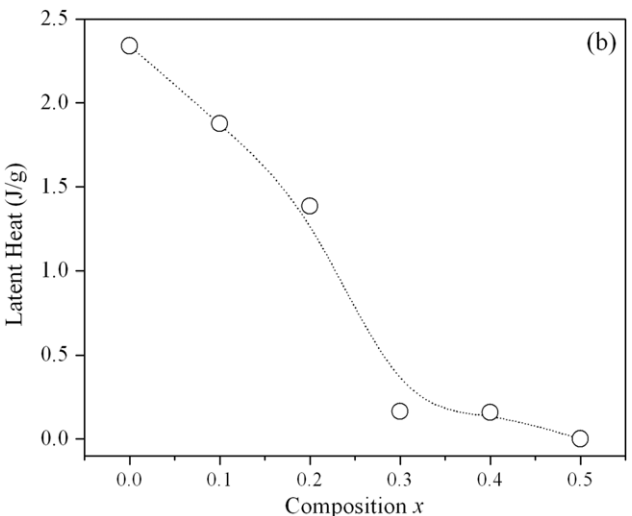


Figure 4. (a) Typical DSC curves for Pb[$Zr_{1-x}(Ni_{1/3}Nb_{2/3})_x$]O₃; x = 0.0–0.5 ceramics. (b) Nonlinear decrease in latent heat with increasing PNN concentration.

temperature reflects typical relaxor FE behaviour arising from the responses of polar micro-domains with the spectrum of relaxation time [28,29].

From dielectric permittivity-temperature measurements and also differential scanning calorimetry (DSC), we investigated the nature of the FE-PE phase transitions in the PZNN system. The transition temperature was determined from both the latent heat anomaly in the DSC data and the peak of the permittivity-temperature plots. Figures 4(a)

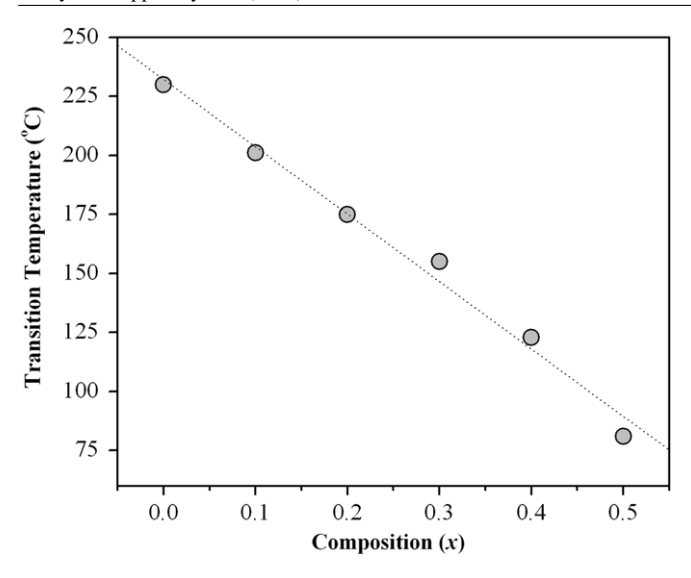


Figure 5. Transition temperatures (T_{max}) as a function of the composition x.

and (b) show the results of the DSC for the PZNN system. As shown in figure 4(a), two anomalies at about 229 and 235 °C have been observed for pure PbZrO₃. The lower temperature corresponds to the transition temperature of the AFE \rightarrow FE phase transition, while the higher temperature corresponds to the FE \rightarrow PE phase transition. The trend of latent heat for the FE phase transition was found to lessen with a progressive increase in the PNN content as shown in figure 4(b). The tricritical point, the composition at which a first-order transition becomes a second-order transition, is close to the composition x = 0.3 which has a tolerance factor of $t \sim 1.0$ using the ionic radii of Shannon [25]. et al [30] reported that in Bi(Ni_{1/2}Ti_{1/2})O₃-PbTiO₃ (BNiT-PT) the tricritical point in the solid solution also corresponded closely to $t \sim 1.0$. Similar behaviour was also observed in the Bi(Mg_{3/4}W_{1/4})O₃–PbTiO₃ (BMW-PT) system by Stringer et al [31] and in the PZT system by Rossetti and Navrotsky [32].

A clear transition in $T_{\rm max}$ (defined as the temperature at which $\varepsilon_{\rm r}$ is maximum at 100 Hz) is observed with $T_{\rm max}$ decreasing with x. The transition temperature ($T_{\rm max}$) as a function of the mole fraction of PNN (x) is represented in figure 5. A good linear relationship between $T_{\rm max}$ and x indicates that this system is a well-behaved and complete solid solution, suggesting that the transition temperature of the PZNN system can be varied over a wide range from -120 to $236\,^{\circ}{\rm C}$ by controlling the amount of PNN in the system. The results show that PNN substitution produces a linear reduction in the transition temperature ($T_{\rm m}$) = $232.19-285x\,^{\circ}{\rm C}$ with the concentration (x). The PNN shifts the transition temperature of this system at a rate of $28.5\,^{\circ}{\rm C}$ mol $^{-1}$, agreeing quantitatively with other lead-based perovskite systems [14, 19, 33].

The relative permittivity of normal FE materials above the maximum relative permittivity temperatures can be expressed by the Curie–Weiss law. However, the broad relative permittivity of the relaxor FE composition more appropriately follows the quadratic law. The relative permittivity can be

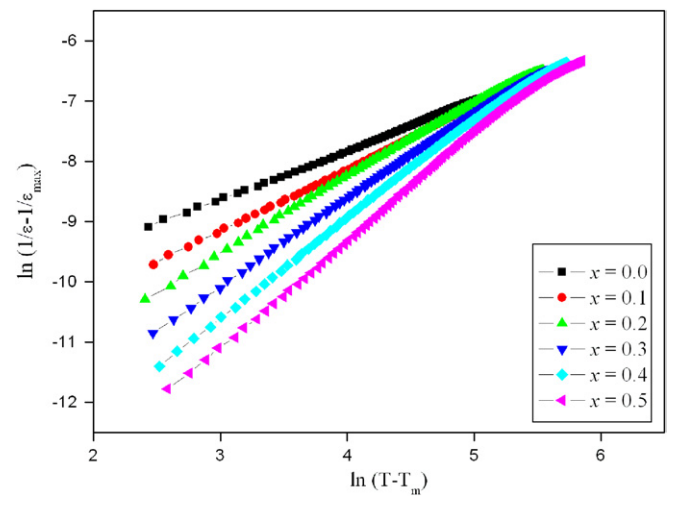


Figure 6. Double logarithmic plot of $\ln(1/\varepsilon - 1/\varepsilon_{\text{max}})$ versus $\ln(T - T_{\text{m}})$ for evaluating the diffusivity exponent γ for the $(\text{Pb}[\text{Zr}_{1-x}(\text{Ni}_{1/3}\text{Nb}_{2/3})_x]O_3\text{ceramic}.$

derived via the following expression [34, 35]:

$$\frac{\varepsilon_{\rm m}'}{\varepsilon'(f,T)} = 1 + \frac{(T - T_{\rm m}(f))^{\gamma}}{2\delta_{\gamma}^2} \qquad (1 \leqslant \gamma \leqslant 2), \quad (2)$$

where $\varepsilon_{\rm m}'$ is the maximum value of the permittivity at $T=T_{\rm m}(f),~\gamma$ is the diffusivity and δ is the diffuseness parameter. The value of γ is the expression of the degree of dielectric relaxation while the parameter δ_{γ} is used to measure the degree of diffuseness of the phase transition. The limiting values $\gamma=1$ and $\gamma=2$ reduce expression (2) to the Curie–Weiss law valid for the case of a normal FE and the quadratic dependence valid for an ideal relaxor, respectively. The quadratic dependence of $1/\varepsilon_{\rm r}$ on temperature has been claimed to be obeyed by several materials with diffuse phase transition behaviour.

By plotting $\ln(1/\varepsilon-1/\varepsilon_{\rm max})$ versus $\ln(T-T_{\rm m})$, γ can be determined directly from the gradient. Figure 6 gives these results; the plotted lines for all specimens show remarkably good linearity within the measured temperature range. Using the intercept and slope of the lines in figure 6, δ_{γ} and γ for each specimen are calculated and shown in figure 7. The values of γ and δ illustrated in figure 7 vary between 1.06 and 1.70, confirming that a diffuse phase transition occurs in the PZNN system. Both diffuseness parameters δ_{γ} and γ increased with an increase in the mole fraction of PNN. As illustrated in figure 7, a near-linear relationship was observed over the wide compositional range which is consistent with a perfect solid solution. The diffuseness of the phase transition in the x=0.5 composition can be attributed to the relaxor nature of PNN.

The dielectric behaviour of Pb containing the relaxor ferroelectrics is generally explained in the literature in terms of small regions of local spontaneous polarization (so-called polar regions) with a nanometre scale size [28, 36]. In a mixed-perovskite system, where the same site is occupied by two differently charged ions (e.g. Ni²⁺ and Nb⁵⁺ in the case of the PNN), a self-limiting mechanism operates for the

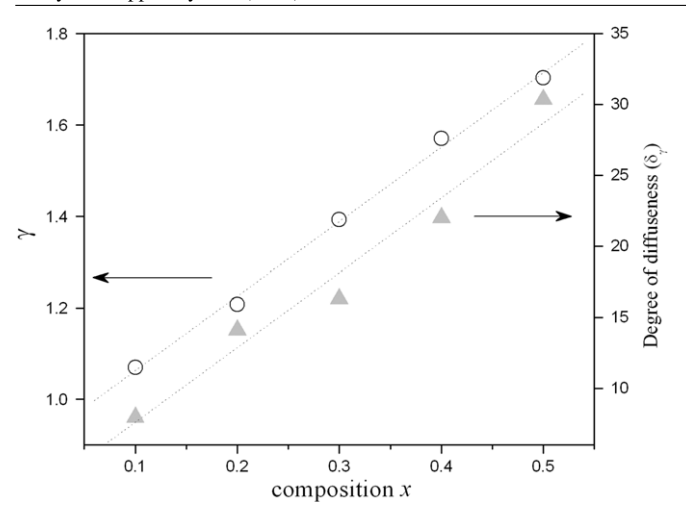


Figure 7. Dependence of γ and the degree of diffuseness (δ_{γ}) for Pb[Zr_{1-x}(Ni_{1/3}Nb_{2/3})_x]O₃, x = 0.1–0.5 ceramics.

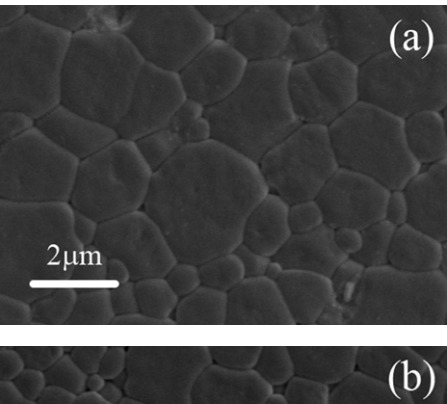
average size of the ordered regions. Although the global value of the Ni: Nb ratio in PNN is 1:2, the local value in the unit cell is 1:1, resulting in a net charge for the unit cell, a situation that cannot exist over too many unit cells. Small ordered (polar) regions are therefore surrounded by disordered regions to compensate for the charge imbalance. These ordered polar regions exhibit relaxational behaviour as observed in the dielectric measurements. There are several theories which attempt to explain these properties. Such materials have some features analogous to magnetic spin glasses [37]. As the PNN content increases, the relaxor characteristic of PZNN is observed to increase because the substitution of $(Ni_{1/3}Nb_{2/3})^{4+}$ for the B site ions Zr⁴⁺ increases the number of polar regions as well as their size. The distribution of the relaxation times depends on the distribution of the size and the polarization strength of the polar regions. It is very possible that the region size is diverse, leading to the broadening of the relaxation time and an increase in the degree of frequency dispersion. A similar tendency has also been observed in several prior investigations [11, 14, 19, 38].

3.3. Microstructure characterization

Figures 8(a) and 8(b) show SEM images of the surfaces of Pb[Zr_{1-x}(Ni_{1/3}Nb_{2/3})_x]O₃ ceramics at x=0.2 and 0.5, respectively. No plate-like grains were observed in either sample, indicating the absence of pyrochlore formation. Other compositions of the system also exhibited a high density and an irregular grain size and shape. By applying the linear intercept methods to these SEM micrographs, the average grain size was calculated to be between 2.6 and 3.8 μ m for all the samples. There was no systematic variation in the grain size as a function of the composition according to the different sintering schedules used.

4. Conclusions

For the first time, we have demonstrated the effect of PNN in stabilizing the rhombohedral phase relative to



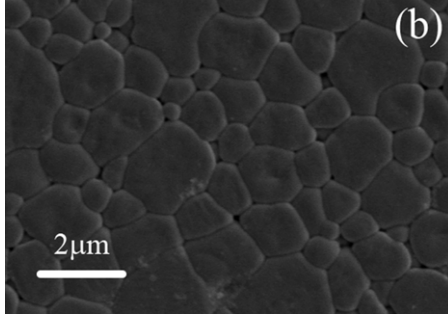


Figure 8. SEM micrographs of thermally etched surfaces of Pb[Zr_{1-x}(Ni_{1/3}Nb_{2/3})_x]O₃ ceramics; (a) x = 0.2, (b) x = 0.5.

the orthorhombic phase in PZ powders and ceramics. Relaxor FE PNN has been found to strongly influence the phase development and dielectric responses of PZ ceramics. The crystal structure data obtained from XRD indicate that the solid solution $Pb[Zr_{1-x}(Ni_{1/3}Nb_{2/3})_x]O_3$, where x = 0.0-0.5, successively transforms from orthorhombic to rhombohedral to pseudo-cubic symmetry with an increase in the PNN concentration. The dielectric constant of Pb[$Zr_{1-x}(Ni_{1/3}Nb_{2/3})_x$]O₃ was found to increase with increased PNN concentration. The PNN shows a clear trend of a reduced temperature $(T_{\rm m})$ of maximum permittivity $(\varepsilon_{\rm m})$, while slightly increasing the diffuse nature of the FE-to-PE phase transition. Furthermore, the transition from the normal FE to the relaxor FE state was clearly observed as the mole fraction of the PNN increased. Furthermore, this transition from the normal to the relaxor FE state was typified by a quasi-linear relationship between the diffuseness parameter δ_{γ} and the PNN mole fraction x. Optimum dielectric properties were observed for the x = 0.4 composition with a permittivity of 16 000.

Acknowledgments

This work was supported by the Thailand Research Fund (TRF), the Commission on Higher Education (CHE), Thailand Graduate Institute of Science and Technology (TGIST) and King Mongkut's Institute of Technology Ladkrabang (KMITL).

References

[1] Jaffe B, Cook W R Jr and Jaffe H 1971 *Piezoelectric Ceramic* (London: Academic)

- [2] Balyunis L E, Topolov V Y, Bah I S and Turik A V 1993 J. Phys.: Condens. Matter 5 1419–26
- [3] Pokharel B P and Pandey D 2002 *Phys. Rev.* B **65** 214108
- [4] Pokharel B P and Pandey D 1999 *J. Appl. Phys.* **86** 3327–32
- [5] Shatalova G E, Filip'ev V S, Kantsel L M and Fesenko E G 1974 Sov. Phys. Crystallogr. 19 257
- [6] Fujishita H, Shiozaki Y and Sawaguchi E 1979 J. Phys. Soc. Japan 16 1391
- [7] Uchino K 2000 Ferroelectric Devices (New York: Dekker)
- [8] Haertling G H 1999 J. Am. Ceram. Soc. 82 797-818
- [9] Lanagan M T, Kim J H, Jang S and Newnham R E 1988 J. Am. Ceram. Soc. 71 311
- [10] Sharma S, Sati R and Choudhary R N P 1993 Can. J. Phys. 71 322
- [11] Yimnirun R, Ananta S and Laoratanakul P 2005 J. Eur. Ceram. Soc. 25 3235–42
- [12] Yimnirun R, Ananta S and Laoratanakul P 2005 J. Eur. Ceram. Soc. 25 3235–42
- [13] Vittayakorn N, Puchmark C, Rujijanagul G, Tan X and Cann D P 2006 *Curr. Appl. Phys.* 6 303–6
- [14] Vittayakorn N, Rujijanagul G, Tan X, He H and Marquardt M A and Cann D P 2006 J. Electroceram. 16 141–9
- [15] Vittayakorn N, Rujijanagul G, Tunkasiri T, Tan X and Cann D P 2004 Mater. Sci. Eng. B 108 258
- [16] Xu Y 1991 Ferroelectric Materials and Their Application (Amsterdam: Elsevier)
- [17] Takeuchi H, Jyomura S and Nakaya C 1985 Japan. J. Appl. Phys. 24 36–40
- [18] Alberta E F and Bhalla A S 2001 Int. J. Inorg. Mater. 3 987

- [19] Vittayakorn N, Rujijanagul G, Tan X, Marquardt M A and Cann D P 2004 J. Appl. Phys. 96 5103
- [20] Cullity B D and Stock S R 2001 *Elements of x-ray Diffraction* (Englewood Cliffs, NJ: Prentice Hall)
- [21] 2000 Powder Diffraction File No. 87-0570, International Centre for Diffraction Data, Newton Square, PA
- [22] Jona F, Shirane G, Mazzi F and Pepinsky R 1957 Phys. Rev. 105 849–56
- [23] 2000 Powder Diffraction File no. 75-1607. International Centre for Diffraction Data, Newtown Square, PA
- [24] Shirane G and Hoshino S 1954 Acta Crystallogr. 7 203
- [25] Shannon R D 1976 Acta. Crysallogr. A 32 751
- [26] Kingary W D, Bowen H K and Uhlmann D R 1976 Introduction to Ceramics (New York: Wiley)
- [27] Yokosuka M 1998 Japan. J. Appl. Phys. 37 5257
- [28] Cross L E 1987 Ferroelectrics 76 241
- [29] Cross L E 1994 Ferroelectrics 151 305
- [30] Choi S M, Stringer C J, Shrout T R and Randall C A 2005 J. Appl. Phys. 98 034108
- [31] Stringer C J, Eitel R E, Shrout T R, Randall C A and Reaney I M 2005 J. Appl. Phys. 97 024101
- [32] Rossetti G A and Navrotsky A 1999 J. Solid State Chem. 144 188
- [33] Vittayakorn N, Rujijanagul G, Tunkasiri T, Tan X and Cann D P 2003 *J. Mater. Res.* 18 2882–9
- [34] Martirena H T and Burfoot J C 1974 Ferroelectrics 7 151
- [35] Uchino K and Nomura S 1982 Ferroelectr. Lett. Sect. 44 55
- [36] Uchino K 1994 Ferroelectrics 151 321
- [37] Viehland D, Jang S J and Cross L E 1990 *J. Appl. Phys.* **68** 2916–21
- [38] Vittayakorn N, Uttiya S, Rujijanagul G and Cann D P 2005 J. Phys. D: Appl. Phys. 38 2942–6

Structural transformation in antiferroelectric PbZrO₃-relaxor ferroelectric Pb(Ni_{1/3}Nb_{2/3})O₃ solid solution system

S. Wirunchit and N. Vittayakorna)

Faculty of Science, Materials Science Research Unit, Department of Chemistry, King Mongkut's Institute of Technology Ladkrabang, Bangkok 10520, Thailand

(Received 8 March 2008; accepted 10 May 2008; published online 18 July 2008)

The solid solution between the antiferroelectric (AFE) PbZrO₃ (PZ) and the relaxor ferroelectric (FE) Pb(Ni_{1/3}Nb_{2/3})O₃ (PNN) was synthesized by the columbite precursor method. The crystal structure, phase transformations, and dielectric and thermal properties of (1-x)PZ-xPNN where x=0.00–0.30 were investigated. With these data, the FE phase diagram between PZ and PNN has been established. The crystal structure data obtained from X-ray diffraction indicate that the solid solution PZ-PNN, where x=0.00–0.30, successively transforms from orthorhombic to rhombohedral symmetry with an increase in the PNN concentration. The AFE phase \rightarrow FE phase transition occurs in compositions of $0.00 \le x \le 0.08$. The AFE \rightarrow FE phase transition shifts to lower temperatures with higher compositions of x. The FE phase temperature range width increases with increased PNN. Apparently the replacement of the Zr⁴⁺ ion by Ni²⁺/Nb⁵⁺ ions decreases the driving force for an antiparallel shift of Pb²⁺ ions because they interrupt the translational symmetry and facilitates the appearance of a rhombohedral FE phase when the amount of PNN is higher than 8 mol %. © 2008 American Institute of Physics. [DOI: 10.1063/1.2956598]

INTRODUCTION

Since the 1990s, many studies on the phase transition between the antiferroelectric (AFE) and the ferroelectric (FE) phase in pure and compositionally modified lead zirconate [PbZrO₃ (PZ)] ceramics have been completed.¹⁻⁴ AFE PZ-based ceramics can undergo transformation from AFE to FE with a large volume change under an external ac bias, temperature, or hydrostatic pressure. 5,6 The maximal longitudinal strain reached 0.87%. These high-strain phenomena have been investigated for applications including charge-storage capacitors, large displacement actuators, and shape memory devices.^{3,8} The relative stability of the AFE and FE phases can be altered through chemical substitutions such as Ba²⁺, Sr²⁺, and Ca²⁺ at the Pb²⁺ site⁹ and Ti⁴⁺ at the Zr⁴⁺ site. The substitution of Ba²⁺ for Pb²⁺ in PZ is of considerable interest for transducer applications since the volume change associated with the field forced AFE to FE transition increases with Ba²⁺ substitution. ¹⁰ Also the switching field for the AFE to FE transition decreases as a result of Ba²⁺ substitution.¹¹

Lead nickel niobate [Pb(Ni_{1/3}Nb_{2/3})O₃ (PNN)] is a relaxor FE having a Ni²⁺ and Nb⁵⁺ complex on the *B*-site of Pb(B'B'')O₃ perovskite with a cubic symmetry at room temperature, ¹² PNN-based ceramics are considered to possess low sintering temperatures and high permittivity, high electrical resistivity, and diffuse phase transition characteristics. Therefore, these materials can be used to fabricate multilayer capacitors with low-temperature melting inner electrodes. ^{13,14} When PNN forms solid solutions with Pb(Zr_{1-x}Ti_x)O₃, the system exhibits excellent piezoelectricity and becomes a potential candidate for use in actuators. ^{15–17}

Since PNN is a relaxor FE with a broad dielectric peak near $T_C \approx -120 \,^{\circ}\text{C}^{18}$ and PZ is AFE with a sharp maximum permittivity at $T_C \sim 230$ °C, the Curie temperature in a PZ-PNN system can be engineered over a wide range of temperatures by controlling the amount of PNN in the system. Although PZ ceramics have better dielectric breakdown strength than PNN, the sintering temperature is also higher.^{9,13} Thus, mixing PNN with PZ is expected to decrease the sintering temperature of PZ ceramics, a desirable move toward lower-cost electrodes. ¹⁹ Moreover, since PZ-PNN is not a pure-relaxor FE system, it is easier to prepare single phase ceramics with a smaller amount of undesirable pyrochlore phases. ¹⁴ Furthermore, no work has been done on the metastable FE phase induced by the B-site substitution in perovskite PZ. With their complimentary characteristics, it is expected that excellent properties can be obtained from ceramics in a PZ-PNN system.

In this study, a metastable FE phase induced by a B-site substitution was studied as a function of composition. The columbite precursor method was used to synthesize the $(1-x)\text{PbZrO}_3-x\text{Pb}(\text{Ni}_{1/3}\text{Nb}_{2/3})\text{O}_3$ (PZ-PNN) with x=0.00-0.30. The structural phase and the dielectric and thermal properties of PZ-PNN ceramics were investigated as a function of composition x. Differential scanning calorimeter (DSC) measurements were also used to study the details of AFE to FE and FE to PE phase transformations accompanied by an evaluation of the thermal behaviors of the PZ-PNN samples. The results are discussed.

EXPERIMENTAL PROCEDURE

Perovskite-phase powders were synthesized using a columbite precursor method to avoid the formation of a pyrochlore phase. Commercial oxide powders of PbO, NiO, Nb₂O₅ (99.9% purity, Aldrich Chemicals, Milwaukee, WI),

a) Author to whom correspondence should be addressed. Tel.: 66-89-7002136. FAX: 66-2-3264415. Electronic mail: naratipemu@yahoo.com.

and ZrO_2 (99% purity, Aldrich Chemicals, Milwaukee, WI) were used as starting materials. NiNb₂O₆ was first formed at 1100 °C for 4 h, and then NiNb₂O₆ and ZrO_2 were mixed with PbO, according to the composition of (1-x)Pb ZrO_3-x Pb $(Ni_{1/3}Nb_{2/3})O_3$, $0.00 \le x \le 0.30$, with an excessive content of 2 mol % PbO.

Each mixture of the starting powders was milled and mixed in a ball mill, as well as wet homogenized with isopropyl alcohol for 18 h using nylon-coated YTZ zirconia milling as media. The mixtures were dried in an oven and calcined at 900-950 °C for 4 h in a double crucible configuration with a heating rate of 20 °C/min. After remilling, drying, and sieving, the various powders were cold pressed into disks 15 mm in diameter and then sintered at temperatures ranging from 950 to 1250 °C using a heating rate of 5 °C/min and a dwell time of 2 h in sealed alumina crucibles. To limit the loss of PbO, the disks were covered with PbZrO₃ powder. X-ray diffraction (XRD) patterns of the sintered pellets were measured using an x-ray diffractometer (PW1729, Philips, Netherlands). $CuK\alpha$ radiation with step scanning was used with a step size of 0.02° and a scan rate of 2 s per step. The density of the sintered PZ-PNN pellets was measured by water immersion (Archimedes method). The relative density of all the sintered pellets was approximately 95%-97% of the theoretical density. To determine dielectric properties, the maximum density of each composition sample was lapped on its major face. Silver electrodes were made from a low-temperature silver paste by firing at 500 °C for 30 min to enable electrical measurements to be taken. Relative permittivity measurements were made using an automated measurement system consisting of an LCR meter (HP-4284, Hewlett-Packard Inc.). The relative permittivity was then calculated from $\varepsilon_r = Cd/\varepsilon_0 A$, where C is the capacitance of the sample, d and A are the thickness of the sample and the area of the electrode, respectively, and ε_0 is the dielectric permittivity of the vacuum $(8.854 \times 10^{-12} \text{ F/m})$. The phase transition temperatures and enthalpy (ΔH) of the phase transitions were determined by DSC at room temperature to 350 °C with a heating rate of 10 °C/min.

RESULTS AND DISCUSSION

Crystal structure

The XRD patterns of (1-x)PZ-xPNN ceramics with various x values are shown in Fig. 1. A complete crystalline solution of perovskite structure is formed throughout the composition range without the presence of pyrochlore or unwanted phases. Ceramics with $0.02 \le x \le 0.08$ have the same crystal structure with pure PZ (x=0.00), i.e., an orthorhombic unit cell at room temperature. Furthermore, the XRD patterns indicate that the replacement of Zr⁴⁺ by Ni²⁺/Nb⁵⁺ ions apparently influenced the orthorhombic PbZrO₃ structure. If the XRD pattern of PZ is indexed on the basis of the pseudocubic cell, then $\frac{1}{4}$ ($h \times l$)-type superlattice reflections representing the antiparallel shifts of Pb²⁺ ions will appear.

In Fig. 1, all the indices were based on the pseudocubic cell and the XRD patterns of the samples with $0.02 \le x \le 0.08$ showed the presence of $\frac{1}{4}$ ($h \ k \ l$)-type superlattice reflections. The intensity ratio of 004/240 peaks and the rela-

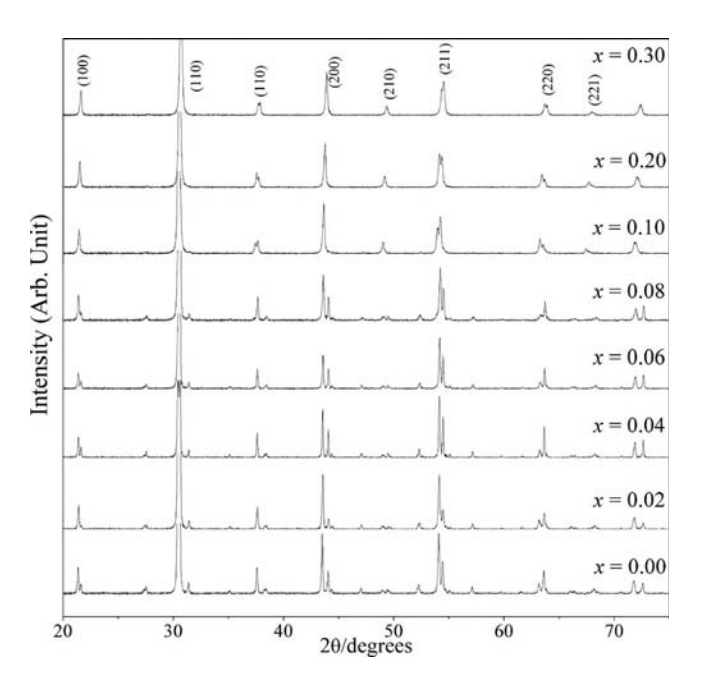


FIG. 1. XRD patterns of (1-x)PZ-xPNN; x=0.0-0.3 ceramics at the optimum sintering conditions.

tive intensity of $\frac{1}{4}$ (h k l)-type superlattice reflections (namely, 130/112) decreased with increased Ni²⁺/Nb⁵⁺ content, as shown in Fig. 2. According to Glaze, ²⁰ these types of reflections represent antiphase tilting of the oxygen octahedra without distortion. Furthermore, the PZ-PNN samples with $0.1 \le x \le 0.3$ showed only the fundamental reflections of the pseudocubic perovskite cell. The relative intensity of superlattice reflections decreased with increased PNN content, as shown in Fig. 2, demonstrating that the superlattice disappeared with the addition of 10 mol % PNN. Figure 2 also shows the results for $\frac{1}{4}$ (h k l)-type superlattice (1 1 1), $(2\ 0\ 0)$, and $(2\ 2\ 0)$ reflections. The samples with $x=0.1,\ 0.2,$ and 0.3 had a split (1 1 1) and (2 2 0) reflection and a single (2 0 0) reflection, confirming that the crystal structure of the samples with x=0.1, 0.2, and 0.3 is primitive rhombohedral perovskite. For a pure rhombohedral structure, the 2 0 0 group of reflections should be a singlet.

Furthermore, the specimens displayed a progressive peak shift toward higher diffraction angle directions with increased PNN. This phenomenon can be qualitatively explained with respect to the unit cell volume caused by the Ni²⁺/Nb⁵⁺ incorporation. According to Shannon's effective ionic radii with a coordination number of 6, the average ionic radius of *B*-site ions $(Ni_{1/3}Nb_{2/3})^{4+}$ has a radius of 0.79 Å, which is close to a radius of Zr^{4+} (0.86 Å).²¹ Therefore, (Ni_{1/3}Nb_{2/3})⁴⁺ can enter into the sixfold coordinated *B*-site of the perovskite structure to substitute for Zr⁴⁺ due to radius matching. The structure of ABO3 type perovskites can be viewed as a network of [BO₆] oxygen octahedra. The substitution of the relatively smaller $(Ni_{1/3}Nb_{2/3})^{4+}$ for the relatively larger Zr⁴⁺ led to a decrease in the unit cell volume. This radius effect is presumably responsible for the steady shift of the XRD peak positions to higher diffraction angle directions with increased PNN. The influence of the addition $(Ni_{1/3}Nb_{2/3})^{4+}$ on the phase structure of the

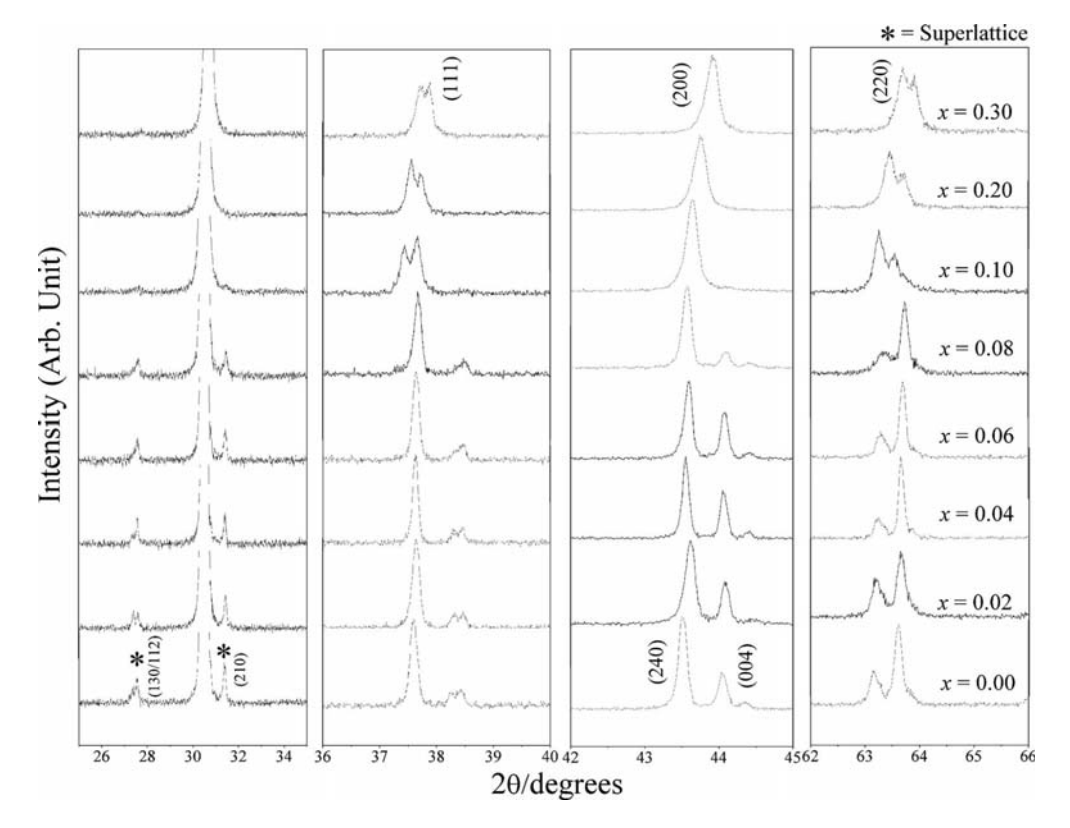


FIG. 2. XRD patterns of the $\frac{1}{4}$ (h k l)-type superlattice reflections, (111), (200), and (220) peaks of (1-x)PZ-xPNN; x=0.0-0.3 ceramics.

PbZrO₃–Pb(Ni_{1/3}Nb_{2/3})O₃ system is similar to the influence of (Pb_{1-x}Ba_x)ZrO₃. The substitution of smaller (Ni_{1/3}Nb_{2/3})⁴⁺ ions with Zr⁴⁺ sites (which implies the transition of the PZ-PNN structure from orthorhombic to rhombohedral, as shown in Fig. 2) may facilitate the parallel displacement along a [1 1 1] direction and the associated displacements of three oxygen ions in the PZ-PNN structure, resulting in an improvement of ferroelectricity. The presence of a polar axis in the [1 1 1] direction has been reported for a FE rhombohedral structure. ²²

Phase transition and dielectric properties

The permittivity temperature dependences of (1) -x)PbZrO₃-xPb(Ni_{1/3}Nb_{2/3})O₃ ceramics were measured at several frequencies from 25 to 350 °C. Figures 3(a)-3(h) show the relative permittivity versus temperature of (1 -x)PbZrO₃-xPb(Ni_{1/3}Nb_{2/3})O₃ ceramics for compositions x=0.00, 0.02, 0.04, 0.06, 0.08, 0.10, 0.20, and 0.30, respectively, at frequencies of 100 Hz, 1 kHz, 10 kHz, 100 kHz, and 500 kHz. For composition x=0.0, the relative permittivity increased slowly until the temperature approached 225 °C. Near 230 °C the relative permittivity increased greatly, passing through a maximum at about 231 °C. With further heating, the relative permittivity decreased in accordance with the Curie-Weiss law, $\varepsilon_r = C/(T-T_0)$, where ε_r is the relative permittivity, T is the temperature, and C and T_0 are constants which, in this study, were 1.04×10^5 and 460.7 K, respectively.

The substitution of PNN lowers the AFE to FE phase transition temperature. The AFE to FE phase transition oc-

curs at 200, 150, and 105 °C for 0.02, 0.04, and 0.06, respectively [see Figs. 3(b)–3(d)]. The jumps in the relative permittivity at the transition temperature are found to be nearly 2250, 1240, and 650 for x=0.02, 0.04, and 0.06, respectively. Furthermore, for x>0.08, no dielectric anomaly corresponding to the AFE-FE transition is observed [Fig. 3(e)].

Since the AFE to FE transition decreases nearly linearly at the rate of 22.5 °C/mol % of PNN with respect to its value for pure PZ, the expected AFE to FE transition temperature for the composition x=0.08 is around 64 °C. No anomaly corresponding to AFE-FE transition in the composition $x \ge 0.08$ was found. From these results, we can conclude that the AFE phase of pure PZ persists in the PZ-PNN system for x < 0.08 only. At the composition $x \ge 0.10$, the relative permittivity peak values became gradually higher in parallel with the decrease in the transition temperature (T_m) . The x=0.2 and 0.3 compositions showed a broadening of the permittivity maxima, and the T_m increased with an increased measurement frequency [Figs. 3(c) and 3(h)], indicating that this composition shows a diffuse phase transition with a strong frequency dispersion which is characteristic of relaxor ferroelectricity.

The DSC technique was also used as the primary tool to confirm the AFE-FE phase transition in the PZ-PNN system. AFE-FE phase transition temperatures, enthalpy, and paraelectric (PE) transitions are summarized in Table I. Figure 4 shows the results of the DSC analysis of the PZ-PNN samples. As shown in Fig. 4, two distinct endothermic peaks were observed for PZ-PNN samples with $0.0 \le x < 0.08$. The lower temperature corresponds to the transition temperature

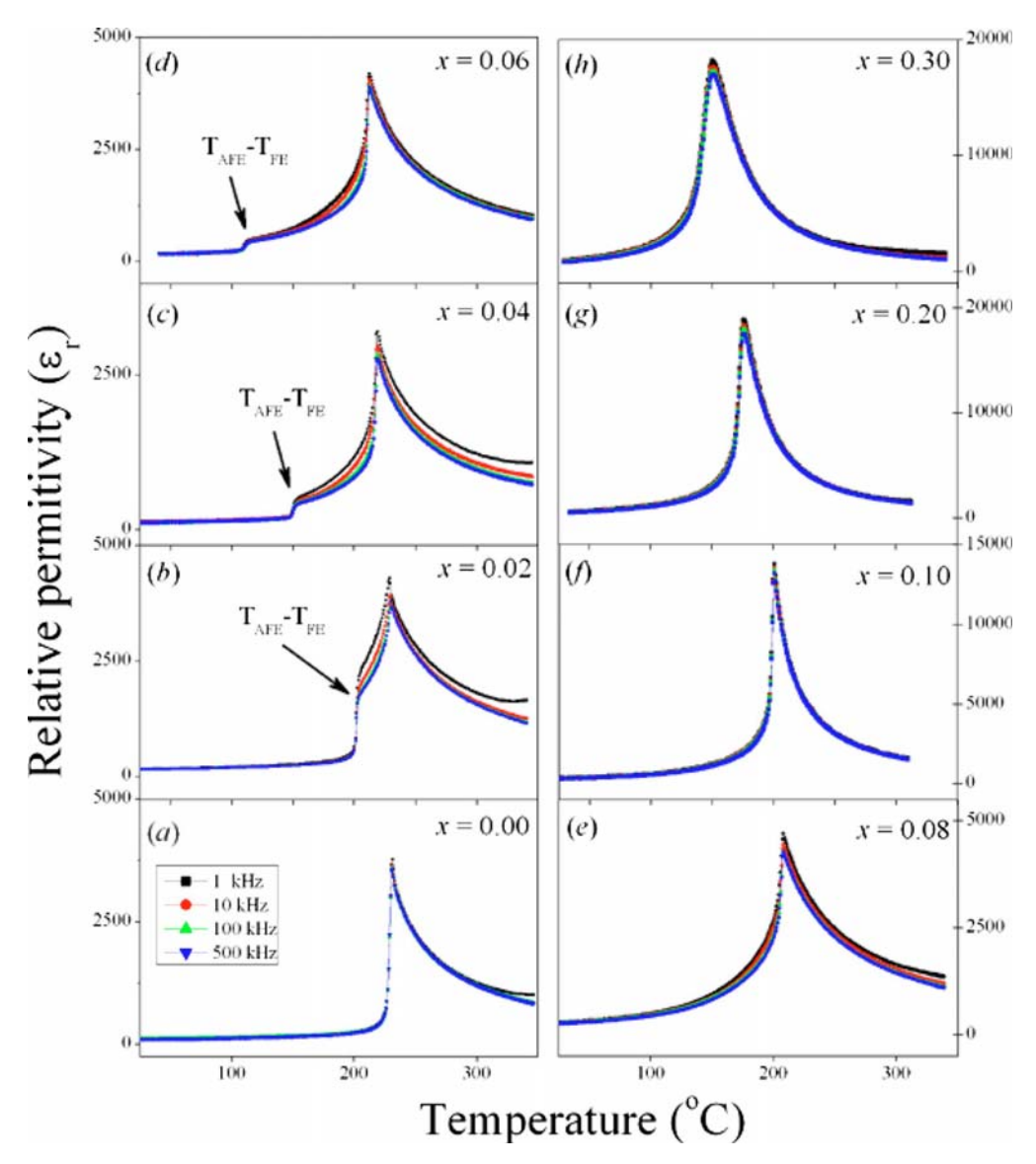


FIG. 3. (Color online) Dielectric properties as a function of temperature on heating at a frequency of 1–500 kHz varies PNN concentration.

of the AFE \rightarrow FE phase transition, while the higher temperature corresponds to the FE \rightarrow PE phase transition. It is well known that good quality ceramics as well as single crystal samples of PZ show two distinct endothermic peaks around

230 and 215 °C corresponding to the PE to FE and FE to AFE transitions, respectively, on heating and cooling. ^{23,24} The AFE \rightarrow FE phase transition was found in compositions of $0.0 \le x < 0.08$. The peaks shift to lower temperatures with

TABLE I. Characteristics of (1-x)PZ-xPNN ceramics with optimized processing conditions (R, rhombohedral; O, orthorhombic).

Composition	Crystal			Phase tra temperati		Enthalpy (J/g)	
(x)	structure	$\varepsilon_{r \text{ room}}$	$\varepsilon_{r\mathrm{max}}$	AFE→FE	FE→PE	AFE→FE	$FE \rightarrow PE$
0.00	0	120	3 370	229.5	235.5	1.53	2.34
0.02	O	166	4 300	200.7	227.0	1.56	2.95
0.04	0	127	3 200	150.2	220.8	1.33	2.89
0.06	0	177	4 200	105.7	213.3	1.10	2.70
0.08	0	319	4 700	• • •	205.5		2.44
0.10	R	375	13 800		200.2		1.88
0.20	R	602	18 900		175.3		1.39
0.30	R	1120	18 200		149.0	• • • •	0.16

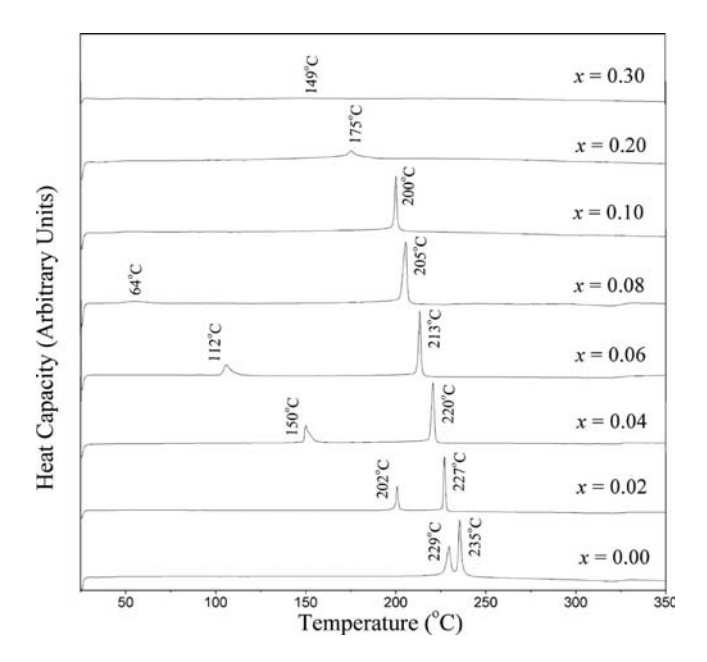


FIG. 4. Typical DSC curves for (1-x)PZ-xPNN; x=0.0-0.3 ceramics.

higher compositions of x. From Table I, the temperature range width of the FE phase continuously increases progressively with the PNN content. The temperature range widths of the FE phase are around 6, 25, 70, and 101 °C for compositions x=0.00, 0.02, 0.04, and 0.06, respectively. Furthermore, the areas under two endothermic peaks in Fig. 4 decreased with increased PNN. Since those areas represent a free-energy difference between the two phases, this result indicates that the addition of PNN decreases the stability of orthorhombic phase. Apparently the replacement of the Zr⁴⁺ ion by $(Ni_{1/3}Nb_{2/3})^{4+}$ ions decreases the driving force for an antiparallel shift of Pb²⁺ ions because they interrupt the translational symmetry.²⁰ This interruption caused the appearance of a rhombohedral FE phase when the amount of PNN was more than 8 mol %. Gotor et al. 25 studied relationships between the structure change of BaTiO3 and its enthalpy by using DSC. They found that the tetragonality (c/a)of BaTiO₃ is reduced along with the reduction in enthalpy. However, in the present work, the decrease in ΔH is proportional to the fraction ratio of the FE and PE phases in the PZ-PNN. The tricritical point (the composition at which a first-order transition becomes a second-order transition) is close to the composition x=0.3, which has a tolerance factor, $t \sim 1.0$, using the ionic radii of Shannon.²¹ Choi et al.²⁶ reported that in the $Bi(Ni_{1/2}Ti_{1/2})O_3-PbTiO_3$, the tricritical point in the solid solution also corresponded closely to t ~ 1.0 . Similar behavior was also observed in the $Bi(Mg_{3/4}W_{1/4})O_3-PbTiO_3$ system by Stringer et al.²⁷ and PZT by Rossetti and Navrotsky.²⁸

Based on the results of XRD, dielectric properties, and DSC data, the FE phase diagram for the (1-x)PZ-xPNN binary system has been established (see Fig. 5). The transition temperature decreases approximately linearly with x, from T_C =235 °C for x=0.0 to 149 °C for x=0.3. The phase diagram consists of three distinct crystallographic phases in this system: high-temperature PE cubic (Pm3m), rhombohe-

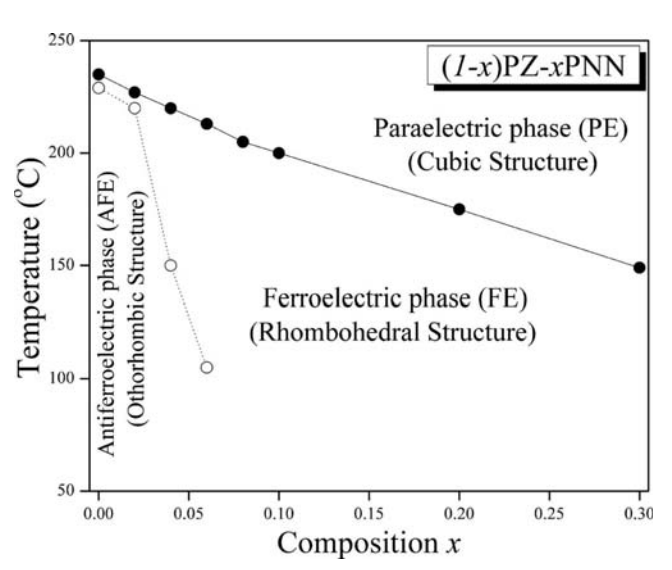


FIG. 5. Phase diagram of (1-x)PZ-xPNN, x=0.0–0.3 binary system determined from room temperature XRD, DSC as a function of temperature. The symbols refer to \bigcirc =the transition temperature from AFE state to FE state; \blacksquare =the transition temperature from FE state to PE state.

dral (R3m), and FE orthorhombic [P2cb (No. 32)]. At low concentrations of PNN $x \le 0.08$, the symmetry can be defined as orthorhombic. The orthorhombic symmetry transforms into rhombohedral at the composition near x = 0.08.

CONCLUSIONS

Relaxor FE PNN has been found to strongly influence crystal structure dielectric responses and thermal properties of PZ ceramics. The crystal structure data obtained from XRD indicate that the solid solution (1-x)PZ-xPNN, where x=0.0-0.3, successively transforms from orthorhombic to rhombohedral symmetry with increased PNN concentration. The AFE

FE phase transition is found in compositions of $0.0 \le x \le 0.08$. The AFE \rightarrow FE phase transition shifts to lower temperatures with higher compositions of x. The temperature range width of the FE phase increases with increased PNN. It is apparent that the replacement of the Zr⁴⁺ ion by Ni²⁺/Nb⁵⁺ ions would decrease the driving force for an antiparallel shift of Pb²⁺ ions because they interrupt the translational symmetry. The dielectric properties of (1-x)PZ-xPNN was found to increase with increased PNN concentration. PNN shows a clear trend toward reducing the temperature (T_m) of maximum permittivity (ε_m) , while slightly increasing the diffuse nature of the FE to PE phase transition. Furthermore the transition from the normal FE to the relaxor FE state was clearly observed as the mole fraction of PNN increased.

ACKNOWLEDGMENTS

This work was supported by the Thailand Research Fund (TRF), the Commission on Higher Education (CHE), Thailand Graduate Institute of Science and Technology (TGIST), and King Mongkut's Institute of Technology Ladkrabang (KMITL)

¹W.-H. Chan, Z. Xu, T. F. Hung, and H. Chen, J. Appl. Phys. **96**, 6606 (2004).

- ²J. Zhai and H. Chen, J. Appl. Phys. **94**, 589 (2003).
- ³K. Uchino, Ferroelectric Devices (Dekker, New York, 2000).
- ⁴E. Sawaguchi, H. Maniwa, and S. Hoshino, Phys. Rev. 83, 1078 (1951).
- ⁵B. P. Pokharel and D. Pandey, J. Appl. Phys. **86**, 3327 (1999).
- ⁶B. P. Pokharel and D. Pandey, Phys. Rev. B **65**, 214108 (2002).
- ⁷W. Y. Pan, C. Q. Dam, Q. M. Zhang, and L. E. Cross, J. Appl. Phys. **66**, 6014 (1989).
- ⁸K. Uchino, *Piezoelectric Actuators and Ultrasonic Motors* (Kluwer Academic, Boston, 1996).
- ⁹B. Jaffe and W. R. Cook, *Piezoelectric Ceramic* (Academic Press, New York, 1971).
- $^{10}\mathrm{G.}$ Rujijanagul and T. Bongkarn, Phase Transitions 80, 209 (2007).
- ¹¹N. Vittayakorn, T. Bongkarn, and G. Rujijanagul, Physica B 387, 415 (2007).
- ¹²L. E. Cross, Ferroelectrics **151**, 305 (1994).
- ¹³G. H. Haertling, J. Am. Ceram. Soc. **82**, 797 (1999).
- ¹⁴T. R. Shrout and A. Halliyal, Am. Ceram. Soc. Bull. **66**, 704 (1987).
- ¹⁵N. Vittayakorn, G. Rujijanagul, X. Tan, M. A. Marquardt, and D. P. Cann, J. Appl. Phys. 96, 5103 (2004).
- ¹⁶E. F. Alberta and A. S. Bhalla, Int. J. Inorg. Mater. **3**, 987 (2001).

- ¹⁷G. Robert, M. Demartin, and D. Damjanovic, J. Am. Ceram. Soc. **81**, 749 (1998).
- ¹⁸S. Sharma, R. Sati, and R. N. P. Choudhary, Can. J. Phys. **71**, 322 (1993).
- ¹⁹Y. Xu, Ferroelectric Materials and Their Application (Elsevier Science, Amsterdam, 1991).
- ²⁰A. M. Glazer, Acta Crystallogr., Sect. A: Cryst. Phys., Diffr., Theor. Gen. Crystallogr. A31, 756 (1975).
- ²¹R. D. Shannon, Acta Crystallogr., Sect. A: Cryst. Phys., Diffr., Theor. Gen. Crystallogr. A32, 751 (1976).
- ²²G. Shirane and S. Hoshino, Acta Crystallogr. 7, 203 (1954).
- ²³G. Shirane, E. Sawaguchi, and Y. Takagi, *Phys. Rev.* **84**, 476 (1951).
- ²⁴R. W. Whatmore and A. M. Glazer, J. Phys. C 12, 1505 (1979).
- ²⁵F. J. Gotor, C. Real, M. J. Dianez, and J. M. Criado, J. Solid State Chem. 123, 301 (1996).
- ²⁶S. M. Choi, C. J. Stringer, T. R. Shrout, and C. A. Randall, J. Appl. Phys. 98, 034108 (2005).
- ²⁷C. J. Stringer, R. E. Eitel, T. R. Shrout, C. A. Randall, and I. M. Reaney, J. Appl. Phys. **97**, 024101 (2005).
- ²⁸G. A. Rossetti and A. Navrotsky, J. Solid State Chem. **144**, 188 (1999).

Ceramic Processing Research

Effect of calcination conditions on phase formation of microwave dielectric cobalt niobate (CoNb₂O₆) powders via a mixed oxide synthesis route

Nopsiri Chaiyo and Naratip Vittayakorn*

King Mongkut's Institute of Technology Ladkrabang Nanotechnology Research Center (NRC), King Mongkut's Institute of Technology Ladkrabang, Bangkok, Thailand 10520

Cobalt niobate ($CoNb_2O_6$) powders have been prepared using a mixed oxide synthesis route. The formation of the $CoNb_2O_6$ phase in the calcined powders has been investigated as a function of calcination conditions by differential thermal analysis (DTA) and X-ray diffraction (XRD) techniques. The morphological evolution was determined by scanning electron microscopy (SEM). It has been found that the minor phases of unreacted Co_3O_4 and the orthorhombic- Nb_2O_5 and monoclinic- β - Nb_2O_5 phase tend to form together with the columbite $CoNb_2O_6$ phase, depending on calcination conditions. It is seen that optimization of calcination conditions can lead to a single-phase orthorhombic $CoNb_2O_6$. The calcination temperature and dwell time have been found to have a pronounced effect on the phase formation of the calcined cobalt niobate ($CoNb_2O_6$) powders. Optimization of calcination conditions can lead to a single-phase $CoNb_2O_6$ in a columbite phase.

Key words: CoNb2O6, Calcination, Powder synthesis.

Introduction

Advances in wireless communication systems are very dependent upon improvements in microwave dielectric materials. In particular, centimetre and millimetre wave wireless applications require high-Q materials that would be less expensive than the known high-Q perovskitestructure, barium-tantalate-based microwave dielectrics and would not need high sintering temperatures [1]. Cobalt niobate CoNb₂O₆ is a potential candidate for mechanical filter coatings and electrical applications such as for resonators and capacitors which has a columbite structure having the general formula AB2O6, with a Pcan (no.60) space group and can be used for capacitors or dielectric resonators for microwave applications due to its low tangent loss (tan δ) and high dielectric constant (ϵ_r) [1, 2]. Figure 1 shows the columbite structure of CoNb₂O₆. Regarding the structure, $[M-O_6]$ (M = Co or Nb) octahedra share edges forming chains along the c-axis. Parallel Co-O₆ and Nb-O₆ chains alternate along the b-axis. CoNb₂O₆ is well known as the key precursor for the successful preparation of single-phase perovskite Pb(Co_{1/3}Nb_{2/3})O₃ (PCoN), which is becoming increasingly important for multilayer ceramic capacitor, transducer, electrostrictor and actuator applications [3, 4]. The objective of this investigation was to study the reaction between the starting cobalt oxide and niobium oxide precursors, phase formation, microstructure and microwave dielectric properties of columbite-structure cobalt niobate ceramics.

Fig. 1. Crystal structure of CoNb₂O₆ compound.

Experimental

Ceramics with the composition CoNb₂O₆ were produced by the conventional mixed-oxide route. All samples in this study were prepared from reagent-grade oxides: Co₃O₄ (99.99%, Aldrich, U.S.A.) and Nb2O5 (99.9%, Aldrich, U.S.A.). Co₃O₄ and Nb₂O₅ powders were weighed and mixed by ball-milling in a polyethylene bottle together with methyl alcohol and partially stabilized zirconia media. Methyl alcohol was removed by heating at 80 °C for appropriate durations. After drying, the reaction of the uncalcined powders taking place during heat treatment was investigated by differential thermal analysis (DTA; Perkin-Elmer 7 series) using a heating rate of 10 Kminute⁻¹ in air from room temperature up to 1350 °C. Based on the DTA results, various calcinations conditions, i.e. temperature ranging from 700-1100 °C and dwell time ranging from 15 to 240 minutes, were applied with a heating/ cooling rate of 5 Kminute-1, in order to investigate the formation of CoNb₂O₆.

Fax: +66-2-3264415

E-mail: naratipemu@yahoo.com

CoNb₂O₆

^{*}Corresponding author: Tel: +66-9-700-2136

All powders were subsequently examined by room temperature X-ray diffraction (XRD; Bruker D8 Advance) using Ni-filtered CuK_{α} radiation to identify the phases formed and optimum calcination conditions for the formation of $CoNb_2O_6$ powders. The relative proportions of $CoNb_2O_6$, Co_3O_4 , orthorhombic- Nb_2O_5 and monoclinic- β - Nb_2O_5 have been calculated according to the following approximate relationship, by analogy with our treatment of the yield of $CoNb_2O_6$ in a related synthesis [5, 6]:

Wt% columbite phase

$$= \left(\frac{I_{col}}{I_{col} + I_{Co_2O_4} + I_{Otho-Nb_2O_5} + I_{\beta-Nb_2O_5}}\right) \times 100$$
 (1)

here I_{col} , $I_{Co_3O_4}$ $I_{Otho-Nb_2O_5}$ and $I_{\beta-Nb_2O_5}$ refer to the intensities of the (311) columbite peak, (311) cubic-Co₃O₄ peak, (180) orthorhombic-Nb₂O₅ and (400) monoclinic- β -Nb₂O₅ peak respectively, these being the strongest reflections in all cases. Microstructural analysis of the ceramic samples was performed by means of scanning electron microscopy (LEO 1455VP, Cambridge, England).

Results and Discussions

Figure 2 shows the DTA curves for the mixture of Co₃O₄ and Nb₂O₅ with a molar ratio of 1 : 3. From Fig. 2, three endothermic peaks centered at 100.6, 357 and 810 °C are observed. The first endothermic peak at 100.6 °C is attributed to the evaporation of water molecules [7]. The second endothermic peak occurring at 357 °C should correspond to the decomposition of the organic species from the milling process [8]. The different temperature, intensities, and shapes of the thermal peaks are probably related to the different nature of the organic species and consequently, caused by the removal of species bounded differently in the network [7, 8]. The third endothermic peak at 810 °C is assigned to the formation of CoNb₂O₆ by combination reactions of Co₃O₄ and Nb₂O₅. According

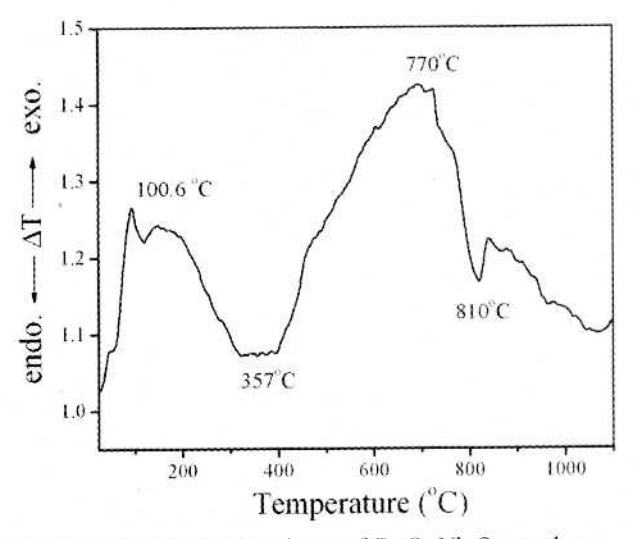


Fig. 2. DTA curve for the mixture of Co₃O₄-Nb₂O₅ powders.

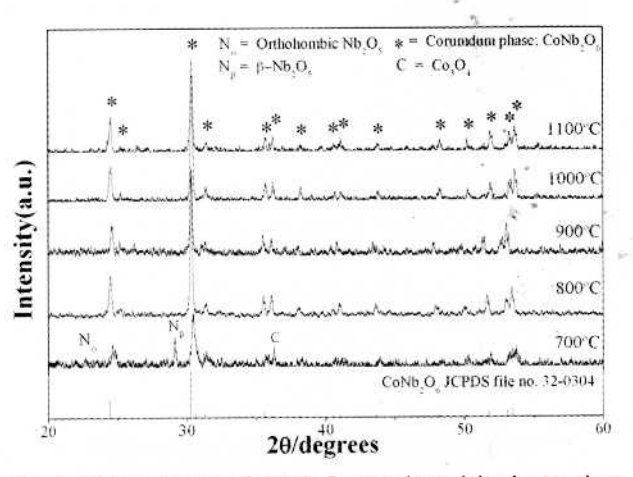


Fig. 3. XRD patterns of CoNb₂O₆ powder calcined at various temperatures for 4 h with heating/cooling rates of 20 Kminute⁻¹.

to the DTA measurements, these data were used to define the range of calcination temperature for XRD investigation between 700 °C and 1100 °C.

XRD paterns of all calcined powders are given in Fig. 3. It is seen that CoNb₂O₆ crystallites were already developed in the powder at a calcination temperature as low as 700 °C, accompanied with cubic-Co₃O₄ (JCPDS files No 78-1969), orthorhombic-Nb₂O₅ (JCPDS files No 27-1003), monoclinic-β-Nb₂O₅ (JCPDS files No 26-0885). No evidence of a cubic phase of CoO was found. The strongest reflection from Co₃O₄, (200), was located at $2\theta = 36.8$ whereas the observed temperature variation of Nb₂O₅ in terms of the intensity and position of the peaks attested to a number of phase changes. In niobium oxide synthesis through precipitation from solution, the calcination temperature has a significant effect on the crystal structure of the resulting oxide. The XRD patterns show that the transformation from the orthorhombic-Nb₂O₅ to monoclinic-β-Nb₂O₅ takes place as the calcination temperature increases, which was reported earlier by Belous et al. [9]. As the temperature increased to 800 °C, the intensity of the columbite CoNb₂O₆ peaks was further enhanced and it became the only phase. Upon calcination at 900, 1000 and 1100 °C, an essentially single of CoNb₂O₆ phase was obtained. This CoNb₂O₆ phase was able to be indexed according to an orthorhombic columbite-type structure with lattice parameters a = 571 pm, b = 1414 pmand c = 504 pm, space group Pcan (no. 60), consistent with JCPDS file number 32-0304. Having established the optimum calcination temperature, dewll times ranging from 15 minute to 120 minute with constant heating/cooling rate of 5 Kminute⁻¹ were applied at 800 °C, as shown in Fig. 4. It can be seen that a single-phase of CoNb₂O₆ powders was also successfully obtained with a calcinations temperature of 800 °C and a dwell time of 120 minutes or more applied. This was apparently a consequence of the enhancement in crystallinity of the CoNb2O6 phase with increasing dwell time. The disappearance of monoclinicβ-Nb₂O₅ and orthorhombic-Nb₂O₅ phase indicated that full crystallization has occurred at relative shorter calcinations

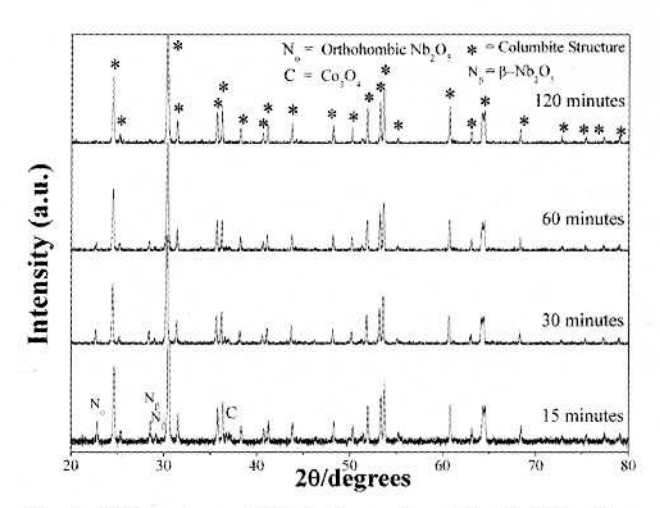


Fig. 4. XRD patterns of CoNb₂O₆ powder calcined with heating/ cooling rates of 20 Kminute⁻¹ at 800 °C for 15-240 minutes.

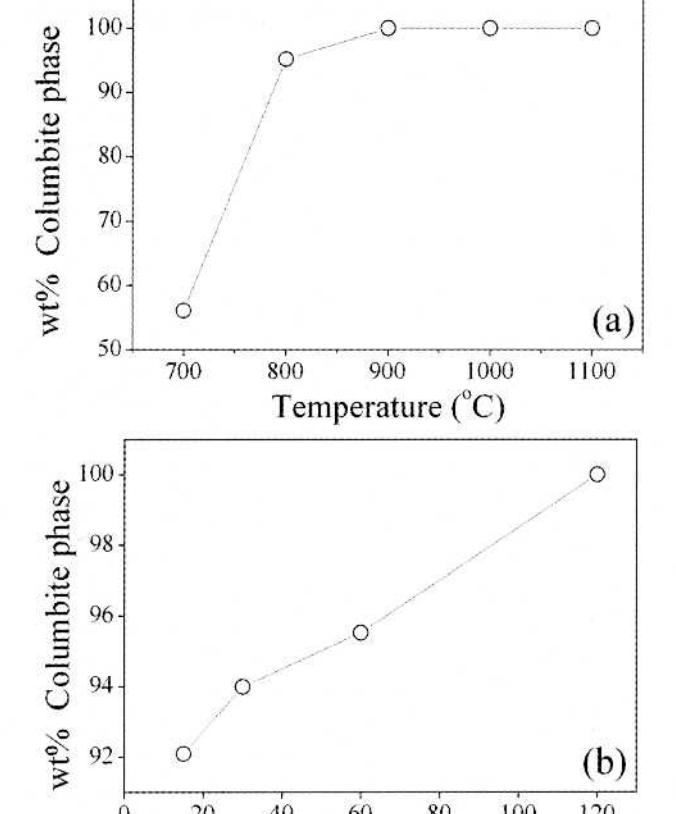


Fig. 5. Fraction of the columbite phase formed in CoNb₂O₆. specimens (a) as a function of calcination temperature (calcined for 4 hours) (b) as a function of calcination time (calcined at 800 °C).

60

Time (minute)

80

100

120

40

0

20

times. The observation that the dwell time may also play an important role in obtaining a single phase product is also consistent with other systems [10, 11]. The columbite phase formation at various calcination temperatures and time is shown in Fig. 5(a) and (b). By increasing the calcination temperature from 700 to 1100 °C, the yield of the columbite phase increased significantly until at 800 °C, a single phase of CoNb₂O₆ was formed. However,

form the present study, there are no significant differences between the powders calcined at temperatures ranging from 800 to 1100 °C. This observation agrees well with those derived from the DTA results. Apart from the calcination temperature, the effect of dwell time was also found to be quite significant (Fig. 4). It is seen that the single phase of CoNb₂O₆ (yield 100% within the limitations of the XRD technique) was found to be in powders, calcined at 800 °C with a dwell time of 120 minutes or more. The average grain sizes were determined from XRD patterns according to the Scherrer's equation:

$$D = \frac{k\lambda}{\beta \cos \theta_R} \tag{2}$$

where D is the average grain size, k is a constant equal to $0.89, \theta_B$ is the (311) peak angle, λ is the X-ray wavelength equal to 1.5406 Å and β is the half peak width. The average grain size of CoNb₂O₆ powders at 800 °C with a dwell time of 120 minutes was about 280 nm.

Because the raw materials used were multiphase, the formation reaction of the columbite phase belongs to a heterogeneous system. A model used to treat multiphase reaction kinetics was derived by Johnson and Mehl and the equation for this reaction is:

$$\ln[1/(1-y)] = (kt)^n \tag{3}$$

where v is the constant of the columbite phase formed, k the reaction rate constant, t the calcination time and nis the reaction order [12, 13]. The relation of $\ln \left[\ln \frac{1}{1-y} \right]$ versus ln t is plotted in Fig. 6. From this graph, it was found that the phase transformation of the columbite phase obeys this theory of phase transformations [14]. This phenomenological model is based on the theory of nucleation and growth and is accurate for a large number of systems. The fact that the data in Fig. 6 closely follow Eq. (3) indicates that the columbite phase grows at a constant rate from a random distribution of point nuclei [14]. SEM micrographs of the calcined CoNb2O6 powders are given in Fig. 7(a) and 7(b). In general, the particles are agglomerated

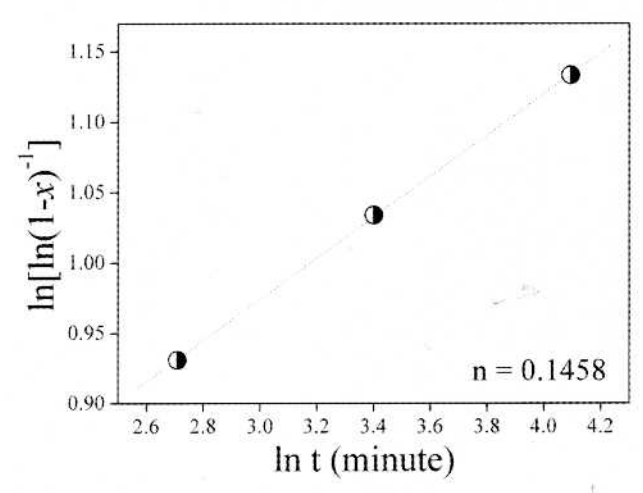


Fig. 6. Johnson-Mehl-Avrami-type for the formation of columbite phase in CoNb2O6 specimens isothermally heat treated at 800 °C.

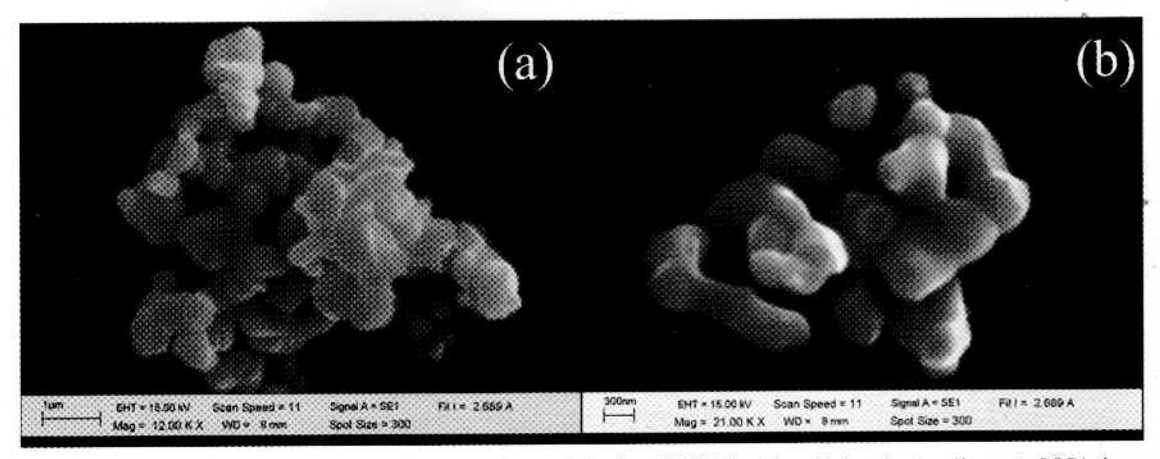


Fig. 7. Scanning electron micrographs of the CoNb₂O₆ powders calcined at 800 °C for 2 h, with heating/cooling rate 5 °C/min.

and basically irregular in shape, with a substantial variation in particle size and morphology. The particle size can be estimated from SEM micrographs to be in the range of 70-300 nm. A detailed study at higher magnification (Fig. 7(b)) showed that the particles had spherical secondary particles, composed of nano-sized primary particulates.

Conclusions

Polycrystalline powder of $CoNb_2O_6$ was synthesized using solid state synthesis using oxides as starting materials. Evidence has been obtained for a 100% yield of $CoNb_2O_6$ at a calcination temperature of 800 °C for 120 minutes with heating/cooling rates of 5 Kminute⁻¹. XRD showed the compound to have the columbite structure, having orthorhombic lattice parameters of $a = 5.06880(\pm 0.0014) \text{Å}$, $b = 14.1348 \ (\pm 0.0046) \text{Å}$ and $c = 5.2230 \ (\pm 0.0072) \text{Å}$.

Acknowlegements

This work was supported by the Thailand Research Fund (TRF), the Commission on Higher Education (CHE), Thailand Graduate Institute of Science and Technology (TGIST), National Research Council of Thailand (NRCT) and King Mongkut's Institute of Technology Ladkrabang.

References

- A.J. Moulson and J.M. Herbert, Electroceramics: Materials, Properties, Applications, Chapman and Hall, New York (1990).
- 2. A.S. Bhalla, R. Guo and R. Roy, Mat. Res. Innovat. 1 (2000)
- N. Vittayakorn and T. Tunkasiri, Phys. Scr. T129 (2007) 199-204.
- T.R. Shrout and A. Halliyal, Am. Ceram. Soc. Bull. 66[4] (1987) 704-711.
- S.L. Swartz and T.R. Shrout, Mater. Res. Bull. 17 (1982) 1245-1250.
- 6. N. Vittayakorn, J. Ceram. Process. Res. 7 (2006) 288-291.
- 7. N. Vittayakom and S. Wirunchit, Smart Mater. Struct. 16 (2007) 851-857.
- 8. A. Ngamjarurojana, O. Khamman, R. Yimnirun and S. Ananta, Materials Letters 60 (2006) 2867-2872.
- A.G. Belous, O.V. Ovchar, D.O. Mishchuk, A.V. Kramarenko, B. Jancar, J. Bezjak and D. Suvorov, Inorg. Mater. 43 (2007) 412-417.
- R. Wongmaneerung, R. Yimnirun and S. Ananta, Materials Letters 60 (2006) 2666-2671.
- R. Wongmaneerung, T. Sarakonsri, R. Yimmirun and S. Ananta, Mat. Sci. Eng. B-Solid. 132 (2006) 292-299.
- 12. M.J. Avrami, J. Chem. Phys. 8 (1940) 212-224.
- 13. M.J. Avrami, J. Chem. Phys. 9 (1941) 177-184.
- J.W. Christian, The Theory of Transformations in Metals and Alloys: Part I., Pergamon Press, Oxford (2002).

Ferroelectric phase stabilization, phase transformations and thermal properties in (1-x)PbZrO₃-xPb(Co_{1/3}Nb_{2/3})O₃ solid solution

Wanwimon Banlue · Naratip Vittayakorn

Received: 12 February 2008 / Accepted: 15 May 2008 / Published online: 6 June 2008 © Springer-Verlag 2008

Abstract The solid solution between the antiferroelectric PbZrO₃ (PZ) and relaxor ferroelectric Pb(Co_{1/3}Nb_{2/3})O₃ (PCoN) was synthesized by the columbite method. The phase structure and thermal properties of (1-x)PZ-xPCoN, where x = 0.0-0.3, were investigated. With these data, the ferroelectric phase diagram between PZ and PCoN has been established. The crystal structure data obtained from XRD indicates that the solid solution PZ-PCoN, where x = 0.0–0.3, successively transforms from orthorhombic to rhombohedral symmetry with an increase in PCoN concentration. The AFE \rightarrow FE phase transition was found in the compositions of $0.0 \le x \le 0.10$. The AFE \rightarrow FE phase transition shift to lower temperatures with higher compositions of x. The width of the temperature range of FE phase was increased with increasing amount of PCoN. It is apparent that the replacement of the Zr^{4+} ion by $(Co_{1/3}Nb_{2/3})^{4+}$ ions would decrease the driving force for antiparallel shift of Pb²⁺ ions, because they interrupt the translational symmetry. This interruption caused the appearance of a rhombohedral ferroelectric phase when the amount of PCoN was more than 10 mol%.

PACS 61.05.cp · 77.80.Bh · 65.40.-b · 77.22.-d · 77.80.-e · 77.84.Dy

W. Banlue · N. Vittayakorn (☒)
Materials Science Research Unit, Department of Chemistry,
Faculty of Science, King Mongkut's Institute of Technology
Ladkrabang, Bangkok 10520, Thailand

e-mail: naratipcmu@yahoo.com

1 Introduction

A lot of attention has been given to the lead zirconate, (PbZrO₃; PZ) and modified-PZ in several recent years as regards theoretical, experimental and industrial applications [1-3]. At room temperature PZ has an antiferroelectric phase (AFE) which has an orthorhombic structure. It undergoes the AFE to a paraelectric phase (PE) and transforms from an orthorhombic structure to a cubic structure at 236 °C [1]. It is reported that there exists a ferroelectric phase (FE) over a very narrow temperature range (230-233 °C). The FE intermediate phase can also be introduced by partial replacement of Pb2+ ions with A-site ions such as Ba²⁺ ions [4] or La³⁺ ions [5]. Due to the differences of AFE and FE phases in the unit cell parameters, this phase transition is accompanied by a nonlinear change in physical properties, such as an abrupt jump in polarization and strain, or a large charge release [4]. Lead cobalt niobate Pb(Co_{1/3}Nb_{2/3})O₃ (PCoN) is one of the first known relaxor ferroelectrics (RFE). The sub-micro-scale heterogeneous distribution of the B-cations is believed to be the origin of their relaxor nature, typically having a diffuse and frequency-dependent maximum in the variation of the relative permittivity with temperature [6]. PCoN was first reported by Smolenskii and Agranovskaya in 1958 [6, 7] that PCoN displays typical RFE behavior with a maximum dielectric constant occurring near -90°C, and at 1 kHz [6].

Since PCoN is a relaxor ferroelectric with a broad dielectric peak near $T_c \approx -90\,^{\circ}\text{C}$ and PZ is an antiferroelectric with a sharp maximum in the permittivity at $T_c \sim 230\,^{\circ}\text{C}$, the Curie temperature in the PZ–PCoN system can be engineered over a wide range of temperature by controlling the amount of PCoN in the system. Although the PZ ceramic has a better dielectric breakdown strength than PCoN, the sintering temperature is also higher [3, 8]. Thus, mixing



PCoN with PZ is expected to decrease the sintering temperature of PZ-based ceramics, a desirable move towards an electrode of lower cost [5]. Moreover, since PZ-PCoN is not a pure-relaxor ferroelectric system, it is easier to prepare single phase ceramics with a lower amount of undesirable pyrochlore phases [9]. Furthermore, no work has been done on the metastable FE phase induced by b-site substitution in perovskite PZ. With their complementary characteristics, it is expected that excellent properties can be obtained from ceramics in the PZ-PCoN system.

In this study, a metastable FE phase induced by b-site substitution was studied as a function of composition and temperature. The columbite precursor method was used to synthesize the $(1-x)\text{PbZrO}_3-x\text{Pb}(\text{Co}_{1/3}\text{Nb}_{2/3})\text{O}_3$ (PZ–PCoN), with x=0.00–0.30. The structural phase, microstructure and thermal properties of the PZ–PCoN ceramics were investigated as a function of composition x. DSC measurements were also used to study the details of AFE to FE and FE to PE phase transformations accompanied with an evaluation of the thermal behavior of the PZ–PCoN samples. The results were discussed.

2 Experimental procedure

The (1 - x)PbZrO₃-xPb(Co_{1/3}Nb_{2/3})O₃ (PZ-PCoN), $0.00 \le x \le 0.30$, ceramics were prepared using a columbite precursor method in order to avoid the formation of a pyrochlore phase. The columbite phase CoNb₂O₆ was formed by reacting CoO (99.9%) with Nb₂O₅ (99.9%) at 1100 °C for 4 hours. The raw materials of PbO, ZrO₂ and CoNb₂O₆ were weighed and mixed. Each mixture of the starting powders was milled and mixed in a ball mill, as well as wethomogenized with ethanol for 18 h using YTZ zirconia grinding media. The suspensions were dried and the powders were ground using an agate mortar and sieved into fine powder. All obtained powders were calcined at 850 °C for 2 h. The calcined powders were milled for 3 hours for reduced particle size. After grinding and sieving, the calcined powder was mixed with 5 wt% poly (vinyl alcohol) binder and uniaxially pressed into a pellet. Binder burnout occurred by slowly heating to 500 °C and holding for 2 hours. Sintering occurred between 1100-1250 °C with a dwell time of 4 hours depending on the composition. To mitigate the effects of lead loss during sintering, the pellets were sintered in a closed alumina crucible containing PbZrO₃ powder. The density of the sintered PZ-PCoN pellets was measured by the water immersion method (Archimedes method). The relative density of all the sintered pellets was approximately 94-96% of the theoretical density. The phase transition temperatures and enthalpy (ΔH) of the phase transitions were determined by DSC. This was operated from room temperature to 250 °C with a heating rate of 10 °C/min.

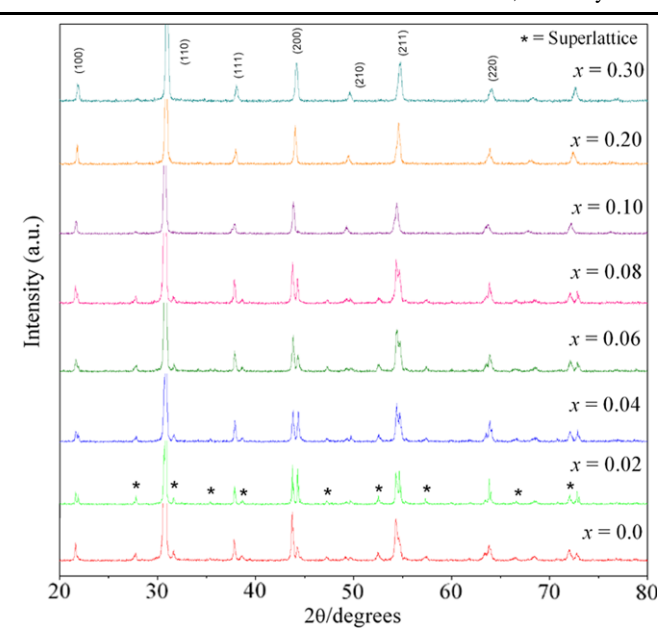


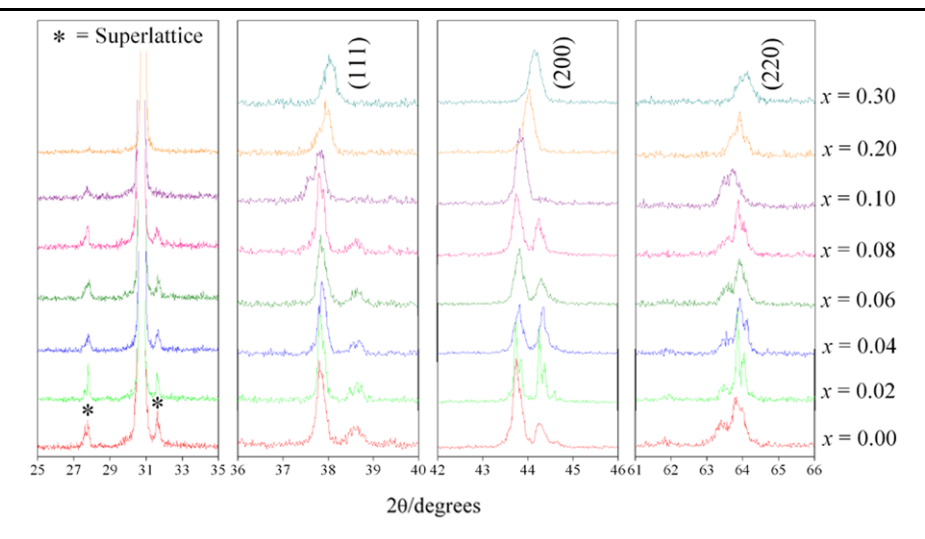
Fig. 1 XRD patterns of (1 - x)PZ–xPCoN ceramics with x = 0.0–0.3 at the optimum sintering conditions

3 Results and discussion

Figure 1 shows XRD patterns of ceramics in the PZ–PCoN system with a well crystallized perovskite structure for all compositions. The pyrochlore phase was not observed in this system at all. Ceramics with $0.02 \le x < 0.1$ had the same crystal structure with PZ, i.e., an orthorhombic unit cell at room temperature. If the XRD pattern of PZ is indexed on the basic of the pseudo-cubic cell, then $1/4(h \ k \ l)$ -type superlattice reflections representing the antiparallel shifts of Pb²⁺ ions will appear. In Fig. 1, all the indices were based on the pseudo-cubic cell, and the XRD patterns of the samples with $0.02 \le x < 0.1$ showed the presence of $1/4(h \ k \ l)$ type superlattice reflections. According to Glazer [10], these types of reflections represent antiphase tilting of the oxygen octrahedra without distortion. In Fig. 1, PZ-PCoN samples with $0.1 \le x \le 0.3$ showed only the fundamental reflections of the pseudo-cubic perovskite cell. The relative intensity of superlattice reflections decreased with increasing PCoN content as shown in Fig. 2. This result demonstrates that the superlattice disappeared with the addition of 10 mol% PCoN. Figure 2 shows the results for $1/4(h \ k \ l)$ -type superlattice reflections, (1 1 1), (2 0 0) and (2 2 0) reflections. The samples with x = 0.1, 0.2 and 0.3 had a split (1 1 1) and (2 2 0) reflection and a single (2 0 0) reflection. This results confirms that the crystal structure of the samples with x = 0.1, 0.2 and 0.3 is primitive rhombohedral perovskite. For the pure rhombohedral structure, the 2 0 0 group of reflections should be a singlet. In the PZ-PCoN system, the A-site is occupied by Pb²⁺ (0.1630 nm) ions, and the Co²⁺, Nb⁵⁺ and Zr⁴⁺ ions occupy the B site of



Fig. 2 XRD patterns of the $1/4(h \ k \ l)$ -type superlattice reflections, and the $(1\ 1\ 1)$, $(2\ 0\ 0)$ and $(2\ 2\ 0)$ peaks of (1-x)PZ-xPCoN ceramics with x=0.0-0.3



the ABO₃ perovskite crystal structure. The average ionic radius of B-site ions in the composition (1 - x)PbZrO₃–xPb(Co_{1/3}Nb_{2/3})O₃ can be calculated from the following equation:

$$r_{\text{B-site}} = (1 - x) \lfloor r_{\text{Zr}^{4+}} \rfloor + x \lfloor 1/3r_{\text{Co}^{2+}} + 2/3r_{\text{Nb}^{5+}} \rfloor,$$
 (1)

where the ionic radii of Co²⁺, Nb⁵⁺ and Zr⁴⁺ are 0.0790, 0.0780 and 0.0860 nm, respectively [11]. In general, the lattice parameters of the perovskite structure also decreased gradually as x increased, undoubtedly because of the introduction of the smaller cobalt niobium ion (r = 0.783 Å)into the zirconium site (r = 0.86 Å), resulting in a decreasing of the unit cell according to the Vegard rule. The effective size of the B-site ion increased with increasing mole fraction of PCoN primarily due to the smaller ionic radii of $(Co_{1/3}Nb_{2/3})^{4+}$. This shift in the B-site ionic radius is shown in the XRD data in Fig. 2 as the diffraction peaks are shifted toward higher angles. The influence of the addition of Pb(Co_{1/3}Nb_{2/3})O₃ on the phase structure of the PbZrO₃-Pb(Co_{1/3}Nb_{2/3})O₃ system is similar to that of $(Pb_{1-x}Ba_x)ZrO_3$ [12]. The substitution of smaller $(Co_{1/3}Nb_{2/3})^{4+}$ ions with Zr^{4+} sites, which implies the transition of the PZ-PCoN structure from orthorhombic to rhombohedral as shown in Fig. 2, may facilitate the parallel displacement along the [1 1 1] direction and the associated displacements of three oxygen ions in the PZ-PCoN structure, resulting in an improvement of ferroelectricity. The presence of a polar axis in the [1 1 1] direction has been reported for the ferroelectric rhombohedral structure [13].

The DSC technique was used as the primary tool to investigate the influence of the addition of Pb(Co_{1/3}Nb_{2/3})O₃ on phase transitions. Transition temperatures, including paraelectric (PE) transitions, are summarized in Table 1. Figure 3 shows the results of a differential scanning calorimeter (DSC) analysis of the PZ–PCoN samples. As shown in Fig. 3, two distinct endothermic peaks were observed for

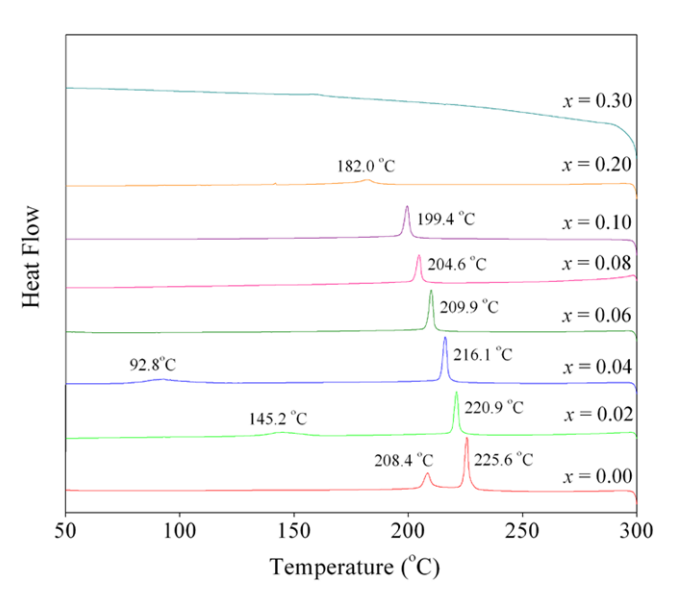


Fig. 3 Typical differential scanning calorimetry (DSC) curves for (1-x)PZ-xPCoN ceramics with x=0.0–0.3

PZ–PCoN samples with $0.0 \le x \le 0.10$. The lower temperature corresponds to the transition temperature of the AFE \rightarrow FE phase transition, while the higher temperature corresponds to the FE \rightarrow PE phase transition. It is well known that the good quality ceramic as well as single crystal samples of PZ show two distinct endothermic peaks around 230 °C and 215 °C corresponding to the PE to FE and FE to AFE transitions, respectively, on cooling [14, 15]. The AFE \rightarrow FE phase transition was found in the compositions of $0.0 \le x \le 0.10$. The peaks shift to lower temperatures with higher compositions of x. From Table 1, the width of the temperature range of FE phase continuously increases with PCoN content. The width of the temperature range of FE phase is around 17.2, 75.7, 123.3 and 176.9 °C for composition x = 0.00, 0.02, 0.04 and 0.06, respectively.



568 W. Banlue, N. Vittayakorn

Table 1 Characteristics of (1 - x)PZ - xPCON ceramics with optimized processing conditions (R, Rhombohedral; O, Orthorhombic)

Composition (x)	Crystal structure	Lattice parameter (Å)			Phase transition temperature (°C)		Enthalpy (J/g)	
		a	b	c	$AFE \rightarrow FE$	$FE \rightarrow PE$	$AFE \rightarrow FE$	$FE \rightarrow PE$
0.00	0	7.27	9.92	8.21	208.4	225.6	1.19	2.63
0.02	О	7.25	9.92	8.21	145.2	220.9	1.60	3.44
0.04	О	7.23	9.91	8.21	92.8	216.1	1.71	3.47
0.06	O	7.27	9.92	8.2	33.3	209.9	1.03	2.83
0.08	О	7.25	9.93	8.22	_	204.6	_	2.78
0.10	R		4.11		_	199.4	_	2.40
0.20	R		4.10		_	182.0	_	1.20
0.30	R		4.09		_	158.2	_	0.44

It is of interest to note that the areas under two endothermic peaks in Fig. 3 decreased with increasing amount of PCoN. Since those areas represent the free-energy difference between the two phases, this result indicates that the addition of PCoN decreases the stability of the orthorhombic phase. It is apparent that the replacement of the Zr⁴⁺ ion by $(Co_{1/3}Nb_{2/3})^{4+}$ ions would decrease the driving force for antiparallel shift of Pb²⁺ ions, because they interrupt the translational symmetry. This interruption caused the appearance of a rhombohedral ferroelectric phase when the amount of PCoN was more than 10 mol%. Gotor et al. [16] studied the relationships between the structure change of BaTiO₃ and its enthalpy by using DSC. They found that the reduction of the tetragonality (c/a) of BaTiO₃ is accompanied by a reduction of the enthalpy. However, in the present work, the decreasing of ΔH is proportional to the fraction ratio of FE and PE phase in PZ-PCoN. Based on the results of x-ray diffraction and DSC data, the phase diagram for the (1 - x)PZ - xPCoN binary system has been established, as shown in Fig. 4. The transition temperature decreases approximately linearly with x, from $T_c = 225.6$ °C for x = 0.0to 158.2 °C for x = 0.3. The phase diagram consists of three distinct crystallographic phases in this system; high temperature paraelectric cubic (Pm3m), rhombohedral (R3m), and ferroelectric orthorhombic (P2cb (no. 32)). At the low concentrations of PCoN with x < 0.1 the symmetry can be defined as orthorhombic. The orthorhombic symmetry transforms into rhombohedral at a composition near x = 0.1.

Figure 5(a) and (b) show scanning electron microscopy (SEM) images of the fracture surfaces of the PZ–PCoN ceramics at x=0.02 and 0.2, respectively. No plate-like grains were observed in both samples, indicating the absence of pyrochlore formation. Other compositions of the system also exhibited a high density and an irregular grain size and shape. By applying the linear intercept methods to these SEM micrographs, the average grain size was calculated to be between 0.57 and 0.59 μ m for all of the samples. There was no systematic variation in grain size as a function

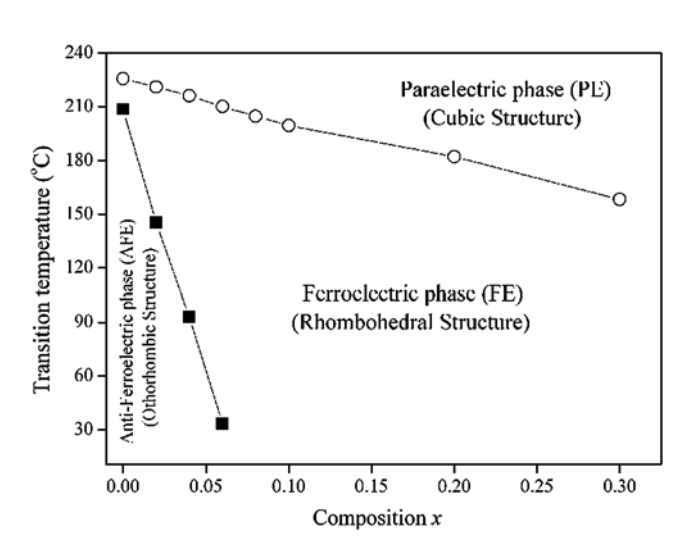


Fig. 4 Phase diagram of the (1-x)PZ-xPCoN binary system with x = 0.0-0.3 determined from room temperature XRD and DSC as a function of temperature. The symbols refer to quantities as follows: \blacksquare = the transition temperature from the antiferroelectric state (AFE) to the ferroelectric state (FE); \bigcirc = the transition temperature from the ferroelectric state (FE) to the paraelectric state (PE)

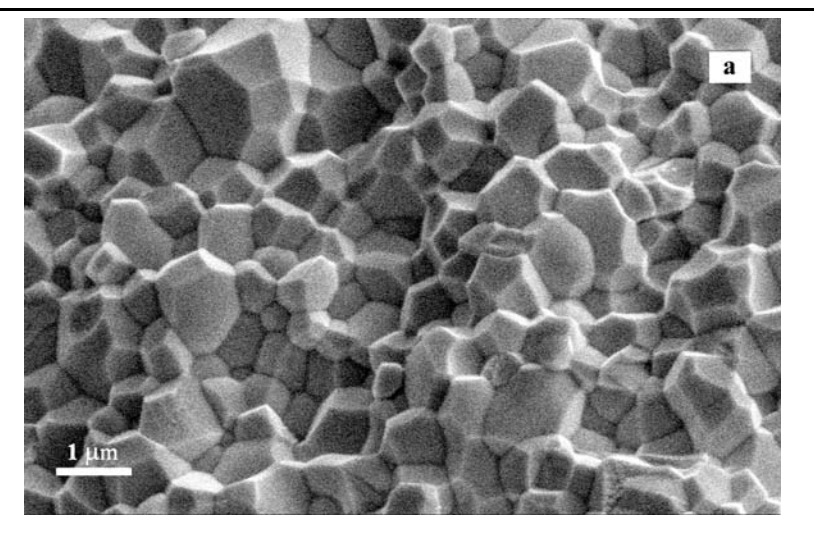
of composition according to the different sintering schedules used.

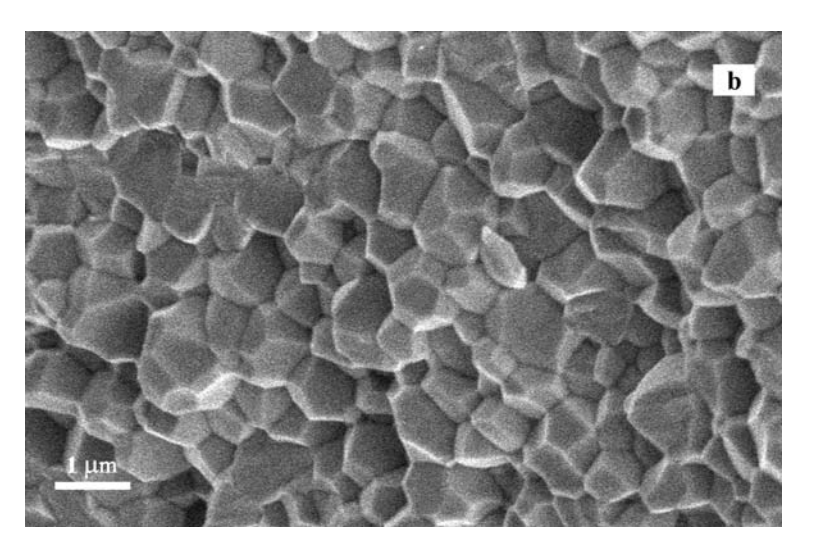
4 Conclusions

We have been the first to demonstrate the effect of PCoN in stabilizing the rhombohedral phase relative to the orthorhombic phase in PZ ceramics. The crystal structure data obtained from XRD indicates that the solid solution PZ–PCoN, where x=0.0–0.3, successively transforms from orthorhombic to rhombohedral symmetry with an increase in PCoN concentration. The AFE \rightarrow FE phase transition was found in the compositions of $0.0 \le x \le 0.10$. The AFE \rightarrow FE phase transition shifts to lower temperatures with higher compositions of x. The width of the temperature range of the FE phase increases with increasing amount



Fig. 5 Fracture surfaces of (1-x)PZ-xPCoN ceramics with (**a**) x = 0.02 and (**b**) x = 0.2





of PCoN. It is apparent that the replacement of the Zr^{4+} ion by $(Co_{1/3}Nb_{2/3})^{4+}$ ions would decrease the driving force for an antiparallel shift of Pb^{2+} ions because they interrupt the translational symmetry. This interruption caused the appearance of a rhombohedral ferroelectric phase when the amount of PCoN was more than 10 mol%.

Acknowledgements This work was supported by the Thailand Research Fund (TRF), National Research Council of Thailand (NRCT) and King Mongkut's Institute of Technology Ladkrabang (KMITL).

References

- 1. E. Sawaguchi, G. Shirane, S. Hoshino, Phys. Rev. 83, 1078 (1951)
- 2. K. Uchino, Ferroelectric Devices (Dekker, New York, 2000)

- 3. G.H. Haertling, J. Am. Ceram. Soc. 82, 797–818 (1999)
- 4. B.P. Pokharel, D. Pandey, Phys. Rev. B 65, 214108 (2002)
- 5. Y. Xu, Ferroelectric Materials and Their Application (Elsevier, Amsterdam, 1991)
- G.A. Smolenskii, A.L. Agranovskaya, Sov. Phys. Tech. Phys. 1380 (1958)
- 7. V.A. Isupov, Sov. Phys. Solid State 5, 136 (1958)
- 8. B. Jaffe, W.R. Cook, *Piezoelectric Ceramic* (R.A.N. Publishers, 1971)
- 9. T.R. Shrout, A. Halliyal, Am. Ceram. Soc. Bull. 66, 704 (1987)
- 10. A.M. Glazer, Acta Crystallogr. A 31, 756 (1975)
- 11. R.D. Shannon, Acta Crystallogr. A 32, 751 (1976)
- 12. B.P. Pokharel, D. Pandey, J. Appl. Phys. **86**, 3327–3332 (1999)
- 13. G. Shirane, S. Hoshino, Acta Crystallogr. 7, 203 (1954)
- 14. G. Shirane, E. Sawaguchi, Y. Takagi, Phys. Rev. **84**, 476 (1951)
- 15. R.W. Whatmore, A.M. Glazer, J. Phys. C 12, 1505 (1979)
- F.J. Gotor, C. Real, M.J. Dianez, J.M. Criado, J. Solid State Chem. 123, 301 (1996)



©2008 The Japan Society of Applied Physics

Synthesis and Dielectric and Ferroelectric Properties of Ceramics in (1-x)Pb $(Zr_{1/2}Ti_{1/2})O_3$ –(x)Pb $(Co_{1/3}Nb_{2/3})O_3$ System

Anurak Prasatkhetragarn*, Naratip Vittayakorn¹, Supon Ananta, Rattikorn Yimnirun, and David P. Cann²

Department of Physics, Faculty of Science, Chiang Mai University, Chiang Mai 50200, Thailand

(Received August 16, 2007; revised September 28, 2007; accepted October 26, 2007; published online February 15, 2008)

Ceramics in a PZT-PCN system with the formula $(1-x)Pb(Zr_{1/2}Ti_{1/2})O_3-(x)Pb(Co_{1/3}Nb_{2/3})O_3$, where x=0.1-0.5, were prepared using a solid-state mixed-oxide technique (the columbite-wolframite precursor method). The phase formation behavior and microstructure were studied using X-ray diffraction (XRD) analysis and scanning electron microscopy (SEM), respectively. The dielectric and ferroelectric properties of the compounds were studied and discussed. Phase-pure perovskites of PZT-PCN ceramics were obtained over a wide compositional range. In addition, the XRD, dielectric, and ferroelectric properties confirmed that the morphotropic phase boundary (MPB) composition between the tetragonal and pseudo cubic phases of this system lied between $0.2 \le x \le 0.3$. [DOI: 10.1143/JJAP.47.998]

KEYWORDS: ferroelectric properties, perovskites, MPB, phase transition

1. Introduction

Lead-based perovskite-type solid solutions consisting of ferroelectric and relaxor materials have attracted more and more fundamental and practical attention because of their excellent dielectric, piezoelectric, and electrostrictive properties, which are useful in actuating and sensing applications. 1) Recently, many piezoelectric ceramic materials have been developed from binary systems containing a combination of relaxor and normal ferroelectric materials²⁾ that yield high dielectric permittivities [e.g., Pb(Zn_{1/3}Nb_{2/3})O₃-PbTiO₃ (PZN-PT)^{3,4)} and Pb($Zr_{1/2}Ti_{1/2}$)O₃-Pb($Ni_{1/3}Nb_{2/3}$)-O₃ (PZT-PNN)⁵], excellent piezoelectric coefficients [e.g., $Pb(Zn_{1/3}Nb_{2/3})O_3-PbTiO_3 (PZN-PT),^{3,4)} Pb(Zr_{1/2}Ti_{1/2})O_3 Pb(Zn_{1/3}Nb_{2/3})O_3$ (PZN-PZT),⁶⁾ and $Pb(Sc_{1/3}Nb_{2/3})O_3$ -PbTiO₃ (PSN-PT)^{7,8)}], and high pyroelectric coefficients [e.g., $Pb(Ni_{1/3}Nb_{2/3})O_3-PbTiO_3-PbZrO_3$ (PNN-PT-PZ)⁹⁾]. Of the lead-based complex perovskites, lead zirconate titanate [Pb(Zr_{1/2}Ti_{1/2})O₃ or PZT] ceramics have been investigated from both fundamental and applied viewpoints. 10) A solid solution of Pb(Zr_{1-x}Ti_x)O₃ (PZT) was found to host exceptionally high value for dielectric and piezoelectric properties for compositions close to the morphotropic phase boundary (MPB). This MPB is located at a $PbTiO_3:PbZrO_3$ of $\sim 1:1$ and separates the Ti-rich tetragonal phase from the Zr-rich rhombohedral phase. 10) Furthermore, it has a high T_C of 390 °C, which allows piezoelectric devices to be operated at relatively high temperatures. Most commercial PZT ceramics are designed in the vicinity of the MPB with various doping methods in order to achieve high properties.

Lead cobalt niobate (PCN) is a perovskite relaxor ferroelectric with a broad diffuse phase transition near $-70 \,^{\circ}\text{C.}^{11)}$ The structure is cubic at room temperature (RT). In this compound, the octahedral sites of the crystal are randomly occupied by Co^{2+} and Nb^{5+} ions. $^{12)}$ Malkov and Venevtsev have indicated that there are large deviations in the temperatures at which the permittivity is maximum (T_{m}) for singlecrystal and ceramic samples. $^{13)}$ The effects of the DC bias on The overall purpose of this study is to determine the phase transition, grain size, and composition dependence of the dielectric properties and ferroelectric behavior of ceramics in a $(1-x)\text{Pb}(\text{Zr}_{1/2}\text{Ti}_{1/2})\text{O}_3-(x)\text{Pb}(\text{Co}_{1/3}\text{Nb}_{2/3})\text{O}_3$ (where x=0.1-0.5) binary system prepared using the columbite-wolframite precursor method.

2. Experimental Procedure

Reagent-grade oxides of PbO, CoO, Nb₂O₅, ZrO₂, and TiO₂ (anatase-structure) were used as raw materials. The columbite CoNb₂O₆ and wolframite ZrTiO₄ precursors were weighed and introduced into the batch calculations. CoNb₂O₆ and ZrTiO₄ powders were prepared at calcination temperatures of 1100 and 1450 °C for 2 h, respectively. In the present work, (1-x)Pb(Zr_{1/2}Ti_{1/2})O₃–(x)Pb(Co_{1/3}-Nb_{2/3})O₃ samples with compositions of x=0.1–0.5 were prepared from ZrTiO₄, CoNb₂O₆, and PbO powders. PZT–PCN powders were synthesized using the solid-state reaction of these raw materials and mixed by a vibro-milling technique in ethanol for 1 h. PbO excess of 2.0 mol % was constantly added to compensate for lead losses during calcination and sintering.¹⁷⁾ After drying, the product was calcined in an alumina crucible at a temperature of 950 °C.

¹Department of Chemistry, Faculty of Science, King Mongkut's Institute of Technology Ladkrabang, Bangkok 10520, Thailand

²Materials Science, Department of Mechanical Engineering, Oregon State University, Corvallis, OR 97331, U.S.A.

the dielectric properties have been reported as a function of temperature for single-crystal Pb(Co_{1/3}Nb_{2/3})O₃ with a diffuse phase transition.¹⁴⁾ Although the paraelectric–ferroelectric transition temperature of PCN is below RT, it can be easily shifted upward with the addition of PbTiO₃ (PT), which is a normal ferroelectric compound with a phase transition at 490 °C. 15) In addition, it is well known that the addition of PZT enhances the piezoelectric, dielectric, and ferroelectric properties in a solid solution with a relaxor ferroelectric such as PZT-PZN, 16,17) PZT-PNN, 5) and PZT-PMN.¹⁸⁾ On the basis of this approach, solid solutions of PZT and PCN are expected to synergistically combine the properties of both the normal ferroelectric PZT and relaxor ferroelectric PCN, which could exhibit piezoelectric and dielectric properties that are better than those of the singlephase PZT and PCN. 12,19) There have been no systematic studies on the electrical properties of ceramics within a wide composition range between PZT and PCN.

^{*}E-mail address: Prasatkhetragarn@yahoo.com

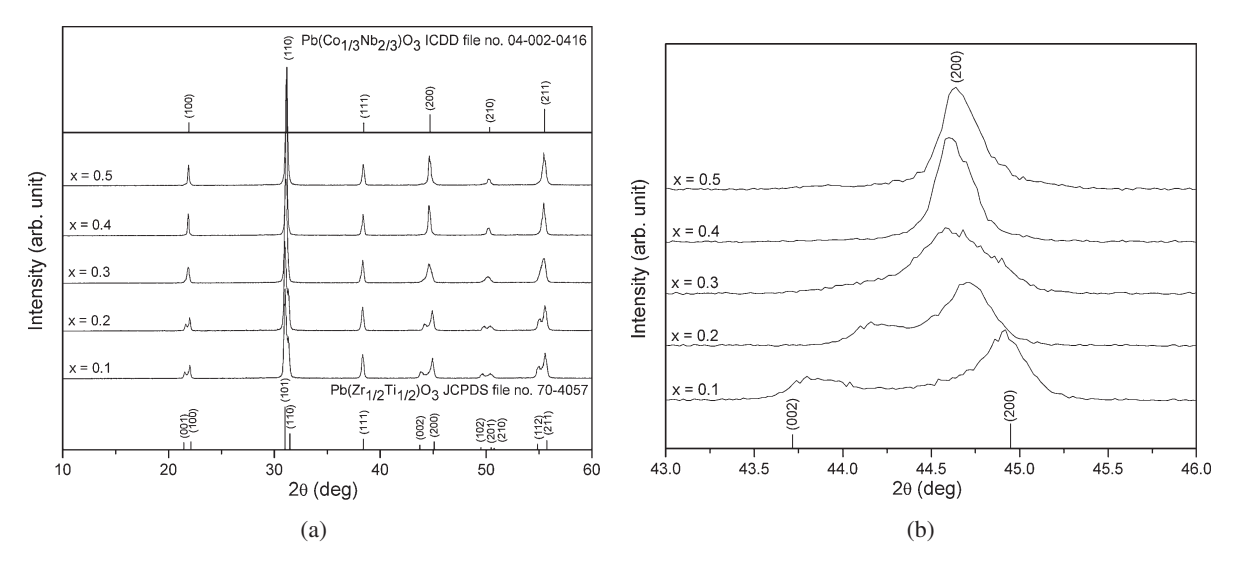


Fig. 1. XRD patterns of (1 - x)PZT-(x)PCN ceramics, where x = 0.1-0.5.

The calcined powders were pressed hydraulically to form disc-shaped pellets with a diameter of 10 mm and a thickness of 1 mm, with 1 wt % poly(vinyl alcohol) (PVA) added as a binder. The pellets were sintered at 1200 °C for 2 h at a heating/cooling rate of 5 °C/min. The phase structure of the powders was analyzed via X-ray diffraction (XRD; Siemens-D500 diffractometer) analysis using Cu K α radiation. The microstructures of the sintered samples were examined using scanning electron microscopy (SEM; JEOL JSM-840A). The dielectric properties of the samples were measured using an automated measurement system. This system consisted of an LCR meter (Hewlett-Packard HP-4284A) in connection with a Delta Design 9023 temperature chamber and a sample holder (Norwegian Electroceramics) capable of high-temperature measurement. The ferroelectric properties were examined using a simple Sawyer-Tower circuit. 18)

3. Results and Discussion

The XRD patterns of (1 - x)PZT-(x)PCN ceramics with various x values are shown in Fig. 1. It can be seen that a complete crystalline solution of the perovskite structure is formed throughout the entire compositional range without the presence of pyrochlore or unwanted phases. From the XRD data, the $Pb(Zr_{1/2}Ti_{1/2})O_3$ ceramic is identified as a single-phase material with a perovskite structure having tetragonal symmetry, which was matched with JCPDS file no. 70-4057. The XRD patterns of the PZT-PCN compositions show a range in symmetry between the tetragonal and pseudo cubic perovskite types.²⁰⁾ For a better comparison, ICDD file no. 04-002-0416 for $Pb(Co_{1/3}Nb_{2/3})O_3$ with pseudo cubic structural symmetry is also displayed in Fig. 1. It is clear that the crystal symmetry should change owing to the effects of increasing the PCN fraction and a corresponding decrease in $T_{\rm C}$. It is well known that in the pseudo cubic phase, the (200) profile will show a single narrow peak, while in the tetragonal phase, the (200) profile should be split into two peaks. More interestingly, the composition at x = 0.3 exhibited peak broadening at a 2θ of \sim 44–45°, indicating the structural transformation from the tetragonal phase, characterized by the shifting of the (002)/(200) peaks to the pseudo cubic phase. This observation is obviously associated with the composition showing the coexistence of two symmetries, which in this case are the tetragonal and pseudo cubic phases. To a first approximation, it could be said that the composition with x = 0.3 is close to the MPB of the (1 - x)PZT-(x)PCN system, where the structure of the PZT-PCN compositions gradually changes from tetragonal to pseudo cubic. The electrical data described later on will further support this assumption.

The SEM images in Fig. 2 reveal that the addition of PCN resulted in significant changes in the microstructure of the ceramics. Some grains are observed to have irregular shapes with both open and close pores as a result of the high rate of the evaporation of PbO during the sintering. 17) The images also show that the grain size of the ceramics varied considerably from 0.43 to 19.56 µm (Table I). However, the average grain size significantly decreased with an increase in the content of PCN. It can also be seen that the maximum density is obtained in the 0.7PZT-0.3PCN ceramics, while the minimum density is observed in the 0.5PZT-0.5PCN ceramics. Interestingly, the density results can be correlated to the microstructure because high-density 0.7PZT-0.3PCN ceramics show high degrees of grain close packing, whereas low-density 0.5PZT-0.5PCN ceramics contain many closed pores.

The dielectric properties of (1 - x)PZT-(x)PCN, where x = 0.1-0.5, are illustrated in Fig. 3. At RT, with an increase in the concentration of PCN, the dielectric constant tends to increase because the transition temperature of the PZT-PCN ceramics shift across RT; hence, the value of the dielectric properties measured at RT increased, as shown in Table II. Other authors have reported a similar behavior.⁵⁾ The temperature dependence of the dielectric constant for the compositions of the (1 - x)PZT-(x)PCN system show broad dielectric peaks with an increase in the concentration of PCN, which indicate a diffuse phase transition. The diffuse phase transition may have been caused by a decrease in grain size; the observed difference in the degree of diffuseness could be a result of the grain size variation, as shown in Table II,²¹⁾ and chemical inhomogenieties within the (1 - x)PZT-(x)PCN solid solution.²⁰⁾

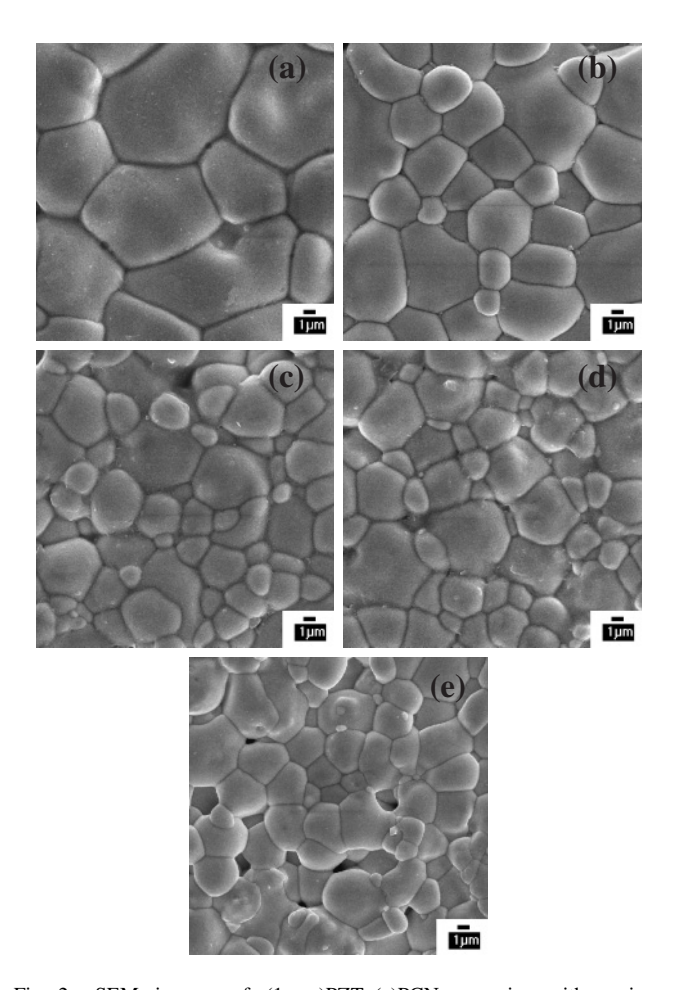


Fig. 2. SEM images of (1-x)PZT-(x)PCN ceramics with various compositions: $x = (a) \ 0.1$, $(b) \ 0.2$, $(c) \ 0.3$, $(d) \ 0.4$, and $(e) \ 0.5$.

It should be noted that the formation of MPB could be clearly seen by the crystal structure analysis as described earlier. As is well known, the value of the dielectric and ferroelectric properties of a solid solution with MPB usually maximize approximately at the MPB. An anomaly at the MPB has been observed by our group in solid solution $(x)PZT-(1-x)PNN.^{5)}$ However, no anomalies approximately at the MPB in the dielectric properties (Table II) could be found in the present work. In addition, the ferroelectric properties at approximately x=0.3 are only slightly different from those of other compositions (x=0.2, 0.4), rather than being "anomalously high". This could possibly be caused by a substitution of Ni^{2+} by Co^{2+} in the B-site, which shifts the MPB composition from x=0.2 in the PZT-PNN system to $0.2 \le x \le 0.3$ in PZT-PCN. Since in this current

Table I. Physical characteristics of (1 - x)PZT-(x)PCN ceramics, where x = 0.1-0.5.

Ceramics $(x = 0.1-0.5)$	Density (g/cm ³)	Grain size range (µm)	Average grain size (µm)
0.9PZT-0.1PCN	7.39 ± 0.05	4.54-19.56	7.45 ± 0.05
0.8PZT -0.2 PCN	7.46 ± 0.05	2.60-12.35	4.13 ± 0.05
0.7PZT-0.3PCN	7.62 ± 0.05	0.43 - 9.48	2.82 ± 0.05
0.6PZT-0.4PCN	7.42 ± 0.05	0.60-10.75	2.77 ± 0.05
0.5PZT-0.5PCN	7.31 ± 0.05	0.47 - 9.53	2.61 ± 0.05

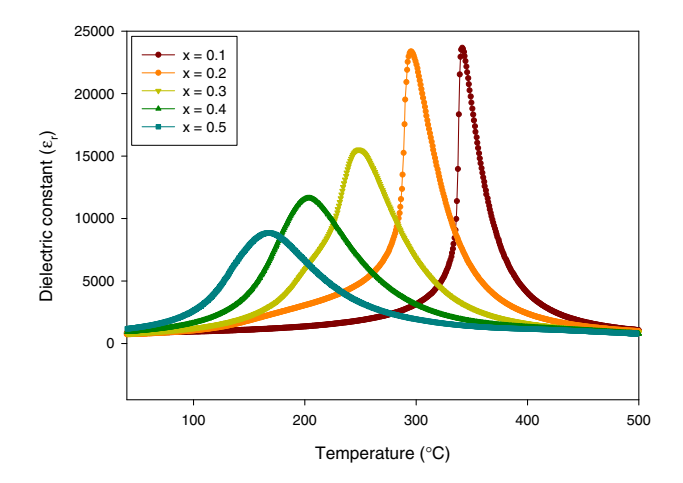


Fig. 3. (Color online) Dielectric constant (ε_r) of (1-x)PZT-(x)PCN ceramics at 100 kHz.

work, we only started with compositions at 0.1 intervals, the exact MPB composition could not be clearly identified. However, as seen in Table II, the argument that the MPB composition should fall between $0.2 \le x \le 0.3$ in PZT–PCN is supported by all the XRD and electrical data, which show drastic decreases in the value of the electrical properties in compositions with x > 0.3.

The temperature dependence of the dielectric constant (ε_r) measured at $100\,\mathrm{kHz}$ for the $(1-x)\mathrm{PZT}-(x)\mathrm{PCN}$ samples with x=0.1–0.5 is shown in Fig. 3. In an ideal solid solution of PZT and PCN, the transition temperature is expected to vary linearly between 341 and $167\,^\circ\mathrm{C}$. As shown in Table II, the Curie temperature decreased as expected with an increase in PCN content. However, the ε_r peaks became broader with increasing PCN content at $x \geq 0.3$. It was confirmed that the composition with $0.2 \leq x \leq 0.3$ is close to the morphotropic phase boundary (MPB) of the $(1-x)\mathrm{Pb}(\mathrm{Zr}_{1/2}\mathrm{Ti}_{1/2})\mathrm{O}_3$ – $(x)\mathrm{Pb}(\mathrm{Co}_{1/3}\mathrm{Nb}_{2/3})\mathrm{O}_3$ system.

Table II. Dielectric and ferroelectric properties of (1 - x)PZT - (x)PCN ceramics, where x = 0.1 - 0.5.

Ceramics $(x = 0.1-0.5)$	T _C (°C)	Dielectric properties			Ferroelectric properties (at 25 °C)			Loop	
		$\varepsilon_{ m max}$	$arepsilon_{ ext{RT}}$	γ	δ	$P_{\rm r}$ $(\mu {\rm C/cm}^2)$	$P_{\rm s}$ ($\mu { m C/cm}^2$)	E _c (kV/cm)	$(R_{\rm sq})$
0.9PZT-0.1PCN	341.40	23700	740	1.52	14.72	2.9	4.1	8.45	1.52
0.8PZT-0.2PCN	295.50	23400	800	1.68	15.73	20.1	21.6	6.84	1.91
0.7PZT-0.3PCN	248.40	15500	840	1.81	16.55	20.9	22.6	6.92	1.94
0.6PZT-0.4PCN	203.50	11600	910	1.82	16.68	18.6	20.3	6.30	1.93
0.5PZT-0.5PCN	167.50	8900	1180	1.97	16.92	14.5	15.2	6.10	1.92

To further understand the dielectric behavior of the PZT–PCN system, the ferroelectric transition can analyzed through the Curie–Weiss relationship. For normal ferroelectrics such as PZT and PCN, above the Curie temperature, the dielectric constant follows the following equation:

$$\varepsilon = \frac{c}{T - T_0},\tag{1}$$

where c is the Curie constant and T_0 is the Curie–Weiss temperature. For a ferroelectric with a diffuse phase transition such as the PZT–PCN solid solutions, the following equation applies:

$$\frac{1}{\varepsilon} \approx (T - T_{\rm m})^2,\tag{2}$$

The above equation has been shown to be valid over a wide temperature range compared with the normal Curie–Weiss law [eq. (1)]. $^{24,25)}$ In eq. (2), $T_{\rm m}$ is the temperature at which the dielectric constant is maximum. If the local Curie temperature distribution is Gaussian, the reciprocal permittivity can be written in the form: $^{5,24)}$

$$\frac{1}{\varepsilon} = \frac{1}{\varepsilon_{\rm m}} + \frac{(T - T_{\rm m})^{\gamma}}{2\varepsilon_{\rm m}\delta^2},\tag{3}$$

where $\varepsilon_{\rm m}$ is the maximum permittivity, γ is the diffusivity, and δ is the diffuseness parameter. For $(1-x){\rm PZT}{-}(x){\rm PCN}$ compositions, the diffusivity (γ) and diffuseness parameter (δ) can be estimated from the slope and intercept of the dielectric data shown in Fig. 4, and tabulated in Table II.

 γ and δ are both material constants depending on the composition and structure of the material. $^{5)}$ γ is the expression of the degree of dielectric relaxation, while δ is used to measure the degree of diffuseness of the phase transition. In a material with a "pure" diffuse phase transition described by the Smolenskii–Isutov relation [eq. (2)], γ is expected to be 2. $^{26)}$ The mean value of the diffusivity (γ) is extracted from these plots by fitting a linear equation. The values of γ vary between 1.52 and 1.97, which confirms that diffuse phase transition occurs in the PZT–PCN system. It is important to note that in perovskite ferroelectrics, it has been established that γ and δ can be affected by microstructure features, density, and grain size. ¹⁸⁾ For PZT-rich ceramics, γ and δ increase with an

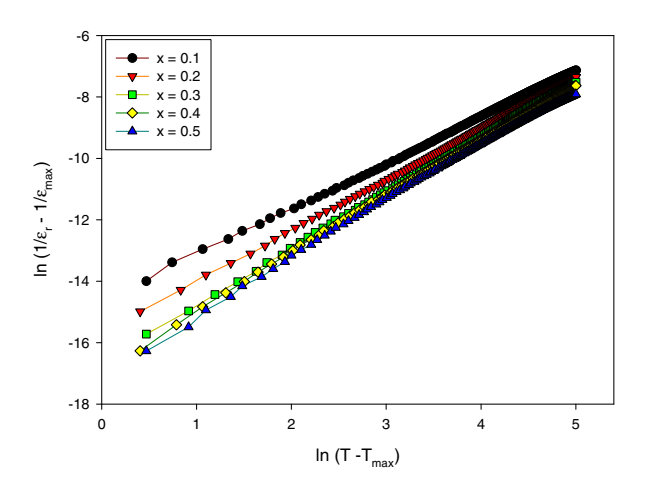


Fig. 4. (Color online) Variation of $\ln(1/\varepsilon_{\rm r}-1/\varepsilon_{\rm max})$ vs $\ln(T-T_{\rm max})$ of $(1-x){\rm PZT}$ – $(x){\rm PCN}$ ceramics.

increase in PCN content, confirming the diffuse phase transitions in PZT–PCN solid solutions. It is clear that the addition of PCN increases the degree of disorder in (1-x)PZT–(x)PCN over the compositional range $0.1 \le x \le 0.5$ with the highest degree of diffuseness exhibited in the 0.5PZT–0.5PCN composition. It should also be mentioned here that different dielectric behaviors could also be caused by grain size variation, x = 0.5PCN as noted in Table I.

The polarization-field (P-E) hysteresis loops of (1 - x)PZT-(x)PCN ceramics measured at 15 kV/cm are shown in Fig. 5. A series of well-developed and mostly symmetric hysteresis loops are observed for all compositions. It is seen that the remanent polarization (P_r) varies significantly across the compositional range. However, the coercive field E_c is relatively constant, as shown in Table II. The ferroelectric parameters obtained from the P-E loops are plotted in Fig. 6. The remnant polarization (P_r) and saturated polarization (P_s) increased from $P_r = 2.9 \,\mu\text{C/cm}^2$ and $P_s = 4.1 \,\mu\text{C/cm}^2$ in 0.9PZT-0.1PCN to reach maximum values of $P_r = 20.9 \,\mu\text{C/cm}^2$ and $P_s = 22.6 \,\mu\text{C/cm}^2$ in 0.7PZT-0.3PCN. At higher PCN contents, they then drop to $P_{\rm r} = 14.5 \,\mu{\rm C/cm^2}$ and $P_{\rm s} = 15.2 \,\mu{\rm C/cm^2}$ in 0.5PZT-0.5PCN. However, it should be noted that the $P_{\rm r}$ (2.9 μ C/ cm²) for the composition x = 0.1 in the present work is

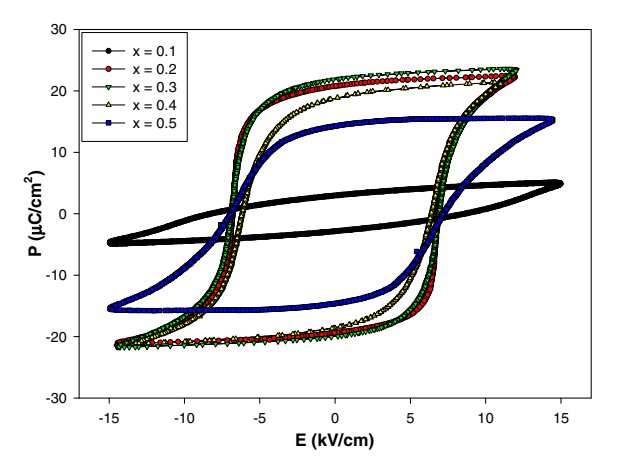


Fig. 5. (Color online) Effect of composition (x) on P–E hysteresis loops for (1 - x)PZT–(x)PCN ceramics with x = 0.1–0.5.

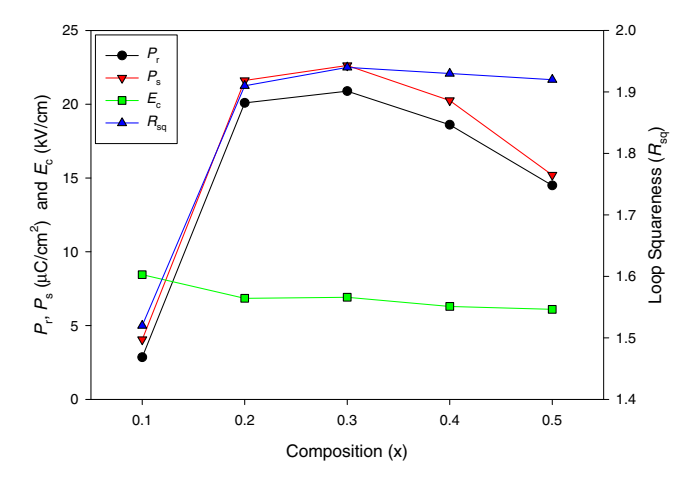


Fig. 6. (Color online) Remnant polarization (P_r) , saturation polarization (P_s) , coercive field (E_c) , and loop squareness (R_{sq}) of (1-x)PZT-(x)PCN ceramics.

lower than the P_r ($\sim 15\,\mu\text{C/cm}^2$) in a previous study,²⁰ probably due to the fact that the solid-state conventional mixed oxide method used in the previous study²⁰ yielded two MPB compositions at x=0.1 and 0.5, which is different from the columbite–wolframite method used in this study, which showed only one MPB composition at approximately $0.2 \le x \le 0.3$. It is well known that ferroelectric values, such as P_r , P_s , and E_c , show maximum values approximately at the MPB composition.

An empirical relationship between remnant polarization (P_r) , saturation polarization (P_s) and polarization at the fields above the coercive field was derived by Haertling and Zimmer.²⁷⁾ This permits the quantification of changes in the hysteresis behavior for the (1-x)PZT-(x)PCN samples through the following equation:

$$R_{\rm sq} = \frac{P_{\rm r}}{P_{\rm s}} + \frac{P_{1.1E_{\rm c}}}{P_{\rm s}},\tag{4}$$

where $R_{\rm sq}$ is the squareness of the hysteresis loop and $P_{1.1E_{\rm c}}$ is the polarization at an electric field equal to 1.1 times the coercive field ($E_{\rm c}$). For an ideal hysteresis loop, $R_{\rm sq}$ is equal to 2.0. As listed in Table II, the loop squareness parameter $R_{\rm sq}$ increased from 1.52 in 0.9PZT–0.1PCN to reach the maximum value of 1.94 in 0.7PZT–0.3PCN before decreasing to 1.92 in the 0.5PZT–0.5PCN composition. This observation is in good agreement with the $P_{\rm c}$ hysteresis loops, as depicted in Fig. 5. The results imply that the addition of 30 mol % PCN into PZT results in an optimized square $P_{\rm c}$ loop.

4. Conclusion

In this study, ceramics within the (1-x)Pb($Zr_{1/2}$ - $Ti_{1/2}$)O₃–(x)Pb($Co_{1/3}$ Nb_{2/3})O₃ solid solution system (where x=0.1–0.5) were successfully prepared using a solid-state mixed-oxide technique. The PZT ceramic was identified by XRD analysis as a single-phase tetragonal perovskite, while the addition of PCN resulted in a gradual shift from tetragonal symmetry to pseudo cubic symmetry, with a possible MPB between the two phases located near the 0.7PZT–0.3PCN composition. However, the dielectric and ferroelectric properties at the 0.7PZT–0.3PCN composition, indicating that the MPB composition shifted to $0.2 \le x \le 0.3$ in the PZT–PCN system.

Acknowledgements

This work was supported by the Commission on Higher

Education (CHE), the Thailand Research Fund (TRF), the Faculty of Science, and the Graduate School of Chiang Mai University.

- A. J. Moulson and J. M. Herbert: Electroceramics: Materials, Properties, Applications (Wiley, Chichester, U.K., 2003).
- S.-E. Park and T. R. Shrout: IEEE Trans. Ultrason. Ferroelectr. Freq. Control 44 (1997) 1140.
- 3) J. Kuwata, K. Uchino, and S. Nomura: Ferroelectrics 37 (1981) 579.
- M. L. Mulvihill, L. E. Cross, W. Cao, and K. Uchino: J. Am. Ceram. Soc. 80 (1997) 1462.
- N. Vittayakorn, G. Rujijanagul, X. Tan, M. A. Marquardt, and D. P. Cann: J. Appl. Phys. 96 (2004) 5103.
- H. Fan, G.-T. Park, J.-J. Choi, J. Ryu, and H.-E. Kim: J. Mater. Res. 17 (2002) 180.
- O. Furukawa, Y. Yamashita, M. Harata, T. Takahashi, and K. Inagaki: 5th Meet. Ferroelectric Materials and Their Applications, Kyoto, 1985, Jpn. J. Appl. Phys. 24 (1985) Suppl. 24-3, p. 96.
- V. J. Tennery, K. W. Hang, and R. E. Novak: J. Am. Ceram. Soc. 51 (1968) 671.
- D. Luff, R. Lane, K. R. Brown, and H. J. Marshallsay: Trans. J. Br. Ceram. Soc. 73 (1974) 251.
- 10) L. E. Cross: Mater. Chem. Phys. 43 (1996) 108.
- G. A. Smolenskii and A. L. Agranovskaya: Sov. Phys. Tech. Phys. 3 (1958) 1380.
- T. Kudo, T. Yazaki, F. Naito, and S. Sugaya: J. Am. Ceram. Soc. 53 (1970) 326
- B. A. Malkov and Y. N. Venevtsev: Izv. Akad. Nauk Neorg. Mater. 13 (1977) 1468 [in Russian].
- V. D. Salniov, Y. S. Kuźminov, and Y. N. Venevtsev: Izv. Akad. Nauk Neorg. Mater. 7 (1971) 1277 [in Russian].
- C. Xu, Z. Duan, X. Wang, D. Yang, and K. Chen: J. Cryst. Growth 281 (2005) 543.
- N. Vittayakorn, C. Puchmark, G. Rujijanagul, X. Tan, and D. P. Cann: Curr. Appl. Phys. 6 (2006) 303.
- N. Vittayakorn, G. Rujijanagul, T. Tankasiri, X. Tan, and D. P. Cann: Mater. Sci. Eng. B 108 (2004) 258.
- R. Yimnirun, S. Ananta, and P. Laoratanakul: J. Eur. Ceram. Soc. 25 (2005) 3235.
- 19) T. Hachiga, S. Fujimoto, and N. Yasuda: J. Phys. D 20 (1987) 1291.
- N. Vittayakorn, S. Wirunchit, S. Traisak, R. Yimnirun, and G. Rujijanagul: Curr. Appl. Phys. 8 (2008) 128.
- R. Yimnirun, S. Ananta, and P. Laoratanakul: Mater. Sci. Eng. B 112 (2004) 79.
- 22) I. W. Chen, P. Li, and Y. Wang: J. Phys. Chem. Solids 57 (1996) 1525.
- 23) G. H. Haertling: J. Am. Ceram. Soc. 82 (1999) 797.
- A. Halliyal, U. Kumar, R. E. Newnham, and L. E. Cross: Am. Ceram. Soc. Bull. 66 (1987) 671.
- R. D. Shannon and C. T. Prewitt: Acta Crystallogr., Sect. B 25 (1969)
- Y.-M. Chiang, D. P. Birnie, and W. D. Kingery: *Physical Ceramics* (Wiley, Chichester, U.K., 1997) p. 522.
- 27) G. H. Haertling and W. J. Zimmer: Am. Ceram. Soc. Bull. 45 (1966) 1084

Phase Transitions and Dielectric Properties in $Bi(Zn_{1/2}Ti_{1/2})O_3-(Na_{1-y}Li_y)NbO_3$ Perovskite Solid Solutions

Chien-Chih Huang, Naratip Vittayakorn¹, Anurak Prasatkhetragarn², Brady J. Gibbons, and David P. Cann

Department of Mechanical Engineering, Oregon State University, Corvallis, OR 97331-6001, U.S.A.

¹Department of Chemistry, King Mongkut's Institute of Technology Ladkrabang, Bangkok 10520, Thailand

Received June 11, 2008; accepted November 24, 2008; published online March 23, 2009

Perovskite solid solutions based on the system $Bi(Zn_{1/2}Ti_{1/2})O_3$ —NaNbO3 were obtained via solid-state processing techniques. The crystal structure and ferroelectric phase transitions were studied by means of X-ray diffraction and dielectric measurements. A stable perovskite phase was obtained for $Bi(Zn_{1/2}Ti_{1/2})O_3$ substitutions up to 10 mol %. The dielectric characterization revealed that as the $Bi(Zn_{1/2}Ti_{1/2})O_3$ content increased, the transition temperature decreased and the transition peak became very diffuse. The polarization hysteresis loop and strain measurements presented evidence of an induced ferroelectric phase with 1 mol % $Bi(Zn_{1/2}Ti_{1/2})O_3$ substitutions. The planar coupling factor (k_p) for $0.01Bi(Zn_{1/2}Ti_{1/2})O_3$ – $0.99NaNbO_3$ was measured to be 0.28. In addition, with the substitution of Li for Na in the $Bi(Zn_{1/2}Ti_{1/2})O_3$ – $(Na_{1-y}Li_y)NbO_3$ system, the diffuseness of the transition peak decreased and the transition temperature increased. © 2009 The Japan Society of Applied Physics

DOI: 10.1143/JJAP.48.031401

1. Introduction

Sodium niobate, NaNbO₃, is a well-known perovskite material which possesses attractive dielectric properties and a complex series of phase transitions.^{1–3)} At room temperature, NaNbO₃ exhibits anti-ferroelectric behavior. However, by replacing Na with a small amount of dopant (e.g., Li or K), a ferroelectric phase can be induced.^{4–6)} Since NaNbO₃ is known to exhibit a wide range of solid solutions with other ABO₃ perovskites, it is a promising candidate for the development of lead-free piezoelectric materials.

In studying past literature reports, solid solutions between NaNbO₃ and other ABO₃ compounds can be divided into two groups.^{7,8)} In the first group, solid solutions with a small amount of a second component ABO₃ (e.g., LiNbO₃)⁴⁾ resulted in an intermediate pseudo-tetragonal ferroelectric phase and the compositional dependence of the transition temperature is rather smooth. In the second group, a ferroelectric orthorhombic phase replaces the anti-ferroelectric phase at a critical mole fraction of the second component (e.g., NaTaO₃).⁹⁾ More importantly, there is an abrupt change in the transition temperature as a function of composition.

There have been many efforts aimed at developing new materials without lead for piezoelectric applications. Perovskite compounds with Bi are excellent candidates for the substitution of Pb since Bi has a similar electronic structure to Pb. In addition, there are numerous Bi-based perovskite compounds that can be used in designing solid solutions to optimize properties. $^{10-12}$ Recently, Suchomel *et al.* reported a new piezoelectric material based on $\text{Bi}(\text{Zn}_{1/2}\text{Ti}_{1/2})\text{O}_3$ –PbTiO₃. Their research revealed that $\text{Bi}(\text{Zn}_{1/2}\text{Ti}_{1/2})\text{O}_3$ acts to increase the transition temperature and enhances the tetragonality of PbTiO₃. 12 However, due to the smaller size of Bi^{3+} compared to Pb^{2+} , $\text{Bi}(\text{Zn}_{1/2}\text{Ti}_{1/2})\text{O}_3$ is unstable in its pure perovskite form.

In previous work, solid solutions within the ternary perovskite system $Bi(Zn_{1/2}Ti_{1/2})O_3$ – $BiScO_3$ – $BaTiO_3$ were explored. A stable perovskite phase was obtained for all compositions with a $BaTiO_3$ content greater than 50 mol %.

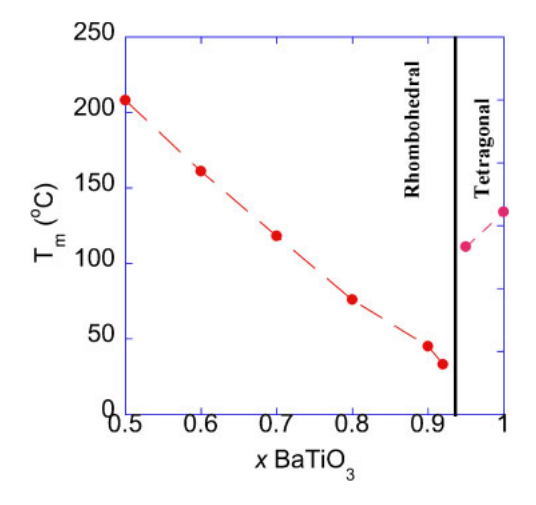


Fig. 1. (Color online) $(1 - x)[Bi(Zn_{1/2}Ti_{1/2})O_3 - BiScO_3] - xBaTiO_3$ system.¹³⁾

Furthermore, a change in symmetry from pseudo-cubic to tetragonal was observed as the mole fraction of BaTiO₃ increased (Fig. 1).¹³⁾ Dielectric measurements showed a dielectric anomaly associated with a phase transformation over the temperature range of 30 to 210 °C for all compositions. Examination of the polarization hysteresis behavior revealed weakly non-linear hysteresis loops. With these data, ferroelectric phase diagrams were derived showing the transition between the pseudo-cubic relaxor behavior to the tetragonal normal ferroelectric behavior. This transition was also correlated to changes in the diffuseness parameter.

In order to develop lead-free piezoelectric materials, NaNbO₃ (NN) was used for this research due to its stable perovskite phase and highly solubility with other perovskite end members. In this paper, the phase equilibria and dielectric properties of the binary solid solution Bi(Zn_{1/2}-Ti_{1/2})O₃-NaNbO₃ (BZT-NN) was examined. The doping effect was also studied to examine the effects of substituting Li for Na in the BZT-NN solid solutions. The purpose of this research is to focus on the influence of BZT on the

²Department of Physics, Chiang Mai University, Chiang Mai 50200, Thailand

perovskite end member NaNbO₃ in terms of the transition temperature and its ferroelectric and dielectric properties.

2. Experimental Procedure

The synthesis of $xBi(Zn_{1/2}Ti_{1/2})O_3-(1-x)Na_{1-y}Li_yNbO_3$ ceramics followed conventional ceramic processing procedures. Reagent grade oxide powders of Bi₂O₃ (≥99.9%), ZnO (>99%), TiO₂ (>99.9%), Na₂CO₃ (>99.5%), Nb₂O₅ $(\geq 99.9\%)$, and Li₂CO₃ $(\geq 99\%)$ were batched in stoichiometric amounts and ball-milled with ethanol and yttriumstabilized zirconia media for 6h. The dried powders were calcined in open crucibles at 920 °C for 6 h followed by an additional milling and drying step. The calcined powders were mixed with 3 wt % poly(vinyl butyral) (PVB) and then uniaxially cold-pressed at 150 MPa into 12.7 mm diameter pellets. Following binder burnout at 400 °C, the pellets were sintered in sealed crucibles between 1110-1150 °C for 2 h. For phase determination, X-ray diffraction (XRD; Bruker-AXS D8) was utilized in the 2θ scan range of $10-80^{\circ}$ using sintered pellets.

Prior to the electrical measurements, the pellets were polished to obtain smooth and parallel surfaces. After polishing, a silver electrode paste (Heraeus C1000) was applied and then fired at 650 °C. An Agilent 4284A LCR meter was used to measure the dielectric properties over a wide temperature range using a NorECS ProboStat high temperature measurement cell. Polarization hysteresis measurements (P-E) were determined at a frequency of 4 Hz using a ferroelectrics test system (Radiant). The strain as a function of applied electric field was obtained by using an optical displacement sensor (MTI-2100). Before the measurement of piezoelectric properties, the samples were sputtered with gold and poled under an electric field of 6-7 kV/mm in silicon oil at room temperature for 10 min. At 24 h after the samples were poled, the planar coupling factors (k_p) were determined by the resonance-antiresonance¹³⁾ method which was measured by using Solartron impedance analyzer (SI-1260). The piezoelectric coefficient, d_{33} , was measured by using a d_{33} meter (Sinocera YE2730A).

3. Results and Discussion

3.1 Crystal structure of Bi(Zn_{1/2}Ti_{1/2})O₃–NaNbO₃ (BZT–NN) solid solutions

The XRD patterns of sintered xBZT-(1-x)NN ceramics shown in Fig. 2 revealed that the perovskite phase was retained with a maximum of 10 mol % BZT added. Higher concentrations of BZT resulted in the formation of numerous secondary phases. Initially, compositions rich in NaNbO₃ exhibited peak splitting consistent with orthorhombic symmetry as expected. However, with increasing BZT content the separation between diffraction peaks corresponding to orthorhombic symmetry became narrower and eventually merged into a single broad peak at about x=0.05. The merging of peaks indicates a decrease in the tilt angle within the monoclinic system.

Figure 3 highlights the diffraction peaks that illustrate the evolution of the crystal structure and symmetry as a function of composition. The data clearly shows that the orthorhombic structure is maintained, though the decrease in peak intensity suggests that the orthorhombic distortion becomes

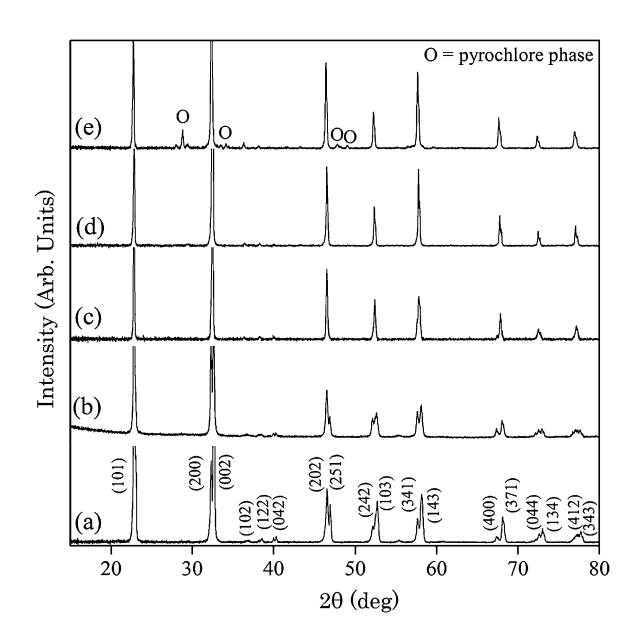


Fig. 2. XRD data for $xBi(Zn_{1/2}Ti_{1/2})O_3-(1-x)NaNbO_3$: (a) x = 0.01, (b) x = 0.05, (c) x = 0.075, (d) x = 0.1, and (e) x = 0.15.

Table I. Physical properties of xBZT-(1-x)NN perovskite ceramics.

			x BZT		
	0	0.01	0.05	0.075	0.1
$\rho_{\text{theoretical}}$ (g/cm ³)	4.575	4.613	4.774	4.877	4.955
ρ (%)	95	92.4	93.2	92.5	93.1

vanishingly small. The following section presents data on the phase transition via dielectric measurements, and it is clear that as the BZT content increases the phase transition approaches room temperature and becomes diffuse. For these reasons, it is not unexpected that the diffraction data is somewhat ambiguous.

3.2 Dielectric properties of BZT-NN solid solutions

Table I shows the densities of the ceramics as a function of BZT content. The measured density decreased slightly when a small amount of BZT was added into the solid solution. The dielectric constant plotted against temperature for $x \text{Bi}(\text{Zn}_{1/2} \text{Ti}_{1/2}) \text{O}_3 - (1-x) \text{NaNbO}_3$ from x=0.01 to 0.1 is presented in Fig. 4. It is shown that the maximum permittivity, ε_{m} , retained similar values for all compositions. However, a diffuse phase transition was observed for compositions where x>0.05 and the transition became more diffuse with increasing BZT content. The dielectric anomaly at around 50 °C for the x=0.01 composition shown in Fig. 4(b) may be related to the phase transition that occurs at a similar temperature in pure NaNbO₃. ³⁾

The temperature at which the maximum dielectric constant appeared, defined as $T_{\rm m}$, is plotted as a function of composition in Fig. 5. It is clear that for small amounts of BZT in the solid solution, a decrease in $T_{\rm m}$ was observed with increasing BZT content. At BZT concentrations greater than x=0.05, $T_{\rm m}$ dramatically decreased. The trend of the transition temperature as a function of composition matches the description of the second group of NaNbO₃-ABO₃ solid solutions in which the antiferroelectric phase transitions to a

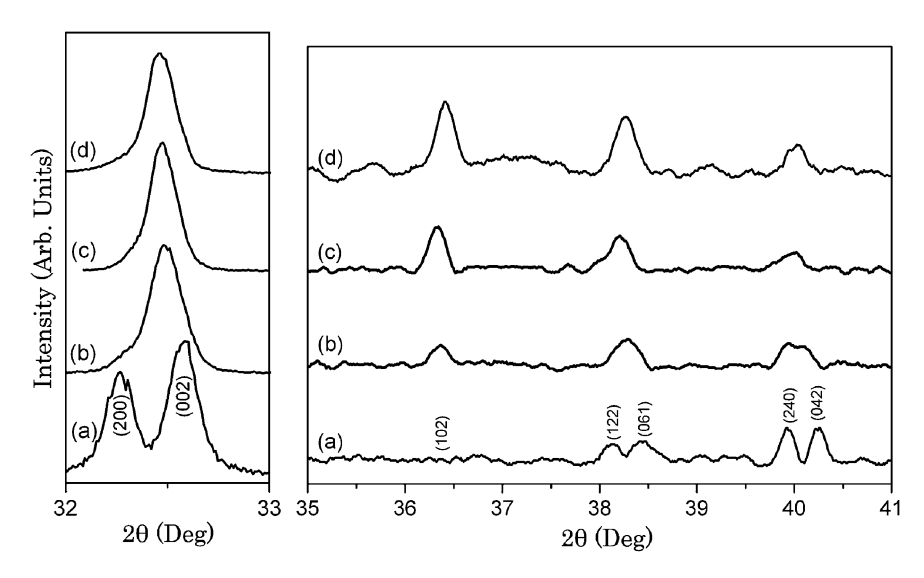


Fig. 3. XRD data for $x \text{Bi}(Z n_{1/2} \text{Ti}_{1/2}) O_3 - (1 - x) \text{NaNbO}_3$: (a) x = 0.01, (b) x = 0.05, (c) x = 0.075, and (d) x = 0.1.

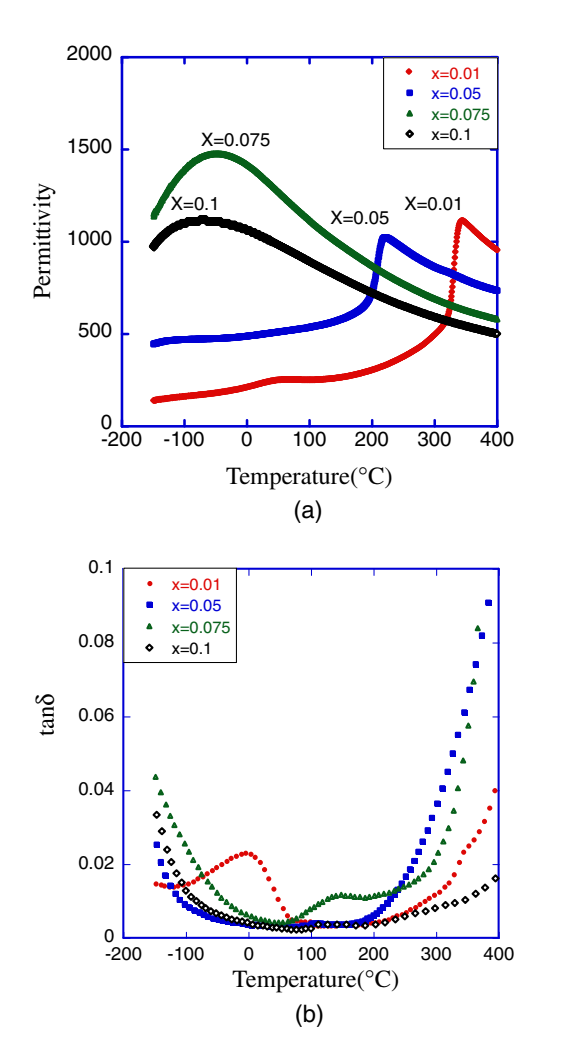


Fig. 4. (Color online) Permittivity and $\tan \delta$ as a function of temperature for $x \text{Bi}(\text{Zn}_{1/2}\text{Ti}_{1/2})\text{O}_3$ – $(1-x)\text{NaNbO}_3$ at a measuring frequency of 10 kHz.

ferroelectric phase with the addition of second component. ⁶⁾ This general trend is also similar to that observed in the ternary $Bi(Zn_{1/2}Ti_{1/2})O_3-BiScO_3-BaTiO_3$ system. Based on these reports, ferroelectric properties can be expected within the $Bi(Zn_{1/2}Ti_{1/2})O_3-NaNbO_3$ solid solution.

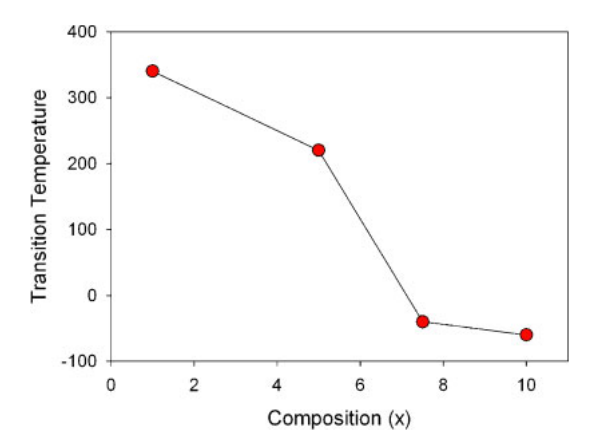


Fig. 5. (Color online) Compositional dependence of the transition temperature for $x \text{Bi}(\text{Zn}_{1/2}\text{Ti}_{1/2})\text{O}_3-(1-x)\text{NaNbO}_3$.

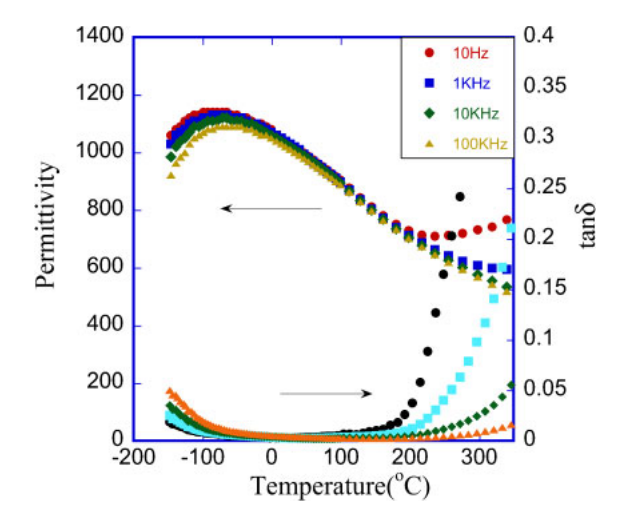


Fig. 6. (Color online) Permittivity and $\tan \delta$ as a function of frequency for 0.1Bi(Zn_{1/2}Ti_{1/2})O₃–0.9NaNbO₃.

The dielectric properties as a function of frequency for the $0.1Bi(Zn_{1/2}Ti_{1/2})O_3-0.9NaNbO_3$ composition is shown in Fig. 6. With only $10\,\text{mol}\,\%$ BZT introduced into the solid solution the maximum dielectric constant is shifted to below room temperature indicating a significant destabilization of

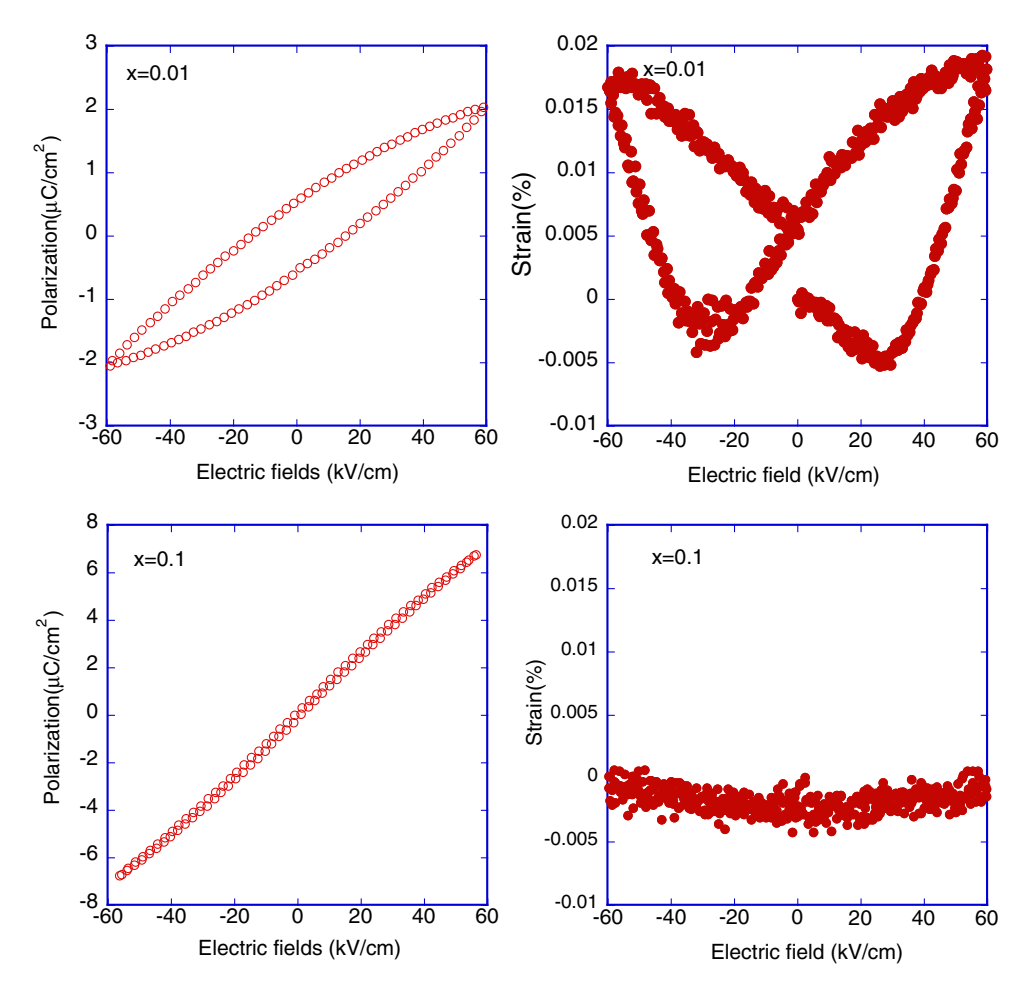


Fig. 7. (Color online) Polarization and strain vs electric field for $x \text{Bi}(\text{Zn}_{1/2}\text{Ti}_{1/2})\text{O}_3 - (1-x)\text{NaNbO}_3$ at 4 Hz at room temperature.

the ferroelectric phase. This is confirmed in the XRD data where room temperature measurements indicated very weak orthorhombic distortions.

At higher temperatures, the increase in permittivity and dielectric loss is most likely not due to a phase transition but rather due to the onset of conduction losses presumably tied to non-stoichiometry. At lower temperatures, a strong frequency dependence characteristic of relaxor ferroelectric behavior was observed in the vicinity of the dielectric maximum.

The polarization and strain as a function of applied electric field was measured at room temperature for a number of BZT–NN solid solutions (Fig. 7). The broad hysteresis loop observed for the 1 mol % BZT composition indicates that ferroelectric behavior was induced with the substitution of BZT. The strain data confirmed the existence of ferroelectric behavior. However at higher BZT concentrations, the *P*–*E* data exhibited linear behavior. The loss of hysteresis can be explained by the decrease of the transition temperature due to the increase in cation disorder at higher BZT concentrations.

The planar coupling factor (k_p) for $0.01 \text{Bi}(\text{Zn}_{1/2} \text{Ti}_{1/2}) \text{O}_3 - 0.99 \text{NaNbO}_3$ was measured to be 0.28 based on the resonance—antiresonance method. The measurement was conducted 24 h after the sample was poled. The piezoelectric coefficient, d_{33} , was measured at 38 pC/N. The depolarization temperature $(T_{\rm d})$ was measured to be 280 °C which is lower than the transition temperature $T_{\rm C} \approx 340$ °C shown

in Fig. 4(a). Combining all the data from the polarization hysteresis, strain, and piezoelectric measurements, the existence of the ferroelectric state can be confirmed with only x = 0.01 mole fraction of BZT added. This behavior is very similar to the effects of small amounts of Li substituted into NaNbO₃. ¹⁵⁾

3.3 Doping effects in BZT-NN

In order to investigate the effect of doping within NaNbO₃-ABO₃ solid solutions, LiNbO₃ was substituted for NaNbO₃. The Li ion is approximately 20% smaller than Na and has been found to introduce an instability into the crystal structure. The effects of replacing Li+ for Na+ in the $0.1Bi(Zn_{1/2}Ti_{1/2})O_3-0.9Na_{1-\nu}Li_{\nu}NbO_3$ composition shown in Figs. 8 and 9. The perovskite structure remained stable with up to 10 mol % Li added. At higher concentrations secondary phases appeared in the diffraction data. As can be seen in the dielectric and P-E hysteresis data, the addition of Li had two effects. First, it increased $T_{\rm m}$ from below room temperature to nearly 100 °C for 10 mol % Li added. This indicates that the stability of the ferroelectric phase was enhanced with the addition of Li which is confirmed by the broadening of the ferroelectric hysteresis loops as shown in Fig. 9. In addition, the phase transition sharpened with the addition of Li as the system shifted from relaxor to normal ferroelectric behavior. Room temperature XRD measurements are mostly inconclusive because the phase transition is in the vicinity of room temperature.

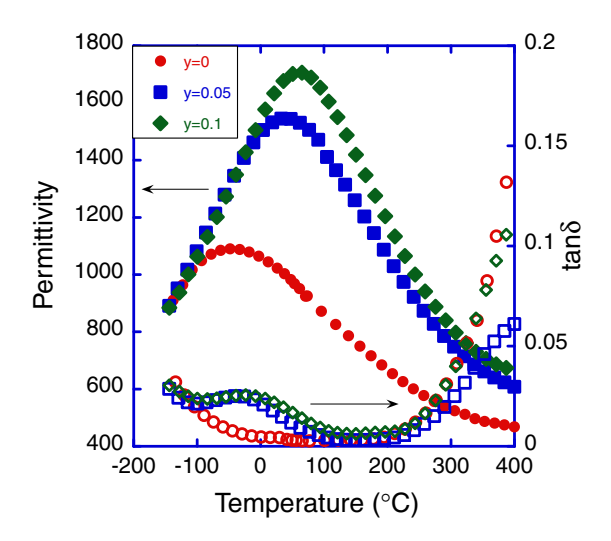


Fig. 8. (Color online) Permittivity and $\tan \delta$ as a function of temperature for 0.1Bi(Zn_{1/2}Ti_{1/2})O₃–0.9Na_{1-y}Li_yNbO₃.

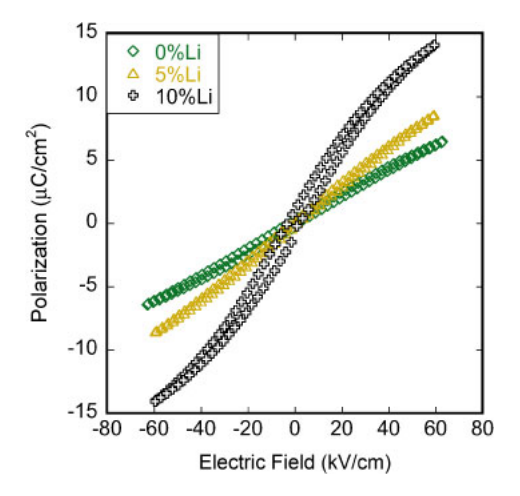


Fig. 9. (Color online) Polarization vs electric field for $0.1Bi(Zn_{1/2}-Ti_{1/2})O_3-0.9Na_{1-\nu}Li_{\nu}NbO_3$ at 4 Hz at room temperature.

Temperature dependent diffraction measurements are currently underway to track the change in symmetry as a function of temperature. These results are very different than

observations in the NaNbO₃–LiNbO₃ and NaNbO₃–KNbO₃ binary system,^{4,6)} where a pseudo-tetragonal phase transition was not observed in XRD and dielectric data.

4. Conclusions

In this work, the phase equilibria and dielectric properties of the binary solid solution $Bi(Zn_{1/2}Ti_{1/2})O_3$ –NaNbO₃ (BZT–NN) were examined. A combination of XRD and dielectric data indicated that a stable perovskite phase with orthorhombic symmetry was observed for compositions rich in NaNbO₃. As the BZT concentration increased the transition temperature dropped below room temperature and correspondingly the orthorhombic distortion weakened. The abrupt decrease of the transition temperature indicates the formation of a ferroelectric phase which was confirmed by P–E loop and strain measurements. The planar coupling factor (k_p) for $0.01Bi(Zn_{1/2}Ti_{1/2})O_3$ – $0.99NaNbO_3$ was measured at 0.28. Through substitution of Li for Na in the NN–BZT solution, the diffuseness of the transition peak decreased and transition temperature increased.

- 1) H. D. Megaw: Ferroelectrics 7 (1974) 87.
- C. N. W. Darlington and K. S. Knight: Acta Crystallogr., Sect. B 55 (1999) 24.
- S. Lanfredi, M. H. Lente, and J. A. Eiras: Appl. Phys. Lett. 80 (2002) 2731.
- 4) T. Nitta: J. Am. Ceram. Soc. 51 (1968) 623.
- 5) M. A. L. Nobre and S. Lanfredi: J. Appl. Phys. 93 (2003) 5557.
- 6) G. Shirane, R. Newnham, and R. Pepinsky: Phys. Rev. 96 (1954) 581.
- G. A. Smolenskii, V. A. Bokov, V. A. Isupov, N. N. Krainik, R. E. Pasynkov, and A. I. Sokolov: Ferroelectrics and Related Materials (Gordon & Breach, New York, 1984) p. 634.
- I. P. Raevski and A. A. Prosandeev: J. Phys. Chem. Solids 63 (2002) 1939.
- 9) H. Iwasaki and T. Ikeda: J. Phys. Soc. Jpn. 18 (1963) 157.
- 10) R. E. Cohen: Nature 358 (1992) 136.
- 11) M. R. Suchomel and P. K. Davies: J. Appl. Phys. 96 (2004) 4405.
- 12) M. R. Suchomel and P. K. Davies: Appl. Phys. Lett. 86 (2005) 262905.
- C.-C. Huang, D. P. Cann, X. Tan, and N. Vittayakorn: J. Appl. Phys. 102 (2007) 044103.
- 14) M. Onoe and H. Jumonji: J. Acoust. Soc. Am. 41 (1967) 974.
- R. R. Zeyfang, R. M. Henso, and W. J. Maier: J. Appl. Phys. 48 (1977)
 3014

High temperature phases in the 0.98PbZrO₃-0.02Pb(Ni_{1/3}Nb_{2/3})O₃ ceramic

W. Qu, 1 X. Tan, 1,a) N. Vittayakorn, 2 S. Wirunchit, 2 and M. F. Besser 3

Department of Materials Science and Engineering, Iowa State University, Ames, Iowa 50011, USA
Department of Chamistry, King Mangkut's Institute of Technology, Ladlyghang, Bangkak 10502, Theila

(Received 28 September 2008; accepted 22 November 2008; published online 13 January 2009)

The phase evolution with temperature in the $0.98 \text{PbZrO}_3 - 0.02 \text{Pb}(\text{Ni}_{1/3} \text{Nb}_{2/3}) \text{O}_3$ ceramic was investigated with dielectric permittivity and polarization measurements, hot stage transmission electron microscopy, and high temperature x-ray diffraction. Below 190 °C, the ceramic is in the antiferroelectric phase with characteristic $\frac{1}{4}\{110\}_c$ superlattice diffractions. In this stage, typical antiferroelectric 180° domains were observed. Between 190 and 220 °C, an intermediate phase, which is characterized by $\frac{1}{2}\{110\}_c$ -type superlattice diffractions, was detected. Evidences are found to suggest that this intermediate phase is ferroelectric. The $\frac{1}{2}\{110\}_c$ -type superlattice diffraction persists even into the paraelectric phase above 220 °C. In addition, there exists an incommensurate phase between the low temperature antiferroelectric phase and the intermediate ferroelectric phase. © 2009 American Institute of Physics. [DOI: 10.1063/1.3065087]

I. INTRODUCTION

The classic antiferroelectric (AFE) compound lead zirconate (PbZrO₃ or PZ) has been extensively studied since 1950s. At temperatures below 220 °C, PbZrO₃ displays an orthorhombic perovskite structure with antiparallel shifts of Pb²⁺ ions along the pseudocubic $\langle 110 \rangle$ direction, which leads to the AFE behavior. The space group for the low temperature AFE phase was determined to be Pbam. At temperatures above 230 °C, PbZrO₃ is in the paraelectric phase with the cubic m3m symmetry. In between the AFE and the paraelectric phase within a narrow temperature range, there is an intermediate phase, which is characterized by $\frac{1}{2}\{110\}_c$ -type superlattice diffractions. Above, the nature of this intermediate phase is still open for debate. Experimental evidence have been found to support either a ferroelectric 2,6,7 or an AFE 5,8 phase.

In our previous study, it has been found that by introducing minor amounts (2–6 mol %) of relaxor ferroelectric Pb(Ni_{1/3}Nb_{2/3})O₃ (PNN) into PZ, the temperature range is expanded for an intermediate phase, which is characterized by an evident frequency dispersion in dielectric permittivity. As a consequence, a series of striking phase transitions was revealed by the dielectric measurement. In the present work, the $0.98 Pb Zr O_3 - 0.02 Pb (Ni_{1/3} Nb_{2/3}) O_3$ (PZ98-PNN2) ceramic was selected to further investigate the phase evolution sequence during heating up to 300 °C with hot stage transmission electron microscopy (TEM) and high temperature x-ray diffraction (XRD).

II. EXPERIMENTAL PROCEDURE

The phase pure PZ98-PNN2 ceramic was prepared using the columbite precursor method in order to avoid the pyrochlore phase formation. Detailed preparation procedures have been reported in our previous publications. ⁹⁻¹¹ The rela-

The surface layers of the sintered pellets were removed by mechanical grinding. XRD analysis was performed with Cu $K\alpha$ radiation at a series of temperatures up to 300 °C on a PANalytical X-Pert Pro diffraction system to investigate the structural evolution. Dielectric properties were measured with an LCR meter (HP-4284A, Hewlett-Packard) on a Auelectroded specimen during heating from room temperature to 300 °C at a rate of 2 °C/min. The electrical polarization versus field hysteresis loops were recorded at a series of temperature with a standardized ferroelectric test system (RT-66A, Radiant Technologies). The peak field was maintained at 20 kV/cm during measurement.

Thin disks with a diameter of 3 mm were cut from the as-sintered ceramic pellet, ground, and polished to a thickness of 0.15 mm for TEM specimen preparation. The central portion of the disks was further thinned and polished by mechanical dimpling. Argon ion mill was then used to per-

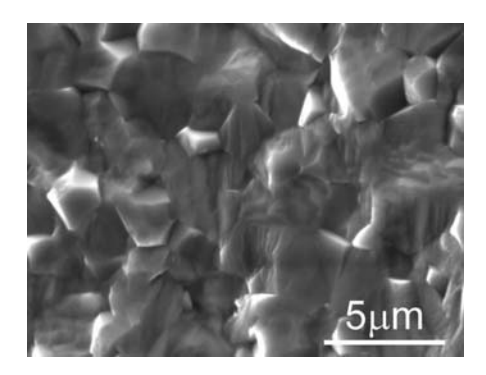


FIG. 1. SEM micrograph of the freshly fractured cross section of the PZ98-PNN2 ceramic.

²Department of Chemistry, King Mongkut's Institute of Technology, Ladkrabang, Bangkok 10502, Thailand ³Materials and Engineering Physics Program, Ames Laboratory, U.S.-DOE, Ames, Iowa 50011, USA

tive density of the as-sintered ceramic was measured using the Archimedes method to be 98%. The grain size was examined by scanning electron microscopy (SEM) (JEOL JSM-606LV). As shown in Fig. 1, the freshly fractured cross section of the PZ98-PNN2 ceramic is almost free of pores and the grain size is in the range of $2-5~\mu m$.

^{a)}Electronic mail: xtan@iastate.edu.

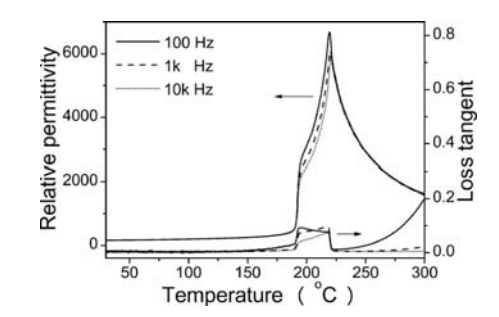


FIG. 2. Dielectric properties during heating at $100~\mathrm{Hz}, 1~\mathrm{kHz}, \mathrm{and}\ 10~\mathrm{kHz}$ in a bulk PZ98-PNN2 ceramic.

forate the disk at the center. Hot-stage TEM observations were performed with a heating rate less than 2 °C/min on a Philips CM30 instrument operating at 300 kV. Bright field images and selected area electron diffraction (SAED) patterns were recorded 10 min after the temperature was stabilized.

III. RESULTS AND DISCUSSION

A. Electrical properties

The temperature dependence of relative dielectric permittivity and loss tangent was measured at frequencies of 100 Hz, 1 kHz, and 10 kHz during heating from 30 to 300 °C and the results are displayed in Fig. 2. Clearly, there are two abrupt changes in both relative permittivity and loss tangent in the PZ98-PNN2 ceramic. The first one occurred at around 190 °C where both relative permittivity and loss tangent increased by one order of magnitude. The second abrupt change took place at the Curie temperature of 220 °C where significant suppression of loss tangent is seen. Therefore, the dielectric response in the PZ98-PNN2 ceramic can be divided into three stages. At temperatures below 190 °C, the relative permittivity and the loss tangent both have low values and show negligible increases with increasing temperatures. At temperatures above 220 °C, the relative permittivity starts to decrease following the Curie-Weiss law, ε_r $=C/(T-T_0)$, where ε_r is the relative permittivity, T is the temperature, and C and T_0 are Curie constant and Curie point, respectively. By fitting the data between 220 and 300 °C in Fig. 2, C and T_0 were determined to be 1.89 $\times 10^5$ and 185.8 °C, respectively. In the intermediate temperature range (190-220 °C), the relative permittivity increases dramatically, while the loss tangent remains high around 0.1. The most remarkable feature of the dielectric behavior in this temperature range is the evident frequency dispersion of both relative permittivity and loss tangent, resembling that in relaxor ferroelectric ceramics. T_{max} , the temperature at which the maximum dielectric permittivity is achieved, was measured to be 219.4 °C at 100 Hz, 220.1 °C at 1 kHz, and 220.4 °C at 10 kHz, respectively, shifting slightly toward higher temperatures with increasing frequency.

To further clarify the dielectric behavior of the different phases in the PZ98-PNN2 ceramic, electrical polarization hysteresis loop measurements were performed under a peak field of 20 kV/cm at a series of temperatures. During heating,

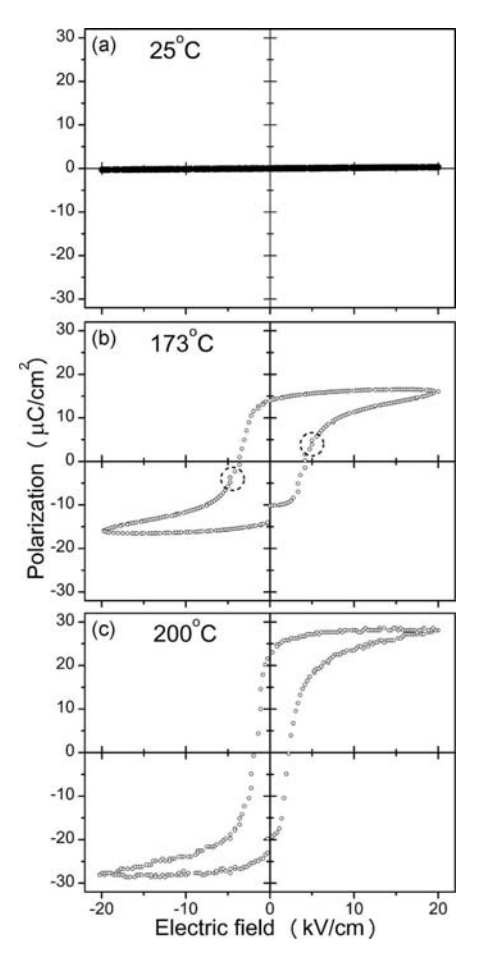


FIG. 3. Polarization hysteresis loops recorded from a bulk PZ98-PNN2 ceramic at 4 Hz during heating at (a) 25 $^{\circ}$ C, (b) 173 $^{\circ}$ C, and (c) 200 $^{\circ}$ C.

the two electrodes were shortened. The loop was recorded after the temperature was stabilized for at least 5 min. As shown in Fig. 3(a), very small polarizations can be induced by the applied electric field in the ceramic at room temperature. This is typical for an AFE ceramic subjected to electric fields that are not sufficient to induce the AFE to ferroelectric phase transition. Such a linear behavior with minimum polarization remains at temperatures up to 170 °C.

When the temperature further increases, a hysteretic behavior starts to develop. As shown in Fig. 3(b), a regular hysteresis loop with a coercive field E_c of 3.9 kV/cm was recorded at 173 °C. However, the observed hysteresis loop does not indicate the presence of a ferroelectric phase. Close examination of the loop in Fig. 3(b) reveals that slight occurred at $\sim 5 \text{ kV/cm}$, marked distortions the two dashed circles on the hysteresis loop. Similar loops were found in distortions on hysteresis $Pb_{0.99}Nb_{0.02}[(Zr_{0.57}Sn_{0.43})_{1-v}Ti_{v}]_{0.98}O_{3}$ ceramics and have been attributed to the onset of the electric field-induced AFE to ferroelectric phase transition. ¹² Therefore, the PZ98-PNN2 ceramic at this temperature is still in the AFE phase. It should be noted that the distortions marked in Fig. 3(b) indicate the AFE-to-ferroelectric phase transition. The distortion associated with the backward ferroelectric-to-AFE transition was not seen because it may overlap with the coercive field of the induced ferroelectric phase. The observed large

polarization is due to the induced ferroelectric phase by the applied field of 20 kV/cm, which is much higher than the critical electric field E_F of \sim 5 kV/cm.

Further increase in temperature leads to the decrease in the critical field E_F and the increase in both the saturation polarization P_s and the remanent polarization P_r . P_r saturates at 25 μ C/cm² when the temperature reaches 177 °C and stays unchanged up to 186 °C. It should be noted that the coercive field E_c (not the critical field E_F) remains the same at 3.9 kV/cm in the temperature range of 172–186 °C. The results suggest that the volume fraction of the ferroelectric phase induced by a field of 20 kV/cm in the ceramic increases with increasing temperatures between 172 and 177 °C. In the temperature range of 177–186 °C, the whole piece of sample was forced into a ferroelectric phase by the external electric field of 20 kV/cm. Therefore, the P_r saturates in this temperature range.

Dramatic change in the coercive field E_c was observed at 186 °C. At this temperature, although a well defined hysteresis loop was still observed, E_c abruptly reduced to 2.4 kV/cm, indicating the appearance of a new phase. Up to 200 °C, the hysteresis loop remains largely unchanged, with the one at 200 °C shown in Fig. 3(c).

Combined with the results presented in Fig. 2, we believe that the abrupt change in E_c at 186 °C marks the phase transition at 190 °C revealed by the dielectric measurement. The discrepancy in temperature is due to the different test conditions. In the dielectric measurement, the ceramic sample was subjected to continuous heating at a rate of 2 °C/min, while in the polarization measurement, the hysteresis loops were recorded after at least 5 min the temperature is stabilized. In summary, the macroscopic property measurements reveal that at temperatures below 190 °C, the PZ98-PNN2 ceramic is AFE with stable and low dielectric permittivity and loss tangent. Under applied electric fields, the AFE phase can be transformed into a ferroelectric phase at temperatures slightly below the transition temperature. An intermediate phase exists between 190 and 220 °C. The increased loss tangent and the well defined hysteresis loops with reduced coercive fields E_c seem to suggest that this phase is ferroelectric.² Further supporting evidence is found in our previous study where the intermediate phase is stabilized down below room temperature in the PZ90-PNN10 ceramic and an undistorted hysteresis loop was observed in this ceramic at room temperature. 10 However, this intermediate phase is a unique ferroelectric phase with evident frequency dispersion in its dielectric behavior.

B. Hot stage TEM

The temperature induced phase transitions were visualized by hot stage TEM during heating. One grain about 3 μ m in size was tilted so that its $\langle 001 \rangle$ -zone axis was aligned with the electron beam direction. The evolution of the SAED pattern with temperature is exemplified in Fig. 4. At room temperature, the primary feature is the presence of the $\frac{1}{4}\{110\}_c$ -type superlattice diffraction spots [Fig. 4(a)], where the subscript c indicates that the indices are based on the parent cubic perovskite unit cell. The superlattice struc-

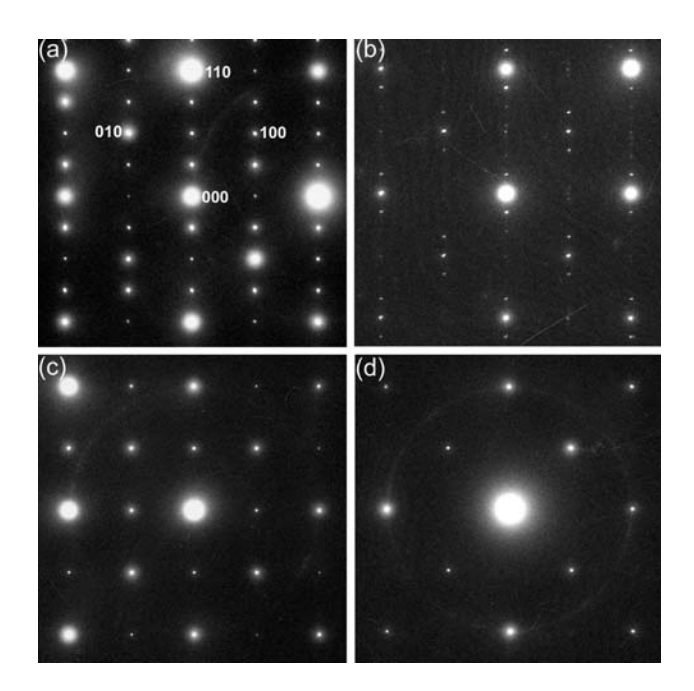


FIG. 4. Hot stage *in situ* TEM experiment on a thin foil specimen of the PZ98-PNN2 ceramic. The $\langle 001 \rangle_c$ -zone axis SAED patterns observed during heating at (a) 25 °C, (b) 179 °C, (c) 194 °C, and (d) 240 °C.

ture is identical to that of PbZrO₃ at room temperature. ^{2,6,7} Therefore, adding 2 mol % of PNN does not change the crystal structure of PbZrO₃. The SAED pattern with the $\frac{1}{4}\{110\}_c$ superlattice spots does not change with increasing temperature up to 179 °C.

At 179 °C, the $\frac{1}{4}\{110\}_c$ superlattice spots disappeared, as shown in Fig. 4(b). Instead, incommensurate superlattice diffraction spots emerged. These extra diffraction spots are of the $\frac{1}{n}\{110\}_c$ -type, where n is not an integer. The value of n is determined to be 6.48 for the PZ98-PNN2 ceramic from Fig. 4(b). The incommensurate superlattice diffraction spots only existed over a narrow temperature range of ~ 3 °C and completely disappeared at 181 °C. This type of incommensurate superlattice diffraction has been previously observed in PbZrO₃ and was attributed to the competition between the low temperature AFE phase and the intermediate ferroelectric phase.

In the temperature range of 181-212 °C, the primary feature in SAED patterns is the presence of $\frac{1}{2}\{110\}_c$ -type superlattice diffraction, as exemplified by the diffraction pattern recorded at 194 °C shown in Fig. 4(c). The $\frac{1}{2}\{110\}_c$ superlattice diffraction was reported previously and has been considered as the signature of the intermediate phase in PbZrO3. However, considerable controversy remains concerning the symmetry and the nature of the intermediate phase. It was reported to be either rhombohedral or orthorhombic, 5,7 either ferroelectric 2,6,7 or AFE. 5,8

The $\frac{1}{2}\{110\}_c$ superlattice diffraction started to become weaker and diffuse at 212 °C and finally vanished at 240 °C. Further increase in temperature up to 300 °C did not lead to any change in the diffraction pattern. The SAED pattern at 240 °C is shown in Fig. 4(d) and can be indexed with the parent cubic perovskite structure.